On elliptic quantum integrability

Vertex models, solid-on-solid models and spin chains

Jules Lamers

Reading committee

Prof. dr. H. Rosengren, Chalmers Tekniska Högskola and Göteborgs Universitet
Prof. dr. J. V. Stokman, Universiteit van Amsterdam
Prof. dr. J.-S. Caux, Universiteit van Amsterdam
dr. D. Schuricht, Universiteit Utrecht
Prof. dr. B. Q. P. J. de Wit, Universiteit Utrecht

ISBN 978-90-393-6579-3

Printed by CPI, Koninklijke Wöhrmann, Zutphen

On elliptic quantum integrability

Vertex models, solid-on-solid models and spin chains

Elliptische kwantumintegreerbaarheid

Vertexmodellen, SOS-modellen en spinketens

(met een samenvatting in het Nederlands)

Proefschrift

ter verkrijging van de graad van doctor aan de Universiteit Utrecht op gezag van de rector magnificus, prof. dr. G. J. van der Zwaan, ingevolge het besluit van het college van promoties in het openbaar te verdedigen op woensdag 1 juni 2016 des middags te 12.45 uur

door

Jules Lamers

geboren op 14 december 1986 te Utrecht

Promotor: Prof. dr. G. E. Arutyunov

This thesis was accomplished with financial support from the Netherlands Organisation for Scientific Research (NWO) under the VICI grant 680-47-602.

to Levi

Contents

List of Figures

Preface

This is an account of work I have done during my PhD at the Institute for Theoretical Physics of Utrecht University. The general theme is quantum integrability in vertex models (Part One) and exact solvability in spin chains (Part Two), with the elliptic case constituting the core of the thesis (Chapters III and IV).

Publications. This thesis is based on my research papers

[1] W. Galleas and J. Lamers, *Reflection algebra and functional equations*, Nucl. Phys. B 886, 1003 (2014), arxiv:1405.4281

[2] W. Galleas and J. Lamers, *Differential approach to on-shell scalar products in six-vertex models*, submitted, arxiv:1505.06870

[3] J. Lamers, *Integral formula for elliptic SOS models with domain walls and a reflecting end*, Nucl. Phys. B 901, 556 (2015), arxiv:1510.00342

as well as the current status of

[4] R. Klabbers and J. Lamers, *A partially isotropic extension of Inozemtsev's elliptic spin chain*, in preparation.

Other papers:

[5] J. Lamers, *A pedagogical introduction to quantum integrability, with a view towards theoretical high-energy physics*, PoS Modave2014 001, arxiv:1501.06805

[6] R. Keesman, J. Lamers, R. A. Duine and G. T. Barkema, *Finite-size scaling at infinite-order phase transitions*, in preparation.

Outline. The two parts of this thesis can be read independently. Part One is about the exact computation of the partition function governing a six-vertex or solid-on-solid model on a lattice of arbitrary but fixed size for a specific choice of boundary conditions. Exact expressions for these quantities were already available due to the work of Korepin and Izergin and others. Using the approach put forward by Galleas we study the partition functions from another point of view. We show that this approach contains that of Korepin–Izergin, while offering an algorithm that allows one to construct, rather than guess, a formula for the partition function. This yields a new expression for that function in the case of a reflecting end and domain walls on the three other ends.

The shorter Part Two is about the question whether the partially anisotropic (think: XXZ) version of Inozemtsev's elliptic spin chain is exactly solvable. This model, interpolating between the XXZ and Haldane–Shastry spin chains, is very interesting from a theoretical viewpoint. Inozemtsev's exact solution of the original fully isotropic (XXX) model is rather intricate, and it would be very interesting to know whether that is an isolated case or part of a more general pattern. A few other modifications of Inozemtsev's spin chain are known to be exactly solvable, yet, unlike the partially isotropic version, those models are not 'continuously connected' to (deformations of) Inozemtsev's spin chain. Although we have not yet found a satisfying answer I think that this question is very interesting, and our findings so far might be of interest to other researchers.

A note on notation. At the risk of pleasing neither I try to cater to both the physics and the mathematics communities. I have chosen to avoid a Bourbaki 'definition–theorem–proof–corollary' style, although I do use the standard typesetting to demarcate proofs to facilitate skipping them if one would wish to do so.

I write $\mathbb{N} := \mathbb{Z}_{>0}$, $\mathbb{N}_0 := \mathbb{N} \cup \{0\}$ and $\mathbb{Z}_L := \mathbb{Z}/L\mathbb{Z}$. In Part One the notation $\overleftarrow{\prod}$ and $\overrightarrow{\prod}$ are used to indicate the ordering of the factors, with indices of the factors increasing in the direction indicated by the harpoons. Sometimes—especially in Part Two—sums or products over two indices are decorated with a star, as in $\sum^\star$ and $\prod^\star$, to indicate that equal values of the indices are to be omitted.

To avoid unwieldy numbers the chapter is suppressed in the numbering of sections, equations, figures and the occasional table. Whenever I refer to, say, an equation in *another* chapter the number of that chapter *is* included: thus (1.27) would refer to the twenty-seventh equation in Section 1 of the current chapter, while (III.1.27) refers to that equation in Chapter III.

Elliptic functions. In mathematics as well as physics 'understanding' amounts to a large extent to 'getting used to'. Typical examples are Weierstraß's δ-ε definition of limits and quantum mechanics. The theory of elliptic functions is much the same. Although one does not need much more than complex analysis to get started, it involves many closely related special functions that satisfy a daunting amount of identities. By definition an *elliptic function* is a meromorphic doubly periodic function on $\mathbb{C}$. Recall that Liouville's theorem in complex analysis says that any holomorphic function that is bounded on $\mathbb{C}$ is constant. Thus, an elliptic function without poles is constant. The odd Jacobi theta function, featuring in Part One and especially Chapter III, is discussed in Appendix III.A. The Weierstraß elliptic functions, appearing in Part Two, are treated in Appendix IV.A.

Justification. Quantum integrability and exact solvability are beautiful topics in mathematical physics. They come with algebraic and analytic structures that provide powerful tools enabling one to analyze the models in great detail. The unavoidable consequence, however, is that this field can be quite technical, which tends to makes it rather inaccessible. Therefore I have chosen to devote a fair portion of this thesis (Chapter I and Section IV.1) to an introduction aimed at non-experts with the hope of making the remainder more accessible. I believe that these pieces may also be useful by themselves as in-

troductions to quantum integrability in vertex models and exact solvability in spin chains.

Parts of Chapter I draw from my lecture notes [5], although the angle is different. New are the introduction to various integrable boundary conditions, with a major role for domain walls and reflection, and dynamical (solid-on-solid or, equivalently, generalized six-vertex) models. I find the language of generalized six-vertex models to be more convenient, and the graphical notation for those models introduced in Sections I.3 and I.3.5 is mine [3], originally inspired by Shibukawa [7]. Although quantum integrability is intimately related to various topics in mathematics—including quantum groups, representation theory, harmonic analysis, and special functions—I have chosen to favour physics as a starting point since that requires fewer prerequisites.

Rather than immediately getting into technicalities related to the elliptic, dynamical, reflecting case we get started in Chapter II with a more simple example to get familiar with the constructive method of Galleas. The material covers work of Galleas, though presented from a somewhat different perspective, supplemented with some improvements that I made in [3] and the current text. New in Chapter II are in particular

- the recovery (II.3.27) of the approach of Korepin–Izergin;
- a proof for the special zeroes;
- the use of the value of the partition function at either of the special points (II.1.16) or (II.1.18) to fix the normalization;
- the explicit relation between the results of the two approaches (Appendix II.A), for which I am indebted to Hjalmar Rosengren.

Chapter III is based on [1, 3]. Since the elliptic solid-on-solid model contains the ordinary six-vertex model as a special case, we directly treat the more general case [3]. Improvements with respect to [3] include

- the recovery of the method of Tsuchiya–Filali–Kitanine within our approach;
- the independence of (III.3.20) of $\lambda_\flat$ and, up to an overall factor, of the choice of sign in $\lambda_\star$; and
- the proof of the normalization in (III.3.23) via either of the special points (III.1.34) or (III.1.35).

Note that the last of these is also much easier than the proof from [1] using the leading behaviour of the partition function as all spectral parameters tend to infinity.

Chapter IV is based on ongoing research together with Rob Klabbers. Credits for the nice Figures IV.3 and IV.4 are due to him.

Part One

Quantum integrability and functional equations

Chapter I

Quantum-integrable vertex models and their friends

Physicists try to understand the inanimate world by formulating theories that describe and predict the result of experiments. Further insight into the underlying mechanisms that *cause* the observed phenomena may be furnished by *models* describing, say, a particular material at smaller length scales. Such an approach is possible because the model does not have to be perfect: often it suffices to give an approximate description that captures only certain key features of the actual physical system. One then tries to compute, at least approximately, quantities whose values can be compared with experiments to test the model. The last century or so has witnessed a tremendous progress in our understanding of nature through such microscopic theories and models. Milestones are the development of statistical and quantum mechanics and of course quantum field theory. These have led to microscopic models for such mundane things as water ice all the way to the Standard Model of elementary particle physics.

There is a special class of models that go further still: they are *exactly solvable* by analytical methods while describing nontrivial physics involving, for example, strongly interacting particles. Several of these models have been found to provide accurate descriptions of certain experiments, as in e.g. [8]. Others are *toy models* that are further away from physics but interesting from a theoretical point of view as they allow us to deepen our understanding of the structure of our theories and models for nature.

One can go on and ask *why* such models are exactly solvable. Of course, generally speaking, questions starting with 'why' are hard to answer—much more so than 'how can we compute'-type questions. Yet in exceptional cases one is lucky and can really find a satisfying reason. One possible answer is the presence of an underlying mathematical structure offering a lot of algebraic or analytic control that renders the model exactly solvable. If this mathematical structure corresponds to a macroscopically large amount of hidden symmetries the model is *quantum integrable*. These models are prime examples of Wigner's 'unreasonable effectiveness of mathematics in the natural sciences' [9].

A common feature of quantum-integrable models is that they are *two-dimensional*, either involving time-dependent processes in one-dimensional space or systems at thermal equilibrium in two spatial dimensions. The physics of two-dimensional systems is very special. For us the most relevant consequence of the low dimensionality can be nicely understood in the context of (quantum) field theory, see also [5, §5.1] and references

therein. In three or more dimensions the Coleman–Mandula, and more generally Haag–Łopuszański–Sohnius, theorem puts severe restrictions on the possible symmetries that any interacting theory may have. In two dimensions one of its assumptions is violated and it *is* possible to have an interesting (interacting) theory with many symmetries.

In this chapter we give an introduction to quantum integrability in statistical physics. The goal is to prepare the reader for Chapters II and III, and to offer physical and mathematical background and motivation. The expert might wish to proceed to those chapters, which start with a recap of the relevant set-up to summarize our conventions, and contain references to the relevant parts of the present chapter for further details.

Before going any further let us get the following out of the way: there is in fact no generally accepted definition of 'quantum integrability' [10]. Rather than attempting to contribute to the debate we use this notion, and that of 'exact solvability', somewhat loosely for now. At the end of this chapter we will give a precise definition of quantum integrability that is most suitable for our purposes.

Outline. The plan of this introductory chapter is as follows. After recalling some preliminaries from statistical physics in Section 1 we introduce the main characters of Part One of this thesis in Section 2.1. These include the six-vertex model (for Chapter II), the solid-on-solid model (for Chapter III), and some of their close relatives. For these models it turns out to matter which boundary conditions are chosen for computations, and we review several options in Section 2.2. Important examples are the case of domain walls (Chapter II) and reflection (Chapter III). Our presentation in the remainder of the present chapter uses the diagrammatic notation introduced in Section 2.3.

Having covered the physical and mathematical background we head in the direction of quantum integrability, which is the toolbox that we will use in Chapters II and III to study our models. First we need to translate the models that we are interested in into an algebraic language. We start locally in Section 3.1, pass to the bulk in Section 3.2, and include the boundary conditions in Sections 3.3–3.4. The dynamical case, relevant for the solid-on-solid model, is treated separately in Section 3.5.

Section 4 deals with quantum integrability. To motivate the definition that we will use, which involves the Yang–Baxter equation, we discuss the relevance of commuting transfer matrices for the six-vertex model with periodic boundary conditions in Section 4.1. The quantum inverse-scattering method is next, in Section 4.2. The dynamical case is discussed in Section 4.3. To conclude this chapter we go through the computations for the algebraic Bethe ansatz in Appendix A: similar calculations will be used in Sections II.3.1 and III.3.1.

1 Preliminaries

We commence by fixing some basic terminology and notation.

Lattices. Most of the models featuring in this thesis are *lattice models*, that is, they are defined on (a piece of) a lattice in space. By a lattice we will mean a graph, consisting of vertices (sites) connected by edges (links), that is invariant under discrete translations along any edge. In one dimension there is only one lattice, $\mathbb{Z}$, up to the choice of the lattice spacing.

In two dimensions there are several inequivalent lattices. We will really only be interested in *square lattices*, whose faces (plaquettes) are squares, with edges connecting *nearest neighbours*. The *dual* of this lattice is the square lattice obtained from the original one by a translation over half an edge in both the horizontal and the vertical direction, such that the dual faces are centred at the original vertices and vice versa.

Physically the vertices usually represent atoms of some material. For the integrable statistical-physical models that we will consider in Part One of this thesis the lattice has dimension (rank) two and represents a (perfect) crystal. For the exactly solvable spin chains in Part Two the lattice is one dimensional, which may be achieved in experiments by trapping ultracold atoms in an optical lattice.

We will mostly be interested in statistical-physical systems of finite size. In the case of a square lattice we will consider a rectangular portion containing K rows and L columns of that lattice. We will sometimes refer to this portion as the *bulk*, and to the (half-)edges at the *boundary* as *external* edges.

Stat phys 101. In a nutshell the aim of statistical physics is to understand thermodynamic properties of a macroscopic physical system starting from a microscopic description. A *statistical-physical model* consists of the following data. The first piece of input is a collection of variables ε_l that are known as the *microscopic degrees of freedom*, which are in some way associated to a geometric object like (a portion of) a lattice. A configuration of these microscopic degrees of freedom is called a *microstate*, or simply *state*, of the system. The second piece of input is a rule $C \longmapsto W(C)$ assigning to every microstate a *statistical weight* that encodes the likelihood of finding the system in that state. These weights typically depend on the temperature via the combination $k_{\mathrm{B}}T$ involving Boltzmann's constant $k_{\mathrm{B}} \approx 1.38 \times 10^{-23} J/K$. If Ω denotes the number of *allowed* ('physical') microstates, which have nonzero weight, then the *entropy* is defined as $S := k_{\mathrm{B}} \log \Omega$.

The microscopic degrees of freedom often take values in a discrete, and even finite, set. We will follow the literature, in which these variables are usually called *spins*, but albeit 'quantized' these variables should not be confused with their quantum-mechanical counterparts valued in vector spaces like $\mathbb{C}^2$.

Example: Ising model. Arguably the most famous models in classical statistical physics are *Ising-type models*. The microscopic degrees of freedom are binary spins $\varepsilon_l \in \{\pm 1\}$ at the vertices of a lattice. These two values are usually depicted by arrows pointing up or down. The (unnormalized) Boltzmann weights are determined by the energy $E(C)$ of the microstates $C = \{\varepsilon_l\}_l$. The prototype is the Ising model in d dimensions: the lattice

is $\mathbb{Z}^d$, and $E(C) = J \sum_{\langle k,l \rangle} \varepsilon_k \varepsilon_l$ involves interactions with coupling strength J between all pairs (k,l) of nearest-neighbouring vertices. Such models describe, for instance, crystals with highly anisotropic—yet 'partially isotropic' in the terminology of Chapter IV—interactions between the atoms positioned at the vertices of the lattice, with the spins representing electric dipoles.

Let us record some properties of the Ising model that will also come back for different models in the next section. Firstly, due to the short-range nature of the interactions, the statistical weights $W(C,T) = \prod_{\langle k,l \rangle} \mathrm{e}^{-J\,\varepsilon_k\,\varepsilon_l/k_{\mathrm{B}}T}$ are *local* in the sense that they are products of 'local' weights, which in this case are associated to the edges of the lattice. Secondly the weights are translationally invariant or *homogeneous*, making them compatible with the lattice structure of the model. Finally, as the energy is quadratic in the spins, the model is invariant under global *spin reversal* acting by $C \longmapsto -C$, i.e. $\varepsilon_l \longmapsto -\varepsilon_l$ for all l. This symmetry can be interpreted as the absence of an external field as the spins do not have a preferred direction, and is also known as the *zero-field* assumption.

The case $d = 1$ was solved by Ising in his 1924 PhD thesis; it does not exhibit any phase transitions [11, §2]. The case $d = 2$ is more interesting. For the square lattice Kramers and Wannier [12] were able to locate the critical temperature in 1941 using the first example of a weak/strong-coupling duality, see also [11, §6]. Three years later Onsager [13] solved the Ising model on the square lattice using the transfer-matrix method. Allowing for different coupling constants in the horizontal and vertical directions, he found that close to the critical temperature the model's behaviour does not depend on the ratio between the couplings. This led to the idea of *universality* in statistical physics, and in the following decades more models were found exhibiting the same critical behaviour [11, §1]. Only in 1972, with Baxter's solution of the eight-vertex model (see also Section 4.3) it became clear that there are several different universality classes.

Partition function. The thermodynamic behaviour of a statistical-physical model, defined on a large but finite portion of a lattice, is governed by the *statistical sum* or (canonical) *partition function*,

$$Z(T) \coloneqq \sum_{C} W(C,T)\,. \tag{1.1}$$

This quantity serves as a normalization for turning the weights into probabilities: $P(C,T) = W(C,T)/Z(T)$ is the probability for finding the system in the state C. Moreover, Z is essentially the moment-generating function of this probability distribution, and determines macroscopic thermodynamic quantities. For any model the problem is to get a grip on the typically *huge* sum in (1.1). Indeed, interesting thermodynamic behaviour, such as a phase transition, is related to non-smooth behaviour of Z in $1/k_{\mathrm{B}}T$. The weights usually depend smoothly on the temperature, in which case non-smoothness can only occur in the *macroscopic* limit where the bulk size tends to infinity. An important

role in that limit is played by the *bulk free energy* per site,

$$f(T) \coloneqq -k_{\mathrm{B}}T \lim_{L\to\infty} \frac{1}{L^2} \log Z \,. \tag{1.2}$$

The typical strategy for computing the partition function consists of two steps. First one tries to compute Z for the model for a *finite* but *arbitrary* system size L. This requires a choice of *boundary conditions*, say periodic or with fixed values of the microscopic degrees of freedom at the boundary. The second, and often less rigorous, step is to take the limit $L \to \infty$ of macroscopic system size. With this strategy in mind one should not really distinguish between models that only differ in size, but rather think of a statistical-physical model as a *family* indexed by the system size $L \in \mathbb{N}$. In practice the choice of boundary conditions is rarely considered to be a part of the data of the model, and sometimes even left implicit. This is related to the expectation that far away from the boundaries the situation is independent of this choice, and therefore the thermodynamic properties are so too. Although this is often indeed the case there are exceptions, see also Section 2.2.

Only in rare cases one is able to evaluate the sum in (1.1) exactly. Well-known examples where this is possible are free models such as non-interacting ideal gasses. There are also some very special interacting statistical models for which there are methods that, in principle, allow for an *exact* evaluation of (1.1). The two-dimensional Ising model on a square lattice is an example of such an exactly solved model. In fact, these kinds of models are the topic of Part I of this thesis, and in the following sections we will encounter several other examples.

Disclaimer. The goal of Chapters II and III will be more modest than to work out the entire above strategy for some of the models introduced in the next section. We will only perform the first step—computing the partition function for *finite* system size—for a *single* choice of boundary conditions in either chapter. Accordingly we henceforth suppress the dependence of the vertex weights and partition function on the temperature as the thermodynamics will not be our focus.

2 Introducing the cast

It is time to meet the main characters of Part One of this thesis. We first give their 'bulk' description, then discuss several interesting boundary conditions, and finally introduce a diagrammatic notation that will be useful in the remainder of this chapter as well as in Chapters II and III.

2.1 Vertex models and their friends

In this section we introduce the classical statistical-physical models starring in Part One of this thesis, focussing on a rectangular portion, say with K rows and L columns, of a square lattice. We will see that the models are closely related to each other.

(a) **(b)**

Figure 1. An example of a microstate for a vertex model in **(a)** the arrow picture, where the edges are decorated with arrows indicating the values of the spins (up or to the right for $\varepsilon = +1$), and **(b)** the line picture (dotted lines for $\varepsilon = +1$).

Vertex models. We start with *vertex models*. As for Ising-type models the microscopic degrees of freedom are binary spins $\varepsilon \in \{\pm 1\}$, yet this time the spins are assigned to the edges, rather than the vertices, of the lattice. When depicting the spins it is convenient to encode their values graphically. This is often done in the *arrow picture*, where the values are indicated by arrows pointing up or to the right for $\varepsilon = +1$, and down or to the left for $\varepsilon = -1$. We usually find it more convenient to work with the *line picture*, also called *path* or *bond* picture, where the same values are represented by dotted ('empty') and thick ('occupied') lines, respectively. An example of a microstate C in the two pictures is shown in Figure 1.

The weight $W(C)$ of a configuration on the lattice is local in the sense that it is the product of *vertex weights* assigned to the vertices of the lattice. Interactions take place between nearest neighbours: the vertex weights only depend on the four surrounding spins. When the model is homogeneous (translationally invariant) the vertex weights can be denoted as follows: given spin variables $\alpha, \beta, \alpha', \beta' \in \{\pm 1\}$ on the four surrounding edges as in Figure 2 (a) we write $w\left(\alpha \begin{smallmatrix} \beta' \\ \beta \end{smallmatrix} \alpha'\right)$. There are sixteen such vertex weights that have to be specified, one for each possible configuration of spins on the surrounding edges.

Six-vertex model. The *six-vertex* or *ice-type* model describes hydrogen-bonded two-dimensional crystals. The vertices of the lattice represent heavier atoms, oxygen in the case of water ice, and the edges model hydrogen bonds: a square lattice, with its four-valent equally spaced vertices, is a reasonable two-dimensional approximation of the hexagonal structure of ice crystals found in nature as depicted in Figure 2 (b). The spin on the edge encodes at which end of each bond the proton is, say with spin +1 corresponding to the right (top) of a horizontal (vertical) edge; in the arrow picture the arrow then points towards the proton on that hydrogen bond. For electric neutrality each oxygen atom should have precisely two hydrogen atoms close by. This translates to the *ice rule*

$$\alpha + \beta = \alpha' + \beta' \tag{2.1}$$

for $w\left(\alpha \begin{smallmatrix} \beta' \\ \beta \end{smallmatrix} \alpha'\right)$, which leaves us with six allowed vertices, with nonzero weights $a_\pm, b_\pm, c_\pm$ as shown in Figure 3. For example, in Figure 1 the ice rule is only satisfied for the two vertices

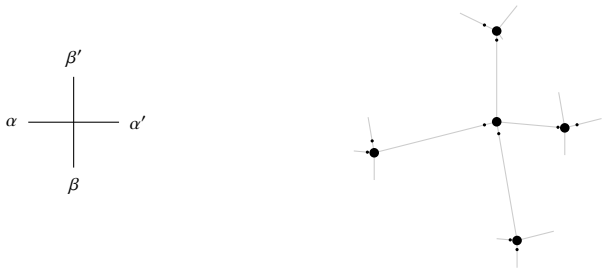

(a) **(b)**

Figure 2. **(a)** A vertex in a square lattice with spins $\alpha, \beta, \alpha', \beta' \in \{\pm 1\}$ on the surrounding (half-)edges, which has vertex weight $w\left(\alpha {}^{\beta'}_{\beta} \alpha'\right)$. **(b)** In ordinary, type $\mathrm{I_h}$, ice the oxygens constitute a (nearly) perfect hexagonal crystal, where the four nearest neighbours of each oxygen form a tetrahedron centred at that oxygen. The hydrogen bonds are indicated in grey. The protons near each oxygen satisfy the ice rule.

on the right. Viewed as (local) Boltzmann weights, $a_+ = \mathrm{e}^{-E_{a_+}/k_\mathrm{B}T}$ and so on, these vertex weights should be nonnegative for physical applications, running from zero to one as the temperature increases. The partition function of the six-vertex model depends on these six parameters, being a polynomial of degree KL in the vertex weights for an $K \times L$ bulk.

The ice rule was first formulated by Bernal and Fowler in 1933 [14]. Two years later Pauling [15] realized that the resulting geometric frustration explains the nonzero residual entropy of water ice observed in experiments. The ice rule is extremely convenient from an algebraic point of view, see Section 4.2, yet it also leads to some pathological properties as we will see in Section 2.2.

In addition *spin-reversal* symmetry is often imposed: $w\left(\alpha {}^{\beta'}_{\beta} \alpha'\right) = w\left(-\alpha {}^{-\beta'}_{-\beta} -\alpha'\right)$. This global $\mathbb{Z}_2$-symmetry further cuts the number of independent vertex weights down to three: a, b, c. We thus obtain the *symmetric* or *zero-field* six-vertex model. Writing $a_\pm = a\ \mathrm{e}^{\pm(H+V)}$ and $b_\pm = b\ \mathrm{e}^{\mp(H-V)}$ shows that physically one can think of the symmetric case as a model in the absence of external horizontal and vertical (electric) fields H and V. In the arrow picture the vertex weights are then invariant under rotations over 180°.

Physically, the values of a, b, c distinguish different systems. There are three prototypical cases. The *ice model* corresponds to the case $a = b = c$ where each vertex is equally likely. Recently Algara-Siller *et al.* reported to have obtained two-dimensional 'square' ice in the laboratory by confining water between two sheets of graphene at room temperature [16]. The ice model also contains the point $a = b = c = 1$ of infinite temperature for the six-vertex model when we think of the vertex weights as local Boltzmann weights. The case $a > b = c$ is known as the *KDP model* for ferroelectric materials, such as potassium dihydrogen phosphate ($\mathrm{KH_2PO_4}$), at low temperatures. Here vertices of type a are energetically favoured and there are two completely polarized ground states, each having

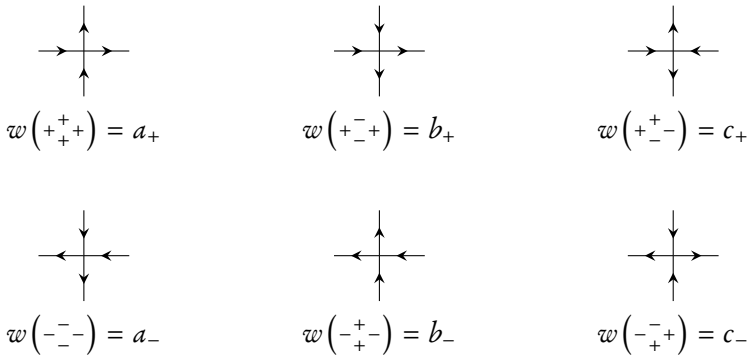

Figure 3. The allowed vertex configurations, which have nonzero weight, for the six-vertex model in the arrow picture. In this setting the ice rule says that the (binary) vector field specifying a microstate is divergence free.

the same spin value at each of its edges. At low temperatures the system is frozen: local changes to either ground state are forbidden by the ice rule, so each excitation requires a macroscopically large energy. The case $a = b < c$ is the *F-model* for antiferroelectric materials. This time the vertices are invariant under rotations over 90° in the arrow picture. By spin-reversal symmetry there are again two ground states, each built from both $c_\pm$ with the same vertex running along diagonals of the lattice, resulting in a *staggered* polarization: the spins on the horizontal edges alternate, and the same is true for the spins on the vertical edges. These three cases were solved (for periodic boundary conditions) in 1967 by Lieb [17, 18], followed by Sutherland's solution of the general symmetric six-vertex model (with periodic boundary conditions) in the same year [19]. Let us briefly discuss the phase diagram. Consider the 'reduced coupling constant' given by the combination

$$\Delta(a, b, c) := \frac{a^2 + b^2 - c^2}{2\,a\,b} \tag{2.2}$$

of vertex weights. The bulk free energy (1.2) has different analytic forms when $\Delta < -1$, $-1 < \Delta < 1$, $\Delta > 1$, allowing one to distinguish ferroelectric, disordered and antiferroelectric phases. The phase diagram is given in Figure 4.

Eight-vertex model. One can generalize the six-vertex model by weakening the ice rule (2.1) to hold modulo four. The resulting vertex model is known as the *eight-vertex model*, as it allows for two more vertices. In the arrow picture these vertices are sources and drains, shown in the middle column of the configuration from Figure 1. The new vertex weights are $d_\pm$, or just d in the symmetric case. The eight vertices are depicted in the line picture in Figure 5.

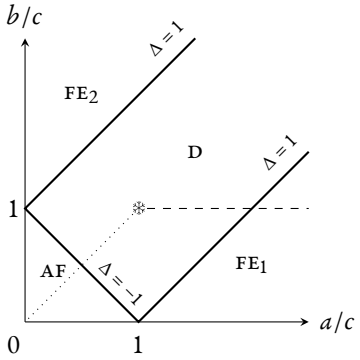

Figure 4. The phase diagram of the symmetric six-vertex model with periodic boundary conditions in both directions [11, §8.11]. Since simultaneous rescalings of the vertex weights only result in an overall factor for the partition function and leaves (2.2) invariant it suffices to consider $a/c : b/c : 1 = a : b : c$. The ice model (at $\Delta = 1/2$) is indicated by ❄. All other models trace out straight lines from the boundary to ❄ as temperature increases. The dashed line is for the KDP-model, and the dotted line corresponds to the F-model. There are two ferroelectric phases (FE_i, $\Delta > 1$), one disordered phase (D, $|\Delta| < 1$), and one antiferroelectric phase (AF, $\Delta < -1$). Interestingly, the entire disordered phase is critical. The phase transition at $\Delta = 1$ is of first order, while the transition at $\Delta = -1$ is of infinite order (Berezinskii–Kosterlitz–Thouless type).

This extension of the six-vertex model is a mathematical one, arising naturally in the line picture, in which the ice rule requires the paths to take a north-easterly course. For the eight-vertex model, instead, the paths may go in any direction. There does not seem to be a completely natural physical interpretation of the eight-vertex model within the vertex-model context. From the point of view of hydrogen-bonded crystals, for instance, it would be more natural to extend the six-vertex model by including *charge defects* in the form of the eight *other* vertices, representing small local charge surpluses and deficits. In any case, the eight-vertex model does not suffer from the restrictive nature of the ice rule and its thermodynamics is in some sense less pathological than that of the six-vertex model, see also Section 2.2. There are two antiferroelectric phases (with largest weight c or d), two ferroelectric ones (with largest weight a or b), and one disordered phase. However, all phases are related by dualities, and the disordered phase is no longer critical. For more we refer to [11, §10.11].

Height models. Another class of statistical-physical models that are defined on a lattice are *height models* describing, for example, crystal growth. After intial nucleation, a crystal in nature grows through the deposit of particles from a vapour onto its surface. We focus on the crystal surface, and will not keep track of the particles in the vapour. The *solid-on-*

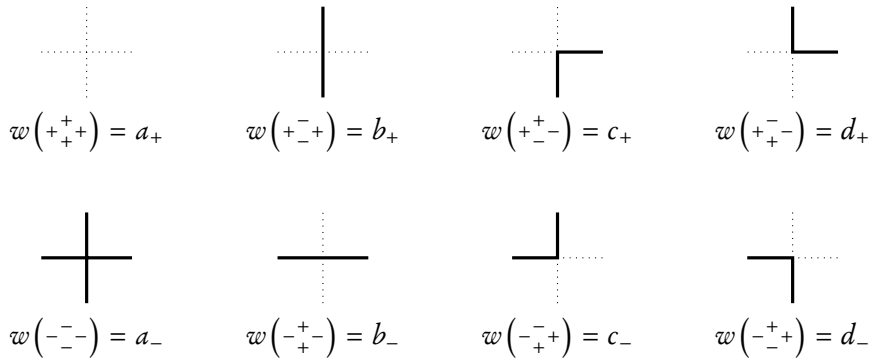

Figure 5. The allowed vertex configurations for the eight-vertex model in the line picture. The right-most vertices are new with respect to Figure 3.

solid condition [20] forbids voids inside the solid and overhangs of the surface. Thus we can describe the shape of the crystal-vapour interface with respect to a flat reference surface by a function on a two-dimensional lattice. The microscopic degrees of freedom are discrete *height* variables h_l associated to the vertices of the lattice. We will consider heights taking values in $\theta + \gamma\,\mathbb{Z}$, where θ is some reference height and γ sets the step size. Microstates $C = \{h_l\}_l$ are functions on the lattice describing height profiles of the surface. The shape of the surface is determined by interactions between these height variables. Again we focus on square lattices.

The simplest such model is Kossel's famous 'terrace-ledge-kink model' for simple cubic crystals [21], see also [20, 22]. The Boltzmann weights are determined by the energy $E(C) = -J\sum_{\langle k,l\rangle}|h_k - h_l|$ counting the nearest neighbours weighted by their height difference; note that the dependence on θ drops out in this case. This model was shown to exhibit a roughening phase transition by Burton, Cabrera and Frank [23].

Solid-on-solid model. Another important subclass of local height models is formed by *face* or (or 'interaction-(a)round-a-face', IRF) models, in which interactions take place between the four vertices sharing a face of the lattice. The weight of a microstate is the product of these face weights.

As will become clear momentarily we will be interested in the case where the heights at adjacent vertices always differ by *one* unit, allowing for six different height profiles around any face as shown in Figure 6. The precise dependence of the face weights on the height has to be specified. In Section 4.3 we will see that there is not much choice if one asks the model to be quantum integrable. We will refer to these particular height models simply as *solid-on-solid* (SOS) models, as is standard in the literature on quantum integrability. The condition that nearest-neighbouring heights differ by one unit makes the square lat-

tice bipartite, where one sublattice only has even heights and the other only odd heights; the surface has no steep cliffs, but cannot have plateaus either. Physically this condition occurs naturally in *body-centred cubic* (*bcc*) crystals, explaining the name 'body-centred solid-on-solid' (BCSOS) models used for these particular models in the crystal-physics community [24].

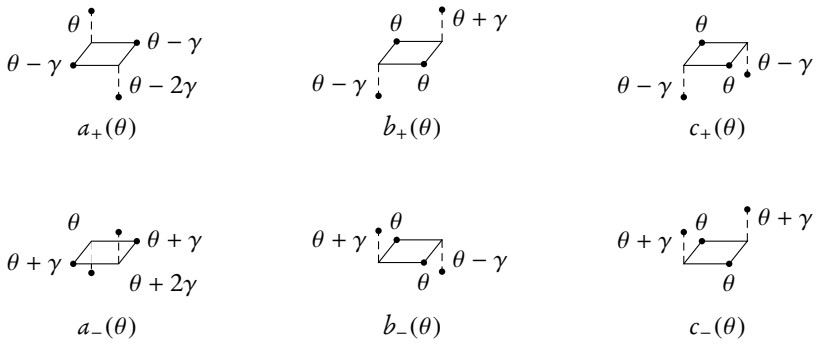

Figure 6. In SOS models where all neighbouring heights differ by one unit there are six possible height profiles around a face: four slopes and two saddles. In each case we have chosen to fix the left top vertex at some reference height θ. Dashed lines connect points over the same vertex.

Some related models. There are many relations and dualities between models in statistical physics. This is also true for vertex and SOS models. Let us discuss the correspondences that are most relevant for us. (In Sections 4.1 and 4.3 we will further see that the six- and eight-vertex models are also closely related to certain spin chains.)

Three-colourings. Lenard [17, note added in proof] found a nice alternative way to think about the six-vertex model, with the spins on the edges giving rise to three-colourings of the square lattice. The microscopic degrees of freedom in the new description are *colours* of the faces of the lattice. Pick an ordering of the colours. When depicting the spins by arrows the rule is as follows: going around a vertex in anti-clockwise direction, the colour increases by one when the arrow on the edge points outwards, and decreases by one otherwise. In the line picture this means that the colour increases (decreases) by one when we cross a thick (dotted) line to a neighbouring face on the left or bottom. The ice rule (2.1) ensures that the colouring is well defined: going once around a vertex we get back to the same colour. Moreover it is clear that no adjacent faces will have the same colour, so three colours (counted cyclically) suffice, and the resulting pattern is a *three-colouring* of the square lattice. An example is given in Figure 7. If the colour of any single face is fixed then a con-

(a) **(b)**

Figure 7. [Colour online] An example of Lenard's correspondence between a six-vertex microstate and a three-colouring of a square lattice, in the **(a)** arrow and **(b)** line picture. The two other three-colourings giving rise to the same six-vertex microstate are obtained by cyclically shifting all colours. The three faces that would have had another colour if we would not have counted the colours cyclically are marked with a ○.

figuration of spins uniquely determines the colouring, so the correspondence with the six-vertex model is three to one. In particular, for the ice model, where all microstates have the same weight, the partition function essentially counts the number of possible three-colourings. This is one reason why the infinite-temperature case $a = b = c = 1$ is known as the *combinatorial point* of the six-vertex model, see also the end of Section 2.2.

Yet another description of the same problem is offered by a 'cyclic' SOS model defined on the *dual* square lattice. Here the colours are reinterpreted as heights at the dual vertices, counted modulo three. The (three-to-one) correspondence with the six-vertex model uses the local dictionary from Figure 8.

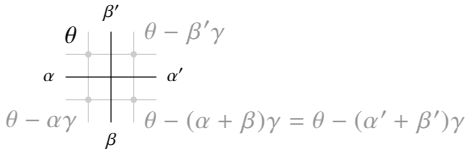

Figure 8. A configuration of spins around a vertex determines all heights on the surrounding faces (or dual vertices) once one of those heights is fixed. The dual lattice is drawn in grey.

Generalized six-vertex model. As we have just seen a spin configuration of a six-vertex model determines a height profile up to shifts in the vertical direction, i.e. changes of θ. The many-to-one relation between microstates of the two settings already allows one to infer interesting physical properties of SOS models from the analysis of the six-vertex model [24]. The reference-height ambiguity can also be resolved by turning to another statistical-physical model that is a sort of hybrid between the six-vertex model and an SOS model, whose microstates are in one-to-one correspondence with those of the SOS model

on the dual lattice.

More preciselyy the *generalized six-vertex model*, sometimes called a vertex-IRF model, has two types of microscopic degrees of freedom: spins ±1 on the edges and heights taking values in $\theta+\gamma\mathbb{Z}$ on the faces. The two are related to each other as before and the spins satisfy the ice rule to ensure that the height profile is well defined. Thus a microstate is completely specified by a choice of spins on all edges together with the height at any single face. The (generalized) vertex weights $w\left(\begin{smallmatrix}\beta' & \\ \alpha & \alpha'\end{smallmatrix}\middle|\theta\right)$ depend on the height at one of the surrounding faces, see Figure 9. The ordinary six-vertex model is recovered by forgetting the heights.

Since SOS models are equivalent to generalized six-vertex models on the dual lattice we are free to switch between the two points of view. This also justifies the identical labelling of the face weights from Figure 6 and the generalized vertex weights from Figure 9, where the way to translate between the two is given by the dictionary from Figure 8.

At this point it might seem that the step from ordinary to generalized six-vertex models is small. As we will see in Section 4.3, however, quantum integrability gives SOS models a life of their own. In particular, they come in three flavours: rational, trigonometric, and elliptic. For comparison, the ordinary six-vertex model is rational or trigonometric, while the eight-vertex model is elliptic.

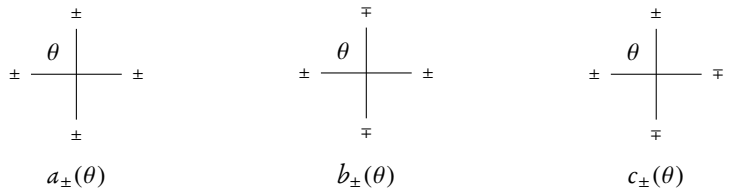

$a_\pm(\theta)$ $b_\pm(\theta)$ $c_\pm(\theta)$

Figure 9. The generalized vertex weights $w\left(\begin{smallmatrix}\beta' & \\ \alpha & \alpha'\end{smallmatrix}\middle|\theta\right)$ dual to the face weights shown in Figure 6. In the line picture these look like the six vertices in Figure 5, decorated with a θ in the top-left face.

Generalized eight-vertex model? It is clear that the eight-vertex model, in which the ice rule only holds modulo four, does not straightforwardly generalize to an SOS (or generalized vertex) model. Indeed, given a spin configuration the ice rule is needed to extend a single specified height to a well-defined height profile as in Figure 8. In the height-model picture one may heuristically think of vertices with weight $d_\pm$ as *screw dislocations* [24], but this leaves room for ambiguities. These screw dislocations come in two 'chiralities', which are related by reversing the surrounding spins. Cliffs that are four units high run between screw dislocations of opposite chirality, but their course is not fixed by the configuration of the eight-vertex model. Correspondingly, in the presence of vertices with weight $d_\pm$, heights are only unique modulo four. In Section 4.3, once we have

developed some algebraic machinery, we will see that the generalized *six*-vertex model is nevertheless closely related to the symmetric *eight*-vertex model in a different way.

2.2 Quantum-integrable boundary conditions

At the end of Section 1 we briefly touched upon the issue of boundary conditions and their role in the computation of the limit of infinite system size. Now that we have met the statistical-physical models starring in this thesis we are in a position to return to this issue. We begin by reviewing some possible boundary conditions, restricting the allowed spins on the external edges, for six-vertex models and SOS models on the dual lattice. We mostly focus on the special cases that are compatible with quantum integrability in the sense that they allow one in some way to use the algebraic tools introduced in Section 4.2. Let us refer to these as *quantum-integrable* boundary conditions; amongst others this does not include the case where the boundary spins are left free.

Periodic boundaries. One of the most common choices of boundary conditions is that of *periodic* or *cyclic* boundaries, where the spins at opposite ends of a row or column must coincide. From a global point of view this may not be very realistic, yet for finite bulk size it is the only choice preserving translational invariance, akin to the model on an (infinite) lattice. In two dimensions one can impose periodicity in both directions; this choice is also known as *toroidal* boundary conditions. In the context of quantum integrability such boundaries were for instance used by Onsager for the Ising model on a square lattice, by Lieb and Sutherland for the symmetric six-vertex model (resulting in the phase diagram from Figure 4), and by Baxter for the symmetric eight-vertex model. For SOS models horizontal periodic boundary conditions require the height profiles on opposite ends to have the same shape, although they might differ by a shift.

Fixed boundaries. For *fixed* boundary conditions the spins at the boundary are fixed to certain values. This should be done according to some pattern specifying the boundary configurations for all bulk sizes at once. The ice rule implies that the partition function vanishes for fixed boundaries *unless* the total numbers of +1's and −1's at the bottom plus left boundary equal those at the top plus right boundary. This restricts the possible choices yielding models with nonzero partition function. In the arrow picture this means that equally many arrows should point in and out of the bulk, which translates to the SOS statement that the corresponding height profile at the boundary is well defined given the height at any single boundary face. A very general, although rather cumbersome, formula for the partition function of the six-vertex model with arbitrary fixed boundaries was found by Baxter [25] in 1987.

Ferroelectric boundaries. Even when the partition function does not vanish the ice rule may still give rise to trivial thermodynamics. This is the case with *ferroelectric*

boundaries. Here all horizontal external edges have the same spins, and the same is true for all vertical external edges. For the SOS model on the dual lattice the boundary heights lie in a tilted plane. There are four such boundary configurations, including the case where all boundary spins are equal to +1, depicted in Figure 10. In each case the system is completely 'frozen' in the sense that there is only allowed microstate (each involving just one of the vertices $a_\pm, b_\pm$), so the entropy is zero and there is a single (ferroelectric) phase [26].

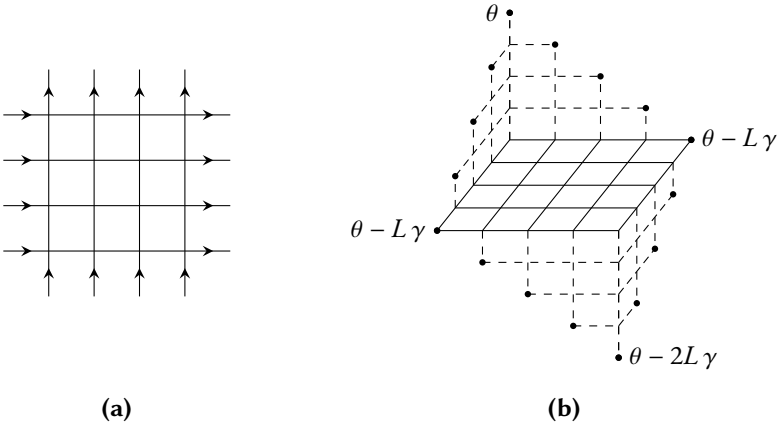

Figure 10. Ferroelectric boundary conditions for **(a)** a vertex model and **(b)** the SOS model on the dual lattice.

Domain walls. A particularly interesting case is that of *domain walls*, where all boundary spins on the bottom and right have, say, value +1 and on the left and the top opposite value −1. In other words, all vertical arrows point inwards and all horizontal arrows point outwards; for the SOS model on the dual lattice the corresponding boundary profile is a saddle, see Figure 11. Because of the ice rule these boundary conditions demand the bulk to be square ($K = L$). Domain-wall boundary conditions were the first example of quantum-integrable fixed boundaries yielding nontrivial thermodynamics, found by Korepin [27] in the context of scalar products of Bethe vectors (see Section 4.2). The corresponding partition function was expressed in closed form as a determinant by Izergin [28], see Section II.2. The phase diagram looks exactly as in Figure 4, yet the details are different: the bulk free energies in the disordered and antiferroelectric phases have another form, and the lines with $\Delta = 1$ are now second-order phase transitions [29, 30]. Domain-wall boundaries are also intimately related to problems in combinatorics as we will see at the end of this section. The six-vertex model with these boundary conditions will be the topic of Chapter II.

Néel boundaries. For completeness let us also mention *Néel* or *anti-ferroelectric* boundary conditions [26], where, in the arrow-picture, the arrows on the external edges

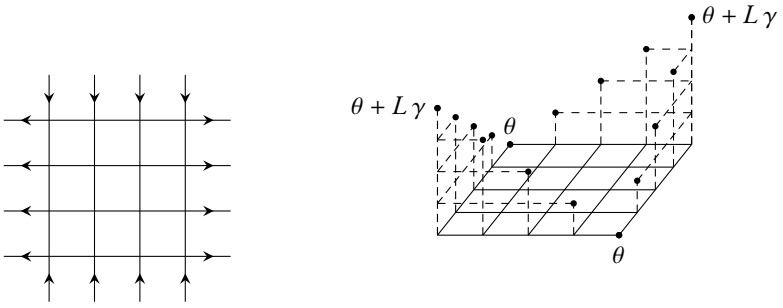

Figure 11. Domain-wall boundary conditions for **(a)** vertex and **(b)** SOS models. Note that the ice rule requires an equal amount of rows and columns.

alternatingly point inwards and outwards as in Figure 12. This choice does *not* appear to be quantum integrable, yet it is interesting for other reasons. From the vertex-model viewpoint Néel boundaries are fairly physical inasmuch as the boundary does not carry a net polarization. Correspondingly, for SOS models the resulting boundary profile is as close as possible to having constant height, see again Figure 12. Korepin *et al.* argue that, amongst all possible fixed boundaries, this choice allows for the largest number of microstates and that, although the entropy is less than that for toroidal boundary conditions at finite system sizes, the entropy for the two cases is expected to become equal as L tends to infinity at the ice point [31].

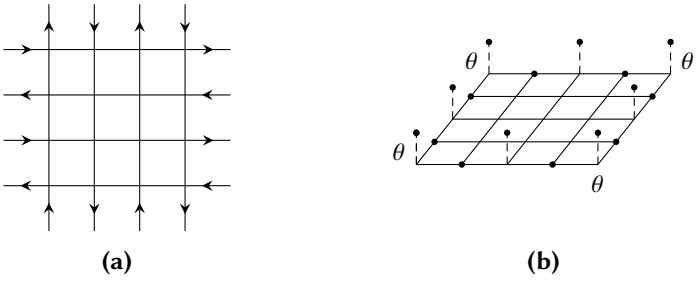

Figure 12. Néel boundary conditions for **(a)** vertex and **(b)** SOS models.

Reflecting boundaries. Besides periodic and certain fixed boundary conditions, another integrable option is that of a *reflecting end*, also called an *open* boundary in the literature on quantum integrability. Here one connects pairs of neighbouring external edges via a two-valent vertex as in Figure 13. In the case of *diagonal* reflection, which is com-

patible with the ice rule in the sense that there are equally many arrows pointing in and out, there are two nonzero (local) *boundary weights*, which we denote by $k_\pm$. Reflection was first considered in the context of integrable field theories by Cherednik in 1984 [32]. Four years later Sklyanin [33] implemented reflection in the context of spin chains and the six-vertex model, and in 1996 Behrend, Pearce and O'Brien [34] did so for SOS models.

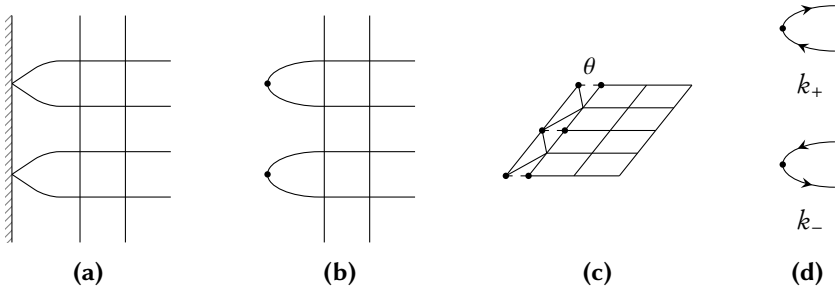

Figure 13. A reflecting end for a vertex model, where the two-valent vertices may be represented by **(a)** a wall or **(b)** U-turns. **(c)** The SOS model on the dual lattice. The vertices connected by dashed lines are identified. **(d)** The two allowed local boundary configurations, with associated boundary weights, for the case of *diagonal* reflection.

In Chapter III we will consider systems with $K = 2L$, one (diagonally) reflecting end, and domain walls on the three other ends. Tsuchiya has shown that the partition function of the the six-vertex model with these boundary conditions can be written as a determinant [35]; the generalization of this result to SOS models with the same boundaries is due to Filali–Kitanine [36] and Filali [37]. The phase diagram once more looks as shown in Figure 4, but the details are not known at present. Recently Ribeiro and Korepin [38] obtained an expression for the free energy in the disordered phase and showed that the entropy at infinite temperature coincides with that for domain walls.

Existence of macroscopic limit. Recall from the end of Section 1 that the partition function in the macroscopic limit $L \to \infty$ is computed as a limit of the partition function for arbitrary finite system size with some choice of boundary conditions. This recipe only yields a well-defined result when the choice of boundaries does not influence the outcome; naively one would indeed expect this to be the case, and there are some rigorous results confirming this expectation to be valid under certain assumptions.

The six-vertex model, however, is a *counterexample* to this anticipation. The above examples of fixed boundary conditions illustrate that the ice rule is so restraining that many choices yield trivial thermodynamic behaviour, as for ferroelectric boundaries. We have also seen that, as first shown around the turn of the millennium by Korepin and Zinn-Justin [29], the macroscopic physics may depend on the boundary conditions also for choices that do allow for interesting thermodynamics: the details of the phase diagram

for periodic and domain-wall boundaries are different. This can again be understood as a consequence of the ice rule, which causes ordered (highly polarized) boundary conditions to 'propagate' into the bulk, freezing portions of the configuration near the boundary and causing macroscopic polarization that makes it possible to detect the boundary conditions even deep inside the bulk. In other words, in some sense the ice rule spoils part of the local nature of the model. Of course domain walls, with their boundary polarization, are not very realistic, and one could hope that at least more physical choices do yield the same thermodynamics. It has been shown that this is indeed true for free and toroidal boundaries [26], and it appears to hold for Néel boundaries as well [31].

Interestingly it can been proven that the thermodynamics of the symmetric *eight*-vertex model, for generic values of the vertex weights, does *not* depend on the choice of boundary conditions: for this model the macroscopic limit *does* exist [26]. The reason is that in this case an $L \times L$ portion with any choice of boundary conditions can be embedded in an $(L+2)\times(L+2)$ bulk with any other choice of boundaries, resulting in an energy difference that does not influence the thermodynamics.

Alternating-sign matrices. To conclude this section we briefly turn an interesting application of six-vertex models with domain-wall boundary conditions at the ice point to combinatorics. We have already seen that the ice model is equivalent ('up to a factor of three') to the three-colouring problem for the square lattice. Another relation with enumerative problems was found by Kuperberg in 1995 [39].

In the six-vertex model let us focus on the vertices with weight $c_\pm$. In any row or column the two must alternate: between any two c_+-vertices there must at some point be a c_-, and reversely; this is particularly clear in the line picture. In the presence of periodic boundary conditions in either direction this implies that every microstate has equal amounts of the two vertices, so without loss of generality one may take $c_+ = c_-$ in that case. For domain walls, instead, it follows that every row and column must have precisely one more vertex of weight c_-. Thus, up to an overall factor of c_-^L, the domain-wall partition function only depends on $c^2 = c_+\, c_-$. (Analogous arguments apply to any choice of fixed boundaries.)

Now consider the mapping from domain-wall microstates to matrices whose entries correspond to the vertices of the lattice, being equal to ±1 for vertex $c_\mp$ and zero else. For instance we have

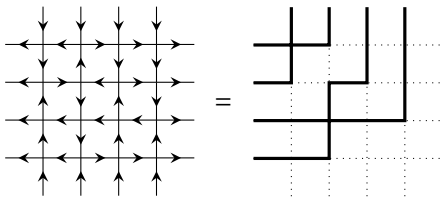

$$\longmapsto \begin{pmatrix} 0 & 1 & 0 & 0 \\ 1 & -1 & 1 & 0 \\ 0 & 0 & 0 & 1 \\ 0 & 1 & 0 & 0 \end{pmatrix}. \tag{2.3}$$

Each matrix obtained in this way is an *alternating-sign matrix* (ASM): its only entries are $-1, 0, +1$, and along each row and column ±1 occur alternatingly in such a way that the

entries on each row and column add to +1. It is easy to see that this correspondence gives a bijection between allowed microstates of the $L \times L$ six-vertex model with domain walls and all $L \times L$ alternating-sign matrices. Here is an example for the inverse of Kuperberg's mapping:

$$\begin{pmatrix} 0 & 1 & 0 & 0 \\ 0 & 0 & 1 & 0 \\ 1 & 0 & 0 & 0 \\ 0 & 0 & 0 & 1 \end{pmatrix} \longmapsto$$

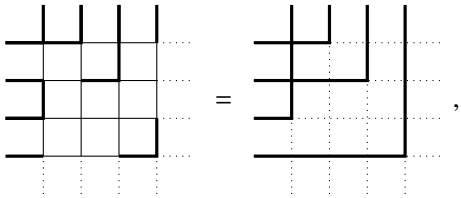

, (2.4)

where the unique way to complete the microstate is dictated by the ice rule—see the next section for the graphical notation. At the combinatorial point all microstates have the same weight, so the partition function just counts the number of allowed configurations. Using the Izergin–Korepin formula for the domain-wall partition function Kuperberg thus obtained a nice proof for the conjecture of Mills, Robins and Rumsey that the number of $L \times L$ alternating-sign matrices is

$$N_L = \prod_{j=1}^{L} \frac{(3j-2)!}{(L+j-1)!} = \frac{1!\,4!\,7!\cdots(3L-2)!}{L!\,(L+1)!\cdots(2L-1)!}\,. \tag{2.5}$$

Kuperberg's result was extended to SOS models with domain walls by Rosengren [40, 41]. There are more examples of relations with the combinatorics of special types of alternating-sign matrices, including the case of Néel boundaries [31] and reflecting boundaries [42]. For more about alternating-sign matrices and Kuperberg's proof see e.g. [43].

2.3 Diagrammatics

Some topics in theoretical physics come with a diagrammatic notation that offers a way of visualizing what is going on. Quantum field theory has Feynman diagrams, which transcend their role of being merely a tool for bookkeeping in perturbation theory by providing intuition for processes in particle physics. In general relativity Penrose came up with a graphical calculus for representing quantities built from tensors. Happily, the models from Section 2.1 also allow for a diagrammatic description, which will moreover facilitate the passage to an algebraic description in Section 3.

Vertex models. The graphical notation for vertex models is based on three rules.

i) The values of the spins on any edge is depicted using arrows, or dotted and thick lines, just as in Figure 1.

ii) The basic building blocks for a diagram are the vertex weights, drawn as in Figure 2.

iii) There is a *summation convention* for internal lines: whenever two vertices are connected by an ordinary line (neither carrying an arrow, nor dotted or thick) we sum over the two possible values of the spins—which we typeset in a small font in all diagrams—on the connecting edge.

Thus

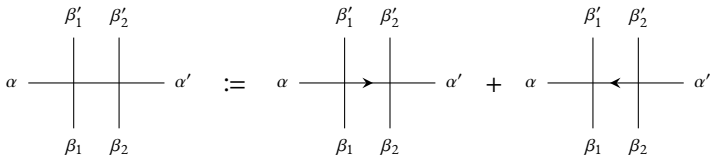

(2.6)

represents $\sum_{\varepsilon\in\{\pm1\}} w\left(\alpha\begin{smallmatrix}\beta_1'\\ \beta_1\end{smallmatrix}\varepsilon\right) w\left(\varepsilon\begin{smallmatrix}\beta_2'\\ \beta_2\end{smallmatrix}\alpha'\right)$. Since vertex weights vanish if the ice rule is violated (2.6) may contain zero, one or two nontrivial terms.

Fixed boundary configurations can be drawn using (ii). To draw the remaining boundaries described in Section 2.2 we need two more rules:

iv) For periodic boundary conditions we draw little hooks at the ends of a line to indicate that opposite edges of a row or column in the lattice are connected.

v) Reflection is depicted as in Figure 13 (a) or (b), with weights (d).

Let us illustrate these rules with a few examples. Consider the diagram from Figure 14. By (iv) all edges are internal, so it encodes a rather complicated expression involving $2KL$ sums as in (2.6), one for every edge. Each summand is a product of KL vertex weights, that is, the weight of a microstate of a vertex model. Comparing this with (1.1) we recognize the diagram as representing nothing but the partition function for a vertex model on a $K \times L$ bulk with toroidal boundaries! Likewise, the diagrams in Figures 10–12 (a) represent partition functions for vertex models on a 4×4 bulk with various fixed boundary conditions.

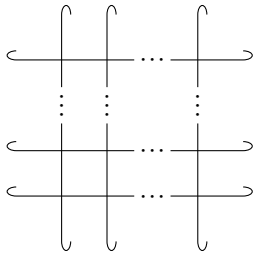

Figure 14. Periodic boundary conditions for a vertex model.

Solid-on-solid and generalized six-vertex model. One can come up with analogous rules for SOS models and generalized vertex models. The building blocks for the former are face weights, with heights that we represent by thick dots as in Figure 6. (Of course one could also simply draw a top view instead.) For the generalized vertex model on the dual lattice we use a decorated version of the above rules for ordinary vertex models, where we now also indicate the height at any single face of the lattice, say the face at the left top of the lattice as e.g. in Figure 9.

Recall that we are free to switch between the two settings. We will mostly use the language of generalized vertex models. The above rules for ordinary vertex models then straightforwardly carry over to this setting, where the heights at the faces are determined from the spins via the dictionary in Figure 8. Here is an example [cf. (2.6) with $\beta_1' = +1$]:

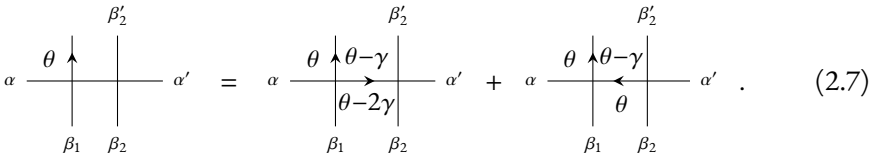

(2.7)

(By the ice rule the first term on the right-hand side vanishes unless $\alpha = \beta_1 = +1$.) As before the entire lattice represents the partition function of a model with certain boundary conditions. Examples for fixed boundary heights are given in Figures 10–12, where in (a) we should decorate the top-left face with a θ, in accordance with (b).

3 Passage to an algebraic formulation

In this section we recast the problem of computing the partition function (1.1) in quantum-mechanical (operator-algebraic) language. The local, and eventually global, Boltzmann weights are encoded in operators. In brief the idea is to cut up the entire lattice, representing the partition function in our diagrammatic notation, into rows. We focus on the ordinary six-vertex model. The extension to SOS-models and generalized six-vertex models is treated in Section 3.5. Although many constructions may also be used for the eight-vertex model they turn out to be less useful in that case as will become clear in Section 4.2.

3.1 Local description: *R*-matrix

The local nature of the vertex and height models presented in Section 2.1 allows us to start the algebraization locally, with the vertex weights.

A bit more diagrammatics. Before we define the local operators it is useful to upgrade the rules for the graphical notation from Section 2.3. First we construct the space on which

the operator containing the local weights acts.

i') Edges are assigned a copy of the two-dimensional vector space $V := \mathbb{C}|+\rangle \oplus \mathbb{C}|-\rangle$ with basis vectors labelled by the values $\varepsilon \in \{\pm 1\}$ of the spin on the edge. We will sometimes need to rotate diagrams, so we need a way to keep track of the orientation. To this end we orient the lines by attaching arrows at the end of straight lines formed by consecutive edges.

For the moment let us ignore the case of reflection, which will be the topic of Section 3.4. In all other diagrams from Section 2 the horizontal and vertical lines get an arrow pointing to the right or up, respectively. These arrows should not be confused with those denoting the spins in the arrow picture. V may thus be represented as

(3.1)

We stress that in the arrow picture, an arrow following the orientation of the line represents spin $\varepsilon = +1$, whilst an arrow going against the orientation indicates $\varepsilon = -1$. This generalizes the convention from Section 2.1, see e.g. Figure 1, when the orientation arrows point up or to the right. To avoid possible confusion about the role of the arrows we will mostly work in the line picture from now on.

Let us remark that the idea of associating a vector space to a line in a diagram might be quite familiar: in Penrose's graphical tensor calculus this is quite clear, but it is true for Feynman diagrams as well. Indeed, in the latter case different kinds of lines (normal, wiggly, spiralling, …) are used for various particles (scalars, photons, gluons, …) that by Wigner correspond to different vector spaces, each carrying a particular representation of the symmetry group. The present case is rather similar; we will also use various types of lines (normal, triple, …) for different vector spaces.

Next consider several copies V_j of (3.1), associated to edges $j = 1, 2, \cdots$. Larger vector spaces are built by taking tensor products of the V_j and come with a lexicographically ordered basis.

ii') The tensor product of two vector spaces is depicted by putting the corresponding lines next to each other. For example,

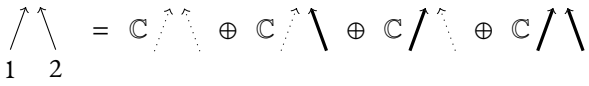

(3.2)

represent $V_1 \otimes V_2$ and its decomposition in terms of basis vectors, ordered as $|{+}{+}\rangle, |{+}{-}\rangle, |{-}{+}\rangle, |{-}{-}\rangle$. (The reason for the tilt of the lines will become clear at the warning below.)

iii') An operator acting on V schematically looks like 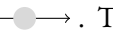 . The composition of operators is represented by concatenating diagrams, where the operators act in the

order indicated by the orientation of the line. In terms of components:

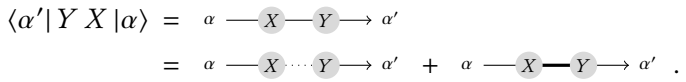

(3.3)

Thus the summation rule for internal lines accounts for the matrix product. Note that it only makes sense to connect lines in a way that preserves the orientations.

Let us introduce the following common notation. If W is a vector space 'End(W)' denotes the space of all linear operators $W \longrightarrow W$ (endomorphisms of W), which correspond to square matrices of size $\dim(W)$.

Warning. One has to be careful when reading off the order of 'outgoing' basis vectors for operators acting on tensor products in our graphical notation. For instance, consider some $S \in \mathrm{End}(V_1 \otimes V_2)$. Such an operator, along with its matrix entries, is drawn as

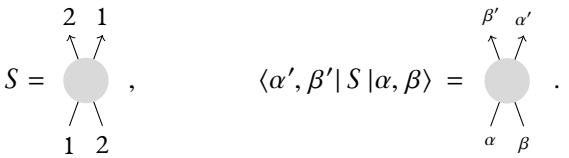

(3.4)

Unlike for the 'incoming' vector $|\alpha, \beta\rangle$, the order of the labels α' and β' is reversed on the right-hand side of (3.4). The reason is that the operator acts as $S\colon V_1 \otimes V_2 \longrightarrow V_1 \otimes V_2$, while the 'outgoing' lines in (3.4) are switched in the diagram. Thus the 'outgoing' copy of $V_1 \otimes V_2$, with basis ordered in the same way as in (3.2), looks like

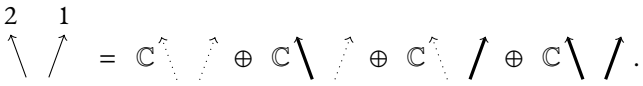

(3.5)

(Some authors avoid this subtlety by instead considering $\check{S}\colon V_1 \otimes V_2 \longrightarrow V_2 \otimes V_1$.) The labels on the 'outgoing' lines in diagrams like the one on the left in (3.4) will be omitted in the graphical notation from now on.

***R*-matrix.** For vertex models the vertex weights from Figure 2 are encoded by an *R-matrix*, which is an operator $R \in \mathrm{End}(V_1 \otimes V_2)$. The preceding discussion allows us to depict this operator simply by a vertex (with oriented edges):

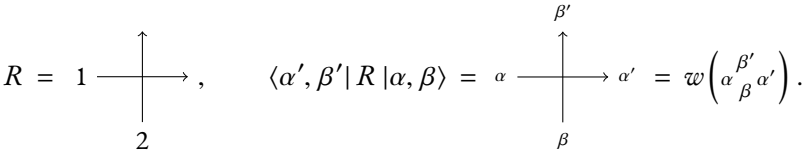

(3.6)

Keeping the above warning in mind we read off from Figures 3 and 5 that, with respect to the basis in (3.2) and (3.5), the R-matrices of the six- and eight-vertex models have matrices

$$R^{6v} = \begin{pmatrix} a_+ & 0 & 0 & 0 \\ 0 & b_+ & c_- & 0 \\ 0 & c_+ & b_- & 0 \\ 0 & 0 & 0 & a_- \end{pmatrix}, \qquad R^{8v} = \begin{pmatrix} a_+ & 0 & 0 & d_- \\ 0 & b_+ & c_- & 0 \\ 0 & c_+ & b_- & 0 \\ d_+ & 0 & 0 & a_- \end{pmatrix}. \tag{3.7}$$

Note that for the *symmetric* six- and eight-vertex models these matrices satisfy

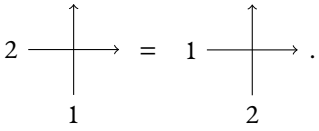

(3.8)

Now that the edges are oriented the ice rule amounts to *line conservation* in the line picture: it requires the number of incoming and outgoing thick lines to be conserved along the direction indicated by the orientation. More algebraically the ice rule can be understood as spin conservation for the R-matrix:

$$[\, h \otimes \mathbb{1} + \mathbb{1} \otimes h, R^{6v} \,] = 0\,, \tag{3.9}$$

where $h \in \mathrm{End}(V)$ is given by the third Pauli matrix $\sigma^z = \mathrm{diag}(1, -1)$, and measures (twice) the spin. Thus the block-diagonal structure of the matrix on the left in (3.7) is equivalent to the ice rule for the vertex weights of the six-vertex model.

3.2 Bulk description: monodromy matrix

The next step is to join R-matrices to form a row of the lattice. Before doing so we need to introduce some notation that is used throughout the literature on quantum integrability.

Tensor-leg notation. Consider an operator $X \in \mathrm{End}(V)$ acting on some vector space V, and form the tensor product $V_1 \otimes \cdots \otimes V_L$ of L copies of this space. Then the operator

$$X_j \coloneqq \underset{1}{\mathbb{1}} \otimes \cdots \otimes \mathbb{1} \otimes \underset{j}{X} \otimes \mathbb{1} \otimes \cdots \otimes \underset{L}{\mathbb{1}} \tag{3.10}$$

acts by X on the jth copy of V and trivially on other factors. In more algebraic terms this tensor-leg notation specifies an embedding $\mathrm{End}(V) \cong \mathrm{End}(V_j) \hookrightarrow \mathrm{End}(V_1 \otimes \cdots \otimes V_L)$.

This notation extends to operators defined on tensor products, with the subscripts specifying the factors on which the 'legs' of the operators act nontrivially. Let us consider some examples. In the form (3.9) the ice rule is an equation for operators on $V_1 \otimes V_2$. In

the tensor-leg notation it reads $[\, h_1 + h_2 \,, R_{12}^{6v}\,] = 0$. Next define the *permutation operator* $P \in \mathrm{End}(V \otimes V)$ by

$$P\,|\alpha, \beta\rangle = |\beta, \alpha\rangle\,. \tag{3.11}$$

Then $R_{21} = P_{12}\, R_{12}\, P_{12}$, and for symmetric vertex models the property (3.8) can be written as $R_{21} = R_{12}$. Finally, on $V_1 \otimes V_2 \otimes V_3$, the operator R_{12} acts as $R \otimes \mathbb{1}$, R_{23} as $\mathbb{1} \otimes R$, while R_{13} acts by $(\mathbb{1} \otimes P)(R \otimes \mathbb{1})(\mathbb{1} \otimes P) = (P \otimes \mathbb{1})(\mathbb{1} \otimes R)(P \otimes \mathbb{1})$.

Monodromy matrix. Consider a row of the lattice. We label the horizontal line by 0 and the vertical lines by $1, \cdots, L$. The corresponding vector space V_0 is called *auxiliary space*, while the tensor product $W := V_1 \otimes \cdots \otimes V_L$ is the (global) *quantum space*. This terminology comes from the spin-chain point of view, see Section 4.1.

For vertex models the *monodromy matrix* $T_0 \in \mathrm{End}(V_0 \otimes W)$ is defined as an ordered product of R-matrices:

$$T_0 := \prod_{L \geq j \geq 1}^{\leftarrow} R_{0j} := R_{0L} \cdots R_{02}\, R_{01}$$

$$= \quad 0 \longrightarrow \quad := \quad 0 \longrightarrow \cdots \longrightarrow \,. \tag{3.12}$$

$1 \cdots L \qquad\qquad 1 \quad 2 \qquad\quad L$

It is customary to omit subscripts corresponding to the entire space W in the tensor-leg notation, whence 'T_0' instead of '$T_{01\ldots L}$'. The harpoon on the product symbol in (3.12) points in the direction of increasing j in the formula; observe that the order of the R-matrices is dictated by rule (iii') in our graphical notation. In the graphical notation we sometimes abbreviate W by a triple line as in (3.12).

The monodromy matrix has size $2^{L+1} \times 2^{L+1}$. Write $|\vec{\beta}\rangle = |\beta_1\rangle \otimes \cdots \otimes |\beta_L\rangle$ for the basis vectors of W. Like in (3.4) the order of the components of the 'outgoing' vectors are partially reversed in the graphical notation:

$$\langle \alpha', \vec{\beta}'\,|\, T_0\, |\alpha, \vec{\beta}\rangle = \quad \alpha \longrightarrow \cdots \longrightarrow \alpha' \,. \tag{3.13}$$

$\beta_1' \quad \beta_2' \qquad\quad \beta_L'$

$\beta_1 \quad \beta_2 \qquad\quad \beta_L$

The bulk contribution to the partition function for a system of size $K \times L$, due to all local vertex weights prior to fixing boundary conditions, is governed by the K-fold product

of monodromy matrices acting on the same quantum space but different auxiliary spaces:

$$\overleftarrow{\prod_{K\geq k\geq 1}} T_{0_k} \;=\;$$

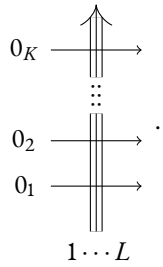

(3.14)

Quantum operators. When we fix the auxiliary spins α, α' in (3.13) we obtain operators with matrices of size $2^L \times 2^L$ acting on the quantum space W:

$A :=$ 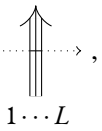 , $B :=$ 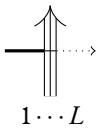 ,

$C :=$ 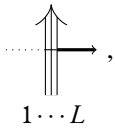 , $D :=$ 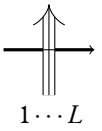 .

(3.15)

In other words, the monodromy matrix $T_0 \in \mathrm{End}(V_0 \otimes W) \cong \mathrm{End}(V_0) \otimes \mathrm{End}(W)$ can be viewed as a matrix acting on V_0 with entries in $\mathrm{End}(W)$:

$$T_0 = \begin{pmatrix} A & B \\ C & D \end{pmatrix}_0 . \tag{3.16}$$

The operators (3.15) will play an important role in Section 4 and Chapters II–III.

The ice rule (3.9) for the six-vertex R-matrix implies that the corresponding monodromy matrix satisfies the ice rule in the form $[\, h_0 + H, T_0^{6v} \,] = 0$, where

$$H := \sum_{j=1}^{L} h_j \in \mathrm{End}(W) \tag{3.17}$$

is the total spin operator on W (so that $L\,\mathbb{1} - H$ is twice the number operator on W for thick lines in the line picture). It follows that the operators (3.15) satisfy

$$\begin{aligned} &[\, H, A \,] = 0\,, && [\, H, B \,] = -2\,B\,, \\ &[\, H, C \,] = 2\,C\,, && [\, H, D \,] = 0\,. \end{aligned} \tag{3.18}$$

In the line picture this is evident, see (3.15): A and D satisfy line conservation, B injects a thick line into W and extracts a dotted line, $(H+2)\,B = B\,H$, while C does the opposite, $(H-2)\,C = C\,H$.

3.3 Algebraic characterization of the partition function

Now that we have an operator-algebraic description of the 'bulk' models from Section 2.1, see (3.14), it remains to include the boundary conditions from Section 2.2. We focus on the ordinary six-vertex model. The case of reflection is a bit more involved, and will be treated separately in the next section.

Periodic boundaries: transfer matrix. For a model with periodic boundary conditions in the horizontal direction the relevant operator is the (row-to-row) *transfer matrix* $t \in \mathrm{End}(W)$ defined in terms of the monodromy matrix (3.12) as

$$t := \mathrm{tr}_0\, T_0 =$$

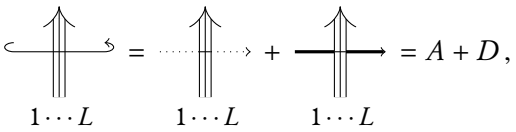

$$= A + D\,, \tag{3.19}$$

where $\mathrm{tr}_0 = \mathrm{tr} \otimes \mathbb{1} \colon \mathrm{End}(V_0 \otimes W) \cong \mathrm{End}(V_0) \otimes \mathrm{End}(W) \longrightarrow \mathbb{C} \otimes \mathrm{End}(W) \cong \mathrm{End}(W)$. From (3.18) it follows that the transfer matrix of the six-vertex model satisfies the ice rule, or line conservation, $[\, H, t\,] = 0$.

In the case of toroidal boundaries as in Figure 14 the partition function for an $K \times L$ bulk is obtained as the trace over W of the K-fold product of transfer matrices:

$$Z^{\mathrm{torus}} = \sum_{\vec{\beta} \in \{\pm 1\}^L} \langle \vec{\beta} |\, t^K \,| \vec{\beta} \rangle = \mathrm{tr}(t^K)\,. \tag{3.20}$$

Thus the *transfer-matrix method* converts the problem of computing the partition function (1.1) into that of diagonalizing the transfer matrix. This technique was devised by Kramers and Wannier [12] and independently by Lassetre and Howe [44], and was famously used by Onsager [13] to solve the two-dimensional Ising model with toroidal boundaries. Subsequently it was employed by Lieb [17, 18] and Sutherland [19] to tackle the six-vertex model, with the help of a coordinate Bethe ansatz to diagonalize the transfer matrix, see e.g. [5, §3].

Fixed boundaries. Vertex models with toroidal boundary conditions usually allow one to express the partition function as a trace of a product of transfer matrices, so that the evaluation of the partition function becomes an eigenvalue problem for the transfer matrix. This is not the case when other types of boundary conditions are considered. Instead, the algebraic formulation allows us to express partition functions for six-vertex models with fixed boundary conditions as n-point correlators. The fixed spins on the left and right boundaries are taken care of by considering the appropriate product of the quantum operators (3.15). For the spins at the bottom and top edges we need some special vectors

in W. There are two *pseudovacua*

$$|\Omega\rangle := |+\,+\cdots+\rangle = \quad \in W\,, \qquad |\bar{\Omega}\rangle := |-\,-\cdots-\rangle = \quad \in W\,, \tag{3.21}$$

and two *Néel vectors*

$$|N\rangle := |+\,-\,+\,-\cdots\rangle \in W\,, \qquad |\bar{N}\rangle := |-\,+\,-\,+\cdots\rangle \in W\,. \tag{3.22}$$

Ferroelectric boundaries. The partition function of a vertex model on an $L \times L$ bulk with ferroelectric boundary conditions as in Figure 10 can be expressed as

$$Z^{\text{ferro}} = \quad = \langle\Omega|A^L|\Omega\rangle\,. \tag{3.23}$$

The three other ferroelectric cases correspond to $\langle\Omega|D^L|\Omega\rangle$, $\langle\bar{\Omega}|A^L|\bar{\Omega}\rangle$ and $\langle\bar{\Omega}|D^L|\bar{\Omega}\rangle$.

In Section 2.2 we already saw that for the six-vertex model these boundaries only allow for one microstate. Let us rederive this result in the present setting.

Proof. As the pseudovacua (3.21) are the only vectors (up to rescalings) with all spins equal, it follows from the ice rule (3.18) that they are eigenvectors of both A and D,

$$\begin{aligned} A\,|\Omega\rangle &= \Lambda_A\,|\Omega\rangle\,, & A\,|\bar{\Omega}\rangle &= \bar{\Lambda}_A\,|\bar{\Omega}\rangle\,, & D\,|\Omega\rangle &= \Lambda_D\,|\Omega\rangle\,, & D\,|\bar{\Omega}\rangle &= \bar{\Lambda}_D\,|\bar{\Omega}\rangle\,, \\ \Lambda_A &= a_+^L\,, & \bar{\Lambda}_A &= b_+^L\,, & \Lambda_D &= b_-^L\,, & \bar{\Lambda}_D &= a_-^L\,. \end{aligned} \tag{3.24}$$

These eigenvalues are easily computed in the graphical notation using (3.13); for example,

$$\Lambda_A = \langle\Omega|\,A\,|\Omega\rangle = \quad = \quad = a_+^L\,, \tag{3.25}$$

where in the third equality the sums over the intermediate spins collapses to a single term by line conservation. From repeated application of (3.24) it follows that the four partition functions each consist of a single term, as we wanted to show. □

Domain walls. Next we examine the partition function of a vertex model on an $L\times L$ bulk with domain-wall boundary conditions (DWBC). For the configuration from Figure 11 it is given by

$$Z^{\text{DWBC}} = \quad = \langle\bar{\Omega}|\,B^L\,|\Omega\rangle\,, \tag{3.26}$$

while its spin-reversed analogue equals $\langle\Omega|\,C^L\,|\bar{\Omega}\rangle$. This partition function is more complicated than (3.23) since the pseudovacua are not eigenvectors of B and C, yet it can be computed with the quantum-integrability toolkit from Section 4, see Chapter II.

Néel boundaries. In case of Néel boundary conditions as in Figure 12, for an $L \times L$ bulk with L even, the partition function can be written as

$$Z^{\text{Néel}} = \langle N | \, (A\,D)^{L/2} \, | N \rangle \,, \tag{3.27}$$

with spin-reversed version $\langle \bar{N} | \, (D\,A)^{L/2} \, | \bar{N} \rangle$. For odd system size L we instead get $\langle \bar{N} | \, B\,(C\,B)^{(L-1)/2} \, | N \rangle$ or $\langle N | \, C\,(B\,C)^{(L-1)/2} \, | \bar{N} \rangle$. There are many more allowed microstates and no exact treatment using the formalism from Section 4.2 is known to date.

3.4 The case of reflection

Reflecting boundaries were analysed in the algebraic framework by Sklyanin in 1988 [33]. This formulation allows one to use quantum integrability, but there are some subtleties. Roughly speaking, quantum integrability requires one to take 'reflection' quite seriously: the proper way to think about two rows of the lattice connected by a reflecting end is as the trajectory of a particle coming in from one side, then reflecting, and going out at the side it started. Indeed, this is the context in which reflection first entered the realm of quantum integrability, with Cherednik's treatment of particles moving on a half-line in an integrable quantum field theory [32]. In the vertex-model language this corresponds to models that are *staggered* in the vertical direction: the vertex weights are different for odd and for even rows of the lattice, thus breaking the vertical homogeneity. This motivates the introduction of the following operator.

Opposite monodromy matrix. In the definition (3.12) of the monodromy matrix we picked an ordering of R-matrices. We may equally well choose the opposite order to get another monodromy matrix $\bar{T}_0 \in \mathrm{End}(V_0 \otimes W)$:

$$\bar{T}_0 \coloneqq \overrightarrow{\prod_{1 \le j \le L}} R_{j0} \coloneqq R_{10}\, R_{20} \cdots R_{L0} =$$

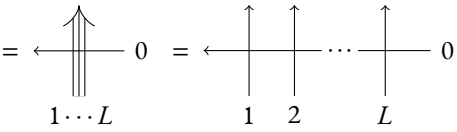

. (3.28)

We stress that, diagrammatically, by rule (iii') from Section 3 the R-matrices must be rotated over 90° in counter-clockwise direction before they can be connected in the correct order. In particular it follows that we now have R_{j0} instead of R_{0j}, though in the symmetric case this distinction is not necessary and (3.28) equals $\overrightarrow{\prod} R_{0j}$.

Moreover, to read off the correct vertex weights using Figure 3 one has to rotate back. In general this leads to different weights for microstates: T_0 and $\bar{T}_0$ are different operators, even in the symmetric case! (In Section 4 we will see that, nevertheless, the two operators are related: they are almost inverse to each other.) This can already be seen for the simplest

case, $L = 1$:

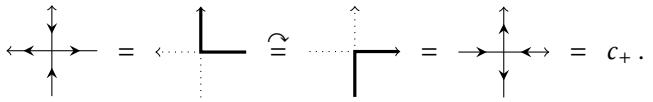

(3.29)

Observe that if we would have ignored the orientations in the arrow picture we would have assigned weight c_- to this vertex instead, while in the line picture we even appear to have a vertex forbidden by the ice rule! Only for the F-model (symmetric with $a = b$) one happens to be able *in the arrow picture* to read off the vertex weights directly from Figure 3 without having to rotate back.

We can again fix the auxiliary spins to get operators acting on W like in (3.15). These quantum operators are the entries of (3.28) viewed as a matrix in auxiliary space:

$$\bar{T}_0 = \begin{pmatrix} \bar{A} & \bar{B} \\ \bar{C} & \bar{D} \end{pmatrix}_0 . \tag{3.30}$$

By the ice rule we have $[\, h_0 + H, \bar{T}_0^{6v} \,] = 0$ yielding relations analogous to (3.18).

Sklyanin's monodromy matrix. The boundary weights for reflection as in Figure 13 are collected in the *K-matrix* $K_0 \in \mathrm{End}(V_0)$ defined by

(3.31)

For diagonal reflection it has matrix

$$K_0 = \begin{pmatrix} k_+ & 0 \\ 0 & k_- \end{pmatrix}_0 , \qquad k_\pm = \tag{3.32}$$

The *boundary* or *double-row* monodromy matrix $\mathcal{T}_0 \in \mathrm{End}(V_0 \otimes W)$ is defined as the composition

$$\mathcal{T}_0 \coloneqq T_0\, K_0\, \bar{T}_0 \;=$$

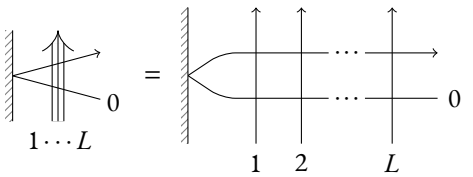

(3.33)

Like in Figure 13 the bends in the horizontal lines just serve to make the diagram more compact; they do not carry any physical significance.

Of course (3.33) can also be viewed as a matrix in auxiliary space with entries in $\mathrm{End}(W)$:

$$\mathcal{T}_0 = \begin{pmatrix} \mathcal{A} & \mathcal{B} \\ \mathcal{C} & \mathcal{D} \end{pmatrix}_0 = \begin{pmatrix} A & B \\ C & D \end{pmatrix}_0 \begin{pmatrix} k_+ & 0 \\ 0 & k_- \end{pmatrix}_0 \begin{pmatrix} \bar{A} & \bar{B} \\ \bar{C} & \bar{D} \end{pmatrix}_0 , \tag{3.34}$$

where the final expression assumes the reflection to be diagonal. In that case the double-row quantum operators inherit the properties in (3.18) from their six-vertex single-row counterparts. Graphically they look like [cf. (3.15)]

$\mathcal{A} :=$ 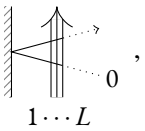

, $\mathcal{B} :=$ 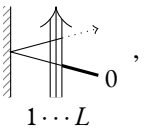

,

$\mathcal{C} :=$ 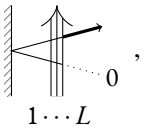

, $\mathcal{D} :=$ 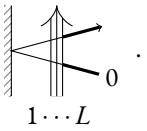

. (3.35)

Remaining ends. The description of reflection so far only fixes the boundary conditions for one end of the lattice. Let us present a few possibilities for the remaining boundaries.

Double reflection. One possibility is to choose the opposite ends to be reflecting as well. This requires a second K-matrix $\bar{K}_0 \in \mathrm{End}(V_0)$,

$\bar{K}_0 =$ 

, (3.36)

which in general may have different weights, $\bar{k}_\pm$ in the diagonal case. The partition function is built from the *double-row transfer matrix* $\tau \in \mathrm{End}(W)$ defined by

$\tau := \mathrm{tr}_0(\bar{K}_0 \mathcal{T}_0) =$ 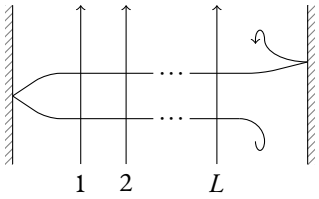

$=:$ 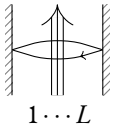

$= \bar{k}_+ \mathcal{A} + \bar{k}_- \mathcal{D}$. (3.37)

The partition function can be expressed in terms of a product of these operators, which is turned into a scalar in a way depending on the choice of boundary conditions for the edges at the bottom and top of the lattice. In this case the computation of the partition function again amounts to the problem of diagonalizing the double-row transfer matrix.

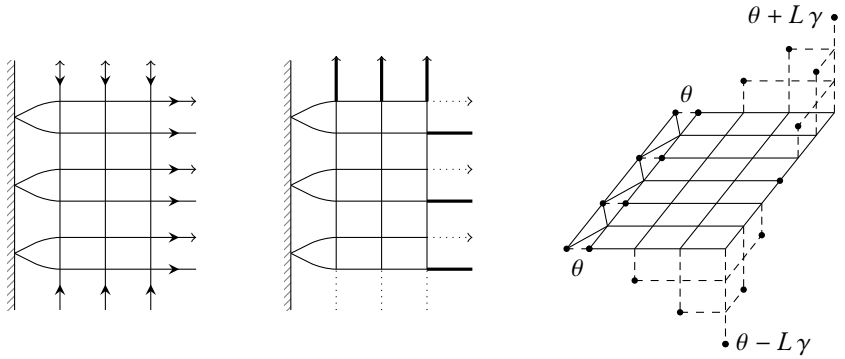

Figure 15. An example of a lattice for a vertex model with domain-wall boundaries and one reflecting end in the **(a)** arrow and **(b)** line pictures. **(c)** The SOS model on the dual lattice. For diagonal reflection the ice rule requires the bulk to have size $L \times 2L$.

Domain walls. One can also choose a fixed spin configuration along the three remaining boundaries. The four ferroelectric choices each allow for a single microstate only. A more interesting possibility is that of domain walls, shown in Figure 15. In the arrow picture these look just like in Figure 11 if we would forget about the orientations. In the line picture the domain walls still correspond to injections of horizontal thick lines and extractions of horizontal dotted lines when we take into account the orientations. Accordingly the partition function has a form that is very similar to (3.26), except that it now involves double-row quantum operators:

$$Z^{\text{refl, DWBC}} = \quad -\vec{\lambda} \quad = \langle \bar{\Omega} | \, \mathcal{B}^L \, | \Omega \rangle \, . \tag{3.38}$$

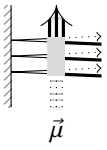

This partition function, along with its dynamical generalization, will be studied in detail in Chapter III. Following Korepin–Izergin, Tsuchiya was able to express (3.38) in terms of a determinant [35], which was extended to the dynamical case by Filali and Kitanine [36] and by Filali [37], see Section III.2. These partition functions were studied from another point of view in [1, 3]: this is the topic of Section III.3.

3.5 Dynamical case

All of the constructions from Sections 3.1–3.4 can be extended to the case of SOS models or, equivalently, generalized six-vertex models. The terminology 'dynamical' for this case

will become more clear in Section 4.3 [see the text following (4.44)].

Dynamical *R*-matrix. The generalized vertex weights from Figure 9 are contained in the 'generalized' or *dynamical R-matrix* $R_{12}(\theta) \in \mathrm{End}(V_1 \otimes V_2)$. The parameter θ, keeping track of the height, is also known as the *dynamical parameter*. It is defined as

$R_{12}(\theta) \;=\;$ 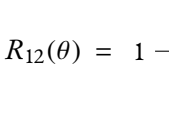

, $\qquad \langle \alpha', \beta' |\, R(\theta) \,| \alpha, \beta \rangle \;=\;$ 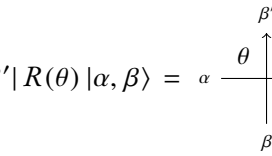

$= w\left(\begin{smallmatrix} \alpha & \beta' \\ \beta & \alpha' \end{smallmatrix} \middle| \theta\right).$ (3.39)

Its matrix is just as in (3.7), but with weights depending on the dynamical parameter. We still have to specify the actual dependence on this parameter. We have come across one possibility for the Kossel model in Section 2.1. Asking for quantum integrability only leaves a few options, see Section 4.3.

Dynamical monodromy matrix. In the graphical notation introduced at the end of Section 2.3 the definition of the *dynamical monodromy matrix* is obvious [cf. (3.12)], yet in the algebraic expression one has to take care to keep track of the heights. This can be done using the spin operators h_j, detecting the spin ± 1 on the upper vertical edges, in the arguments of the dynamical R-matrices in the ordered product:

$T_0(\theta) \;=\;$ 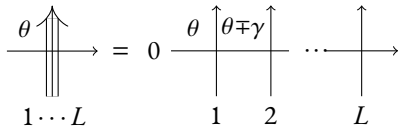

$= \overleftarrow{\prod_{L \geq j \geq 1}} R_{0j}\Big(\theta - \gamma \sum_{i=1}^{j-1} h_i\Big)\,.$ (3.40)

Through the dynamical parameter each dynamical R-matrix in (3.40) is sensitive to the spin in any V_i present to the left (in the graphical notation) of the $V_0 \otimes V_j$ on which that R-matrix acts. This makes sure that each R-matrix depends on the height, which is fixed at the top left face in (3.40), in the correct way. Indeed, the first operator, $R_{01}(\theta)$, is just the dynamical R-matrix (3.39). *After* it acts the height $\theta \mp \gamma$ is found using h_1 to get the correct value of the dynamical parameter [cf. (2.7) where h_1 acts by $\beta_1' = +1$]. This means that the second operator in (3.40), i.e. $R_{02}(\theta - \gamma\, h_1)$, acts on $V_0 \otimes V_2$ in a way that depends on the value of the spin in V_1 (measured after $R_{01}(\theta)$ has acted). Since h_1 is diagonal the matrix of $R_{02}(\theta - \gamma\, h_1)$ on V_1, with entries in $\mathrm{End}(V_0 \otimes V_2)$, takes a simple form:

$$R_{02}(\theta - \gamma\, h_1) = \begin{pmatrix} R_{02}(\theta - \gamma) & 0 \\ 0 & R_{02}(\theta + \gamma) \end{pmatrix}_1 . \tag{3.41}$$

The remaining terms in the product (3.40) are interpreted in a similar way. Through the dynamical parameter the jth factor in the product senses the spins in all local quantum spaces $V_i, 1 \le i \le j-1$, present to the left of V_j.

Of course (3.40) gives rise to four quantum operators like in (3.15), now depending on θ, and obeying relations as in (3.18) due to the ice rule.

Partition functions. The discussion from Section 3.3 extends in a fairly straightforward manner to the generalized six-vertex model.

Fixed boundaries. For boundary conditions with fixed spins the monodromy matrix (3.12) must be replaced by its dynamical counterpart (3.40). The spins at the left boundary determine the shifts in the quantum operators, and can be read off from the figures in Section 2.2. For example, the dynamical domain-wall partition function reads [cf. Figure 11 and (3.26)]

$$Z^{\text{DWBC}}(\theta) = \quad = \langle\bar{\Omega}| \overleftarrow{\prod_{L\ge j\ge 1}} B(\theta+(L-j)\gamma)\,|\Omega\rangle\,. \tag{3.42}$$

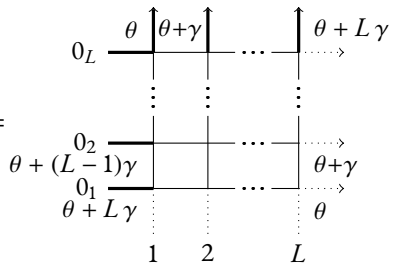

Reflection. In the presence of a reflecting end as in Section 3.4 we also need the opposite monodromy matrix

$$\bar{T}_0(\theta) = \quad 0 \quad = \quad \cdots \quad 0 \quad = \overrightarrow{\prod_{1\le j\le L}} R_{j0}\Big(\theta - \gamma\sum_{i=1}^{j-1} h_i\Big)\,. \tag{3.43}$$

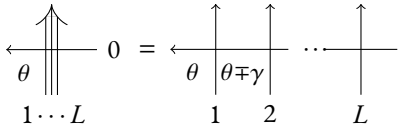

Note that this time the height is fixed in the bottom left face due to the rotation as in (3.29). When passing to faces above the horizontal line to extend this to a full height profile as dictated by the spin configuration, the dictionary from Figure 8 should be used *after* rotating the dynamical R-matrices in $\bar{T}_0(\theta)$ back as in (3.29).

Diagonal reflection means that the height at the boundary on the left is constant,

$$K_0(\theta) = \begin{pmatrix} k_+(\theta) & 0 \\ 0 & k_-(\theta) \end{pmatrix}_0, \qquad k_\pm(\theta) = \quad , \tag{3.44}$$

in accordance with Figure 13. Thus the dynamical double-row monodromy matrix $\mathcal{T}_0(\theta) \in \mathrm{End}(V_0 \otimes W)$ is

$\mathcal{T}_0(\theta) =$ 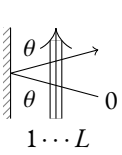

$=$ 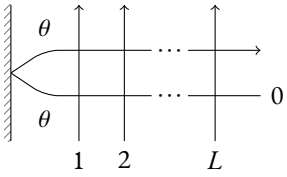

$= T_0(\theta)\, K_0(\theta)\, \bar{T}_0(\theta)\,, \qquad (3.45)$

and the dynamical partition function with domain walls and one reflecting end does *not* involve any shifts in the argument of the quantum operators [cf. (3.38)]:

$Z^{\text{refl, DWBC}}(\theta) =$ 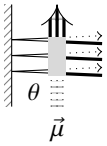

$-\vec{\lambda} = \langle\bar{\Omega}|\, \mathcal{B}(\theta)^L\, |\Omega\rangle\,. \qquad (3.46)$

This quantity is the topic of Chapter III.

4 Quantum integrability

In this section we consider the quantum-integrable versions of the models introduced in Section 2. As in Section 3 the ordinary six-vertex model is treated first. The eight-vertex model and generalized six-vertex model are discussed in Section 4.3.

4.1 Commuting transfer matrices and hidden symmetries

To motivate the definition for quantum integrability that we will give in Section 4.2, in terms of some algebraic condition on the R-matrix, let us study the case of toroidal boundary conditions for the symmetric six-vertex model.

Commuting transfer matrices. Consider the *symmetric* six-vertex model with *toroidal* boundary conditions, and view the vertex weights as parameters specifying the physical system under consideration. The various operators introduced in Section 3 depend on these parameters. By the transfer-matrix method, computing the partition function (3.20) amounts to diagonalizing the transfer matrix. Lieb [17, 18] and Sutherland [19] realized that this can be done, at least in principle, by a Bethe-ansatz analysis. The precise method is not relevant for us here; it is summarized in Section IV.1.3 and described in detail in [5, §2]. The striking result is that, although the transfer matrix $t = t(a, b, c)$ depends on all three vertex weights, its eigenvectors turn out *only* to depend on the combination

$\Delta(a,b,c)$ defined in (2.2). Varying the values of a,b,c while keeping (2.2) fixed therefore does not change the eigenvectors (though the eigenvalues do change). This means that transfer matrices for all six-vertex models yielding the same value of (2.2) are simultaneously diagonalized:

$$[\, t(a,b,c),\ t(a',b',c')\,] = 0 \qquad \text{if} \quad \Delta(a,b,c) = \Delta(a',b',c')\,. \tag{4.1}$$

As we will see soon this observation holds the key to understanding the integrability of the six-vertex model.

Spectral parameters. To analyse the consequences of (4.1) let us first look at the degrees of freedom contained in the six-vertex model's parameters (a,b,c). Simultaneous nonzero rescalings $(a,b,c) \longmapsto (r\,a, r\,b, r\,c)$ do not affect the combination (2.2) and only modify the partition function (3.20) by an overall factor. Motivated by this let us replace (a,b,c) by the ratio $a : b : c$ and fix the value of the function (2.2). This leaves a single remaining degree of freedom, known as the *spectral parameter*, which we denote by λ. Observe that, through the vertex weights, the transfer matrix also depends on the spectral parameter: $t(\lambda) = t\,(a(\lambda), b(\lambda), c(\lambda))$. We can now recast (4.1) in the form

$$[\, t(\lambda),\ t(\lambda')\,] = 0 \qquad \text{for all } \lambda, \lambda'\,. \tag{4.2}$$

That is, we have a one-parameter family of six-vertex models, with $a : b : c$ for fixed Δ parametrized by varying λ, whose transfer matrices $t(\lambda)$ commute with each other.

***Z*-invariant models.** How should the commutator (4.2) be interpreted from the vertex-model viewpoint? Diagrammatically it consists of two terms of the form

$t(\lambda)\,t(\lambda') \;=$

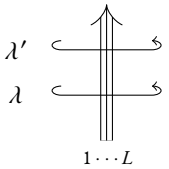

(4.3)

with a separate spectral parameter associated to each row as indicated. This diagram can be viewed as a portion of a vertex model with different values of the spectral parameter—hence different vertex weights, yielding the same value of (2.2)—for each row of horizontal edges in the lattice. By (4.2) the partition function Z (3.20) of such vertex models are invariant under the exchange of any two rows in the lattice; accordingly those models are sometimes called *Z-invariant*.

Analyticity. Baxter realized that for the analysis of the six-vertex models it is extremely useful to allow for complex vertex weights and let $\lambda \in \mathbb{C}$. For example,

$$a(\lambda) = r\,\sinh(\lambda+\gamma)\,, \qquad b(\lambda) = r\,\sinh(\lambda)\,, \qquad c(\lambda) = r\,\sinh(\gamma)\,, \tag{4.4}$$

gives an *analytic* parametrization of the six-vertex weights in terms of (λ,γ,r) that is even *entire* in λ; in fact (4.4) is naturally found by seeking an entire parametrization, see [11,

§9.7]. Note that in this parametrization c is independent of the spectral parameter. The *crossing* or *anisotropy* parameter γ, which one can also take to be complex, parametrizes the value of (2.2) since $\Delta(a(\lambda), b(\lambda), c(\lambda)) = \cosh(\gamma)$. The power of the transfer-matrix method lies in the fact that all functions $\lambda \longmapsto \langle \vec{\beta}' | \, t(\lambda) \, | \vec{\beta} \rangle$ are entire as well, because they are polynomial in a, b, c. Analyticity considerations will also play a prominent role in the analysis of Chapters II and III.

Hidden symmetries. Let us put together the ingredients discussed above to appreciate the importance of commuting transfer matrices as in (4.2). Consider a symmetric six-vertex model with toroidal boundaries, vertex weights (a_0, b_0, c_0) and transfer matrix $t_0 := t(a_0, b_0, c_0)$. Setting $\Delta_0 := \Delta(a_0, b_0, c_0)$, we have seen that there exists a one-parameter family of six-vertex models with commuting transfer matrices, like in (4.2), such that $t(\lambda_0) = t_0$ for some $\lambda_0 \in \mathbb{C}$. To get a better understanding of the importance of the relation (4.2) let us parametrize the vertex weights as in (4.4). Since the transfer matrix is a Laurent polynomial in e^{λ} it makes sense to take logarithmic derivatives and define operators H_k on W via the *trace identities*

$$H_k := \frac{\mathrm{d}^k}{\mathrm{d}\lambda^k}\bigg|_{\lambda=\lambda_*} \log t(\lambda) \tag{4.5}$$

for some value λ_* of the spectral parameter—we will see momentarily that $\lambda_* = 0$ is a convenient choice for the parametrization (4.4). Then (4.2) implies that

$$[\, H_k, t_0 \,] = [\, H_k, H_l \,] = 0 \qquad \text{for all } k, l. \tag{4.6}$$

Now we can see the fruits of our labour more clearly. The trace identities produce operators that commute with t_0. Moreover, these symmetry operators commute with each other (they are *in involution*). From the original six-vertex model's perspective the one-parameter family $t(\lambda)$ generates a discrete Euclidean 'time' evolution with respect to which the H_k are 'conserved'. The presence of such a macroscopic number of commuting symmetries is a very special property; it 'proves' that the model is 'quantum integrable' in analogy with the notion of Liouville integrability in classical mechanics.

Since the transfer matrix consists of a product of R-matrices it is easy to find a particularly convenient choice for the special value λ_* at which the logarithmic derivatives are evaluated in (4.5). Using the parametrization (4.4) we observe that $b(0) = 0$ vanishes, while $a(0) = c$. Thus at $\lambda_* = 0$ the six-vertex R-matrix from (3.7) becomes proportional to the permutation operator (3.11):

$$R_{12}(0) = c \, P_{12} \, . \tag{4.7}$$

This makes the computation of the symmetries (4.5) quite simple, at least for low k, see e.g. [5, §4.1]. For $k = 0$ the result is the *shift operator*, shifting the lattice by one unit in

the horizontal direction. Interestingly for $k = 1$ one obtains, up to some constants, the Hamiltonian of the periodic *Heisenberg–Ising* or 'xxz' spin chain,

$$H_{\mathrm{xxz}} = -J \sum_{j \in \mathbb{Z}_L} (S_j^x S_{j+1}^x + S_j^y S_{j+1}^y + \Delta S_j^z S_{j+1}^z) , \tag{4.8}$$

which acts on W. Here $J \in \mathbb{R}$ is a coupling constant setting the energy scale, $\mathbb{Z}_L$ labels the L sites of a periodic spin chain, $S^\alpha = \sigma^\alpha/2$ ($\alpha = x, y, z$) are the three $\mathfrak{su}_2$ spin operators for spin 1/2, and $\Delta = \cosh(\gamma)$ is now interpreted as the *anisotropy* parameter. The xxz spin chain will be discussed in more detail in Section IV.1.1. From the preceding discussion it follows that H_{xxz} can be diagonalized simultaneously with the six-vertex model's transfer matrix.

Incidentally, the appearance of a spin chain explains the origin of the quantum-mechanical terminology, such as 'quantum' and 'auxiliary' space in Section 3.2, 'pseudo-vacuum' and 'Néel vector' in Section 3.3. In the spin-chain picture the ice rule amounts to *partial isotropy* $[\, H, H_{\mathrm{xxz}} \,] = 0$ where H is the total spin operator (3.17) on W, generating the subgroup $U(1)_z \subseteq SU(2)$ of rotations about the z-axis. In the limit $\gamma \to 0$ the isotropy is restored to $SU(2)$ for finite system sizes. In the vertex-model picture this limit yields the *rational* six-vertex model, whose weights are obtained from (4.4) via $a_{\mathrm{rat}}(\lambda) := \lim_{\gamma \to 0} a(\gamma\, \lambda)/\lambda = r\,(\lambda + 1)$ and so on.

4.2 Quantum inverse-scattering method

We are finally ready to get to the heart of quantum integrability: the Yang–Baxter equation and the resulting quantum-algebraic structure, allowing one to obtain exact results. This algebraic formalism is known as the *quantum inverse-scattering method* (QISM) and was devised by the Leningrad school of Faddeev *et al.* in the late 1970s, see e.g. [45] and the references therein.

Still a bit more diagrammatics. It is useful to update our graphical notation one more time. We extend rule (i') from Section 3.1 to include spectral parameters:

i") To any (oriented) edge we assign a copy of the vector space $V = \mathbb{C}\,|+\rangle \oplus \mathbb{C}\,|-\rangle$ and a spectral parameter $\lambda \in \mathbb{C}$.

As in (4.3) each line carries its own spectral parameter, so we may now label the lines by the spectral parameters instead. Rules (ii') and (iii') remain the same.

The R-matrix acts on two copies of the auxiliary space, $V_1 \otimes V_2$, so it can depend on two spectral parameters. The rule is that it does so via their *difference*, which makes sense

when we think of the slopes of the lines as encoding the values of the spectral parameters:

$$R_{12}(\lambda_1 - \lambda_2) \;=\; \qquad =$$

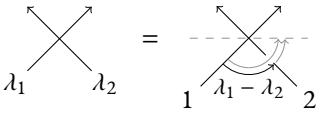

. (4.9)

The spectral parameters in the diagram in the middle should not to be confused with spin variables $\alpha, \beta, \cdots$, which is why we use a small font size for the latter in diagrams.

For some purposes such a geometric interpretation of the spectral parameters is very illuminating. It should be compared with factorized scattering in $(1+1)$-dimensional field theory. There the two-particle S-matrix may be depicted in a spacetime diagram as in (4.9) wit time increasing upwards, the two lines are the worldlines of the particles that scatter, and their slopes encode their rapidities λ_j. By translational invariance the S-matrix can only depend on the difference of the momenta. In this setting the Yang–Baxter equation below is a consistency condition for the factorization of many-particle scattering into successive two-particle processes. See also [5, §5.1].

Yang–Baxter equation. The take-away message from Section 4.1 is that, for the symmetric six-vertex model with toroidal boundaries, given an analytic parametrization of the vertex weights there exists a one-parameter family of commuting transfer matrices that gives rise to a tower of hidden symmetries rendering the model solvable. (In Appendix A we will see how the transfer matrix can be diagonalized in practice.)

Let us demonstrate that the machinery from Sections 3.1–3.2 allows one to formulate algebraic conditions that apply to models with more general boundary conditions while guaranteeing commuting transfer matrices in the case of horizontal periodicity. These algebraic conditions take the form of a 'local' relation involving the R-matrix only.

Assume that we have a vertex model whose R-matrix satisfies the following *Yang–Baxter equation* (YBE) on $V_1 \otimes V_2 \otimes V_3$:

$$\begin{aligned} &R_{12}(\lambda_1 - \lambda_2)\, R_{13}(\lambda_1 - \lambda_3)\, R_{23}(\lambda_2 - \lambda_3) \\ &\qquad = R_{23}(\lambda_2 - \lambda_3)\, R_{13}(\lambda_1 - \lambda_3)\, R_{12}(\lambda_1 - \lambda_2)\,. \end{aligned} \tag{4.10}$$

This equation can be drawn as

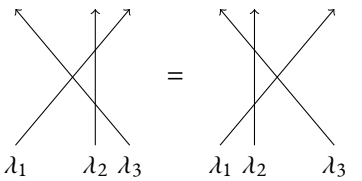

. (4.11)

The corresponding equation for the components—the vertex weights—is known as the *star-triangle equation*. A direct check shows that the symmetric six-vertex R-matrix (3.7)

does indeed satisfy the YBE when its entries are parametrized as in (4.4). Reversely, symmetric R-matrices of six-vertex form, with three sets of vertex weights (a, b, c), (a', b', c') and (a'', b'', c''), solve the YBE $R_{12}R'_{13}R''_{23} = R''_{23}R'_{13}R_{12}$ provided that $\Delta(a, b, c) = \Delta(a', b', c') = \Delta(a'', b'', c'')$, see e.g. [5, §C], which then leads to the entire parametrization (4.4). In Section 4.1 we promised that this implies that the corresponding transfer matrices commute. Let us rederive this conclusion in the present algebraic setting. The 'local' YBE is turned into a 'bulk' relation for the monodromy matrix as follows.

From local to bulk. There exists R-matrices $R_{12}(\lambda) \in \mathrm{End}(V_1 \otimes V_2)$ obeying the YBE (4.10) if and only if for every system size $L \in \mathbb{N}$ the corresponding monodromy matrices commute up to conjugation by the R-matrix:

$$R_{00'}(\lambda - \lambda')\, T_0(\lambda)\, T_{0'}(\lambda') = T_{0'}(\lambda')\, T_0(\lambda)\, R_{00'}(\lambda - \lambda')\,. \tag{4.12}$$

Proof. It is clear that the Yang–Baxter equation is necessary in order to have (4.12) for all $L \in \mathbb{N}$: setting $L = 1$ in (4.12) gives (4.10) up to renaming the spectral parameters as $\lambda = \lambda_1 - \lambda_2$ and $\lambda' = \lambda_1 - \lambda_3$. To see that (4.10) is also sufficient we use the following graphical (yet rigorous!) 'train argument', which essentially is a proof by induction on L.

Diagrammatically (4.11) says that any of the three lines can be moved through the crossing of the two other lines, representing the R-matrix acting on the vector spaces associated with those other lines. Consider a monodromy matrix (3.12) for some fixed value of L. Then L applications of (4.11) with $\lambda_1 = \lambda$, $\lambda_2 = \lambda'$ and $\lambda_3 = 0$ do the job:

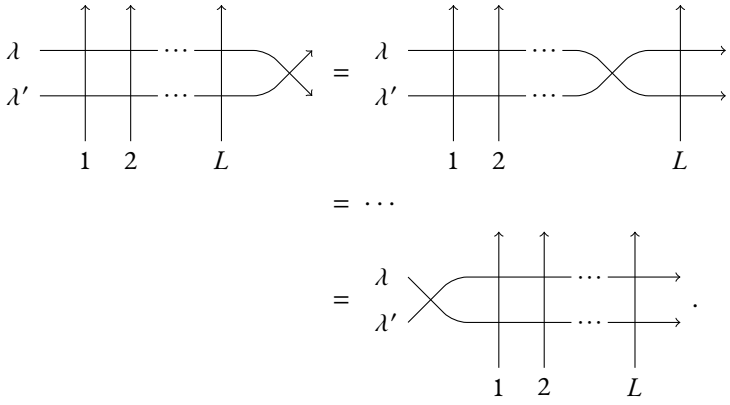

(4.13)

The first and last diagrams in these series of equalities are just the graphical notation for the two sides of (4.12). □

Equation (4.12) is often called the *RTT-relation* for obvious reasons. Note that the train argument effectively allows us to replace any single line in (4.11) by a triple line representing

the quantum space W:

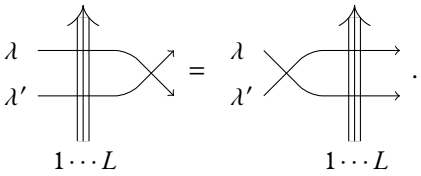

(4.14)

Quantum integrability. We will call a model *quantum integrable* if it comes with operators $R_{12}(\lambda) \in \mathrm{End}(V_1 \otimes V_2)$ satisfying the following *quantum-integrable data*:

- the functions $\lambda \longmapsto \langle \alpha', \beta' | \, R(\lambda) \, | \alpha, \beta \rangle$ are meromorphic,
- $R_{12}(\lambda)$ is invertible for generic (i.e. almost all) values of $\lambda \in \mathbb{C}$, and
- $R_{12}(\lambda)$ satisfies the YBE (4.10).

For exact solvability the boundary conditions should be compatible with the above in some way; whether this is true has to be investigated case by case.

The power of a definition of quantum integrability in terms of quantum-integrable data as above is that it includes quite a few more systems than just the symmetric six-vertex model with toroidal boundaries. It can also be adapted to the dynamical case, see Section 4.3. Let us turn to some examples of quantum-integrable models.

Periodic boundaries. It is easy to see that the YBE is indeed instrumental for having commuting transfer matrices: given the above quantum-integrable data the resulting one-parameter family of transfer matrices $t(\lambda)$ commute for almost all values of the spectral parameter.

Proof. Since the entries of the monodromy matrix are polynomial in the vertex weights they inherit the meromorphic dependence on the spectral parameter. So do the entries of the transfer matrix (3.19). For generic $\lambda, \lambda' \in \mathbb{C}$ we can multiply both sides in (4.14) from the left by the inverse of the R-matrix. Taking the trace over both auxiliary spaces we see that $t(\lambda)$ and $t(\lambda')$ commute by the cyclic property of the trace. □

By the discussion in Section 4.1 this guarantees the existence of hidden symmetries for the symmetric six-vertex model with horizontal periodicity. Indeed, we already noted that the parametrization (4.4) of the vertex weights is in fact entire. The corresponding R-matrix has determinant $a(\lambda)^2 \, (b(\lambda)^2 - c(\lambda)^2)$, which only vanishes at a discrete subset, $\lambda \in \mathrm{i}\pi\,\mathbb{Z} \pm \gamma$. Moreover, as the transfer matrix is entire, the commutativity extends to all values of the spectral parameter as in (4.2). In Appendix A we will see how quantum integrability can be used to find the spectrum of the transfer matrix.

Inhomogeneities. A variation of the above goes as follows. When the R-matrix depends on the difference of spectral parameters as in (4.9) one can introduce an *inhomogeneity parameter* μ_j, which is also taken to be complex, for each vertical row of the lattice.

The monodromy matrix for the inhomogeneous six-vertex model is

$$T_0(\lambda;\vec{\mu}) \coloneqq \prod_{L\geq j\geq 1}^{\leftarrow} R_{0j}(\lambda-\mu_j) =$$

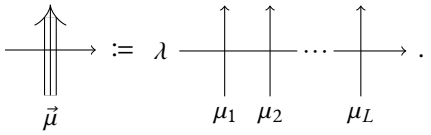

(4.15)

The introduction of inhomogeneities breaks translational invariance (homogeneity) of the corresponding lattice in the horizontal direction, but it does so in a way that preserves quantum integrability. Indeed, the RTT-relation (4.12) remains valid; we only have to take $\lambda_3 = \mu_j$ at step $L-j+1$ in (4.13). (In view of the geometric interpretation of spectral parameters it might be more appropriate to give each vertical line in (4.15) a slightly different slope, but we will refrain from doing so.)

Fixed boundaries. Recall the various fixed boundary conditions from Sections 2.2 and 3.3. Ferroelectric boundaries lead to a trivial model whose partition function is easily obtained for any six-vertex model. Domain walls are rather interesting from the present point of view. Unlike for toroidal boundaries the partition function can not be computed using a Bethe ansatz. However, the model is quantum integrable, which does still allow for the exact computation of the domain-wall partition function. This is precisely the topic of Chapter II. In contrast, no such way of treating the partition function for Néel boundaries is known. At the end of this section we will discuss the case of reflection.

Yang–Baxter algebra. The following algebraic construction lies at the core of the QISM. It provides the mathematical setting for the computations in the framework of the algebraic Bethe ansatz (see Appendix A) as well as a way to compute the domain-wall partition function from Figure 11.

Recall from Section 3.2 that the monodromy matrix contains four (one-parameter families of) quantum operators $A(\lambda),\cdots,D(\lambda)\in \mathrm{End}(W)$, see (3.16). These operators generate a (unital, associative) algebra, known as the *Yang–Baxter algebra* (YBA), whose commutation rules are given by the RTT-relation (4.12). The latter encodes $\dim(V_0\otimes V_{0'}) = 16$ relations in $\mathrm{End}(V_0\otimes V_{0'})$ for the generators (3.15). The explicit form of these relations can be found from (4.12) by straightforward matrix multiplication or using the graphical form (4.14), see [5, §4.2]. For the symmetric six-vertex model, with R-matrix containing vertex weights $a(\lambda), b(\lambda), c(\lambda)$, the result is as follows:

$$[\,A(\lambda),A(\lambda')\,] = [\,B(\lambda),B(\lambda')\,] = [\,C(\lambda),C(\lambda')\,] = [\,D(\lambda),D(\lambda')\,] = 0\,, \tag{4.16}$$

$$[\,A(\lambda)+D(\lambda),A(\lambda')+D(\lambda')\,] = 0\,, \tag{4.17}$$

$$A(\lambda)\,B(\lambda') = \frac{a(\lambda'-\lambda)}{b(\lambda'-\lambda)}\,B(\lambda')\,A(\lambda) - \frac{c(\lambda'-\lambda)}{b(\lambda'-\lambda)}\,B(\lambda)\,A(\lambda')\,, \tag{4.18}$$

$$D(\lambda)\,B(\lambda') = \frac{a(\lambda-\lambda')}{b(\lambda-\lambda')}\,B(\lambda')\,D(\lambda) - \frac{c(\lambda-\lambda')}{b(\lambda-\lambda')}\,B(\lambda)\,D(\lambda')\,, \tag{4.19}$$

$$C(\lambda)\,A(\lambda') = \frac{a(\lambda-\lambda')}{b(\lambda-\lambda')}\,A(\lambda')\,C(\lambda) - \frac{c(\lambda-\lambda')}{b(\lambda-\lambda')}\,A(\lambda)\,C(\lambda')\,, \tag{4.20}$$

$$B(\lambda)\,D(\lambda') = \frac{a(\lambda'-\lambda)}{b(\lambda'-\lambda)}\,D(\lambda)\,B(\lambda') - \frac{c(\lambda'-\lambda)}{b(\lambda'-\lambda)}\,D(\lambda)\,B(\lambda')\,, \tag{4.21}$$

$$[\,C(\lambda), B(\lambda')\,] = \frac{c(\lambda'-\lambda)}{b(\lambda'-\lambda)}\,(A(\lambda)\,D(\lambda') - A(\lambda')\,D(\lambda))\,. \tag{4.22}$$

In (4.18)–(4.22) we assume that the spectral parameters are distinct. According to (4.17) the transfer matrices (3.19) form a commutative subalgebra of the Yang–Baxter algebra. Next, (4.18) says that when we commute an A past a B, besides some factors, we pick up an additional term where the operators have interchanged their spectral parameters. By (4.20) the situation is similar when we move an A past a C to its left. Note that the entries of the R-matrix play the role of structure constants for the Yang–Baxter algebra. From this point of view the YBE (4.10), which is cubic in the 'structure constants', is the analogue of the Jacobi identity.

The physical use of the YBA stems from the *quantum inverse-scattering problem*, which asks whether it is possible to reconstruct arbitrary operators in $\mathrm{End}(V_j)$, and thus those in $\mathrm{End}(W)$, from the monodromy matrix. It suffices to construct the local spin operators together with the identity, since those span $\mathrm{End}(V_j)$. The solution to this problem was found for many models, including the six-vertex model, in [46]. The conclusion is that $A(\lambda), \cdots, D(\lambda)$ generate all of $\mathrm{End}(W)$.

Ice rule revisited. The algebraic consequence of the ice rule (line conservation) is that operators such as the transfer matrix (3.19) are block diagonal,

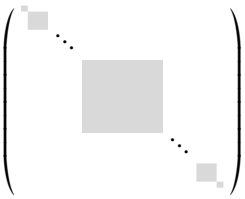

(4.23)

where we reorder the basis to group together vectors with the same number of spins equal to −1 (thick lines). More precisely, according to (3.18) the quantum space W splits into H-eigenspaces of fixed total spin, and the decomposition

$$W = \bigoplus_{M=0}^{L} W[L-2M]\,, \qquad\qquad H\,|\vec{\beta}\rangle = s\,|\vec{\beta}\rangle \text{ iff } |\vec{\beta}\rangle \in W[s]\,, \tag{4.24}$$

is preserved by $A(\lambda)$ and $D(\lambda)$, and in particular by the transfer matrix $t(\lambda) = A(\lambda) + D(\lambda)$. In the line picture vectors in the *M-particle sector* $W[L-2M]$ contain precisely M

thick lines; it follows that $\dim(W[L-2M]) = \binom{L}{M}$. For example, $W[\pm L]$ are both one dimensional with basis consisting of the pseudovacua (3.21). The Néel vectors (3.22) lie in the largest subspaces, $W[0]$ when L is even and $W[\pm 1]$ for L odd.

Bethe vectors. By (3.18) the operator $B(\lambda)$ maps $W[L-2M]$ into $W[L-2(M+1)]$ for each M, while $C(\lambda)$ acts in the opposite direction. Starting from the pseudovacuum $|\Omega\rangle$, which is annihilated by $C(\lambda)$, we thus have candidates for raising and lowering operators. To diagonalize the transfer matrix in an arbitrary M-particle sector the *algebraic Bethe ansatz* (ABA) proposes to seek for eigenvectors of the form

$$|\Psi_M;\vec{\lambda}\rangle \coloneqq B(\lambda_1)\cdots B(\lambda_M)\,|\Omega\rangle = \quad \in W[L-2M]\,, \tag{4.25}$$

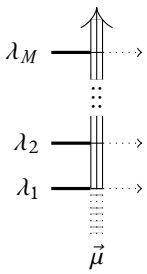

for suitable values of the spectral parameters λ_m. By (4.16) the order of the B's does not matter. In Appendix A use the relations of the Yang–Baxter algebra to demonstrate that this ansatz does indeed work provided the λ_m obey a set of coupled equations known as the Bethe-ansatz equations.

In the maximal case $M = L$ the Bethe vector (4.25) must be proportional to $|\bar{\Omega}\rangle$. We recognize $\langle\bar{\Omega}|\Psi_L;\vec{\lambda}\rangle$ as nothing but the domain-wall partition function (3.26) for an inhomogeneous six-vertex model with boundary conditions as in Figure 11!

Reflecting end. A reflecting end is made compatible with the quantum-integrable data in the following way. In view of (4.9) we use the rule that for reflection the 'incoming' spectral parameter is $-\lambda$, which is then turned into 'outgoing' parameter λ by the reflection. For quantum integrability Cherednik [32] realized that the K-matrix has to obey the *boundary Yang–Baxter* or *reflection equation*

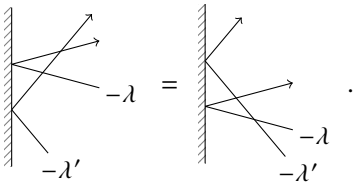

(4.26)

Note that like the YBE this relation can be interpreted as the invariance under translations of lines, which in this case are reflected. With the help of (4.9) we read off the algebraic

form of the reflection equation:

$$\begin{aligned} R_{00'}(\lambda-\lambda')\,K_0(\lambda)\,R_{0'0}(\lambda+\lambda')\,K_{0'}(\lambda') \\ = K_{0'}(\lambda')\,R_{00'}(\lambda+\lambda')\,K_0(\lambda)\,R_{0'0}(\lambda-\lambda')\,. \end{aligned} \tag{4.27}$$

Note that on each side of this equation the R-matrix in between the two K-matrices depends on the *sum* of spectral parameters. For the six-vertex R-matrix with vertex weights (4.4) the diagonal solution of the reflection equation reads [cf. (3.44)]

$$k_\pm(\lambda) = \sinh(\zeta \pm \lambda)\,, \tag{4.28}$$

where $\zeta \in \mathbb{C}$ is a fixed boundary parameter.

The above can be adapted to turn the (local) reflection equation into an algebraic relation governing the bulk as well as the reflecting end. Consider the opposite monodromy matrix $\bar{T}_0(\lambda)$ [cf. (3.28)]:

$$\bar{T}_0(\lambda) = \overrightarrow{\prod_{1\le j\le L}} R_{j0}(\lambda+\mu_j) \;=\; \tag{4.29}$$

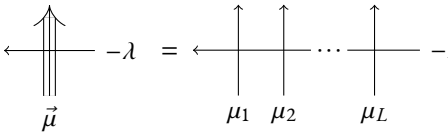

By virtue of the YBE it obeys the relations

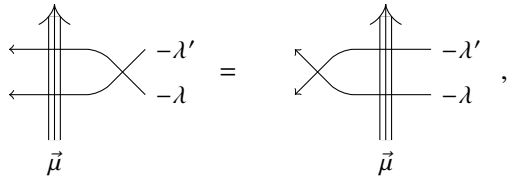

(4.30)

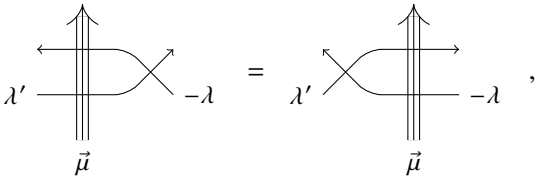

(4.31)

which are established just as in (4.13). Following Sklyanin [33] one now checks that, together with the reflection equation (4.26), these bulk relations imply that the double-row

monodromy matrix (3.33) satisfies a global reflection equation in the form

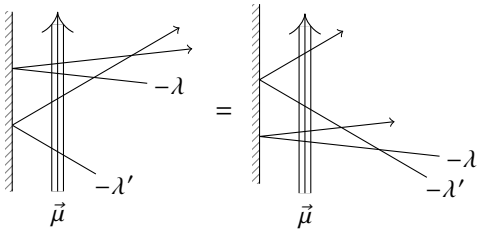

(4.32)

or

$$R_{00'}(\lambda-\lambda')\,\mathcal{T}_0(\lambda)\,R_{0'0}(\lambda+\lambda')\,\mathcal{T}_{0'}(\lambda') = \mathcal{T}_{0'}(\lambda')\,R_{00'}(\lambda+\lambda')\,\mathcal{T}_0(\lambda)\,R_{0'0}(\lambda-\lambda')\,. \tag{4.33}$$

This equation encodes commutation rules for the double-row quantum operators (3.34): these are the defining relations for the *reflection algebra*, which is the double-row analogue of the Yang–Baxter algebra.

For double reflection with (3.36) satisfying a mirrored version of (4.26) the relation (4.33) ensures that the double-row transfer matrices (3.37) once more commute, which shows that double reflection is also quantum integrable. Again there is an algebraic Bethe ansatz, where Bethe vectors are now constructed with the help of the double-row creation operator $\mathcal{B}$ from (3.34)–(3.35). For domain walls on the three remaining boundaries the situation is again quite interesting: this is the topic of Chapter III.

4.3 Dynamical case revisited

Thus far we have extensively studied the six-vertex model with the various boundary conditions from Section 2.2. Now we turn to the other models from Section 2.1: the eight-vertex model and the SOS model, or equivalently, generalized six-vertex model. In the context of quantum integrability these models turn out to be intimately related.

In this section we use a grey background for the diagrammatic notation for the eight-vertex model to distinguish it from its six-vertex counterpart.

Symmetric eight-vertex model. We start with the symmetric eight-vertex model, with R-matrix

$$R^{8v} = \begin{pmatrix} a & 0 & 0 & d \\ 0 & b & c & 0 \\ 0 & c & b & 0 \\ d & 0 & 0 & a \end{pmatrix} = \quad 1 \quad \text{ 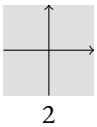 } \quad 2 \,. \tag{4.34}$$

Such an R-matrix solves the Yang–Baxter equation $R_{12}R'_{13}R''_{23} = R''_{23}R'_{13}R_{12}$ provided that the vertex weights obey $\Delta(a,b,c,d) = \Delta(a',b',c',d') = \Delta(a'',b'',c'',d'')$ and

$\Gamma(a,b,c,d) = \Gamma(a',b',c',d') = \Gamma(a'',b'',c'',d'')$, where

$$\Delta(a,b,c,d) \coloneqq \frac{a^2+b^2-c^2-d^2}{2(ab+cd)}\,, \qquad \Gamma(a,b,c,d) \coloneqq \frac{a\,b-c\,d}{a\,b+c\,d}\,. \tag{4.35}$$

As for the six-vertex model the equations are invariant under simultaneous rescalings $(a,b,c,d) \longmapsto (r\,a, r\,b, r\,c, r\,d)$, which together with fixing the values of (4.35) once more leaves one degree of freedom, the spectral parameter. Quantum-integrable data requires a meromorphic parametrization of the eight-vertex weights in terms of λ such that (4.35) are independent of λ. Again it turns out to be possible to find an *entire* parametrization in terms of elliptic functions, see e.g. [11, §10.4], giving rise to Baxter's elliptic R-matrix [47].

In the case of horizontal periodic boundary conditions the preceding implies that the corresponding eight-vertex transfer matrices commute. Via the trace identities (4.5) one finds the completely anisotropic XYZ spin chain amongst the conserved quantities:

$$H_{\text{XYZ}} = -J \sum_{j\in\mathbb{Z}_L} (S^x_j\,S^x_{j+1} + \Gamma\,S^y_j\,S^y_{j+1} + \Delta\,S^z_j\,S^z_{j+1})\,. \tag{4.36}$$

The trigonometric limit of vanishing d corresponds to $\Gamma \to 1$ yielding the six-vertex model and XXZ spin chain.

***TQ*-equation.** The next thing one would like to do is to use the corresponding Yang–Baxter algebra to find the spectrum of the transfer matrix. However, since (4.34) violates the ice rule there is no pseudovacuum to start from. In 1972 Baxter constructed another one-parameter family of commuting operators $Q(\lambda) \in \mathrm{End}(W)$ that also commute with the $t(\lambda')$ and at coinciding spectral parameters satisfy the *TQ-relations*

$$t^{8\text{v}}(\lambda)\,Q(\lambda) = \varphi(\lambda-\gamma)\,Q(\lambda+2\gamma) + \varphi(\lambda+\gamma)\,Q(\lambda-2\gamma)\,, \tag{4.37}$$

where φ is a known function. By (simultaneously) diagonalizing t and Q this yields a functional equation that determines the eigenvalues of the transfer matrix. More about the TQ-method can be found in [11, §9–10], or [45, §4–5] for an account using the QISM.

Face-vertex transformation. One year after Baxter obtained the eigenvalues of $t^{8\text{v}}$ using (4.37) he realized that it is possible to transform the problem into another setting that does admit a pseudovacuum. One way [45] of looking at this *vertex-IRF* or *face-vertex transformation* is as a site-dependent ('gauge') transformation such that the transformed R-matrix *does* obey the ice rule and the transformed monodromy matrix also differs from $T^{8\text{v}}_0$ by a linear transformation. More precisely [48, §6] one can explicitly write down a (generically) invertible operator $S(\lambda,\theta) \in \mathrm{End}(V)$, depending on an additional parameter θ, such that

$$\begin{aligned} R^{8\text{v}}_{00'}(\lambda_1-\lambda_2)\,S_0(\lambda_1,\theta)\,S_{0'}(\lambda_2,\theta-\gamma\,h_0) \\ = S_{0'}(\lambda_2,\theta)\,S_0(\lambda_1,\theta-\gamma\,h_{0'})\,R_{00'}(\lambda_1-\lambda_2,\theta)\,. \end{aligned} \tag{4.38}$$

The transformed $R_{00'}(\lambda_1 - \lambda_2, \theta)$ is precisely the dynamical R-matrix of a generalized six-vertex model! In fact, this is the context in which generalized six-vertex models first appeared [47]. If we draw S and its entries as

$$S(\lambda,\theta) = \quad , \qquad \langle\alpha'|\, S(\lambda,\theta)\, |\alpha\rangle = \tag{4.39}$$

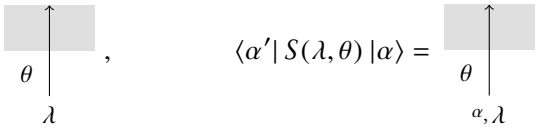

we see that (4.38) is like a YBE of mixed ordinary and generalized vertex type:

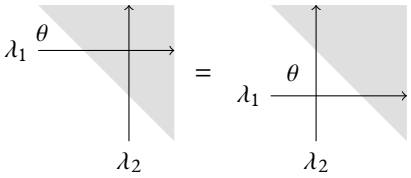

(4.40)

Multiplying (4.38) from the left by the appropriate inverses, drawn as

$$S(\lambda,\theta)^{-1} = \quad , \qquad = \quad , \qquad = \tag{4.41}$$

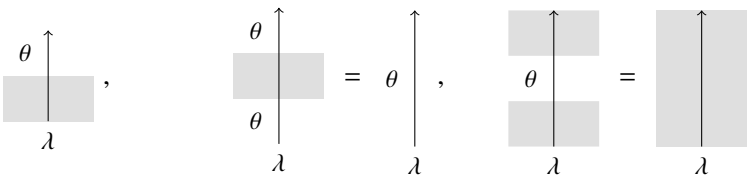

with the line depicting the identity on V, the 'gauge' transformation looks like

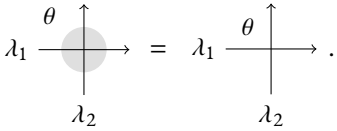

(4.42)

Thus the eight-vertex monodromy matrix is related to the dynamical six-vertex monodromy (3.40) as

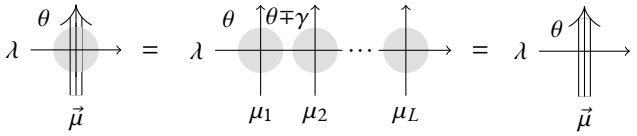

(4.43)

Note that the face-vertex transformation requires a choice of θ: this is precisely the ambiguity in the choice of reference height θ that we discussed in Section 2.1. Thus the correspondence is many-to-one at the level of microstates. At the end of the day all physical results for the eight-vertex model turn out to be independent of this choice, as should be the case.

Generalized six-vertex model. Through the face-vertex transformation the symmetric eight-vertex R-matrix is mapped into a dynamical R-matrix, which, not surprisingly, features elliptic functions. The YBE for the eight-vertex model translates to the *dynamical Yang–Baxter equation* (DYBE)

$$\begin{aligned} R_{12}(\lambda_1-\lambda_2,\theta-\gamma\,h_3)\,R_{13}(\lambda_1-\lambda_3,\theta)\,R_{23}(\lambda_2-\lambda_3,\theta-\gamma\,h_1) \\ = R_{23}(\lambda_2-\lambda_3,\theta)\,R_{13}(\lambda_1-\lambda_3,\theta-\gamma\,h_2)\,R_{12}(\lambda_1-\lambda_2,\theta)\,. \end{aligned} \tag{4.44}$$

This equation was first written down by Gervais and Neveu in 1984 [49] in the context of (Liouville) conformal field theory and later independently obtained by Felder [50] as the quantization of the modified classical YBE. Let us remark in passing that the latter is the reason for the terminology 'dynamical': such classical R-matrices are dynamical in the sense that they depend on the phase space coordinates, cf. e.g. [51]. The appropriate quantum-algebraic setting is that of elliptic quantum groups [52, 53]. The DYBE (4.44) has the usual graphical form (4.11) decorated by a fixed height θ in the left-most face of both sides of the equation:

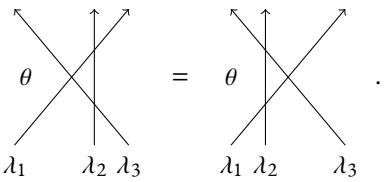

(4.45)

The elliptic solution of (4.45) is of the non-symmetric six-vertex form (3.7). We will work with the following parametrization of the entries from Figure 9:

$$a_\pm(\lambda,\theta)=f(\lambda+\gamma)\,,\quad b_\pm(\lambda,\theta)=f(\lambda)\,\frac{f(\theta\mp\gamma)}{f(\theta)}\,,\quad c_\pm(\lambda,\theta)=\frac{f(\theta\pm\lambda)}{f(\theta)}\,f(\gamma)\,. \tag{4.46}$$

Here $f(\lambda) := -\mathrm{i}\,\mathrm{e}^{-\mathrm{i}\pi\tau/4}\,\vartheta_1(\mathrm{i}\lambda|\tau)/2$ is basically the odd Jacobi theta function with elliptic nome $\mathrm{e}^{\mathrm{i}\pi\tau}\in\mathbb{C}$ such that $\mathrm{Im}(\tau)>0$, see Appendix III.A. In view of (4.38) the resulting elliptic generalized six-vertex (equivalently: SOS) model is sometimes referred to as the '8VSOS model', even though its dynamical R-matrix obeys the ice rule. It is a two-parameter extension of the six-vertex model, with additional parameters θ and $\mathrm{e}^{\mathrm{i}\pi\tau}$.

Like for the ordinary eight-vertex model, the elliptic dynamical R-matrix contains two degenerate cases: the trigonometric limit, in which $\lim_{\tau\to\mathrm{i}\infty} f(\lambda)=\sinh(\lambda)$, and the rational limit $\gamma\to 0$, which is taken as we described just before Section 4.2. Note that in each of these cases the factors in (4.46) that involve the dynamical parameter θ come in ratios. The vertices $c_\pm$ are no longer constant, but like for the six-vertex model we do have $b_\pm(0,\theta)=0$ and $c_\pm(0,\theta)=f(\gamma)$.

To make contact with the ordinary six-vertex model one takes the trigonometric limit and subsequently lets $\theta\to\infty$, which yields the ($U_q(\widehat{\mathfrak{sl}_2})$-invariant form of the) six-vertex model's R-matrix from Section 4.2. This finally also justifies our notation, where γ denotes the step size for height models as well as the crossing parameter in vertex models.

Dynamical Yang–Baxter algebra. The parametrization (4.46) is meromorphic and yields a generically invertible dynamical R-matrix, so it defines a dynamical quantum-integrable model. One can now proceed like we did in Section 4.2 for the ordinary six-vertex model. Using the ice rule and a 'train argument' as in (4.13) we obtain a decorated version of (4.14):

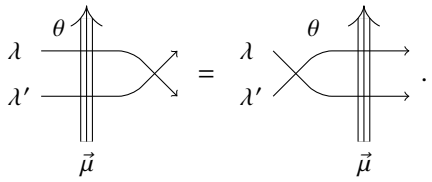

(4.47)

This is the dynamical analogue of the RTT-relation [cf. (4.12)],

$$\begin{aligned} R_{00'}(\lambda-\lambda',\theta-\gamma H)\,T_0(\lambda,\theta)\,T_{0'}(\lambda',\theta-\gamma h_0) \\ = T_{0'}(\lambda',\theta)\,T_0(\lambda,\theta-\gamma h_{0'})\,R_{00'}(\lambda-\lambda',\theta)\,, \end{aligned} \tag{4.48}$$

where H is the total spin operator (3.17). Writing the dynamical monodromy matrix as a matrix in auxiliary space we obtain four (two-parameter) families of quantum operators [cf. (3.15)]

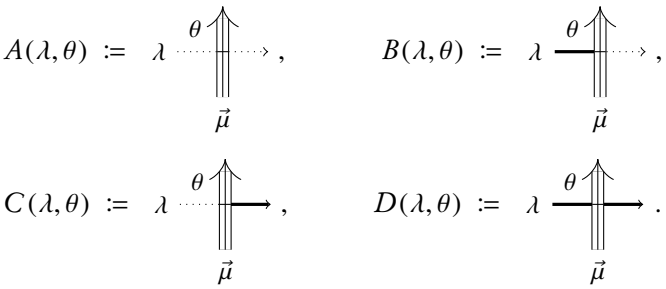

(4.49)

The graphical notation shows that the ice rule translates to [cf. (3.18)]

$$\begin{aligned} &[\,H,A(\lambda,\theta)\,]=0\,, && [\,H,B(\lambda,\theta)\,]=-2\,B(\lambda,\theta)\,, \\ &[\,H,C(\lambda,\theta)\,]=2\,C(\lambda,\theta)\,, && [\,H,D(\lambda,\theta)\,]=0\,. \end{aligned} \tag{4.50}$$

Together with (4.48) this implies that (4.49) and H satisfy the defining relations of the *dynamical Yang–Baxter algebra* (DYBA).

Algebraic Bethe ansatz. Let us conclude this section with a brief discussion of how the dynamical six-vertex model can be used to construct eigenvectors for the transfer matrix of the eight-vertex model with horizontal periodic boundary conditions. First we consider elliptic SOS model with the same boundary conditions. The algebraic Bethe ansatz

now reads

$$|\Psi_M;\vec{\lambda},\theta\rangle \coloneqq \prod_{M\geq m\geq 1}^{\leftarrow} B(\lambda_m,\theta+(M-m)\gamma)\,|\Omega\rangle =$$

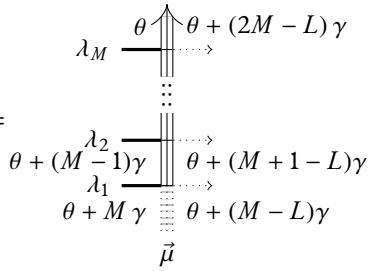

. (4.51)

One can verify that this ansatz produces eigenvectors of the dynamical transfer matrix $t(\lambda,\theta) = \mathrm{tr}_0\, T_0(\lambda,\theta)$, with eigenvalues that are independent of θ, provided the parameters $\vec{\lambda}$ satisfy certain Bethe-ansatz equations. The computation uses (4.48) and the trick from Appendix A. These Bethe vectors can then be transformed back to obtain eigenvectors of the eight-vertex transfer matrix, see e.g. [48]. As before when $M = L$ the vector (4.51) is essentially the dynamical domain-wall partition function (3.42). One can also recover (the functional form of) the TQ-equation in this way [48, §6]. Finally one can also accommodate for reflection in the dynamical setting; we leave this topic for Section III.1.1.

A Computations for the algebraic Bethe ansatz

This appendix is devoted to showing how the Yang–Baxter algebra is used to diagonalize the transfer matrix in practice, via a Fock-space construction of the space of states in terms of creation and annihilation operators. This computation will also be useful for Sections II.3.1 and III.3.1. Define the *Bethe vectors* [cf. (4.25)]

$$|\Psi_M;\vec{\lambda}\rangle \coloneqq B(\lambda_1)\cdots B(\lambda_M)\,|\Omega\rangle \in W[L-2M]\,, \tag{A.1}$$

featuring M spectral parameters λ_m. The strategy for showing that these vectors do the job goes as follows:

1. Use the relations from the Yang–Baxter algebra to work out $t(\lambda_0)\,|\Psi_M;\vec{\lambda}\rangle$.
2. Read off $\Lambda_M(\lambda_0;\vec{\lambda})$ from the *wanted* terms, proportional to $|\Psi_M;\vec{\lambda}\rangle$ as in (A.1).
3. Determine the values of the $\vec{\lambda}$ such that the remaining *unwanted* terms cancel.

We assume that all spectral parameters are distinct so that we can use (4.18).

All computational effort goes into the first step, which can be done using a nice trick that is due to Faddeev. We use the Latin alphabet for indices $m, m', \cdots$ ranging through $\{1,2,\cdots,M\}$, and Greek for indices $\nu, \rho, \cdots$ in $\{0,1,2,\cdots,M\}$.

Step 1. Our task is to calculate

$$t(\lambda_0)\,|\Psi_M;\vec{\lambda}\rangle = A(\lambda_0)\prod_{m=1}^{M} B(\lambda_m)\,|\Omega\rangle + D(\lambda_0)\prod_{m=1}^{M} B(\lambda_m)\,|\Omega\rangle\,. \tag{A.2}$$

We start with the first term on the right-hand side. Using (4.18) we can move A past the B, where at every step the two quantum operators may swap spectral parameters. Continuing in this way we obtain 2^M terms, each proportional to some $(\prod_{\rho\neq\nu} B(\lambda_\rho))A(\lambda_\nu)$ for $0 \leq \nu \leq M$. As $|\Omega\rangle$ is an eigenvector of $A(\lambda_\nu)$, see (3.24), the result of the first term on the right-hand side of (A.2) must be of the form

$$A(\lambda_0)\,|\Psi_M;\vec{\lambda}\rangle = \sum_{\nu=0}^{M} \dot{M}_\nu(\lambda_0;\vec{\lambda})\prod_{\substack{\rho=0\\ \rho\neq\nu}}^{M} B(\lambda_\rho)\,|\Omega\rangle\,. \tag{A.3}$$

(We use a dot to distinguish these coefficients from closely related but different coefficients in Section II.3.) Two of the coefficients $\dot{M}_\nu$ are easy to compute. Firstly, only one of the 2^M terms contributes to $\nu = 0$: this is the term where we always pick up the first term in (4.18), giving

$$\dot{M}_0(\lambda_0;\vec{\lambda}) = a(\lambda_0)^L \prod_{m=1}^{M} \frac{a(\lambda_m-\lambda_0)}{b(\lambda_m-\lambda_0)}\,, \tag{A.4}$$

where the prefactor is the eigenvalue Λ_A from (3.24). Secondly, the coefficient for $\nu = 1$ also only has one contribution: this comes from swapping $\lambda_0 \leftrightarrow \lambda_1$ as A moves past the first B and subsequently always picking up the first term in (4.18). Thus we find

$$\dot{M}_1(\lambda_0;\vec{\lambda}) = -a(\lambda_1)^L\,\frac{c(\lambda_1-\lambda_0)}{b(\lambda_1-\lambda_0)}\prod_{m'=2}^{M}\frac{a(\lambda_{m'}-\lambda_0)}{b(\lambda_{m'}-\lambda_0)}\,. \tag{A.5}$$

The other coefficients receive more and more contributions, and their calculation appears to be a complicated task. Luckily there is a neat trick that exploits the YBA to obtain the other coefficients without much effort. Indeed, recall that by (4.16) the B's commute. Therefore we may rearrange the creation operators in (4.25) in any way we like; in particular we may put any $B(\lambda_m)$ in front. Then, by switching 1 and m in (A.5), the above argument immediately yields

$$\dot{M}_m(\lambda_0;\vec{\lambda}) = -a(\lambda_m)^L\,\frac{c(\lambda_m-\lambda_0)}{b(\lambda_m-\lambda_0)}\prod_{\substack{m'=1\\ m'\neq m}}^{M}\frac{a(\lambda_{m'}-\lambda_m)}{b(\lambda_{m'}-\lambda_m)}\,. \tag{A.6}$$

The coefficients $\dot{N}_\nu(\lambda_0;\vec{\lambda})$ in

$$D(\lambda_0)\,|\Psi_M;\vec{\lambda}\rangle = \sum_{\nu=0}^{M} \dot{N}_\nu(\lambda_0;\vec{\lambda}) \prod_{\substack{\rho=0\\ \rho\neq\nu}}^{M} B(\lambda_\rho)\,|\Omega\rangle \tag{A.7}$$

are computed in a similar way, now using relation (4.19) from the YBA together with (3.24) and of course the trick. The result is

$$\begin{aligned} \dot{N}_0(\lambda_0;\vec{\lambda}) &= b(\lambda_0)^L \prod_{m=1}^{M} \frac{a(\lambda_0-\lambda_m)}{b(\lambda_0-\lambda_m)}\,,\\ \dot{N}_m(\lambda_0;\vec{\lambda}) &= -b(\lambda_m)^L\, \frac{c(\lambda_0-\lambda_m)}{b(\lambda_0-\lambda_m)} \prod_{\substack{m'=1\\ m'\neq m}}^{M} \frac{a(\lambda_m-\lambda_{m'})}{b(\lambda_m-\lambda_{m'})}\,. \end{aligned} \tag{A.8}$$

Step 2. Since only the terms with $\nu = 0$ in (A.3) and (A.7) are of the wanted form, the eigenvalues of the transfer matrix on $W[L-2M]$ are given by

$$\Lambda_M(\lambda_0;\vec{\lambda}) = a(\lambda_0)^L \prod_{m=1}^{M} \frac{a(\lambda_m-\lambda_0)}{b(\lambda_m-\lambda_0)} + b(\lambda_0)^L \prod_{m=1}^{M} \frac{a(\lambda_0-\lambda_m)}{b(\lambda_0-\lambda_m)}\,. \tag{A.9}$$

Step 3. The remaining terms in (A.3) and (A.7) cancel when $\dot{M}_m(\lambda_0;\vec{\lambda}) + \dot{N}_m(\lambda_0;\vec{\lambda}) = 0$ for all $1 \le m \le M$, that is, when the spectral parameters solve the system of coupled equations

$$\left(\frac{b(\lambda_m)}{a(\lambda_m)}\right)^L = \prod_{\substack{m'=1\\ m'\neq m}}^{M} \frac{a(\lambda_{m'}-\lambda_m)}{b(\lambda_{m'}-\lambda_m)}\, \frac{b(\lambda_m-\lambda_{m'})}{b(\lambda_m-\lambda_{m'})}\,, \qquad 1 \le m \le M\,. \tag{A.10}$$

where we used that $b(\lambda_m-\lambda_0) = -b(\lambda_0-\lambda_m)$. The relations (A.10) are the *Bethe-ansatz equations* for the M-particle sector.

Thus we have shown that the algebraic Bethe ansatz produces eigenvectors of the six-vertex transfer matrix provided the rapidities are *on shell*, i.e. satisfy (A.10), at least for distinct rapidities. The eigenvalue of the transfer matrix is (A.9). According to the trace identities (4.5) this quantity gives the eigenvalues of the hidden symmetries by taking logarithmic derivatives. It is now easy to show that the momentum and energy are *additive*: they are the sum of contributions that can be ascribed to the $B(\lambda_m)$ separately, see e.g. [5, §4.3]. In the spin-chain picture, where a row of the six-vertex bulk can be interpreted as the spin chain at discrete times with time increasing upwards, this allows one to view the excitations created by the B as quasiparticles.

Chapter II

Warm-up: The six-vertex model with domain walls

The topic of this chapter is the inhomogeneous zero-field six-vertex model on an $L \times L$ lattice with domain-wall boundary conditions as in Figure I.11. We will study the partition function of this model, which is known as the *domain-wall partition function*. Our goal is to prepare ourselves for Chapter III by introducing the analysis that we will use there in a more simple setting, postponing a few additional layers of technicalities as well as cumbersome formulas so that we can focus on the analysis itself.

Since its first appearance the domain-wall partition function has been studied by numerous researchers and from many different perspectives; let us mention some of the highlights. The domain-wall partition function was introduced by Korepin in 1982 [27] in the context of scalar products of Bethe vectors [cf. Section I.2.2 and Appendix I.A]. He showed that it is uniquely determined by some properties including a recurrence relation relating the partition functions for successive system sizes. Five years later Izergin [28] found an elegant and concise formula for the solution in the form of a determinant.

In 1995 Kuperberg [39] demonstrated that the six-vertex model with domain walls also has applications in combinatorics [cf. the end of Section I.2.2] and evaluated the homogeneous limit of Izergin's determinant.

The thermodynamic limit $L \to \infty$ of infinite system size was studied by Zinn-Justin at the turn of the millennium [30], who obtained an asymptotic expression for the partition function. These asymptotics were rigorously established by Bleher *et al.* in the series of papers [54]. Korepin and Zinn-Justin found that the bulk free energy is different when computed using toroidal or domain-wall boundaries at finite L. This makes the six-vertex model an important counterexample to the naive expectation that the thermodynamics should be independent of the choice of boundary conditions used at an intermediate step of the calculation [cf. Sections I.1 and I.2.2].

Outline. This chapter is organized as follows. After recalling the algebraic characterization of the domain-wall partition function and using it to derive several properties of this quantity in Section 1 we review the method of Korepin and Izergin in Section 2.

An alternative approach, due to Galleas [55–59], is presented in Section 3. We use the relations of the Yang–Baxter algebra to derive a functional equation for the domain-wall

partition function in Section 3.1. We proceed along the lines of [3] to show that this equation uniquely determines the partition function up to an overall constant factor, culminating in other formulas for the domain-wall partition function in terms of a symmetrized sum or, equivalently, a repeated contour integral. The former is a special case of a very general, yet rather involved, expression obtained by Baxter. The two approaches are compared in the concluding Section 4, while Appendix A contains a direct proof of the equality of their results.

Functional equations. Since functional equations play an important role in this chapter and the following, let us first briefly introduce them. Some general references are [60, 61]. In short, a *functional equation* is an equation that implicitly defines a function. Usually one excludes differential or integral equations, as well as ordinary algebraic equations, from the definition. (A precise definition can be found in [61] but is not very insightful.) The general theory of functional equations is much more subtle—and thus less developed—than, for instance, that of differential equations. Let us give a flavour of this with a few examples.

Cauchy's equation. Functional equations depending on more than one variable can often be studied by specialization of variables. Consider the *Cauchy equation* for additive functions

$$F(x+y) = F(x) + F(y) \tag{0.1}$$

to be solved for an unknown function F of one variable over some domain, say $\mathbb{R}$. By appropriate specializations of the variables one sees that $F(0) = 0$, so $F(-x) = -F(x)$; moreover $F(n\,x) = n\,F(x)$ for all $n \in \mathbb{N}$ and thus $F(r) = r\,F(1)$ for all $r \in \mathbb{Q}$. Clearly, a solution is $F(x) = F(1)\,x$ for any $F(1) \in \mathbb{R}$. Under mild assumptions, like continuity at any single point, these are the only solutions. The axiom of choice can be used to construct further non-continuous solutions. These so-called Hamel solutions are quite pathological; for instance, their graph is dense in $\mathbb{R}^2$.

Sometimes one can find sufficiently regular solutions by reduction to differential equations. For F differentiable, taking the derivative of (0.1) with respect to x it follows that F' is constant, which again yields $F(x) = F(1)\,x$ since $F(0) = 0$.

Cyclic functional equation. For $n \in \mathbb{N}$ consider the *cyclic* functional equation

$$\sum_{j=1}^{n} F(z_j, z_{j+1}, \cdots, z_{j+n-1}) = 0 \tag{0.2}$$

over $\mathbb{C}^n$, where we identify $z_{j+n} \equiv z_j$ for all j. It is not hard to see that the solution must be of the form $F(z_1, \cdots, z_n) = G(z_1, \cdots, z_n) - G(z_2, \cdots, z_n, z_1)$ for some function G. Reversely, for any choice of G this combination obeys (0.2). We see that a single (linear) functional equation may admit many linearly independent solutions also in reasonable function spaces.

Baxter's *TQ*-equation. In the context of this thesis one of the most famous functional equations is of course Baxter's TQ-equation (I.4.37) from Section I.4.3.

1 Domain-wall partition function

In this section we swiftly review the domain-wall partition function and derive the properties that will be useful in the rest of this chapter.

1.1 Algebraic description

Let us briefly recall the algebraic characterization of the domain-wall partition function, with references to the relevant parts of Chapter I for further details.

***R*-matrix.** Let $V = \mathbb{C}|+\rangle \oplus \mathbb{C}|-\rangle$ and fix the spectral parameter $\lambda \in \mathbb{C}$ to a generic value. The R-matrix $R(\lambda) \in \mathrm{End}(V \otimes V)$ is given by

$$R(\lambda) = \begin{pmatrix} a(\lambda) & 0 & 0 & 0 \\ 0 & b(\lambda) & c(\lambda) & 0 \\ 0 & c(\lambda) & b(\lambda) & 0 \\ 0 & 0 & 0 & a(\lambda) \end{pmatrix}, \tag{1.1}$$

where we parametrize the vertex weights as [cf. (I.4.4)]

$$a(\lambda) = \sinh(\lambda + \gamma)\,, \qquad b(\lambda) = \sinh(\lambda)\,, \qquad c(\lambda) = \sinh(\gamma)\,, \tag{1.2}$$

with $\gamma \in \mathbb{C}$ the crossing parameter. This is the solution of the Yang–Baxter equation (YBE) in $\mathrm{End}(V_1 \otimes V_2 \otimes V_3)$ [cf. (I.4.10)–(I.4.11)],

$$\begin{aligned} R_{12}(\lambda_1 - \lambda_2)\, R_{13}(\lambda_1 - \lambda_3)\, R_{23}(\lambda_2 - \lambda_3) \\ = R_{23}(\lambda_2 - \lambda_3)\, R_{13}(\lambda_1 - \lambda_3)\, R_{12}(\lambda_1 - \lambda_2)\,, \end{aligned} \tag{1.3}$$

that is symmetric, $R_{21}(\lambda) = R_{12}(\lambda)$, and obeys the ice rule [cf. (I.3.9)]

$$[\, h_1 + h_2, R_{12}(\lambda)\,] = 0\,, \tag{1.4}$$

where $h \in \mathrm{End}(V)$ is the Cartan generator keeping track of the weights (twice the spin in the z-direction) via $h|\pm\rangle = \pm|\pm\rangle$. The YBE (1.3) contains a spectral parameter $\lambda_j \in \mathbb{C}$ for each copy $V_j \cong V$ and is written using the tensor-leg notation, in which subscripts indicate on which factors V_j the operators act nontrivially [cf. Section I.3.2].

Yang–Baxter algebra. Fix L inhomogeneities $\mu_j \in \mathbb{C}$ and write $\vec{\mu} := (\mu_1, \cdots, \mu_L)$ and $W := V_1 \otimes \cdots \otimes V_L$. The monodromy matrix $T_0(\lambda; \vec{\mu}) \in \mathrm{End}(V_0 \otimes W)$ is defined as

$$T_0(\lambda;\vec{\mu}) := \prod_{L\geq j\geq 1}^{\leftarrow} R_{0j}(\lambda-\mu_j) = \quad \lambda \quad = \quad \lambda \quad \cdots \quad . \tag{1.5}$$

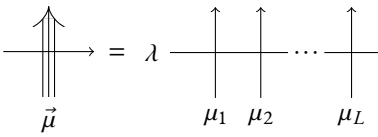

As a consequence of the Yang–Baxter equation it satisfies the RTT-relation [cf. (I.4.12)]

$$R_{00'}(\lambda_1-\lambda_2)\, T_0(\lambda_1;\vec{\mu})\, T_{0'}(\lambda_2;\vec{\mu}) = T_{0'}(\lambda_2;\vec{\mu})\, T_0(\lambda_1;\vec{\mu})\, R_{00'}(\lambda_1-\lambda_2)\,. \tag{1.6}$$

Therefore the entries of T_0, written as a matrix in auxiliary space as [cf. (I.3.15)]

$$T_0(\lambda;\vec{\mu}) = \begin{pmatrix} A(\lambda;\vec{\mu}) & B(\lambda;\vec{\mu}) \\ C(\lambda;\vec{\mu}) & D(\lambda;\vec{\mu}) \end{pmatrix}_0 , \tag{1.7}$$

furnish a representation of the Yang–Baxter algebra, which we denote by $\mathfrak{A} = A_\gamma(\mathfrak{sl}_2)$, on the quantum space W [cf. Section I.4.2]. These four quantum operators in $\mathrm{End}(W)$ have entries that are polynomial in (1.2), so they depend meromorphically on the spectral parameter.

Pseudovacua. Note that, via the total weight operator $H := \sum_{j=1}^{L} h_j \in \mathrm{End}(W)$, this representation admits a weight decomposition as in (I.4.24):

$$W = \bigoplus_{M=0}^{L} W[L-2M]\,, \qquad\qquad H|_{W[s]} = s\ \mathbb{1}\ . \tag{1.8}$$

The $\mathfrak{sl}_2$ highest- and lowest-weight vectors, or *pseudovacua*, [cf. (I.3.21)]

$$|\Omega\rangle := |+\,+\cdots+\rangle \in W[+L]\,, \qquad |\bar{\Omega}\rangle := |-\,-\cdots-\rangle \in W[-L]\,, \tag{1.9}$$

are eigenvectors of the quantum operators on the diagonal in (1.7),

$$\begin{aligned} A(\lambda;\vec{\mu})\,|\Omega\rangle &= \Lambda_A(\lambda;\vec{\mu})\,|\Omega\rangle\,, & A(\lambda;\vec{\mu})\,|\bar{\Omega}\rangle &= \bar{\Lambda}_A(\lambda;\vec{\mu})\,|\bar{\Omega}\rangle\,, \\ D(\lambda;\vec{\mu})\,|\Omega\rangle &= \Lambda_D(\lambda;\vec{\mu})\,|\Omega\rangle\,, & D(\lambda;\vec{\mu})\,|\bar{\Omega}\rangle &= \bar{\Lambda}_D(\lambda;\vec{\mu})\,|\bar{\Omega}\rangle\,. \end{aligned} \tag{1.10}$$

with (pseudo)vacuum eigenvalues [cf. (I.3.24)]

$$\Lambda_A(\lambda;\vec{\mu}) = \bar{\Lambda}_D(\lambda;\vec{\mu}) = \prod_{j=1}^{L} a(\lambda-\mu_j)\,, \quad \bar{\Lambda}_A(\lambda;\vec{\mu}) = \Lambda_D(\lambda;\vec{\mu}) = \prod_{j=1}^{L} b(\lambda-\mu_j)\,. \tag{1.11}$$

Partition function. The domain-wall partition function for system size L can be expressed as

$$Z(\vec{\lambda};\vec{\mu}) = \quad = \langle\bar{\Omega}| \prod_{j=1}^{L} B(\lambda_j;\vec{\mu})\,|\Omega\rangle\,. \tag{1.12}$$

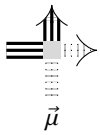

This quantity depends meromorphically on L spectral parameters λ_j and inhomogeneities μ_j, as well as the crossing parameter γ. Fix $\vec{\mu} \in \mathbb{C}^L$ and $\gamma \in \mathbb{C}$ to generic values and consider the λ_j as variables. Accordingly we suppress the inhomogeneity parameters in our notation from now on and write e.g. $Z(\vec{\lambda})$.

1.2 Properties

The domain-wall partition function (1.12) has several properties that can be established for general L without too much effort and pave the way for the analysis in Section 2 as well as Section 3.

Case $L = 1$. For length one we have [cf. Figure I.5]

$$Z(\lambda) = \quad = c(\lambda-\mu) = \sinh\gamma\,. \tag{1.13}$$

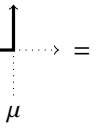

Polynomial structure. Introduce multiplicative spectral parameters $x_j := \mathrm{e}^{2\lambda_j}$. Then the 'renormalized' partition function

$$\bar{Z}(\vec{x}) := Z(\vec{\lambda}) \prod_{j=1}^{L} x_j^{(L-1)/2} \tag{1.14}$$

is a multivariate polynomial that has degree at most $L-1$ when viewed as a polynomial in any single variable x_j. (Again there is an analogous statement with respect to the inhomogeneities.)

Proof. Notice that all contributions involving x_j must be due to row j of the lattice. By the domain-wall boundaries we have at least one vertex of type c [cf. the paragraph preceding (I.2.3)], which is constant. Thus there are at most $L-1$ vertices of type a and b, each yielding a factor of the form $(g\,x_j - g^{-1})\,x_j^{-1/2}$ for some constant g involving $\vec{\mu}$ and possibly γ. □

Another way to describe the polynomial structure of the partition function is saying that $Z(\vec{\lambda})$ is a multivariate *trigonometric polynomial* of degree at most $L-1$ in each variable λ_j separately. (The name 'hyperbolic polynomial' might be more appropriate.) Since we are working over $\mathbb{C}$ this is the same as a multivariate Laurent polynomial in $\bar{x}_j := \mathrm{e}^{\lambda_j} = x_j^{1/2}$ with terms of degrees $-(L-1), \cdots, L-1$ in each variable. In particular, the degree of a trigonometric polynomial in λ_j is equal to the absolute value of the maximal and minimal degrees of the corresponding Laurent polynomial in $\bar{x}_j$.

Doubly symmetric. The partition function is invariant under the exchange of any two spectral parameters, or any two inhomogeneities.

Proof. The symmetry in spectral parameters follows immediately from the relation $B(\lambda_1)\,B(\lambda_2) = B(\lambda_2)\,B(\lambda_1)$ contained in (1.6). It is actually easy to see this directly from the RTT-relation: we have

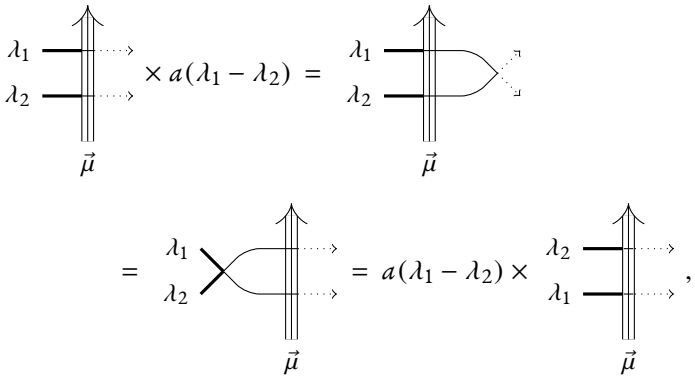

(1.15)

where we apply the ice rule in the outer equalities. The commutativity of the B's follows as the factors $a(\lambda_1 - \lambda_2)$ are generically nonzero. Likewise one shows that the partition function is also symmetric in the μ_j. □

Special points. At the point $\vec{\lambda} = \vec{\mu}$ the partition function collapses to a single term:

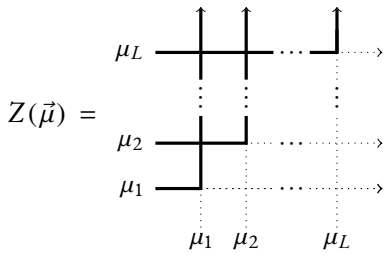

$$= c(0)^L \prod_{\substack{i,j=1 \\ i\neq j}}^{L} a(\mu_i-\mu_j) = [\gamma]^L \prod_{\substack{i,j=1 \\ i\neq j}}^{L} [\mu_i-\mu_j+\gamma], \quad (1.16)$$

where on the right-hand side we abbreviate $[\lambda] := \sinh(\lambda)$.

Proof. The first equality in (1.16) is a consequence of the domain-wall boundary and $b(0) = 0$, which allows us to force the thick lines to turn at the vertices on the anti-diagonal by appropriate choices of the spectral parameters. For example, due to the domain walls the top-right vertex in $Z(\vec{\lambda})$ in general must have weight $b(\lambda_L - \mu_L)$ or $c(\lambda_L - \mu_L)$, so setting $\lambda_L = \mu_L$ selects the latter. Together with the ice rule this determines the entire configuration on the top row and the right-most column. That is, if we for a moment use $\vec{\lambda}$ to denote $(\lambda_1, \cdots, \lambda_{L-1})$, $\vec{\mu}$ for $(\mu_1, \cdots, \mu_{L-1})$, and a triple line for $V_1 \otimes \cdots \otimes V_{L-1}$, we have

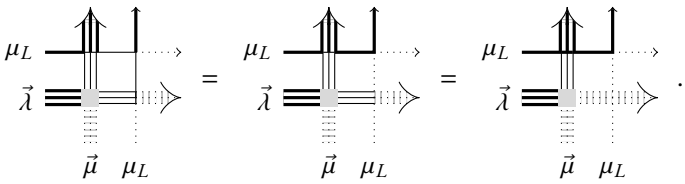

(1.17)

Repeating this argument L times we arrive at the microstate drawn in (1.16). To read off the weights we use Figure I.5 and (I.4.9). □

By symmetry in the homogeneities there are actually $L!$ special points, arising by permuting the components of $\vec{\mu}$. In fact there are $L!$ further points at which the domain-wall partition function only has one contributing configuration, yielding the same value:

$$Z(\mu_L - \gamma, \cdots, \mu_1 - \gamma) =$$

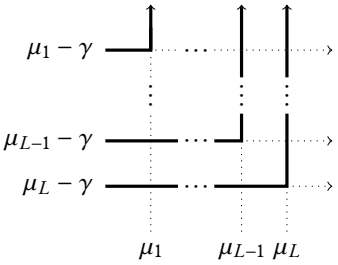

$$= [\gamma]^L \prod_{\substack{i,j=1 \\ i \neq j}}^{L} [\mu_i - \mu_j + \gamma] \,. \quad (1.18)$$

Proof. The argument is similar. This time we use $a(-\gamma) = 0$ to force the thick lines to turn at the vertices on the diagonal. For instance, because of the domain-wall boundaries the bottom-right vertex in Z must in general be of type a or c; by setting $\lambda_1 = \mu_1 - \gamma$ we select the latter. The ice rule then fixes the entire bottom row and the column on the right. Apply this reasoning L times. In the second equality we use $[\mu_j - \gamma - \mu_i] = -[\mu_i - \mu_j + \gamma]$ yielding an even number, $L(L-1)$, of signs. □

Figure 1 shows the configurations from (1.16) and (1.18) in the height-model picture, where they correspond to the highest and lowest profiles allowed by domain walls.

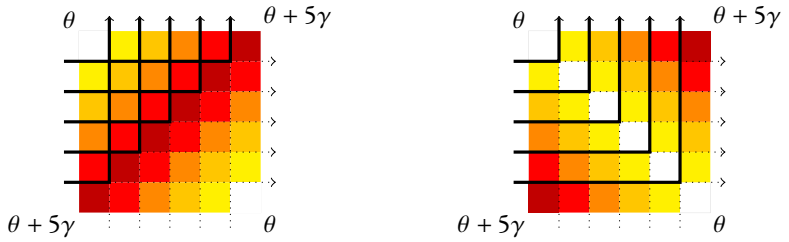

Figure 1. [Colour online] Height profiles corresponding to the only microstates that contribute to the domain-wall partition function (1.12) for $L = 5$ at the special points **(a)** $\vec{\lambda} = \vec{\mu}$, corresponding to (1.16), and **(b)** $\vec{\lambda} = (\mu_L - \gamma, \cdots, \mu_1 - \gamma)$, for (1.18). The heights run from white (low) to dark red (high). Recall that the height profile is determined by the spin configuration via the dictionary in Figure I.8.

2 Korepin–Izergin method

Korepin found a simple recurrence relation between domain-wall partition functions for consecutive system sizes, which was solved in terms of an elegant formula by Izergin. In this section we briefly discuss this approach based on the exposition in [29, 39, 62]. We write Z_L if we want to stress the system size L for the partition function.

Korepin's recurrence relation. By specializing $\lambda_{L+1} = \mu_{L+1}$ one obtains a recurrence relation for the domain-wall partition function:

$$\begin{aligned} Z_{L+1}(\vec{\lambda}, \mu_{L+1}; \vec{\mu}, \mu_{L+1}) &= \Big(c(0) \prod_{j=1}^{L} a(\lambda_j - \mu_{L+1})\, a(\mu_{L+1} - \mu_j)\Big)\, Z_L(\vec{\lambda}; \vec{\mu}) \\ &= \Big([\gamma] \prod_{j=1}^{L} [\lambda_j - \mu_{L+1} + \gamma\,, \mu_{L+1} - \mu_j + \gamma]\Big)\, Z_L(\vec{\lambda}; \vec{\mu})\,, \end{aligned} \tag{2.1}$$

where again $[\lambda] := \sinh(\lambda)$, and $[\lambda_1, \lambda_2] := [\lambda_1][\lambda_2]$. By the symmetry of Z in the spectral parameters, and in the inhomogeneities, one finds a similar relation for any specialization $\lambda_i = \mu_j$.

Proof. The argument is simple: it is as in (1.17), now with $L + 1$ instead of L. □

Actually, rather setting $\lambda_i = \mu_j - \gamma$ [cf. (1.18)] we obtain similar recurrence relations,

including

$$\begin{aligned} Z_{L+1}(\mu_{L+1}-\gamma,\vec{\lambda};\vec{\mu},\mu_{L+1}) &= \Big(c(0)\prod_{j=1}^{L} b(\lambda_j-\mu_{L+1})\,b(\mu_{L+1}-\mu_j-\gamma)\Big)\,Z_L(\vec{\lambda};\vec{\mu}) \\ &= \Big([\gamma]\prod_{j=1}^{L}[\lambda_j-\mu_{L+1},\mu_{L+1}-\mu_j-\gamma]\Big)\,Z_L(\vec{\lambda};\vec{\mu})\,. \end{aligned} \tag{2.2}$$

However, (2.1) already suffices by the following observation.

Uniqueness. The recurrence relation (2.1), together with its analogues for $\lambda_i = \mu_j$, completely determines Z_{L+1} in terms of Z_L. Indeed, for each spectral parameter λ_i we have $L+1$ distinct values at which Z_{L+1} can be expressed in terms of Z_L. Since Z_{L+1} has degree at most L in λ_i, the recurrence relation has a unique solution matching (1.13) for $L = 1$, if there exists such a solution. (Note that this argument uses that the inhomogeneities μ_j have generic values to get sufficient different points; in particular, it fails in the homogeneous case.)

Izergin's solution. We have seen that in the present approach it is not hard to find a recurrence relation (2.1) for the partition function. The difficulty lies in finding a closed expression for the solution. Izergin obtained a remarkably concise formula for the partition function in terms of a determinant:

$$\begin{aligned} Z_L(\vec{\lambda};\vec{\mu}) &= [\gamma]^L\,\frac{\prod_{i,j=1}^{L}[\lambda_i-\mu_j,\lambda_i-\mu_j+\gamma]}{\prod_{1\le i<j\le L}[\lambda_i-\lambda_j,\mu_j-\mu_i]}\,\det K(\vec{\lambda};\vec{\mu})\,, \\ K_{ij}(\vec{\lambda};\vec{\mu}) &\coloneqq \frac{1}{[\lambda_i-\mu_j,\lambda_i-\mu_j+\gamma]}\,. \end{aligned} \tag{2.3}$$

This expression goes under the name *Izergin–Korepin formula*. Note that $\det K(\vec{\lambda};\vec{\mu})$ is an antisymmetric (alternating) function in the λ_i and in the μ_j. Such a doubly alternating determinant is known as a *double alternant*. The prefactor in (2.3) hides another double alternant: a hyperbolic version of the Cauchy determinant,

$$\frac{\prod_{i,j=1}^{L}[\lambda_i-\mu_j]}{\prod_{1\le i<j\le L}[\lambda_i-\lambda_j,\mu_j-\mu_i]} = \frac{1}{\det L(\vec{\lambda};\vec{\mu})}\,, \qquad L_{ij}(\vec{\lambda};\vec{\mu}) \coloneqq \frac{1}{[\lambda_i-\mu_j]}\,. \tag{2.4}$$

Proof. It is not hard to check that (2.3) has the desired properties, in which case it must be the unique solution. For $L = 1$ we immediately recover (1.13). The double symmetry is also clear as both the overall factor and the determinant are antisymmetric under the exchange of two spectral parameters or two inhomogeneities. For the polynomial structure the crucial observations are [39, p. 6]

- $\det K \prod_{i,j}[\lambda_i - \mu_j + \gamma\,, \lambda_i - \mu_j]$ is a trigonometric polynomial in the vertex weights, of degree at most $2(L-1)$ in each variable;
- $\prod_{i<j}[\lambda_i - \lambda_j]$ divides that polynomial [the simple pole in (2.3) arising as $\lambda_i \to \lambda_j$ has vanishing residue] by antisymmetry of the determinant, thus reducing the degree in each variable by $L-1$.

Finally, to check that (2.3) obeys Korepin's recurrence relation note that as $\lambda_L \to \mu_L$ the simple zero in the prefactor is (precisely) countered by the simple pole in K_{LL}, and the remaining factors yield (2.1). [By focussing on the zero and pole due to $a(\lambda_i - \mu_j)$ rather than $b(\lambda_i - \mu_j)$ one likewise sees that (2.3) satisfies (2.2) too.] □

In the decades following the papers of Korepin and Izergin further insight was gained into the structure of Izergin's determinant and related expressions due to work of Stroganov, Lascoux, and others; see e.g. [63, §3.1] for an account of some of the results in this direction.

3 Constructive method

Another way to compute the partition function, based on functional equations for *fixed* system size L, was found by Galleas. For the domain-wall partition function the first such functional equation was derived in [55] and then solved in [56] in terms of a repeated contour integral. The method was further simplified in [57, 58] for the generalized six-vertex model on the same lattice. The analysis was streamlined in later work of Galleas and me [1, 3] in the case of a reflecting end: this is the topic of Chapter III.

In this section we discuss the derivation and analysis of such a functional equation for the domain-wall partition function (1.12) following [3] to illustrate the workings of Chapter III in the simplest possible setting, without the complications due to reflection or the dynamical nature of SOS models and generalized six-vertex models. The resulting functional equation is simpler than the original one from [55] and was first written down by Galleas in [59]. We present a systematic and complete analysis of the equation, emphasizing that it provides a constructive alternative to the Korepin–Izergin approach of Section 2.

Like in Appendix I.A we use the Latin alphabet for indices $i, j, \cdots$ taking values in $\{1, 2, \cdots, L\}$, and Greek for indices $\nu, \rho, \cdots$ in $\{0, 1, 2, \cdots, L\}$.

3.1 Functional equations from the Yang–Baxter algebra

Let us show that the domain-wall partition function for system size L satisfies the functional equation

$$\sum_{\nu=0}^{L} M_\nu(\lambda_0; \vec{\lambda})\, Z(\lambda_0, \cdots, \widehat{\lambda_\nu}, \cdots, \lambda_L) = 0\,, \tag{3.1}$$

where the caret indicates that the ν'th spectral parameter is omitted, and the coefficients are

$$\begin{aligned} M_0(\lambda_0;\vec{\lambda}) &= \bar{\Lambda}_A(\lambda_0;\vec{\mu}) - \Lambda_A(\lambda_0;\vec{\mu}) \prod_{j=1}^{L} \frac{a(\lambda_j-\lambda_0)}{b(\lambda_j-\lambda_0)}\,, \\ M_i(\lambda_0;\vec{\lambda}) &= \Lambda_A(\lambda_i;\vec{\mu})\, \frac{c(\lambda_i-\lambda_0)}{b(\lambda_i-\lambda_0)} \prod_{\substack{j=1\\ j\neq i}}^{L} \frac{a(\lambda_j-\lambda_i)}{b(\lambda_j-\lambda_i)}\,. \end{aligned} \tag{3.2}$$

As before we often suppress the dependence on the inhomogeneities, which are fixed to generic values.

Proof (Galleas). The starting point is the algebraic formula (1.12) for the domain-wall partition function. Since both pseudovacua (1.9) are eigenvectors of $A(\lambda_0)$ we can introduce the latter quantum operator at the expense of an eigenvalue (1.10):

$\bar{\Lambda}_A(\lambda_0)\, Z(\vec{\lambda}) =$ 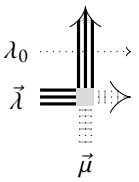 $= \langle\bar{\Omega}|\, A(\lambda_0) \prod_{j=1}^{L} B(\lambda_j)\, |\Omega\rangle\,.$ (3.3)

Using the relations of the Yang–Baxter algebra we can move A to the other side of the product of B's, where it may or may not exchange spectral parameters with every B it passes. This computation is the same as the one for the algebraic Bethe ansatz from Appendix I.A for the special case $M = L$, using the trick that exploits the commutativity of the B's. The result is a linear combination of terms of the form

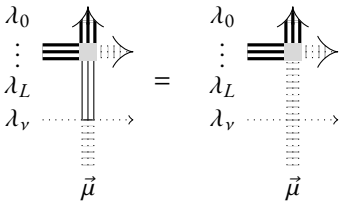 $= \Lambda_A(\lambda_\nu)\, Z(\lambda_0,\cdots,\widehat{\lambda_\nu},\cdots,\lambda_L)\,.$ (3.4)

The conclusion is that the domain-wall partition obeys the functional equation

$$\bar{\Lambda}_A(\lambda_0)\, Z(\vec{\lambda}) = \sum_{\nu=0}^{L} \dot{M}_\nu(\lambda_0;\vec{\lambda})\, Z(\lambda_0,\cdots,\widehat{\lambda_\nu},\cdots,\lambda_L)\,, \tag{3.5}$$

where the coefficients $\dot{M}_\nu$ reduce to (I.A.4)–(I.A.6) in the homogeneous limit. This yields (3.8)–(3.9) with $M_0 = \bar{\Lambda}_A - \dot{M}_0$ and $M_i = -\dot{M}_i$. □

Since the preceding derivation can also be viewed as the application of the (linear) *functional* $\pi_L = \langle\tilde{\Omega}| \cdot |\Omega\rangle$ to the Yang–Baxter-*algebra* relation

$$A(\lambda_0)\prod_{j=1}^{L} B(\lambda_j) = \prod_{j=1}^{L}\frac{a(\lambda_j-\lambda_0)}{b(\lambda_j-\lambda_0)}\prod_{j=1}^{L} B(\lambda_j)\,A(\lambda_0) - \sum_{i=1}^{L}\frac{c(\lambda_i-\lambda_0)}{b(\lambda_i-\lambda_0)}\prod_{\substack{j=1\\ j\neq i}}^{L}\frac{a(\lambda_j-\lambda_i)}{b(\lambda_j-\lambda_i)}\prod_{\substack{\rho=0\\ \rho\neq i}}^{L} B(\lambda_\rho)\,A(\lambda_i)\,, \tag{3.6}$$

this way of extracting functional equations is also known as the *algebraic-functional method*.

The functional equation (3.1) is said to be of 'type A'. As the pseudovacua are also eigenvectors of $D(\lambda_0)$ we could equally well have inserted the latter operator to derive a functional equation of 'type D', instead using [cf. (I.A.8)]

$$D(\lambda_0)\prod_{j=1}^{L} B(\lambda_j) = \prod_{j=1}^{L}\frac{a(\lambda_0-\lambda_j)}{b(\lambda_0-\lambda_j)}\prod_{j=1}^{L} B(\lambda_j)\,D(\lambda_0) - \sum_{i=1}^{L}\frac{c(\lambda_0-\lambda_i)}{b(\lambda_0-\lambda_i)}\prod_{\substack{j=1\\ j\neq i}}^{L}\frac{a(\lambda_i-\lambda_j)}{b(\lambda_i-\lambda_j)}\prod_{\substack{\rho=0\\ \rho\neq i}}^{L} B(\lambda_\rho)\,D(\lambda_i)\,. \tag{3.7}$$

Originally Galleas worked with a functional equation of 'type C', whose form is rather more complicated [55, 56]. In the following sections we will see that the functional equation (3.1)–(3.2) already suffices to characterize the partition function, and we do not need the explicit form of the other functional equations.

3.2 Properties of the functional equation and its solutions

Let us reserve the symbol 'Z' for the domain-wall partition function (1.12), and study the functional equation

$$\sum_{\nu=0}^{L} M_\nu(\lambda_0;\vec{\lambda})\,F(\lambda_0,\cdots,\widehat{\lambda_\nu},\cdots,\lambda_L) = 0\,, \tag{3.8}$$

with coefficients (3.2) explicitly given by

$$
\begin{aligned}
M_0(\lambda_0;\vec{\lambda};\vec{\mu}) &= \prod_{j=1}^{L}[\lambda_0-\mu_j]-\prod_{j=1}^{L}[\lambda_0-\mu_j+\gamma]\,\frac{[\lambda_j-\lambda_0+\gamma]}{[\lambda_j-\lambda_0]}\,,\\
M_i(\lambda_0;\vec{\lambda};\vec{\mu}) &= \frac{[\gamma]}{[\lambda_i-\lambda_0]}\prod_{j=1}^{L}[\lambda_i-\mu_j+\gamma]\prod_{\substack{j=1\\ j\neq i}}^{L}\frac{[\lambda_j-\lambda_i+\gamma]}{[\lambda_j-\lambda_i]}\,,
\end{aligned}
\tag{3.9}
$$

where we once more abbreviate $[\lambda] \coloneqq \sinh(\lambda)$. We will also use the n-ary extension $[\lambda_1,\lambda_2,\cdots] \coloneqq [\lambda_1][\lambda_2]\cdots$. In the terminology of [61], (3.8) is a cyclic linear functional equation, cf. (0.2). Observe that it features $L+1$ variables whilst the partition function depends on only L spectral parameters.

The properties of the domain-wall partition function listed in Section 1.2 tell us to seek a solution F on $\mathbb{C}^L$ in the class of symmetric multivariate trigonometric polynomials that in each variable are of degree at most $L-1$. Since our functional equation is linear in F it can at best determine any solution up to an overall constant (i.e. $\vec{\lambda}$-independent) factor. As we will see in Section 3.3, the solution is indeed unique up to such a constant. Thus the desired normalization can be fixed by computing the value of the partition function Z at any single point at which it does not vanish. Convenient choices are sending all spectral parameters to infinity to fix the leading coefficient [55], or more simply either of the special points (1.16) or (1.18).

The many nice properties of the domain-wall partition function are reflected in the functional equation. In this section we take a closer look at the equation and derive several properties of any nice-enough solution.

Properties of the functional equation. Recall that we use i,j for indices running through $\{1,\cdots,L\}$. The coefficients (3.9) are manifestly symmetric in the μ_j. Moreover, in view of the commutativity of the B's, the proof in Section 3.1 also shows that the equation (3.1) is invariant under the interchange of variables $\lambda_i \leftrightarrow \lambda_j$. This means that the coefficients (3.2), viewed as functions M_ν on $\mathbb{C}^{L+1}$, enjoy the following symmetries:

- $M_0(\lambda_0;\vec{\lambda})$ is symmetric in all λ_j ;
- $M_i(\lambda_0;\vec{\lambda})$ is symmetric in the λ_j with $j\neq i$; (3.10)
- $M_i(\lambda_0;\vec{\lambda})|_{\lambda_i\leftrightarrow\lambda_j} = M_j(\lambda_0;\vec{\lambda})$.

This is also evident from (3.2).

When we instead exchange $\lambda_0 \leftrightarrow \lambda_i$ in (3.1) we get another functional equation, of the same form (3.1) but with different coefficients. Thus, in fact, we obtain L additional

functional equations

$$\sum_{\nu=0}^{L} M_{i,\nu}(\lambda_0;\vec{\lambda})\, F(\lambda_0,\cdots,\widehat{\lambda_\nu},\cdots,\lambda_L) = 0\,, \qquad 1 \le i \le L\,, \tag{3.11}$$

all satisfied by the solution to any single of these equations; here we assume that F is symmetric, which will be justified soon, to rearrange it arguments. For example, when $L = 3$ switching λ_0 and λ_2 gives

$$\begin{aligned} &M_0(\lambda_0;\vec{\lambda})|_{\lambda_0\leftrightarrow\lambda_2}\, F(\lambda_1,\lambda_0,\lambda_3) + M_1(\lambda_0;\vec{\lambda})|_{\lambda_0\leftrightarrow\lambda_2}\, F(\lambda_2,\lambda_0,\lambda_3) \\ &\quad + M_2(\lambda_0;\vec{\lambda})|_{\lambda_0\leftrightarrow\lambda_2}\, F(\lambda_2,\lambda_1,\lambda_3) + M_3(\lambda_0;\vec{\lambda})|_{\lambda_0\leftrightarrow\lambda_2}\, F(\lambda_2,\lambda_1,\lambda_0) = 0\,. \end{aligned} \tag{3.12}$$

Reordering the arguments of F we read off that $M_{2,0}(\lambda_0;\vec{\lambda}) = M_2(\lambda_2;\lambda_1,\lambda_0,\lambda_3) = M_1(\lambda_2;\lambda_0,\lambda_1,\lambda_3)$, where in the last equality we carefully use (3.10) to rearrange the arguments. Likewise we find that $M_{2,1}(\lambda_0;\vec{\lambda}) = M_1(\lambda_2;\lambda_1,\lambda_0,\lambda_3) = M_2(\lambda_2;\lambda_0,\lambda_1,\lambda_3)$ while $M_{2,2}(\lambda_0;\vec{\lambda}) = M_0(\lambda_2;\lambda_1,\lambda_0,\lambda_3) = M_0(\lambda_2;\lambda_0,\lambda_1,\lambda_3)$ and finally $M_{2,3}(\lambda_0;\vec{\lambda}) = M_3(\lambda_2;\lambda_1,\lambda_0,\lambda_3) = M_3(\lambda_2;\lambda_0,\lambda_1,\lambda_3)$. For general L and i the coefficients in (3.11) can similarly be written in terms of the original coefficients (3.2) as

$$\begin{aligned} M_{i,\nu}(\lambda_0;\vec{\lambda}) &= \begin{cases} M_i(\lambda_0;\vec{\lambda})|_{\lambda_0\leftrightarrow\lambda_i} & \nu = 0\,, \\ M_0(\lambda_0;\vec{\lambda})|_{\lambda_0\leftrightarrow\lambda_i} & \nu = i\,, \\ M_\nu(\lambda_0;\vec{\lambda})|_{\lambda_0\leftrightarrow\lambda_i} & \nu \in \{1,\cdots,L\}\setminus\{i\}\,, \end{cases} \\ &= \begin{cases} M_{\nu+1}(\lambda_i;\lambda_0,\cdots,\widehat{\lambda_i},\cdots,\lambda_L) & \nu \in \{0,\cdots,i-1\}\,, \\ M_0(\lambda_i;\lambda_0,\cdots,\widehat{\lambda_i},\cdots,\lambda_L) & \nu = i\,, \\ M_\nu(\lambda_i;\lambda_0,\cdots,\widehat{\lambda_i},\cdots,\lambda_L) & \nu \in \{i+1,\cdots,L\}\,. \end{cases} \end{aligned} \tag{3.13}$$

In any case, the resulting system of $L+1$ functional equations can be recast in the form

$$\begin{pmatrix} M_0(\lambda_0;\vec{\lambda}) & M_1(\lambda_0;\vec{\lambda}) & \cdots & M_L(\lambda_0;\vec{\lambda}) \\ M_{1,0}(\lambda_0;\vec{\lambda}) & M_{1,1}(\lambda_0;\vec{\lambda}) & \cdots & M_{1,L}(\lambda_0;\vec{\lambda}) \\ \vdots & \vdots & \ddots & \vdots \\ M_{L,0}(\lambda_0;\vec{\lambda}) & M_{L,1}(\lambda_0;\vec{\lambda}) & \cdots & M_{L,L}(\lambda_0;\vec{\lambda}) \end{pmatrix} \begin{pmatrix} F(\lambda_1,\cdots,\lambda_L) \\ F(\lambda_0,\lambda_2,\cdots,\lambda_L) \\ \vdots \\ F(\lambda_0,\cdots,\lambda_{L-1}) \end{pmatrix} = 0\,. \tag{3.14}$$

As the partition function certainly is nonzero we know that there exists a nontrivial solution, so this matrix must have vanishing determinant. This can indeed be verified by analytic or numerical inspection for given L.

Properties of solutions. Any sufficiently nice solution F of the functional equation (3.8) automatically has several of the properties of the domain-wall partition function Z listed in Section 1.2.

Bound on the degree. The functional equation also gives an upper bound for the polynomial degree of its solutions in any single variable: any solution F that is a multivariate trigonometric polynomial has degree at most $L-1$ in each of its variables.

Proof. Let us remove all poles in the coefficients by defining rescaled versions

$$\bar{M}_\nu(\lambda_0;\vec{\lambda}) \coloneqq M_\nu(\lambda_0;\vec{\lambda}) \prod_{0\le\rho<j\le L} [\lambda_\rho - \lambda_j]\,. \tag{3.15}$$

From the explicit expressions (3.9) we read off that, as a trigonometric polynomial, $\bar{M}_0$ is of degree at most $2L$ in λ_0 and degree at most L in each λ_j, while $\bar{M}_i$ has degree $L-1$ in λ_0, degree $2L-1$ in λ_i, and degree L in the other λ_j, $j\neq i$. The actual degrees of $\bar{M}_0$ might be lower due to cancellations between its two terms. To investigate this possibility let us determine the leading behaviour of $\bar{M}_0$ for large $\bar{x}_0 \coloneqq \mathrm{e}^{\lambda_0}$,

$$\begin{aligned}\bar{M}_0(\lambda_0;\vec{\lambda}) &\propto \prod_{j=1}^{L}[\lambda_0-\mu_j\,,\lambda_0-\lambda_j] - \prod_{j=1}^{L}[\lambda_0-\mu_j+\gamma\,,\lambda_0-\lambda_j-\gamma]\\ &\propto (1-1)\,\bar{x}_0^{2L} - \Big(\sum_{j=1}^{L}\mathrm{e}^{2\mu_j}+\mathrm{e}^{2\lambda_j}-\mathrm{e}^{2(\mu_j-\gamma)}-\mathrm{e}^{2(\lambda_j+\gamma)}\Big)\,\bar{x}_0^{2(L-1)}+\dots\,,\end{aligned} \tag{3.16}$$

where we drop an overall factor of $2^{-2L}\prod_j \mathrm{e}^{-\mu_j-\lambda_j}$ in the second proportionality sign. The terms in (3.16) involving $\bar{x}_0^{2L}$ come from the leading behaviour $[\lambda_0-\mu]\sim 2^{-1}\,\mathrm{e}^{-\mu}\,\bar{x}_0$, the terms with $\bar{x}_0^{2(L-1)}$ arise by picking up a subleading part $-2^{-1}\,\mathrm{e}^{\mu}\,\bar{x}_0^{-1}$ for one factor in the first line, and the dots indicate terms of lower order in $\bar{x}_0$. Therefore, when $\gamma\neq 0$, $\bar{M}_0$ actually has degree $2(L-1)$ as a trigonometric polynomial in λ_0. It is easy to see that the coefficients of the leading terms of $\bar{M}_0$ in the other variables are generically nonzero, so the degree of $\bar{M}_0$ in the λ_j is equal to L.

Now consider the functional equation (3.8) with both sides multiplied with the same factor as in (3.15). The degree of the desired solution follows by comparing the degrees of the various terms of this rescaled functional equation in the variables. [The degree could again be lower if cancellations occur between different terms in (3.8).] □

Symmetric. Although (3.8) is not manifestly symmetric in *all* spectral parameters, cf. the above discussion, in [57] it was first noticed that if F is meromorphic then it is symmetric in the spectral parameters as well. We follow the proof of [1].

Proof. The coefficients (3.9) exhibit singularities for coinciding spectral parameters. Since the right-hand side of the functional equation is zero any poles must either cancel each other or be countered by zeroes. In the limit $\lambda_0\to\lambda_i$ only M_0 and M_i have poles,

which are simple. Interestingly, the residues only differ by a sign:

$$\begin{aligned}\mathrm{Res}_{\lambda_0=\lambda_i} M_0(\lambda_0;\vec{\lambda}) &= -\mathrm{Res}_{\lambda_0=\lambda_i} M_i(\lambda_0;\vec{\lambda}) \\ &= [\gamma]\prod_{j=1}^{L}[\lambda_i-\mu_j+\gamma]\prod_{\substack{j=1\\ j\neq i}}^{L}\frac{[\lambda_j-\lambda_i+\gamma]}{[\lambda_j-\lambda_i]}\,,\end{aligned} \tag{3.17}$$

where we use $\mathrm{Res}_{\lambda_0=\lambda_i} 1/[\lambda_i-\lambda_0] = -1/\sinh'(0) = -1$. Under the assumptions on F we thus see that the residue of the left-hand side of (3.8) is

$$\Big(F(\lambda_1,\cdots,\lambda_L) - F(\lambda_0,\cdots,\widehat{\lambda_i},\cdots,\lambda_L)\big|_{\lambda_0=\lambda_i}\Big)\,\mathrm{Res}_{\lambda_0=\lambda_i} M_0(\lambda_0;\vec{\lambda})\,. \tag{3.18}$$

This expression must vanish for any F solving the functional equation. Since the quantities in (3.17) are generically nonzero, this implies that such F obeys $F(\lambda_i,\lambda_1,\cdots,\widehat{\lambda_i},\cdots,\lambda_L) = F(\lambda_1,\cdots,\lambda_L)$. In other words, sufficiently regular solutions are invariant under cyclic permutations of the first i arguments.

Recall that any two cycles of length two and L already generate the entire permutation group S_L. Using the above argument for $i=2$ and $i=L$ we may thus conclude that any meromorphic solution is necessarily symmetric. □

The symmetry of the coefficients (3.9) in the inhomogeneity parameters implies that switching two inhomogeneities in the functional equation (3.8) maps solutions to solutions. Once we have shown that (reasonable) solutions are unique up to normalization, see Section 3.3, this implies that F is also symmetric in the inhomogeneities.

Special zeroes. Finally, any solution F of (3.8) vanishes whenever we set $\lambda_i = \mu_k - \gamma$ and $\lambda_j = \mu_k$ for some $i,j,k \in \{1,\cdots,L\}$ with $i \neq j$. [Note that this vanishing property certainly holds for the partition function (1.12): by symmetry in the variables and inhomogeneities one can take $j=k=L$ and use Korepin's relation (2.1) or (2.2).] Following [57] we refer to the L pairs $(\mu_k-\gamma,\mu_k)$ as *special zeroes* of F.

Proof. Choose a $k \in \{1,\cdots,L\}$. By symmetry in the spectral parameters we may assume that $i = L-1$ and $j = L$. Observe that for any $1 \le k \le L$ the coefficients M_{L-1} and M_L vanish when $\lambda_{L-1} = \mu_k - \gamma$ and $\lambda_L = \mu_k$, so F must satisfy

$$\sum_{\nu=0}^{L-2} M_\nu(\lambda_0;\lambda_1,\cdots,\lambda_{L-2},\mu_k-\gamma,\mu_k)\,F(\lambda_0,\cdots,\widehat{\lambda_\nu},\cdots,\lambda_{L-2},\mu_k-\gamma,\mu_k) = 0\,. \tag{3.19}$$

Since all quantities are analytic in the inhomogeneities we are free to set $\mu_k = \lambda_0$. The coefficients in (3.19) then become rather simple:

$$\begin{aligned}\check{M}_\nu &:= M_\nu(\lambda_0;\lambda_1,\cdots,\lambda_{L-2},\mu_k-\gamma,\mu_k)\big|_{\mu_k=\lambda_0} \\ &= [\gamma]\prod_{\substack{j=1\\ j\neq k}}^{L}[\lambda_\nu-\mu_j+\gamma]\prod_{\substack{\rho=0\\ \rho\neq\nu}}^{L-2}\frac{[\lambda_\rho-\lambda_\nu+\gamma]}{[\lambda_\rho-\lambda_\nu]}\,.\end{aligned} \tag{3.20}$$

As we described above, see (3.11), swapping $\lambda_0 \leftrightarrow \lambda_j$ in (3.19) gives rise to $L-2$ more functional equations of a similar form. When we write this system of equations in matrix form as in (3.14), our task is to show that the determinant of the resulting $(L-1)\times(L-1)$ matrix is nonzero. By (3.13) this matrix is given by

$$\begin{pmatrix} \check{M}_0 & \check{M}_1 & \cdots & \check{M}_{L-3} & \check{M}_{L-2} \\ \check{M}_1 & \check{M}_0 & & \check{M}_{L-3} & \check{M}_{L-2} \\ \vdots & & \ddots & & \vdots \\ \check{M}_{L-3} & \check{M}_1 & & \check{M}_0 & \check{M}_{L-2} \\ \check{M}_{L-2} & \check{M}_1 & \cdots & \check{M}_{L-3} & \check{M}_0 \end{pmatrix}. \tag{3.21}$$

By subtracting the first row from all other rows and then adding to the first column all other columns we obtain an upper-triangular matrix:

$$\begin{pmatrix} \check{M}_0+\cdots+\check{M}_{L-2} & \check{M}_1 & \cdots & \check{M}_{L-3} & \check{M}_{L-2} \\ 0 & \check{M}_0-\check{M}_1 & & 0 & 0 \\ \vdots & & \ddots & & \vdots \\ 0 & 0 & & \check{M}_0-\check{M}_{L-3} & 0 \\ 0 & 0 & \cdots & 0 & \check{M}_0-\check{M}_{L-2} \end{pmatrix}. \tag{3.22}$$

Thus the determinant of (3.21) is a simple product, $(\check{M}_0+\cdots+\check{M}_{L-2})\prod_{j=1}^{L-2}(\check{M}_0-\check{M}_j)$. From the text below (3.16) it follows that if we remove the denominators of the (3.20), as in (3.15), then $\check{M}_\nu$ has highest degree in λ_ν. This implies that each factor in the determinant is generically nonzero, so that (3.21) is invertible, which is what we wanted to show. □

3.3 Reduction, recursion and solution

According to the above discussion we may look for solutions within the class of trigonometric polynomials. Note that the functional equation (3.8) involves $L+1$ variables whilst F only has L arguments. This motivates looking for special values to which we can specialize any single variable in the equation, cf. the solution to Cauchy's equation (0.1). For $k \in \{1,\cdots,L\}$ we see from (3.9) that the greatest simplifications in (3.8) occur when either

- $\lambda_i = \mu_k - \gamma$, so that M_i vanishes;
- $\lambda_0 = \mu_k - \gamma$, whence M_0 becomes a single $\vec{\lambda}$-independent product, $\bar{\Lambda}_A(\mu_k-\gamma)$, that is nonzero for generic inhomogeneities and crossing parameter.

The first option yields a functional equation with L terms in which all F's involve $\lambda_i = \mu_k - \gamma$. The second option is more interesting.

Case $L = 1$. For $L = 1$ the functional equation (3.8) has two terms. The first option is not useful as $M_0(\lambda_0; \mu_1 - \gamma) = M_1(\lambda_0; \mu_1 - \gamma) = 0$. However, since $M_0(\mu_1 - \gamma; \lambda_1) = -M_1(\mu_1 - \gamma; \lambda_1) = -[\gamma]$, the specialization $\lambda_0 = \mu_1 - \gamma$ implies that any solution $F(\lambda_1) = F(\mu_1 - \gamma)$ is a constant. Adjusting this constant to agree with (1.16) we recover the partition function (1.13). [For $L = 1$ one arrives at the same conclusion by setting $\lambda_0 = \mu_1$.]Alternatively one can expand M_0 and M_1 in e^{λ_ν} and separate variables to arrive at the same conclusion.

Reduction. For $L \geq 2$ fix a choice of $k \in \{1, \cdots, L\}$ and write $\lambda_\star := \mu_k - \gamma$. Any analytic solution F of (3.8) can be written as

$$F(\vec{\lambda}) = \sum_{i=1}^{L} M_i(\lambda_\star; \vec{\lambda})\, \widetilde{F}_\star(\lambda_1, \cdots, \widehat{\lambda_i}, \cdots, \lambda_L) \prod_{\substack{j=1 \\ j\neq i}}^{L} [\lambda_j - \mu_k]\,, \tag{3.23}$$

where $\widetilde{F}_\star$ is a trigonometric polynomial in $\mathbb{C}^{L-1}$ of degree $L-2$ in each variable that is symmetric in the spectral parameters.

Proof. For general system size L the second option for suitable specializations above allows us to solve for $F(\vec{\lambda})$ in terms of L other F's that are evaluated at $\lambda_0 = \lambda_\star$:

$$F(\vec{\lambda}) = -\bar{\Lambda}_A(\lambda_\star)^{-1} \sum_{i=1}^{L} M_i(\lambda_\star; \vec{\lambda})\, F(\lambda_\star, \lambda_1, \cdots, \widehat{\lambda_i}, \cdots, \lambda_L)\,. \tag{3.24}$$

When $L \geq 2$ this formula can be further simplified by exploiting the special zeroes. Indeed, the functions F on the right-hand side of (3.24) vanish whenever any of their variables equals μ_k. To get rid of these zeroes we define the following function on $\mathbb{C}^L$:

$$\widetilde{F}_\star(\lambda_1, \cdots, \lambda_{L-1}; \vec{\mu}) := -\frac{F(\lambda_1, \cdots, \lambda_{L-1}, \lambda_\star; \vec{\mu})}{\bar{\Lambda}_A(\lambda_\star) \prod_{j=1}^{L-1} [\lambda_j - \mu_k]}\,, \tag{3.25}$$

where we include the constant $-\bar{\Lambda}_A(\lambda_\star)$ to get rid of that factor in (3.24). [$\widetilde{F}_\star = \widetilde{F}_k$ clearly depends on the choice of $\lambda_\star = \mu_k$.] By symmetry of F in the λ_j we have

$$F(\lambda_\star, \lambda_1, \cdots, \widehat{\lambda_i}, \cdots, \lambda_L) = -\bar{\Lambda}_A(\lambda_\star)\, \widetilde{F}_\star(\lambda_1, \cdots, \widehat{\lambda_i}, \cdots, \lambda_L) \prod_{\substack{j=1 \\ j\neq i}}^{L} [\lambda_j - \mu_k]\,, \tag{3.26}$$

which allows us to rewrite (3.24) as in (3.23).

Since the denominator in (3.25) is a symmetric trigonometric polynomial of degree one in each λ_j ($j \neq i$) with zeroes matching the (special) zeroes of the numerator, it follows that $\widetilde{F}_\star$ has the stated polynomial structure from that of F. Symmetry in the spectral parameters is clear since both numerator and denominator in (3.25) have this symmetry. □

For $\lambda_\star = \mu_L - \gamma$ (i.e. $k = L$) write $\widetilde{F} \coloneqq \widetilde{F}_L$. The specialization $\lambda_L = \mu_L$ in (3.23) yields

$$\begin{aligned} F(\lambda_1, \cdots, \lambda_{L-1}, \mu_L) &= M_L(\lambda_\star; \vec{\lambda})|_{\lambda_L = \mu_L} \widetilde{F}(\lambda_1, \cdots, \lambda_{L-1}) \prod_{\substack{j=1 \\ j \neq i}}^{L} [\lambda_j - \mu_L] \\ &= \Big([\gamma] \prod_{j=1}^{L-1} [\lambda_j - \mu_L + \gamma, \mu_L - \mu_j + \gamma] \Big) \widetilde{F}(\lambda_1, \cdots, \lambda_{L-1}) \,. \end{aligned} \tag{3.27}$$

We have recovered Korepin's relation (2.1) in the present approach! [By symmetry of the left-hand side there are again similar relations for any $\lambda_i = \mu_L$.] This suggest that $\widetilde{F}$ should obey a functional equation like (3.8) for system size $L - 1$. Our next task is to show that this is indeed the case.

Recursion. Next we demonstrate that if F solves the functional equation (3.8) then $\widetilde{F}_\star = \widetilde{F}_k$ defined by (3.25) obeys (3.8) for system size $L - 1$ but with inhomogeneities shifted as $\mu_j \longmapsto \mu_{j+1}$ whenever $j \in \{k, \cdots, L-1\}$. In particular, $\widetilde{F} \coloneqq \widetilde{F}_L$ is a solution of (3.8) for system size $L - 1$.

Proof. When we plug (3.23) into (3.8) and set $\lambda_L = \mu_k$ only two types of contributions survive: those with $\nu = L$ in (3.8) and those with $i = L$ in (3.23). Carefully doing this we find that $\widetilde{F}_\star$ satisfies the functional equation

$$\sum_{\nu=0}^{L-1} \widetilde{M}_{\nu,\star}(\lambda_0; \lambda_1, \cdots, \lambda_{L-1}) \, \widetilde{F}_\star(\lambda_0, \cdots, \widehat{\lambda_\nu}, \cdots, \lambda_{L-1}) = 0 \tag{3.28}$$

whose coefficients are explicitly given in terms of (3.9) and $\lambda_\star = \mu_k - \gamma$ by

$$\begin{aligned} \widetilde{M}_{\nu,\star}(\lambda_0; \lambda_1, \cdots, \lambda_{L-1}) \coloneqq \Big(& M_\nu(\lambda_0; \lambda_1, \cdots, \lambda_{L-1}, \mu_k) \, M_L(\lambda_\star; \lambda_0, \cdots, \widehat{\lambda_\nu}, \cdots, \lambda_{L-1}, \mu_k) \\ & + M_L(\lambda_0; \lambda_1, \cdots, \lambda_{L-1}, \mu_k) \, M_{\nu+1}(\lambda_\star; \lambda_0, \cdots, \lambda_{L-1}) \Big) \\ & \times \prod_{\substack{\rho=0 \\ \rho \neq \nu}}^{L-1} [\lambda_\rho - \mu_k] \,. \end{aligned} \tag{3.29}$$

One can check that different choices of $\lambda_\star$ only lead to overall (ν-independent) factors if the inhomogeneities are shifted in the appropriate way. Even more is true: the ratio between $\widetilde{M}_{\nu,\star}$ on the one hand, and the coefficient M_ν from (3.9) for system size $L-1$ with

$\mu_j \longmapsto \mu_{j+1}$ whenever $j \in \{k, \cdots, L-1\}$ on the other hand, equals

$$[\gamma\,, \lambda_0 - \mu_k] \prod_{j=1}^{L-1} [\lambda_j - \lambda_\star] \prod_{\substack{j=1 \\ j\neq k}}^{L} [\mu_k - \lambda_\star]\,. \tag{3.30}$$

Since this ratio does not depend on ν we conclude that the left-hand side of (3.28) for system size L is proportional to that of the functional equation (3.8) for system size $L-1$, up to shifting some inhomogeneities as before. □

Uniqueness. A corollary of the preceding discussion is that the functional equation (3.8) has, up to normalization, a *unique* solution within the class of trigonometric polynomials.

Proof. We use induction on L. The base case, $L = 1$, was furnished at the start of our analysis. Suppose that F is an analytic solution of (3.8) for system size L. Then we have seen that the function $\widetilde{F}_\star$ in (3.25) is analytic and solves the equation for system size $L-1$. Hence, according to the induction hypothesis, $\widetilde{F}_\star$ is unique up to a constant normalization factor. But (3.23) determines F in terms of $\widetilde{F}_\star$, so F is unique up to normalization too. □

As this proof exploits the recursion between the functional equation for successive system sizes it also applies to the functional equations derived in [57, 58], in which a flawed argument for uniqueness was given.

Doubly symmetric. Having established uniqueness it follows that F is symmetric in the inhomogeneity parameters as well as the spectral parameters, inheriting the symmetry in the μ_j from the coefficients (3.9) of the functional equation.

Solution. An interesting byproduct of our analysis is that (3.23) provides an *algorithm* for finding a closed expression for the solution by recursion in L. By uniqueness, when we normalize the solution to match (1.16), the result of iterating the recursion step is a closed formula for the domain-wall partition function (1.12).

Symmetrized sum. The solution to the functional equation (3.8) can be written as the following symmetrized sum:

$$F(\vec{\lambda}) = \Omega_L \sum_{\sigma\in S_L} \prod_{l=1}^{L} M_l(\mu_l - \gamma; \lambda_{\sigma(1)}, \cdots, \lambda_{\sigma(l)}) \prod_{1\leq i<j\leq L} [\lambda_{\sigma(i)} - \mu_j]\,, \tag{3.31}$$

where Ω_L is a constant, S_L denotes the symmetric group in L symbols, and the factor M_l is to be understood as given by (3.9) for system size l. When Ω_L is fixed by (1.16) we obtain the formula for the domain-wall partition function found in [56]:

$$Z(\vec{\lambda}) = [\gamma]^L \sum_{\sigma\in S_L} \prod_{1\leq i<j\leq L} [\lambda_{\sigma(i)} - \mu_j\,, \lambda_{\sigma(j)} - \mu_i + \gamma] \frac{[\lambda_{\sigma(i)} - \lambda_{\sigma(j)} + \gamma]}{[\lambda_{\sigma(i)} - \lambda_{\sigma(j)}]}\,. \tag{3.32}$$

Proof. The proof of (3.31) is by induction on L. For $L = 2$ the statement follows from (3.23) with $k = L$ since $F(\lambda) \propto M_1(\mu_1 - \gamma; \lambda)$ while $M_2(\mu_2 - \gamma; \lambda_2, \lambda_1) = M_1(\mu_2 - \gamma; \lambda_1, \lambda_2)$ by (3.10). The inductive step is straightforward, again using (3.23) for $k = L$ and (3.10), together with the bijection of labelling sets $\{1, \cdots, L\} \times S_{L-1} \xrightarrow{\sim} S_L$ given by $(i, \sigma) \longmapsto (i, i+1, \cdots, L) \circ \sigma'$, where $\sigma' \in S_L$ is the extension of σ fixing L.

One obtains (3.32) using the explicit expression (3.9) of the M_l. To verify (1.16) we notice that at $\vec{\lambda} = \vec{\mu}$ the last factor in (3.32) is zero except when σ is the identity, making the computation very easy. □

Let us take a closer look at the result (3.32), which is in fact a special case of the (somewhat intransparent) formula found by Baxter in 1987 [25] for general fixed boundaries. In Appendix A we explicitly show that (3.32) coincides with Izergin's formula (2.3). Unlike for the latter, the 'partially homogeneous limit' $\vec{\mu} \to 0$ is manifestly regular in (3.32). The same is true for $\lambda_i \to \mu_j$ [cf. (1.16)]; in particular Korepin's recurrence relation (2.1) is immediate: when $\lambda_L = \mu_L$ the last factor in (3.32) is zero except when σ fixes L, for which the terms with $j = L$ give the desired prefactor. As in (2.3) we do still have an apparent singularity at coinciding spectral parameters $\lambda_i = \lambda_j$. However, the residues at those poles cancel pairwise between summands in (3.32) whose permutations differ by the transposition $(i, j) \in S_L$ swapping the two variables. Let us also point out that in algebraic software (2.3) can be much more efficiently implemented for generic parameters than (3.32).

Multiple-integral formula. To conclude this section we show that (3.32) can also be written as a repeated contour integral as in [57]:

$$Z(\vec{\lambda}) = [\gamma]^L \oint\limits_{(\Gamma_{\vec{\lambda}})^{\times L}} \frac{\mathrm{d}^L \vec{z}}{(2\pi \mathrm{i})^L} \frac{\prod_{1 \le i < j \le L} [z_i - \mu_j, z_j - \mu_i + \gamma, z_j - z_i, z_i - z_j + \gamma]}{\prod_{i,j=1}^{L} [z_i - \lambda_j]}, \tag{3.33}$$

where each z_i is integrated over the contour $\Gamma_{\vec{\lambda}}$ consisting of small counter-clockwise oriented loops around all the λ_j, $1 \le j \le L$. In fact this can be done for any symmetric function due to the following trick, which appears to be common lore. Anticipating the next chapter let us formulate the precise statement for a more general set-up; presently $f(\lambda) = \sinh(\lambda) = [\lambda]$.

Consider $L \ge 1$ and let $\vec{\lambda} \in \mathbb{C}^L$ be generic. Suppose that $F : \mathbb{C}^L \to \mathbb{C}$ is a meromorphic function that in each argument is regular in a neighbourhood of λ_j $(1 \le j \le L)$, and that $f : \mathbb{C} \to \mathbb{C}$ is analytic in a neighbourhood of the origin and satisfies $f(0) = 0 \ne f'(0)$. Then we can write

$$\sum_{\sigma \in S_L} F(\lambda_{\sigma(1)}, \cdots, \lambda_{\sigma(L)}) = f'(0)^L \oint\limits_{(\Gamma_{\vec{\lambda}})^{\times L}} \frac{\mathrm{d}^L \vec{z}}{(2\pi \mathrm{i})^L} \frac{\prod_{i,j=1}^{\star\, L} f(z_i - z_j)}{\prod_{i,j=1}^{L} f(z_i - \lambda_j)} F(\vec{z}), \tag{3.34}$$

where the star indicates that equal i and j are to be omitted from the product.

Proof. Again one proceeds by induction on L. For $L = 1$ the statement follows immediately from Cauchy's residue theorem for the single pole at $z = \lambda$, with residue $1/f'(0)$.

For $L \geq 2$ we assume that $\vec{\lambda} \in \mathbb{C}^L$ is such that $f(\lambda_i - \lambda_j) \neq 0$ for all $i \neq j$; in particular this means that the components λ_j should all be distinct. The inductive step entails applying the residue theorem to integrate over z_L, then employing the induction hypothesis (3.34) to the L functions $F(\vec{z})|_{z_L=\lambda_i} \prod_{j=1}^{L-1} f(\lambda_i - z_j)$, and finally using $\{1, \cdots, L\} \times S_{L-1} \xrightarrow{\sim} S_L$ as in the proof of (3.31) above. □

This relation elucidates the appearance of multiple-integral formulae in [1, 57, 58, 64].

4 Summary and discussion

Summary. In this chapter we studied the domain-wall partition function, that is, the partition function of the inhomogeneous symmetric (zero-field) six-vertex model on an $L \times L$ lattice with domain-wall boundary conditions. The main motivation for doing so is that this is the simplest setting in which we can demonstrate the entire analysis of Chapter III without the added technicalities that arise there due to reflection, the dynamical nature of SOS models, and elliptic functions—although we will see in Chapter III that the latter actually simplifies some matters in a certain sense.

Within the framework of the quantum inverse-scattering method the domain-wall partition function admits an algebraic expression (1.12) as a sort of L-point correlation function of operators from the Yang–Baxter algebra. This algebraic setting was recalled in Section 1, where we also used it to derive several properties of the partition function.

The seminal work of Korepin and Izergin, forming the backdrop for the remainder of this chapter, was reviewed in Section 2. In particular this includes Korepin's recurrence relation (2.1) and Izergin's elegant solution (2.3) in the form of a double alternant.

The key part of this chapter is Section 3, in which we worked through the approach put forward by Galleas. The algebraic-functional method for extracting functional equations from the Yang–Baxter algebra was explained in Section 3.1. In Sections 3.2 and 3.3 we gave a detailed account of the complete analysis of the functional equation. This analysis was pioneered by Galleas [55–58] and further developed by Galleas and me [1] and finally by me in [3] and the present text. The resulting symmetrized sum can be recognized as a special case of a rather general yet somewhat opaque formula that was found by Baxter [25], and may be recast in the form of a repeated contour integral by virtue of its symmetry.

Discussion. A common feature of the functional equation (3.8) and others obtained via the algebraic-functional method [1, 3, 55–59, 64] is their structure: they can be described as cyclic linear functional equations [61]. Of course the coefficients, presently (3.9), differ from case to case.

Comparison with Korepin–Izergin. It is instructive to compare the methods from Sections 2 and 3. In both cases the starting point is the algebraic characterization (1.12) of the domain-wall partition function, and one needs several properties of Z that can be surmised from (1.12) as in Section 1.2. In particular, the possible values at which one evaluates one argument of the partition function to get Korepin's recurrence relation (2.1) or (2.2) reappear as 'special zeroes' in the constructive method, see (3.23).

Besides such similarities there are many obvious differences between the two approaches. On the one hand it is clear that the constructive approach of Section 3 is more involved than that of Section 2, and the resulting formula (3.32) for the domain-wall partition function is *computationally* much less efficient for generic values of the parameters than Izergin's determinant (2.3) is. On the other hand, the limit $\vec{\mu} \to 0$ of vanishing inhomogeneities is straightforward using (3.32), while for (2.3) this limit requires a more care, cf. Kuperberg [39]. In addition the analysis in Section 3.3 gives an *algorithm* for finding a closed expression for the partition function.

We have seen that for the domain-wall partition function the method of Korepin–Izergin can be recovered within the constructive approach. One may wonder whether the latter might apply to settings where the former fails. Since both techniques require an algebraic characterization in the framework of the quantum inverse-scattering method, however, it is not clear whether this could be true. To date all cases in which the constructive method has been used to obtain a closed expression were previously tackled using the Korepin–Izergin method:

- Korepin–Izergin for the domain-wall partition function [27, 28, 65];
- Slavnov for scalar products in which the dual Bethe vector is on shell [66];
- Tsuchiya for vertex models with domain walls and a reflecting end [35];
- Wang and Kitanine *et al.* for scalar products of Bethe vectors of the open (reflecting) XXX and XXZ spin chains [67, 68];
- Rosengren for the dynamical (SOS) generalization of Korepin–Izergin [40]; and
- Filali–Kitanine for the extension of Tsuchiya's result to the dynamical case [36, 37].

Within the constructive method, the corresponding references are [55] and the present chapter; [64]; [1]; [69]; [57, 58]; and [3] together with Chapter III of this thesis. In any case, at the very least the constructive approach might be useful in cases where it is hard to guess the determinant formula. One can envision a hybrid approach, in which the constructive approach—possibly with guidance from a property like Korepin's relation (2.1) to locate the special zeroes—is used to come up with a formula that can be proven to be correct by checking that it obeys all conditions from the Korepin–Izergin method. Finally we cannot help noticing that the constructive method provides a beautiful example of the rigid structure imposed by the underlying algebra, which is reflected in the many remarkable properties of the functional equations obtained in this way.

Partial differential equations. Unlike Korepin's recurrence relation the algebraic-functional method yields a functional equation for a fixed system size L. Galleas [56, §4] realized that this allows one, in the rational and trigonometric cases, to derive a set of partial differential equations (PDEs). The way of turning the functional equation into a PDE is easy; let us briefly illustrate one way of doing this starting from (3.8). In Section 1.2 we saw that in terms of multiplicative variables $x_j := \mathrm{e}^{2\lambda_j}$ the 'renormalized' partition function (1.14) is a multivariate polynomial of degree at most $L-1$ in each variable. Thus we can perform a Taylor expansion of $\bar{Z}(x_0,\cdots,\widehat{x_i},\cdots,x_L)$ in x_0 around x_i to obtain

$$\bar{Z}(x_0,\cdots,\widehat{x_i},\cdots,x_L) = \sum_{n=0}^{L-1} \frac{1}{n!}\,(x_0-x_i)^n\,\frac{\partial^n \bar{Z}}{\partial x_i^n}(\vec{x})\,, \tag{4.1}$$

where we used the symmetry to rearrange the order of the arguments on the right-hand side. Applying this relation for $\nu \in \{1,\cdots,L\}$ in (3.8) one obtains a rather complicated PDE of the form $\mathcal{L}(x_0;\vec{x})\,\bar{Z}(\vec{x}) = 0$, where the differential operator $\mathcal{L}$ contains all coefficients of the functional equation. However, the entire dependence on x_0 now resides in $\mathcal{L}$, which is rational in x_0. Once more peeling away some overall factors to ensure that the differential operator becomes polynomial in x_0 [cf. (3.15)], one can now collect equal powers of x_0 to get an equation of the form

$$\sum_{n=0}^{N} x_0^n\;\mathcal{L}_n(\vec{x})\,\bar{Z}(\vec{x}) = 0\,, \tag{4.2}$$

where the value of the maximal degree N follows from the analysis of the coefficients in Section 1.2. Now each of the coefficients must vanish separately, which yields a hierarchy of PDEs, $\mathcal{L}_n(\vec{x})\,\bar{Z}(\vec{x}) = 0$, for the partition function. Such PDEs were e.g. studied for the open (reflecting) XXZ spin chain in [2]. Albeit currently still in its infancy, such an approach via differential equations might also give rise to interesting new insights into properties of the partition function.

Dynamical case. To conclude this section we comment on the extension to SOS models. Recall from Section I.4.3 that the dynamical case comes with additional parameters, the reference height θ and, in the elliptic case, the elliptic nome. Besides the spectral parameters the vertex weights depend on a dynamical parameter valued in $\theta+\gamma\mathbb{Z}$, and the same is true for all operators from Section 1.1. The precise algebraic set-up will be recalled in Section III.1.1. Domain walls were extended to SOS models in [29]. The dynamical domain-wall partition function involves shifts in the dynamical parameter when written in terms of the generators of the dynamical Yang–Baxter algebra, see (I.3.42). Rosengren [40] generalized the Korepin–Izergin method from Section 2 to the case of elliptic SOS models with domain-wall boundary conditions, yielding a sum of 2^L determinants, and extended Kuperberg's work [39] on applications to alternating-sign matrices [see also

the end of Section I.2.2]. The dynamical domain-wall partition function was analysed within the framework of Section 3 by Galleas [57, 58], who recently [70] obtained an expression for this quantity in terms of a single determinant, although it is not yet clear what further benefits that expression has. In the following chapter we will study the partition function of the elliptic SOS model with domain walls and one reflecting end.

A Relation with Korepin–Izergin formula

In this appendix we give a direct proof showing that, for generic values of the parameters, the symmetrized sum (3.32) coincides with Izergin's formula (2.3). Similar steps were originally taken by Rosengren [40, 71] to obtain an expression for the partition function of the elliptic SOS model with domain-wall boundaries starting from a symmetrized sum.

Proof (Rosengren). In order to remove the denominator in the prefactor of (2.3) let us multiply both expressions by $\prod_{i<j}[\lambda_i - \lambda_j, \mu_j - \mu_i]$. Since $\prod_{i<j}[\lambda_{\sigma(i)} - \lambda_{\sigma(j)}] = \operatorname{sgn}\sigma \times \prod_{i<j}[\lambda_i - \lambda_j]$ our task is to show that

$$[\gamma]^L \sum_{\sigma\in S_L} \operatorname{sgn}\sigma \prod_{1\le i<j\le L} [\lambda_{\sigma(i)} - \mu_j, \lambda_{\sigma(j)} - \mu_i + \gamma, \lambda_{\sigma(i)} - \lambda_{\sigma(j)} + \gamma, \mu_j - \mu_i] \tag{A.1}$$

is equal to

$$[\gamma]^L \prod_{i,j=1}^{L} [\lambda_i - \mu_j, \lambda_j - \mu_i + \gamma] \sum_{\sigma\in S_L} \operatorname{sgn}\sigma \prod_{i=1}^{L} \frac{1}{[\lambda_{\sigma(i)} - \mu_i, \lambda_{\sigma(i)} - \mu_i + \gamma]}, \tag{A.2}$$

where we have rewritten Izergin's alternant as an antisymmetrized sum using Leibnitz's formula for the determinant. Using the partial fraction decomposition $1/[z, z+\gamma] = \mathrm{e}^z(1/[z] - \mathrm{e}^\gamma/[z+\gamma])/[\gamma]$ and working out the product we can further express (A.2) as

$$\begin{aligned} &\mathrm{e}^{|\vec{\lambda}|-|\vec{\mu}|} \prod_{i,j=1}^{L} [\lambda_i - \mu_j, \lambda_j - \mu_i + \gamma] \\ &\quad\times \sum_{\sigma\in S_L} \operatorname{sgn}\sigma \sum_{I\subseteq\{1,\cdots,L\}} (-\mathrm{e}^\gamma)^{L-\#I} \prod_{i\in I} \frac{1}{[\lambda_{\sigma(i)} - \mu_i]} \prod_{i\notin I} \frac{1}{[\lambda_{\sigma(i)} - \mu_i + \gamma]}, \end{aligned} \tag{A.3}$$

where we abbreviate $|\vec{\lambda}| := \sum_{j=1}^{L} \lambda_j$ and likewise for $\vec{\mu}$. We will demonstrate that (A.1) can also be written as (A.3) using a version of Lagrange interpolation.

To this end we note that with respect to any λ_i (A.1) lies in $\bigoplus_{a=1-L}^{L-1} \mathbb{C}\,\mathrm{e}^{2a\,\lambda_i}$, which is a subspace of the slightly bigger space $U_i := \mathrm{e}^{\lambda_i} \cdot \bigoplus_{a=1-L}^{L} \mathbb{C}\,\mathrm{e}^{(2a-1)\lambda_i}$ containing (A.3). If

$z_1, \cdots, z_{2L} \in \mathbb{C}$ are pairwise distinct numbers then

$$\varphi_a(\lambda_i) \coloneqq \mathrm{e}^{\lambda} \prod_{\substack{b=1 \\ b\neq a}}^{2L} [\lambda_i - z_b] \in U_i\,, \qquad 1 \le a \le 2L \tag{A.4}$$

form a basis of U_i. Indeed, these $2L = \dim(U_i)$ functions are independent since only φ_a is nonzero at $\lambda_i = z_a$, i.e. $\varphi_a(z_b) \propto \delta_{ab}$. It thus follows that any $F \in U_i$ can be expressed as $F(\lambda_i) = \sum_{a=1}^{2L} F(z_a)\,\varphi_a(\lambda_i)/\varphi_a(z_a)$. This interpolation extends to functions in L variables: any $F \in \bigotimes_{i=1}^{L} U_i$ can be written as

$$F(\vec{\lambda}) = \sum_{a_1,\cdots,a_L=1}^{2L} \frac{F(z_{a_1},\cdots,z_{a_L})}{\varphi_{a_1}(z_{a_1})\cdots\varphi_{a_L}(z_{a_L})}\,\varphi_{a_1}(\lambda_1)\cdots\varphi_{a_L}(\lambda_L)\,. \tag{A.5}$$

Let us apply this relation to (A.1) with $(z_1, \cdots, z_{2L}) = (\mu_1 - \gamma, \cdots, \mu_L - \gamma, \mu_1, \cdots, \mu_L)$. Happily, most of the $(2L)^L$ summands in (A.5) vanish in this case. To see this, note that (A.1) is only nonzero if for every i the values $\mu_i - \gamma$ and μ_i do not both occur (due to the factors $[\lambda_{\sigma(i)} - \lambda_{\sigma(j)} + \gamma]$, cf. the special zeroes), and if either of these only occurs once (by antisymmetry). Thus we must have

$$z_{a_i} = z_{\tau(i),I} \coloneqq \begin{cases} \mu_{\tau(i)} & \tau(i) \in I\,, \\ \mu_{\tau(i)} - \gamma & \tau(i) \notin I\,, \\ 0 & \text{else}\,. \end{cases} \tag{A.6}$$

where $I \subseteq \{1, \cdots, L\}$ specifies whether we pick up μ_j or $\mu_j - \gamma$, and $\tau \in S_L$ shuffles the indices. Thus, in our case, we are left with a sum over $L! \times 2^L$ terms:

$$F(\vec{\lambda}) = \sum_{\tau\in S_L} \sum_{I\subseteq\{1,\cdots,L\}} \frac{F(z_{\tau(1),I},\cdots,z_{\tau(L),I})}{\varphi_{\tau(1),I}(z_{\tau(1),I})\cdots\varphi_{\tau(L),I}(z_{\tau(L),I})}\,\varphi_{\tau(1),I}(\lambda_1)\cdots\varphi_{\tau(L),I}(\lambda_L)\,. \tag{A.7}$$

We will show that this coincides with (A.3) term by term.

First we focus on the term in (A.7) with $\tau = e \in S_L$ and $I = \{\nu + 1, \cdots, L\}$ for some $0 \le \nu \le L$. Interestingly in this case one finds that

$$F(\mu_1-\gamma,\cdots,\mu_\nu-\gamma,\mu_{\nu+1},\cdots,\mu_L) = \mathrm{e}^{-|\vec{\mu}|}(-\mathrm{e}^{\gamma})^{\nu} \prod_{i=1}^{\nu} \varphi_{\mu_i-\gamma}(\mu_i-\gamma) \prod_{i=\nu+1}^{L} \varphi_{\mu_i}(\mu_i)\,, \tag{A.8}$$

where the left-hand side is calculated by observing that the only term in (A.1) that is nonzero at $\vec{\lambda} = (\mu_1 - \gamma, \cdots, \mu_\nu - \gamma, \mu_{\nu+1}, \cdots, \mu_L)$ is the one with $\sigma = e$, while the right-hand side can be found from

$$\prod_{i=1}^{\nu} \varphi_{\mu_i-\gamma}(\lambda_i) \prod_{i=\nu+1}^{L} \varphi_{\mu_i}(\lambda_i) = \mathrm{e}^{|\vec{\lambda}|}\,\frac{\prod_{i,j=1}^{L}[\lambda_i - \mu_j\,, \lambda_i - \mu_j + \gamma]}{\prod_{i\in I}[\lambda_i - \mu_i]\prod_{i\notin I}[\lambda_i - \mu_i + \gamma]}\,. \tag{A.9}$$

Putting the two factors together we precisely reproduce the term in (A.3) with $\sigma = e$ and $I = \{\nu+1, \cdots, L\}$.

Recall that (A.1) is doubly antisymmetric: antisymmetry in the λ_i is manifest, while for the μ_j it was proven at the end of Section 3.3. For general $\tau \in S_L$ the point $\vec{z}_{\tau,I} := (z_{\tau(1),I}, \cdots, z_{\tau(L),I})$ differs from $\vec{z}_{e,I}$ by reshuffling the entries, which can be undone using the antisymmetry of (A.1) in the λ_i at the cost of a factor $\operatorname{sgn}\tau$. Doing this and switching to $\sigma := \tau^{-1}$ we can recast (A.7) in the form

$$F(\vec{\lambda}) = \sum_{\sigma\in S_L} \operatorname{sgn}\sigma \sum_{I\subseteq\{1,\cdots,L\}} \frac{F(z_{1,I},\cdots,z_{L,I})}{\varphi_{1,I}(z_{1,I})\cdots\varphi_{L,I}(z_{L,I})}\, \varphi_{1,I}(\lambda_{\sigma(1)})\cdots\varphi_{L,I}(\lambda_{\sigma(L)})\,. \quad \text{(A.10)}$$

Observe that the summands in this expression depend on σ, λ_i and μ_j in the same way as those in (A.3) do. The equality of the terms for $\tau = e$ and $I = \{\nu+1, \cdots, L\}$ thus implies that (A.7) and (A.3) match term by term, which is what we wanted to prove. □

Chapter III

The elliptic solid-on-solid model with domain walls and a reflecting end

In this chapter we use the method presented in Section II.3 to find a new expression for the partition function of the inhomogeneous elliptic solid-on-solid (SOS) model on an $L \times 2L$ lattice with one reflecting end and domain-wall boundary conditions on the three other ends as in I.15. As a special case this quantity, which we will call the (dynamical) *reflecting-end partition function*, includes the partition function of the symmetric six-vertex model on the same lattice.

In the realm of quantum integrability, reflection was first proposed in the context of factorized scattering by Cherednik in 1984 [32] for systems associated to Weyl groups of type B_N. Four years later Sklyanin [33] treated reflection in the framework of the quantum inverse-scattering method, in which it also governs the boundaries of 'open' (Heisenberg) spin chains. Only in 1998 reflection found its way to quantum-integrable vertex models in the work of Tsuchiya [35], who applied the Korepin–Izergin method to find a determinant expression for the reflecting-end partition function. This once more found an application in combinatorics by work of Kuperberg [42]. It is also closely related to the surface free energy of the XXZ spin chain at finite temperature [72]. The study of the thermodynamic limit of the reflecting-end partition function was initiated recently by Ribeiro and Korepin [38].

In the meanwhile, in 1996, Behrend, Pearce and O'Brien generalized reflection to SOS models [34]. During the 2000s Cao *et al.* [73] and Yang and Zhang [74] found that the trigonometric case arises naturally by applying a face-vertex transformation to the six-vertex model with nondiagonal reflection to diagonalize the boundary operator. Tsuchiya's work was extended to the trigonometric SOS case by Filali and Kitanine in 2010 [36] and the following year to the elliptic case by Filali [37].

Outline. This chapter is set up in the same way as Chapter II to facilitate the comparison between the two. We begin in Section 1 with the quantum-algebraic setting, combining the material introduced in Sections I.3.4 and I.4.3, to provide an algebraic description of the reflecting-end partition function and to study its properties. The work of Tsuchiya, Filali and Kitanine is surveyed in Section 2.

In Section 3 we apply Galleas's method to study the reflecting-end partition function

from a different viewpoint. The dynamical reflection algebra allows us to extract a functional equation for the partition function in Section 3.1. As in Chapter II this equation characterizes the partition function up to normalization, allowing us to find novel formulas for the reflecting-end partition function. We conclude with a discussion and some open issues in Section 4. The appendices contain the relevant facts about Jacobi theta functions and the computation of certain eigenvalues.

1 Reflecting-end partition function

In this section we introduce the dynamical reflection algebra and describe how the partition function fits into that framework. Subsequently we use this to derive several useful properties of that function.

1.1 Algebraic description

Consider an sos model with height variables taking values in $\theta + \gamma\mathbb{Z}$. The *dynamical* parameter θ sets a reference height, whilst the *crossing* or *anisotropy* parameter γ controls the step size. Quantum integrability requires that neighbouring heights differ by one, thus allowing for six types of height profiles around any face, each with an associated local (Boltzmann) weight as shown in Figure I.6.

We find it convenient to use the language of generalized vertex models. The passage to that model, which lives on the dual lattice, goes via the the dictionary from Figure I.8. Since the original height profiles are well defined ('single valued') the arrows around the dual vertex must satisfy the ice rule from the six-vertex model. In the presence of a reflecting boundary we prefer to convert the arrows into signs or dotted and thick lines, where we take a plus (dotted or 'vacant' line) for arrows following some fixed orientation of the line, which goes up and to the right in Figure I.9.

In this section we set up our notation and conventions as in [3], which mostly follow [1, 57, 58], culminating in an algebraic expression for the partition function. The set-up for the bulk is similar to that in Section II.1.1, including (shifts of) the dynamical parameter θ in the appropriate places. More details can be found in Chapter I, in particular Section I.3.4 for the algebraic formulation of reflection, and Section I.4.3 for the treatment of dynamical models in the quantum inverse-scattering method.

Dynamical *R*-matrix. Let $V := \mathbb{C}|+\rangle \oplus \mathbb{C}|-\rangle$ be a complex two-dimensional vector space with standard basis vectors $|\pm\rangle$, to which we assign *weights* $\mathrm{wt}(|\pm\rangle) = \pm 1$. This grading of $V = V[+1] \oplus V[-1]$ by weights is conveniently accounted for via the $\mathfrak{sl}_2$ Cartan generator on V, which we denote by $h \in \mathrm{End}(V)$ and is given by the third Pauli matrix, $h|\pm\rangle = \pm|\pm\rangle$. Write $\mathfrak{h} \subseteq \mathfrak{sl}_2$ for the corresponding Cartan subalgebra.

Let $\lambda, \theta, \gamma \in \mathbb{C}$ be generic complex numbers. We think of the spectral parameter λ and the dynamical parameter θ as variables, and of the crossing parameter γ as fixed.

The vertex weights are encoded in the dynamical R-matrix $R(\lambda, \theta) \in \mathrm{End}(V \otimes V)$, which must be invertible for generic λ and θ and is required to satisfy the *dynamical Yang-Baxter equation* on $V_1 \otimes V_2 \otimes V_3$ [cf. (I.4.44)–(I.4.45)]:

$$\begin{aligned} R_{12}(\lambda_1 - \lambda_2, \theta - \gamma\, h_3)\, R_{13}(\lambda_1 - \lambda_3, \theta)\, R_{23}(\lambda_2 - \lambda_3, \theta - \gamma\, h_1) \\ = R_{23}(\lambda_2 - \lambda_3, \theta)\, R_{13}(\lambda_1 - \lambda_3, \theta - \gamma\, h_2)\, R_{12}(\lambda_1 - \lambda_2, \theta)\,. \end{aligned} \tag{1.1}$$

Here we employ the usual tensor-leg notation, where subscripts indicate on which of the $V_j \cong V$ in the tensor product the operators act nontrivially.

Consider the subspace $\mathrm{End}_{\mathfrak{h}}(V \otimes V) \subseteq \mathrm{End}(V \otimes V)$ of $\mathfrak{h}$-invariant, i.e. weight-preserving, operators on $V \otimes V$. In other words, an element of $\mathrm{End}_{\mathfrak{h}}(V \otimes V)$ satisfies the ice rule: it commutes with $h_1 + h_2 \in V \otimes V$ [cf. (II.1.4)]. The SOS model that we are interested in corresponds to the elliptic solution of (1.1) lying in $\mathrm{End}_{\mathfrak{h}}(V \otimes V)$,

$$R(\lambda, \theta) = \begin{pmatrix} a_+(\lambda,\theta) & 0 & 0 & 0 \\ 0 & b_+(\lambda,\theta) & c_-(\lambda,\theta) & 0 \\ 0 & c_+(\lambda,\theta) & b_-(\lambda,\theta) & 0 \\ 0 & 0 & 0 & a_-(\lambda,\theta) \end{pmatrix}. \tag{1.2}$$

The entries of this dynamical R-matrix are given by [cf. Figure I.9 and (I.4.46)]

$$a_\pm(\lambda,\theta) = f(\lambda+\gamma)\,, \quad b_\pm(\lambda,\theta) = f(\lambda)\,\frac{f(\theta \mp \gamma)}{f(\theta)}\,, \quad c_\pm(\lambda,\theta) = \frac{f(\theta \pm \lambda)}{f(\theta)}\, f(\gamma)\,, \tag{1.3}$$

where in turn $f(\lambda) := -\mathrm{i}\, \mathrm{e}^{-\mathrm{i}\pi\tau/4}\, \vartheta_1(\mathrm{i}\lambda|\tau)/2$ is essentially the odd Jacobi theta function with elliptic nome $\mathrm{e}^{\mathrm{i}\pi\tau} \in \mathbb{C}$ satisfying $\mathrm{Im}(\tau) > 0$. What we need to know about f is summarized in Appendix A.1. Note that the conventions for this chapter are chosen such that throughout one obtains the expressions from [1] simply by ignoring the dynamical arguments (any factor involving θ's, which always come in ratios) and interpreting $f(\lambda) \propto \vartheta_1(\mathrm{i}\lambda|\tau)$ as its trigonometric degeneration $\sinh(\lambda)$. Phrased differently, when expanding f as a series in the elliptic nome $\mathrm{e}^{\mathrm{i}\pi\tau}$ near the origin the trigonometric case accounts for the zeroth order.

Properties. We will need the following *unitarity* property of the R-matrix:

$$R_{12}(\lambda,\theta)\, R_{21}(-\lambda,\theta) = f(\gamma+\lambda)\, f(\gamma-\lambda)\; \mathbb{1}\,. \tag{1.4}$$

Here $R_{21}(\lambda,\theta) = P\, R_{12}(\lambda,\theta)\, P \in \mathrm{End}_{\mathfrak{h}}(V \otimes V)$ with $P \in \mathrm{End}_{\mathfrak{h}}(V \otimes V)$ the permutation operator. Notice that the proportionality factor in (1.4) does not depend on the dynamical parameter. Finally we record that transposing the first leg of the R-matrix yields an

operator satisfying the ice rule in the form $[\,-h_1+h_2, R^{t_1}_{12}(\lambda,\theta)\,]=0$ and the *crossing symmetry*

$$-\sigma^y_1 : R^{t_1}_{12}(-\lambda-\gamma,\theta+\gamma\, h_1): \sigma^y_1 \,\frac{f(\theta-\gamma\, h_2)}{f(\theta)} = R_{21}(\lambda,\theta)\,. \tag{1.5}$$

Here $\sigma^y \in \mathrm{End}(V)$ is the second Pauli matrix, $\sigma^y|\pm\rangle = \pm \mathrm{i}|\mp\rangle$, and the colons around the R-matrix indicates that the h_1 is taken to act *after* (on the left of) the transposed R-matrix. (The precise form of the relation expressing crossing symmetry depends on the parametrization of the vertex weights.)

Monodromy matrices. The dynamical monodromy matrix, introduced in [48], is built out of solutions of (1.1) lying in $\mathrm{End}_{\mathfrak{h}}(V\otimes V)$. Focus on any row of the lattice, with associated 'auxiliary space' $V_0 \cong V$ and spectral parameter $\lambda\in\mathbb{C}$. Every column $1\le j\le L$ comes with a 'local quantum space' $V_j\cong V$ and an inhomogeneity parameter μ_j. The 'global quantum space' is the same as before, $W := V_1\otimes V_2\otimes\cdots\otimes V_L$. As in Chapter II we will often suppress the inhomogeneity parameters in our notation.

The even an odd rows of the lattice (counted from the bottom) are described by (dynamical) monodromy matrices $T_0(\lambda,\theta), \bar T_0(\lambda,\theta)\in \mathrm{End}(V_0\otimes W)$, respectively. These operators are defined as oppositely ordered products [cf. (I.3.40), (I.4.15) and (I.4.29)]

$$T_0(\lambda,\theta;\vec\mu) := \prod_{L\ge j\ge 1}^{\leftarrow} R_{0j}\Big(\lambda-\mu_j,\theta-\gamma\sum_{i=1}^{j-1}h_i\Big) = \quad \lambda \xrightarrow[\vec\mu]{\theta} ,$$

$$\bar T_0(\lambda,\theta;\vec\mu) := \prod_{1\le j\le L}^{\rightarrow} R_{j0}\Big(\lambda+\mu_j,\theta-\gamma\sum_{i=1}^{j-1}h_i\Big) = \quad \xleftarrow[\vec\mu]{\theta} -\lambda \ . \tag{1.6}$$

The total spin-z operator $H := \sum_{j=1}^L h_j$, representing the generator of the Cartan subalgebra $\mathfrak{h}\subseteq\mathfrak{sl}_2$ on W, endows W with a grading by weights as in (II.1.8): $H\,|\vec\beta\rangle = \mathrm{wt}(|\vec\beta\rangle)\,|\vec\beta\rangle$ for basis vectors $|\vec\beta\rangle\in W$. We write $W[s]$ for the subspace of vectors of weight s. Since $R(\lambda,\theta)\in\mathrm{End}_{\mathfrak{h}}(V\otimes V)$ we have $T_0(\lambda,\theta), \bar T_0(\lambda,\theta)\in\mathrm{End}_{\mathfrak{h}}(V_0\otimes W)$, where the ice rule now entails commuting with $h_0+H\in\mathrm{End}(V_0\otimes W)$.

Properties. Usually only one of the monodromy matrices in (1.6) is considered since by (1.4) the two are essentially inverse to each other:

$$T_0(\lambda,\theta)\,\bar T_0(-\lambda,\theta) = \Big(\prod_{j=1}^L f(\gamma-\lambda+\mu_j)f(\gamma+\lambda-\mu_j)\Big)\,\mathbb{1}_0\otimes\mathbb{1}\ . \tag{1.7}$$

In addition the two monodromy matrices are related by crossing symmetry, following from the ice rule for the transposed R-matrix and (1.5),

$$(-1)^L \sigma_0^\gamma : T_0^{t_0}(-\lambda-\gamma, \theta+\gamma h_0) : \sigma_0^\gamma \frac{f(\theta-\gamma H)}{f(\theta)} = \bar{T}_0(\lambda,\theta)\,. \tag{1.8}$$

For our purposes, however, it will be convenient to include both T and $\bar{T}$ in our description.

Dynamical Yang-Baxter algebra. The monodromy matrices (1.6) can be viewed as matrices in auxiliary space with entries acting on W [cf. (I.4.49)]:

$$T_0(\lambda,\theta) = \begin{pmatrix} A(\lambda,\theta) & B(\lambda,\theta) \\ C(\lambda,\theta) & D(\lambda,\theta) \end{pmatrix}_0, \qquad \bar{T}_0(\lambda,\theta) = \begin{pmatrix} \bar{A}(\lambda,\theta) & \bar{B}(\lambda,\theta) \\ \bar{C}(\lambda,\theta) & \bar{D}(\lambda,\theta) \end{pmatrix}_0 . \tag{1.9}$$

Together with the ice rule, the dynamical Yang-Baxter equation (1.1) implies that T obeys the quadratic RTT-relation [cf. (I.4.47)–(I.4.48)]

$$\begin{aligned} R_{00'}(\lambda_1-\lambda_2,\theta-\gamma H)\, T_0(\lambda_1,\theta)\, T_{0'}(\lambda_2,\theta-\gamma h_0) \\ = T_{0'}(\lambda_2,\theta)\, T_0(\lambda_1,\theta-\gamma h_{0'})\, R_{00'}(\lambda_1-\lambda_2,\theta)\,. \end{aligned} \tag{1.10}$$

It follows that the entries of T as in (1.9) furnish W with a representation of the operator algebra associated with $E_{\tau,\gamma}(\mathfrak{sl}_2)$, known as the *(dynamical) Yang-Baxter algebra*, which we denote by $\mathfrak{A} = A_{\tau,\gamma}(\mathfrak{sl}_2)$.

Since $T_0(\lambda,\theta) \in \mathrm{End}_{\mathfrak{h}}(V_0 \otimes W)$ preserves the grading by weights of $V_0 \otimes W$, and not that of W, the generators on the anti-diagonal of (1.9) are not $\mathfrak{h}$-invariant [cf. (I.4.50)]:

$$\begin{aligned} &[\,H, A(\lambda,\theta)\,] = 0\,, && [\,H, B(\lambda,\theta)\,] = -2\,B(\lambda,\theta)\,, \\ &[\,H, C(\lambda,\theta)\,] = 2\,C(\lambda,\theta)\,, && [\,H, D(\lambda,\theta)\,] = 0\,. \end{aligned} \tag{1.11}$$

Nevertheless the dynamical Yang-Baxter algebra is compatible with the grading of W when $\mathfrak{A} = \bigoplus_{s\in 2\mathbb{Z}} \mathfrak{A}[s]$ itself is viewed as a graded algebra: B and C have weights -2 and 2 respectively, while A and D have weight zero. (Thus, $\mathfrak{A}[0]$ is represented in $\mathrm{End}_{\mathfrak{h}}(W)$.)

Likewise the generators contained in $\bar{T}$ are seen to have weights $\mathrm{wt}(\bar{B}) = -2, \mathrm{wt}(\bar{C}) = 2$ and $\mathrm{wt}(\bar{A}) = \mathrm{wt}(\bar{D}) = 0$. The monodromy matrix $\bar{T}$ obeys [cf. (I.4.30)]

$$\begin{aligned} R_{0'0}(\lambda_1-\lambda_2,\theta)\, \bar{T}_0(\lambda_1,\theta-\gamma h_{0'})\, \bar{T}_{0'}(\lambda_2,\theta) \\ = \bar{T}_{0'}(\lambda_2,\theta-\gamma h_0)\, \bar{T}_0(\lambda_1,\theta)\, R_{0'0}(\lambda_1-\lambda_2,\theta-\gamma H)\,. \end{aligned} \tag{1.12}$$

This relation is equivalent to (1.10) due to the unitarity relations (1.4) and (1.7). In particular, the entries of $\bar{T}$ as in (1.9) subject to the relations encoded in (1.12) also provide a representation of $\mathfrak{A}$. From (1.7) and (1.10) it follows that the generators A, B, C, D and $\bar{A}, \bar{B}, \bar{C}, \bar{D}$ are connected by (1.7) as well as by the relations contained in [cf. (I.4.31)]

$$\begin{aligned} T_0(\lambda_1,\theta-\gamma h_{0'})\, R_{00'}(\lambda_1+\lambda_2,\theta)\, \bar{T}_{0'}(\lambda_2,\theta-\gamma h_0) \\ = \bar{T}_{0'}(\lambda_2,\theta)\, R_{00'}(\lambda_1+\lambda_2,\theta-\gamma H)\, T_0(\lambda_1,\theta)\,. \end{aligned} \tag{1.13}$$

Reflecting end. One can regard the Yang-Baxter algebra, or its dynamical version, as governing the bulk of the lattice. The reflecting boundary is described by an operator $K_0(\lambda,\theta) \in \mathrm{End}(V_0)$ satisfying the reflection equation [cf. (I.4.26)–(I.4.27)]

$$\begin{aligned} &R_{00'}(\lambda_1-\lambda_2,\theta)\, K_0(\lambda_1,\theta)\, R_{0'0}(\lambda_1+\lambda_2,\theta)\, K_{0'}(\lambda_2,\theta) \\ &\quad = K_{0'}(\lambda_2,\theta)\, R_{00'}(\lambda_1+\lambda_2,\theta)\, K_0(\lambda_1,\theta)\, R_{0'0}(\lambda_1-\lambda_2,\theta)\,. \end{aligned} \tag{1.14}$$

Although this relation features dynamical R-matrices there are no shifts in the dynamical argument: this is just the ordinary reflection equation. We are interested in the solution of (1.14) that lies in $\mathrm{End}_{\mathfrak{h}}(V_0)$, which first appeared in [34] and reads [cf. (I.3.44)]

$$K_0(\lambda,\theta) = \quad = \begin{pmatrix} k_+(\lambda,\theta) & 0 \\ 0 & k_-(\lambda,\theta) \end{pmatrix}_0, \tag{1.15}$$

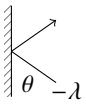

with nonzero entries [cf. (I.4.28)]

$$k_+(\lambda,\theta) = f(\zeta+\lambda)\,\frac{f(\theta+\zeta-\lambda)}{f(\theta+\zeta+\lambda)}\,, \qquad k_-(\lambda,\theta) = f(\zeta-\lambda) \tag{1.16}$$

depending on a fixed boundary parameter $\zeta \in \mathbb{C}$.

Sklyanin's monodromy matrix. The (dynamical) *boundary* or *double-row* monodromy matrix $\mathcal{T}_0(\lambda,\theta) \in \mathrm{End}_{\mathfrak{h}}(V_0 \otimes W)$ is defined as the composition [cf. (I.3.33)]

$$\mathcal{T}_0(\lambda,\theta) := T_0(\lambda,\theta)\, K_0(\lambda,\theta)\, \bar{T}_0(\lambda,\theta) \;=\; \tag{1.17}$$

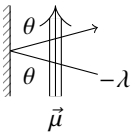

(Like in Section I.3.4 we use a calligraphic font for 'double-row operators'.) As in [33] one can use the relations (1.10)–(1.13) for $\mathfrak{A}$ and the reflection equation (1.14) to show that this operator satisfies the following quadratic relation [cf. (I.4.32)–(I.4.33)]:

$$\begin{aligned} &R_{00'}(\lambda_1-\lambda_2,\theta-\gamma H)\, \mathcal{T}_0(\lambda_1,\theta)\, R_{0'0}(\lambda_1+\lambda_2,\theta-\gamma H)\, \mathcal{T}_{0'}(\lambda_2,\theta) \\ &\quad = \mathcal{T}_{0'}(\lambda_2,\theta)\, R_{00'}(\lambda_1+\lambda_2,\theta-\gamma H)\, \mathcal{T}_0(\lambda_1,\theta)\, R_{0'0}(\lambda_1-\lambda_2,\theta-\gamma H)\,. \end{aligned} \tag{1.18}$$

Note that, as for the K-matrix in (1.14) but unlike for the monodromy matrices in (1.10) and (1.12)–(1.13), the relation (1.18) does not involve shifts in the dynamical parameters of any monodromy matrix. This permits us to think of θ as a constant and [unlike in (I.3.34)] suppress the dependence on this parameter when writing (1.17) as a matrix in auxiliary space with entries in $\mathrm{End}(W)$ [cf. (I.3.34)–(I.3.35)]:

$$\mathcal{T}_0(\lambda,\theta) = \begin{pmatrix} \mathcal{A}(\lambda) & \mathcal{B}(\lambda) \\ \mathcal{C}(\lambda) & \mathcal{D}(\lambda) \end{pmatrix}_0. \tag{1.19}$$

Dynamical reflection algebra. The entries of (1.19) together with H, subject to the relations contained in (1.18) and the ice rule for $\mathcal{T}$, endow W with a representation of the *(elliptic, dynamical) reflection algebra* [75], which we denote by $\mathfrak{B}$ for 'boundary'. For our purposes it will be convenient to follow [33, Prop. 7 and §5] and replace the generator $\mathcal{D}$ of $\mathfrak{B}$ by the combination

$$\widetilde{\mathcal{D}}(\lambda) := \mathcal{D}(\lambda) - \frac{f(\gamma)\, f(\theta - \gamma(H-1) + 2\lambda)}{f(2\lambda+\gamma)\, f(\theta - \gamma(H-1))}\, \mathcal{A}(\lambda)\,. \tag{1.20}$$

Just as for $\mathfrak{A}$, the ice rule for the double-row monodromy matrix endows $\mathfrak{B}$ with a grading by weights: $\mathrm{wt}(\mathcal{B}) = -2$, $\mathrm{wt}(C) = 2$ and $\mathrm{wt}(\mathcal{A}) = \mathrm{wt}(\mathcal{D}) = \mathrm{wt}(\widetilde{\mathcal{D}}) = 0$. That is, (1.11) also holds for $\mathcal{A}, \mathcal{B}, C, \widetilde{\mathcal{D}}$ and it follows that

$$\begin{aligned} f(H)\,\mathcal{A}(\lambda) &= \mathcal{A}(\lambda)\, f(H)\,, & f(H)\,\mathcal{B}(\lambda) &= \mathcal{B}(\lambda)\, f(H-2)\,, \\ f(H)\,C(\lambda) &= C(\lambda)\, f(H+2)\,, & f(H)\,\widetilde{\mathcal{D}}(\lambda) &= \widetilde{\mathcal{D}}(\lambda)\, f(H)\,. \end{aligned} \tag{1.21}$$

[Thus, instead of including H as one of the generators of $\mathfrak{B}$, one may equivalently view $\mathfrak{B} = \bigoplus_{s\in 2\mathbb{Z}} \mathfrak{B}[s]$ as a graded algebra, with grading by weights.] Finally, with the help of (1.13) and (1.21) one can check that (1.8) implies that $\mathcal{B}$ enjoys the crossing symmetry

$$\mathcal{B}(-\lambda-\gamma) = -\frac{f(2\lambda+2\gamma)\, f(\theta+\zeta+\lambda)}{f(2\lambda)\, f(\theta+\zeta-\lambda-\gamma)}\, \mathcal{B}(\lambda)\,. \tag{1.22}$$

Pseudovacua. The highest- and lowest-weight vectors [cf. (I.3.21)]

$$|\Omega\rangle := |+\,+\cdots+\rangle \in W[+L]\,, \qquad |\bar{\Omega}\rangle := |-\,-\cdots-\rangle \in W[-L]\,, \tag{1.23}$$

span the subspaces $W[\pm L]$, so they are also eigenvectors for the quantum operators $\mathcal{A}, \mathcal{D}, \widetilde{\mathcal{D}} \in \mathrm{End}_{\mathfrak{h}}(W)$. We will need the following 'vacuum' eigenvalues:

$$\mathcal{A}(\lambda)\,|\Omega\rangle = \Lambda_{\mathcal{A}}(\lambda)\,|\Omega\rangle\,, \qquad \widetilde{\mathcal{D}}(\lambda)\,|\Omega\rangle = \Lambda_{\widetilde{\mathcal{D}}}(\lambda)\,|\Omega\rangle\,, \qquad \mathcal{A}(\lambda)\,|\bar{\Omega}\rangle = \bar{\Lambda}_{\mathcal{A}}(\lambda)\,|\bar{\Omega}\rangle\,. \tag{1.24}$$

Their expressions are more complicated than their non-dynamical single-row counterparts, cf. (II.1.11). In Appendix B we show that these eigenvalues are given by

$$\Lambda_{\mathcal{A}}(\lambda,\theta;\vec{\mu}) = [\zeta+\lambda]\frac{[\theta+\zeta-\lambda]}{[\theta+\zeta+\lambda]}\prod_{j=1}^{L}[\lambda-\mu_j+\gamma\,,\lambda+\mu_j+\gamma]\,,$$

$$\Lambda_{\widetilde{\mathcal{D}}}(\lambda,\theta;\vec{\mu}) = [\zeta-\lambda-\gamma]\frac{[2\lambda\,,\theta+\zeta+\lambda+\gamma\,,\theta-L\gamma]}{[2\lambda+\gamma\,,\theta+\zeta+\lambda\,,\theta-(L-1)\gamma]}\prod_{j=1}^{L}[\lambda-\mu_j\,,\lambda+\mu_j]\,,$$

$$\begin{aligned}\bar{\Lambda}_{\mathcal{A}}(\lambda,\theta;\vec{\mu}) &= [\zeta-\lambda]\frac{[\gamma\,,\theta+(L-1)\gamma-2\lambda]}{[2\lambda+\gamma\,,\theta+(L-1)\gamma]}\prod_{j=1}^{L}[\lambda-\mu_j+\gamma\,,\lambda+\mu_j+\gamma]\\ &\quad+[\zeta+\lambda+\gamma]\frac{[2\lambda\,,\theta+\zeta-\lambda-\gamma\,,\theta+L\gamma]}{[2\lambda+\gamma\,,\theta+\zeta+\lambda\,,\theta+(L-1)\gamma]}\prod_{j=1}^{L}[\lambda-\mu_j\,,\lambda+\mu_j]\,,\end{aligned}\tag{1.25}$$

where from now on we abbreviate $[\lambda] \coloneqq f(\lambda)$ and $[\lambda_1,\lambda_2,\cdots] \coloneqq [\lambda_1][\lambda_2]\cdots$ like we did in Chapters I–II. For later use we point out that

$$\Lambda_{\mathcal{A}}(-\lambda-\gamma,\theta;\vec{\mu}) = \frac{[2\lambda+\gamma\,,\theta+\zeta+\lambda\,,\theta-(L-1)\gamma]}{[2\lambda\,,\theta+\zeta-\lambda-\gamma\,,\theta-L\gamma]}\,\Lambda_{\widetilde{\mathcal{D}}}(\lambda,\theta;\vec{\mu})\,,\tag{1.26}$$

which is an incarnation of crossing symmetry.

Partition function. Within the setting of the dynamical reflection algebra the (dynamical) reflecting-end partition function, governing the inhomogeneous sos model with domain walls and one reflecting end as in Figure I.15, can be written as

$$Z(\vec{\lambda},\theta;\vec{\mu}) = \quad = \langle\bar{\Omega}|\prod_{j=1}^{L}\mathcal{B}(\lambda_j)\,|\Omega\rangle\,.\tag{1.27}$$

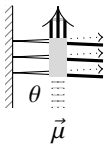

It depends on all parameters of the model: L spectral parameters $\vec{\lambda} = (\lambda_1,\cdots,\lambda_L)$, the dynamical parameter θ, L inhomogeneities μ_j, the crossing parameter γ, the boundary parameter ζ, and the elliptic nome $e^{i\pi\tau}$. As for the generators of the dynamical reflection algebra we often omit the dependence on all but the spectral parameters.

1.2 Properties

Let us collect several properties of the reflecting-end partition function that will be useful in the remainder of this chapter. These properties should be compared with those listed in Section II.1.2 for the domain-wall partition function of the ordinary six-vertex model without reflection.

Case $L = 1$. For system size one we have [cf. Figure I.9 and (I.3.29)]

$$
\begin{aligned}
Z(\lambda) \;=\; & \\
& = b_+(\lambda-\mu,\theta)\, k_+(\lambda,\theta)\, c_+(\lambda+\mu,\theta) + c_-(\lambda-\mu,\theta)\, k_-(\lambda,\theta)\, b_+(\lambda+\mu,\theta) \\
& = [\gamma\,,\zeta-\mu\,,2\lambda]\,\frac{[\theta+\zeta+\mu\,,\theta-\gamma]}{[\theta+\zeta+\lambda\,,\theta]}\,.
\end{aligned}
\tag{1.28}
$$

The last equality uses the addition rule (A.2) for f to combine the two terms into a compact final expression. Unlike (II.1.13) the result is not a constant; both the reflecting end and the dynamical character of the model contribute factors involving λ.

Polynomial structure. Tracing back the dependence on the spectral and dynamical parameters it is clear that the reflecting-end partition function, being polynomial in the statistical weight (1.3) and boundary weights (1.16), is meromorphic. Moreover, up to an overall factor originating from the denominator in (1.16), Z is entire in the spectral parameters: the 'renormalized' partition function

$$
\bar{Z}(\vec{\lambda}) \coloneqq Z(\vec{\lambda}) \prod_{j=1}^{L} [\theta+\zeta+\lambda_j]
\tag{1.29}
$$

is a theta function of order $2(L+1)$ and norm $(L-1)\gamma$ when viewed as a function of any single λ_j. The basics of higher-order theta functions, which are also known as *elliptic polynomials*, are summarized in Appendix A.2. For a proof we refer to [37], in which a factorizing Drinfel'd twist [76] is used to determine the dependence of the partition function on the spectral parameters.

In fact, in [37] it is shown that $\bar{Z}$ can be further written as $\prod_{j=1}^{L}[2\lambda_j]$ times a higher-order theta function of order $2(L-1)$ and norm $(L-1)\gamma$ in each variable, but (1.29) suffices for the purposes of Section 3. This should be compared with the analogous property in Chapter II: the factors $[2\lambda_j]$ are due to the reflecting end, and $2(L-1)$ is twice the degree of (II.1.14) as a result of the double-row structure in the present case.

Doubly symmetric. The partition function (1.27) is symmetric in the spectral parameters λ_i, and also in the inhomogeneity parameters μ_j.

Proof. Symmetry in the λ_i is due to the reflection-algebra relation

$$
\mathcal{B}(\lambda_1)\,\mathcal{B}(\lambda_2) = \mathcal{B}(\lambda_2)\,\mathcal{B}(\lambda_1)\,.
\tag{1.30}
$$

This relation is again obtained from the $(1,4)$-component in $\mathrm{End}(V_0 \otimes V_{0'})$ of (1.18) [cf. (II.1.15)]:

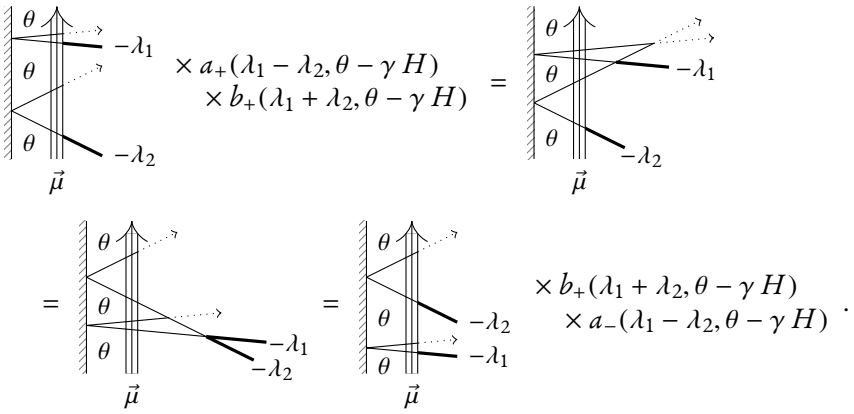

(1.31)

Here the outer equalities use the ice rule for the vertex weights as well as (1.21). Since $a_+(\lambda,\theta) = a_-(\lambda,\theta)$ the factors on both sides cancel.

For the symmetry in the μ_j the reflecting end is not relevant. The proof only uses the dynamical Yang–Baxter equation and is rather similar to (II.1.15); the vertical staggering (alternating orientations of the horizontal lines) does not affect it. □

Crossing symmetry. Let us finally record that the double-row texture is also visible in crossing symmetry for the reflecting-end partition function (1.27), which it inherits from (1.22): for any $1 \le i \le L$ it satisfies

$$Z(\vec{\lambda})|_{\lambda_i \longmapsto -\lambda_i - \gamma} = \frac{[-2(\lambda_i+\gamma), \theta+\zeta+\lambda_i]}{[2\lambda_i, \theta+\zeta-\lambda_i-\gamma]}\, Z(\vec{\lambda})\,. \tag{1.32}$$

This property is not a necessary ingredient for our approach in Section 3, but it is useful for a better understanding of certain issues that we will encounter along the way.

Special points. Like its counterpart from Chapter II the reflecting-end partition function reduces to a single term at $\vec{\lambda} = \vec{\mu}$, where the only contributing configuration is

$Z(\vec{\mu}) =$ 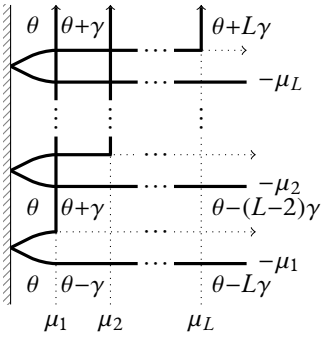

. (1.33)

The corresponding height profile on the faces is shown in Figure 1 (a). Note that if we would delete the odd rows (counted from the bottom) in the configuration in (1.33) we precisely find that of (II.1.16). Accordingly, amongst the various factors of the value of (1.33) we recognize the value in (II.1.16):

$$\begin{aligned} Z(\vec{\mu}) &= \prod_{i=1}^{L} k_-(\mu_i, \♪)\, c_-(0, \♪)\, b_+(2\mu_i, \theta + (i-1)\gamma) \\ &\quad \times \prod_{1\le i<j\le L} a_+(\mu_i - \mu_j, \♪)\, a_-(\mu_j - \mu_i, \♪)\, a_-(\mu_i + \mu_j, \♪) \\ &\qquad \times b_+(\mu_j + \mu_i, \theta + (2i - j - 1)\gamma) \\ &= [\gamma]^L \frac{[\theta - \gamma]}{[\theta + (L-1)\gamma]} \prod_{i=1}^{L} [\zeta - \mu_i, 2\mu_i] \frac{[\theta + (2i - L - 2)\gamma]}{[\theta + (i-2)\gamma]} \\ &\quad \times \prod_{i,j=1}^{L}{}^{\star} [\mu_i - \mu_j + \gamma] \prod_{1\le i<j\le L} [\mu_i + \mu_j + \gamma, \mu_i + \mu_j], \end{aligned} \tag{1.34}$$

where we write ♪ for the dynamical arguments of the vertex weights that are independent of that argument in any case, and the star means that equal values of i and j are to be omitted from the product.

Proof. The proof is like in Section II.1.2. By setting $\lambda_L = \mu_L$ the top-right vertex is tuned to be a $c_-(0, \♪) = [\gamma]$. Through the ice rule this determines the configuration on the two top rows as well as the right column [cf. (II.1.17)]. Continuing in this way we arrive at the microstate depicted in (1.33).

The formula in (1.34) can be directly read off from (1.33) using Figure I.6 or I.9 and (I.3.29). Alternatively one can prove (1.34) by induction in L, which boils down to the repeated application of the recurrence relation (2.1) below. □

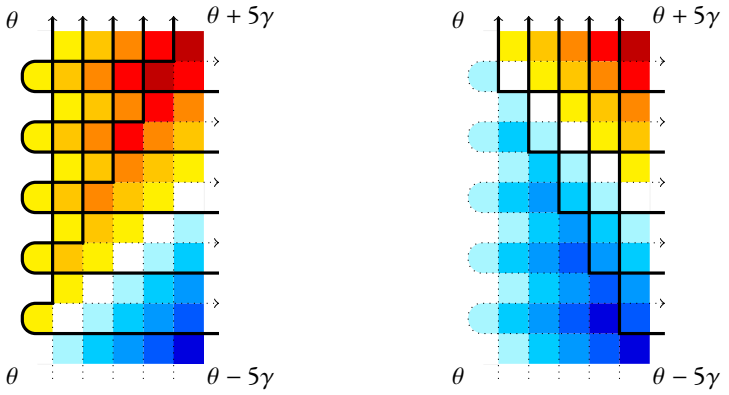

Figure 1. [Colour online] The height profiles for the sole microstates contributing to the reflecting-end partition function (1.27) for $L = 5$ at the special points **(a)** $\vec{\lambda} = \vec{\mu}$, corresponding to (1.33), and **(b)** $\vec{\lambda} = (-\mu_L, \cdots, -\mu_1)$, for (1.35). The reflecting end is depicted as a U-turn like in Figure I.13 (b). Heights range from dark blue (low) to dark red (high).

Another special point at which it is easy to see that the partition function consists of a single term is $\vec{\lambda} = (-\mu_L, \cdots, -\mu_1)$:

$$\begin{aligned} Z(-\mu_L, \cdots, -\mu_1; \vec{\mu}) &= \prod_{i=1}^{L} k_+(-\mu_i, \theta)\, c_+(0, \boldsymbol{\cdot}) \, b_+(-2\mu_i, \theta - (i-1)\gamma) \\ &\quad \times \prod_{1 \le i < j \le L} a_+(\mu_i - \mu_j, \boldsymbol{\cdot}) \, a_-(\mu_j - \mu_i, \boldsymbol{\cdot}) \, a_+(-\mu_i - \mu_j, \boldsymbol{\cdot}) \\ &\quad \times b_+(-\mu_j - \mu_i, \theta - (2i - j - 1)\gamma) \\ &= (-1)^L \, Z(\vec{\mu}; \vec{\mu}) \prod_{j=1}^{L} \frac{[\theta + \zeta + \mu_j]}{[\theta + \zeta - \mu_j]} \prod_{1 \le i < j \le L} \frac{[\mu_i + \mu_j - \gamma]}{[\mu_i + \mu_j + \gamma]}, \end{aligned} \tag{1.35}$$

where the last equality can be verified by direct inspection. The sole contributing microstate is drawn in Figure 1 (b); this time deleting the *even* rows results in (a mirror image of) the configuration from (II.1.16), and an alternative derivation uses (2.2) below. Note that the configurations in Figure 1 give the highest and lowest possible height profiles.

Using symmetry in the inhomogeneities together with crossing symmetry we get many more special points. In particular this includes the point in (II.1.18). It is not clear that this is a special point from the algebraic or graphical expressions for $Z(\mu_L - \gamma, \cdots, \mu_1 - \gamma)$, which

might be related to the fact that crossing symmetry ultimately follows from an algebraic identity for f. One could hope to find special points such that we obtain the configuration from (II.1.18) when erasing the odd or even rows, but it does not seem possible to do so. For instance, the top-left vertex only has one adjacent edge whose spin is fixed, so we are able to kill one out of three possibilities in this case, but this still allows for at least two different microstates.

2 Korepin–Izergin method

As in Section II.2 we write Z_L if we want to stress the system size for the reflecting-end partition function on a $2L \times L$ bulk.

Recurrence relation. By specializing $\lambda_{L+1} = \mu_{L+1}$ in the partition function for system size $L+1$ one obtains the recurrence relation

$$\begin{aligned} Z_{L+1}(\vec{\lambda}, \mu_{L+1}; \vec{\mu}, \mu_{L+1}) &= c_-(0, \text{♪})\, k_-(\mu_{L+1}, \text{♪})\, b_+(2\mu_{L+1}, \theta + L\gamma)\, Z_L(\vec{\lambda}; \vec{\mu}) \\ &\quad \times \prod_{i=1}^{L} a_+(\lambda_i - \mu_{L+1}, \text{♪})\, a_-(\mu_{L+1} - \mu_i, \text{♪})\, a_-(\mu_{L+1} + \mu_i, \text{♪}) \\ &\quad\quad \times b_+(\lambda_i + \mu_{L+1}, \theta + (2i - L - 2)\gamma) \\ &= [\gamma, \zeta - \mu_{L+1}, 2\mu_{L+1}] \frac{[\theta + (L-1)\gamma]}{[\theta + L\gamma]}\, Z_L(\vec{\lambda}; \vec{\mu}) \\ &\quad \times \prod_{i=1}^{L} [\lambda_i - \mu_{L+1} + \gamma, \mu_{L+1} - \mu_i + \gamma, \mu_{L+1} + \mu_i + \gamma] \\ &\quad\quad \times [\lambda_i + \mu_{L+1}] \frac{[\theta + (2i - L - 3)\gamma]}{[\theta + (2i - L - 2)\gamma]}, \end{aligned} \tag{2.1}$$

were we once more write ♪ instead of irrelevant dynamical arguments. Instead setting $\lambda_1 = -\mu_{L+1}$ yields another recurrence relation:

$$\begin{aligned} Z_{L+1}(-\mu_{L+1}, \vec{\lambda}; \vec{\mu}, \mu_{L+1}) &= c_+(0, \text{♪})\, k_+(-\mu_{L+1}, \theta)\, b_+(-2\mu_{L+1}, \theta - L\gamma)\, Z_L(\vec{\lambda}; \vec{\mu}) \\ &\quad \times \prod_{i=1}^{L} a_-(\lambda_i + \mu_{L+1}, \text{♪})\, a_+(-\mu_{L+1} - \mu_i, \text{♪})\, a_+(-\mu_{L+1} - \mu_i, \text{♪}) \\ &\quad\quad \times b_+(\lambda_i - \mu_{L+1}, \theta - (2i - L - 2)\gamma)\,. \end{aligned} \tag{2.2}$$

Here we used the symmetry of Z in the spectral parameters to specialize λ_1 rather than λ_{L+1} in order to simplify the graphical computation. The explicit form of the factors multiplying Z in (2.2) is obtained from (2.1) by replacing μ_{L+1} by $-\mu_{L+1}$ and multiplying with $k_+(-\mu_{L+1}, \theta)/k_-(-\mu_{L+1}, \text{♪}) = [\zeta - \mu_{L+1}, \theta + \zeta + \mu_{L+1}]/[\zeta + \mu_{L+1}, \theta + \zeta - \mu_{L+1}]$.

By the symmetry of Z in the spectral parameters, and in the inhomogeneities, one finds a similar relation for any specialization $\lambda_i = \mu_j$. In fact, by crossing symmetry there are still more relations. These relations were first obtained by Tsuchiya [35] for the ordinary six-vertex models with a reflecting end and domain walls, and later by Filali–Kitanine [36] and Filali [37] for the trigonometric and elliptic case, respectively, of the SOS model with the same boundary conditions.

Uniqueness. By symmetry in the spectral parameters we can focus on any single variable λ_i. Since the renormalized partition function (1.29) is a higher-order theta function of order $2(L+1)$ and norm $(L-1)\gamma$ in λ_i, it is completely determined by its value in $2(L+1)$ points that are distinct modulo the quasiperiods. In fact, due to symmetry and crossing symmetry, we have recurrence relations like (2.1)–(2.2) at $4L$ points $\lambda_i \in \{\pm\mu_j, \pm\mu_j - \gamma \mid 1 \le j \le L\}$. By induction in L it follows that there is a unique solution matching (1.28) when $L = 1$.

Solution. Tsuchiya, Filali and Kitanine succeeded in finding a formula for the reflecting-end partition function involving a double alternant:

$$\begin{aligned} Z_L(\vec{\lambda};\vec{\mu}) &= [\gamma]^L \prod_{i=1}^{L} [\zeta-\mu_i, 2\lambda_i] \frac{[\theta+\zeta+\mu_i, \theta+(2i-L-2)\gamma]}{[\theta+\zeta+\lambda_i, \theta+(L-i)\gamma]} \\ &\quad \times \frac{\prod_{i,j=1}^{L} [\lambda_i+\mu_j+\gamma, \lambda_i-\mu_j+\gamma, \lambda_i+\mu_j, \lambda_i-\mu_j]}{\prod_{1\le i<j\le L} [\lambda_i+\lambda_j+\gamma, \lambda_i-\lambda_j, \mu_j+\mu_i, \mu_j-\mu_i]} \det K(\vec{\lambda};\vec{\mu}), \qquad (2.3) \\ K_{ij}(\vec{\lambda};\vec{\mu}) &:= \frac{1}{[\lambda_i+\mu_j+\gamma, \lambda_i-\mu_j+\gamma, \lambda_i+\mu_j, \lambda_i-\mu_j]}. \end{aligned}$$

Notice that this K_{ij} is the crossing-invariant extension of that from (II.2.3). The same is true for the numerator and denominator in the second line of (2.3). The product in the first line reveals the dynamical nature of the model and contains the contributions due to reflection.

Proof. It is clear that (2.3) is correct for $L = 1$ and satisfies crossing symmetry. By straightforward checks analogous to those in Section II.2 one further verifies that the expression is doubly symmetric and satisfies (2.1)–(2.2). For the polynomial structure one also proceeds as in the domain-wall case, noticing that

- the numerator of the second line times the determinant is a higher-order theta function of order $4(L-1)$ and norm $2(L-1)\gamma$ in each λ_i;
- the denominator in the second line divides this polynomial by antisymmetry of the determinant and invariance under crossing, thus reducing the order by $2(L-1)$ and the norm by $(L-1)\gamma$ for each variable. □

3 Constructive method

In this section we show that the techniques introduced in Section II.3 can be used to analyse the reflecting-end partition function through a functional equation for that quantity. As in Section II.3 the Latin alphabet is used for indices $i, j, \cdots$ running through $\{1, 2, \cdots, L\}$ and Greek for indices $\nu, \rho, \cdots$ in $\{0, 1, 2, \cdots, L\}$.

3.1 Functional equations from the dynamical reflection algebra

Let us show that the reflecting-end partition function (1.27) obeys, for system size L, the linear functional equation

$$\sum_{\nu=0}^{L} M_\nu(\lambda_0; \vec{\lambda})\, Z(\lambda_0, \cdots, \widehat{\lambda_\nu}, \cdots, \lambda_L) = 0\,, \tag{3.1}$$

where, as in Chapter II, the caret indicates that the ν'th spectral parameter is omitted, and the coefficients M_ν feature the vacuum eigenvalues from (1.25):

$$\begin{aligned}
M_0(\lambda_0; \vec{\lambda}) &:= \bar{\Lambda}_{\mathcal{A}}(\lambda_0, \theta; \vec{\mu}) - \Lambda_{\mathcal{A}}(\lambda_0, \theta; \vec{\mu}) \prod_{j=1}^{L} \frac{[\lambda_j - \lambda_0 + \gamma\,, \lambda_j + \lambda_0]}{[\lambda_j - \lambda_0\,, \lambda_j + \lambda_0 + \gamma]}\,,\\
M_i(\lambda_0; \vec{\lambda}) &:= \frac{[\gamma\,, 2\lambda_i\,, \theta + (L-1)\gamma + \lambda_i - \lambda_0]}{[\lambda_i - \lambda_0\,, 2\lambda_i + \gamma\,, \theta + (L-1)\gamma]}\, \Lambda_{\mathcal{A}}(\lambda_i, \theta; \vec{\mu}) \prod_{\substack{j=1\\ j\neq i}}^{L} \frac{[\lambda_j - \lambda_i + \gamma\,, \lambda_j + \lambda_i]}{[\lambda_j - \lambda_i\,, \lambda_j + \lambda_i + \gamma]}\\
&+ \frac{[\gamma\,, \theta + (L-2)\gamma - \lambda_i - \lambda_0\,, \theta - (L-1)\gamma]}{[\lambda_i + \lambda_0 + \gamma\,, \theta + (L-1)\gamma\,, \theta - L\gamma]}\, \Lambda_{\widetilde{\mathcal{D}}}(\lambda_i, \theta; \vec{\mu}) \prod_{\substack{j=1\\ j\neq i}}^{L} \frac{[\lambda_i - \lambda_j + \gamma\,, \lambda_i + \lambda_j + 2\gamma]}{[\lambda_i - \lambda_j\,, \lambda_i + \lambda_j + \gamma]}\,.
\end{aligned} \tag{3.2}$$

The structure of (3.1) is the same as that of (II.3.1). The first coefficient, M_0 also has a form that is rather similar to that in (II.3.2), while the M_i now consist of two terms. Conceptually the proof is just as in Section II.3.1, although the dynamical reflection algebra forces us to use $\widetilde{\mathcal{D}}$ instead of $\mathcal{D}$.

Proof. The idea for obtaining our functional equation for the partition function (1.27) is to use (1.24) to insert an $\mathcal{A}$ on one side of the product of $\mathcal{B}$'s in (1.27) [cf. (II.3.3)] and use the reflection-algebra relations to move it to the other side.

To save space let us indicate the arguments of the generators of $\mathfrak{B}$ as subscripts, e.g. $\mathcal{A}_0 := \mathcal{A}(\lambda_0)$. We start by finding the appropriate algebraic relations in the dynamical reflection algebra $\mathfrak{B}$. The required relations are (1.30) together with those obtained from

the (1, 3)- and (3, 4)-components in $\mathrm{End}(V_0 \otimes V_{0'})$ of (1.18). Using (1.21) to move vertex weights containing H past the double-row quantum operators these relations are

$$\begin{aligned}\mathcal{A}_0\,\mathcal{B}_1 = {}& \frac{[\lambda_1-\lambda_0+\gamma\,,\lambda_1+\lambda_0]}{[\lambda_1-\lambda_0\,,\lambda_1+\lambda_0+\gamma]}\,\mathcal{B}_1\,\mathcal{A}_0 \\ & - \frac{[\gamma\,,2\lambda_1\,,\theta-\gamma(H+1)+\lambda_1-\lambda_0]}{[\lambda_1-\lambda_0\,,2\lambda_1+\gamma\,,\theta-\gamma(H+1)]}\,\mathcal{B}_0\,\mathcal{A}_1 \\ & - \frac{[\gamma\,,\theta-\gamma(H+2)-\lambda_1-\lambda_0]}{[\lambda_1+\lambda_0+\gamma\,,\theta-\gamma(H+2)]}\,\mathcal{B}_0\,\widetilde{\mathcal{D}}_1\,,\end{aligned} \tag{3.3}$$

$$\begin{aligned}\widetilde{\mathcal{D}}_0\,\mathcal{B}_1 = {}& \frac{[\lambda_0-\lambda_1+\gamma\,,\lambda_1+\lambda_0+2\gamma\,,\theta-\gamma H\,,\theta-\gamma(H+1)]}{[\lambda_0-\lambda_1\,,\lambda_1+\lambda_0+\gamma\,,\theta-\gamma(H-1)\,,\theta-\gamma(H+2)]}\,\mathcal{B}_1\,\widetilde{\mathcal{D}}_0 \\ & - \frac{[\gamma\,,2(\lambda_0+\gamma)\,,\theta-\gamma H\,,\theta-\gamma(H+1)+\lambda_0-\lambda_1]}{[\lambda_0-\lambda_1\,,2\lambda_0+\gamma\,,\theta-\gamma(H-1)\,,\theta-\gamma(H+2)]}\,\mathcal{B}_0\,\widetilde{\mathcal{D}}_1 \\ & + \frac{[2(\lambda_0+\gamma)\,,2\lambda_1\,,\gamma\,,\theta-\gamma H\,,\theta-\gamma H+\lambda_0+\lambda_1]}{[2\lambda_0+\gamma\,,2\lambda_1+\gamma\,,\lambda_1+\lambda_0+\gamma\,,\theta-\gamma(H-1)\,,\theta-\gamma(H+1)]}\,\mathcal{B}_0\,\mathcal{A}_1\,,\end{aligned} \tag{3.4}$$

where $\widetilde{\mathcal{D}}$ was defined in (1.20) such that no term proportional to $\mathcal{B}_1\,\mathcal{A}_0$ appears on the right-hand side of (3.4). By repeated application (1.18) gives rise to relations involving more than two generators. In particular, (1.30) allows us to suppress the harpoon in (1.27), and we can use Faddeev's trick from Appendix I.A to proceed. In this way one can use (3.3)–(3.4), together with (1.21), to show that

$$\begin{aligned}\mathcal{A}_0\prod_{j=1}^{L}\mathcal{B}_j = {}& \prod_{j=1}^{L}\frac{[\lambda_j-\lambda_0+\gamma\,,\lambda_j+\lambda_0]}{[\lambda_j-\lambda_0\,,\lambda_j+\lambda_0+\gamma]}\prod_{j=1}^{L}\mathcal{B}_j\,\mathcal{A}_0 \\ & - \sum_{i=1}^{L}\frac{[\gamma\,,2\lambda_i\,,\theta-\gamma(H+1)+\lambda_i-\lambda_0]}{[\lambda_i-\lambda_0\,,2\lambda_i+\gamma\,,\theta-\gamma(H+1)]} \\ & \qquad \times\prod_{\substack{j=1\\ j\neq i}}^{L}\frac{[\lambda_j-\lambda_i+\gamma\,,\lambda_j+\lambda_i]}{[\lambda_j-\lambda_i\,,\lambda_j+\lambda_i+\gamma]}\prod_{\substack{\nu=0\\ \nu\neq i}}^{L}\mathcal{B}_\nu\,\mathcal{A}_i \\ & - \frac{[\theta-\gamma(H+2L-1)]}{[\theta-\gamma(H+2L)]}\sum_{i=1}^{L}\frac{[\gamma\,,\theta-\gamma(H+2)-\lambda_i-\lambda_0]}{[\lambda_i+\lambda_0+\gamma\,,\theta-\gamma(H+1)]} \\ & \qquad \times\prod_{\substack{j=1\\ j\neq i}}^{L}\frac{[\lambda_i-\lambda_j+\gamma\,,\lambda_i+\lambda_j+2\gamma]}{[\lambda_i-\lambda_j\,,\lambda_i+\lambda_j+\gamma]}\prod_{\substack{\nu=0\\ \nu\neq i}}^{L}\mathcal{B}_\nu\,\widetilde{\mathcal{D}}_i\,.\end{aligned} \tag{3.5}$$

Now we multiply this relation from the left by $\langle\bar{\Omega}|$ and from the right by $|\Omega\rangle$. This yields the desired functional equation with coefficients (3.2). □

Rather than inserting an $\mathcal{A}(\lambda_0)$ in (1.27) one could just as well use $\widetilde{\mathcal{D}}(\lambda_0)$. From the structural similarity between (3.3) and (3.4) it is clear that the resulting equation of 'type D' (cf. Section II.3.1) is also of the form (3.1) but with different coefficients. In the next sections we will see that, as in Chapter II, the functional equation (3.1)–(3.2) fully determines the partition function, so we will not need the explicit form of the functional equation of type D.

3.2 Properties of the functional equation and its solutions

We set aside the symbol 'Z' for the reflecting-end partition function (1.27) and consider the functional equation

$$\sum_{\nu=0}^{L} M_\nu(\lambda_0;\vec{\lambda})\, F(\lambda_0,\cdots,\widehat{\lambda_\nu},\cdots,\lambda_L) = 0 \tag{3.6}$$

with coefficients (3.2). In view of the analytic properties of the partition function discussed in Section 1.2 we look for solutions F to this equation in the space of symmetric higher-order theta functions (up to an overall factor) on $\mathbb{C}^L$.

Properties of the functional equation. The coefficients (3.2) inherit the symmetry in the inhomogeneity parameters μ_j from the vacuum eigenvalues (1.25). The symmetry in the λ_i (recall that $1 \le i \le L$), by (1.30), and crossing symmetry (1.26) are reflected in the following properties of the coefficients, regarded as functions $M_\nu : \mathbb{C}^{L+1} \to \mathbb{C}$:

- $M_0(\lambda_0;\vec{\lambda})$ is symmetric in all λ_j and invariant under $\lambda_j \mapsto -\lambda_j - \gamma$;
- $M_i(\lambda_0;\vec{\lambda})$ is symmetric in the λ_j with $j \neq i$
  and invariant under $\lambda_j \mapsto -\lambda_j - \gamma$ for those j ; (3.7)
- $M_i(\lambda_0;\vec{\lambda})|_{\lambda_i \leftrightarrow \lambda_j} = M_j(\lambda_0;\vec{\lambda})$, while
$$M_i(\lambda_0;\vec{\lambda})|_{\lambda_i \mapsto -\lambda_i - \gamma} = \frac{[-2(\lambda_i+\gamma)\,,\theta+\zeta+\lambda_i]}{[2\lambda_i\,,\theta+\zeta-\lambda_i-\gamma]}\, M_i(\lambda_0;\vec{\lambda})\ .$$

In addition, like we described at the end of Section II.3.1, by swapping $\lambda_0 \leftrightarrow \lambda_i$ in (3.1) we get L more functional equations that are of the form (II.3.11) with coefficients obtained from (3.2) by exchanging the spectral parameters precisely as in (II.3.13). When writing the corresponding system of $L+1$ equations in matrix form as in (II.3.14) one can check numerically that the matrix is singular for any L.

Properties of solutions. As in the domain-wall case from the previous chapter the functional equation determines many of the properties of sufficiently nice solutions.

Polynomial structure. Because of (1.29) we expect a simple pole at $-\theta-\zeta$. Up to these poles, the solution is a higher-order theta function whose order and norm in the spectral parameters are determined by the functional equation: if F is a meromorphic solution then the rescaled function

$$\bar{F}(\vec{\lambda}) := F(\vec{\lambda}) \prod_{j=1}^{L} [\theta+\zeta+\lambda_j] \tag{3.8}$$

is a theta function of order $2(L+1)$ and norm $(L-1)\gamma$ with respect to each λ_j.

Proof. Remove all denominators from the functional equation written in terms of (3.8) by setting [cf. (II.3.15)]

$$\begin{aligned} \bar{M}_\nu(\lambda_0;\vec{\lambda}) := {} & [\theta+(L-1)\gamma\,,\theta+\zeta+\lambda_\nu]\, M_\nu(\lambda_0;\vec{\lambda}) \\ & \times \prod_{\rho=0}^{L} [2\lambda_\rho+\gamma] \prod_{0\le\rho<j\le L} [\lambda_j-\lambda_\rho\,,\lambda_j+\lambda_\rho+\gamma] \end{aligned} \tag{3.9}$$

for each $\nu \in \{0,1,\cdots,L\}$. [The ν-dependent term $\theta+\zeta+\lambda_\nu$ completes the product coming from (3.8) to form an overall (ν-independent) factor. The coefficients (3.9) have the symmetry properties from (3.7).] If F solves (3.6) then $\bar{F}$ obeys

$$\sum_{\nu=0}^{L} \bar{M}_\nu(\lambda_0;\vec{\lambda})\, \bar{F}(\lambda_0,\lambda_1,\cdots,\widehat{\lambda_\nu},\cdots,\lambda_L) = 0\,. \tag{3.10}$$

First we focus on the dependence on λ_0. The explicit form of the coefficients, see (1.25) and (3.2), show that $\bar{M}_0$ has no poles in λ_0 whilst (for generic $\vec{\lambda}$) the $\bar{M}_i$ only have simple zeroes in λ_0. Therefore $\bar{F}$ is entire in λ_0. Next one checks that $\bar{M}_0$ is a theta function of order $2(2L+3)$ and norm $(L+2)\gamma-\theta$, whereas each $\bar{M}_i$ is a theta function of order $2(L+2)$ and norm $3\gamma-\theta$. Thus comparing the λ_0-dependence of the terms in (3.10) we conclude that $\bar{F}$ must be a theta function of order $2(L+1)$ and norm $(L-1)\gamma$ in λ_0.

One proceeds likewise for the dependence on λ_i for any fixed $1\le i\le L$. With respect to this variable $\bar{M}_i$ is a theta function of order $2(2L+3)$ and norm $(2L+1)\gamma$ while each $\bar{M}_\nu$ with $\nu\neq i$ is a theta function of order $2(L+2)$ and norm $(L+2)\gamma$. We conclude that F is also a theta function of order $2(L+1)$ and norm $(L-1)\gamma$ in the λ_i. □

Notice that this proof is neater than its counterpart in Section II.3.2. In that case the trigonometric structure in that case makes it easy to check things explicitly. Presently this is no longer feasible, forcing one to think further, which results in a deeper understanding.

It is also worth pointing out that, unlike for the dynamical version of (II.3.8) obtained in [57, 58], similarly focussing on the dependence on the dynamical parameter θ in (3.10) does not give us more information: the $\bar{M}_\nu$ are theta functions of the same order, 2, and

norm, $-\lambda_0 + \zeta + (L-1)\gamma$, in θ for each $\nu \in \{0, 1, \cdots, L\}$. This is in accordance with our notation, in which we do not indicate the dependence on θ of the coefficients or the solution (or partition function).

Symmetric. Any analytic solution is symmetric in the L spectral parameters.

Proof. The proof is analogous to that in Section II.3.2. Consider the functional equation (3.6) in the limit $\lambda_0 \to \lambda_i$ for some $1 \le i \le L$. When F is analytic, so that the previous paragraph applies, (3.2) shows that the only singularities in (3.6) are the simple poles in M_0 and M_i [recall that f is entire]. The residues of these two coefficients are opposite [cf. (II.3.17)]

$$\begin{aligned}\operatorname{Res}_{\lambda_0=\lambda_i} M_0(\lambda_0;\vec{\lambda}) &= -\operatorname{Res}_{\lambda_0=\lambda_i} M_i(\lambda_0;\vec{\lambda}) \\ &= \frac{[\gamma, 2\lambda_i]}{f'(0)\,[2\lambda_i+\gamma]}\Lambda_{\mathcal{A}}(\lambda_i)\prod_{\substack{j=1\\ j\neq i}}^{L}\frac{[\lambda_j-\lambda_i+\gamma, \lambda_j+\lambda_i]}{[\lambda_j-\lambda_i, \lambda_j+\lambda_i+\gamma]}\,. \end{aligned} \tag{3.11}$$

Computing the residue of (3.6) as $\lambda_0 \to \lambda_i$ we thus obtain (II.3.18). Since (3.11) is generically nonzero and F is analytic, this implies that F is invariant under cyclic permutations of its first i arguments. As we argued below (II.3.18) this implies that F is symmetric. □

The situation with respect to the inhomogeneity parameters is as in Section II.3.2: once we show that (reasonable) solutions to the functional equation are unique—see Section 3.3—it follows that the solution inherits the symmetry in the inhomogeneities from the coefficients (3.2).

Crossing symmetry. Any analytic solution F enjoys the crossing symmetry

$$F(\vec{\lambda})|_{\lambda_i \longmapsto -\lambda_i-\gamma} = \frac{[-2(\lambda_i+\gamma), \theta+\zeta+\lambda_i]}{[2\lambda_i, \theta+\zeta-\lambda_i-\gamma]}\,F(\vec{\lambda})\,. \tag{3.12}$$

Proof. We proceed like we did to prove the symmetry in the spectral parameters above, this time letting λ_0 tend to the 'crossed' value of λ_i, that is, to $-\lambda_i-\gamma$. If the solution F is analytic it has the polynomial structure described above, whence the sole singularities in (3.6) are once more simple poles in M_0 and M_i, with residues related as

$$\operatorname{Res}_{\lambda_0=-\lambda_i-\gamma} M_0(\lambda_0;\vec{\lambda}) = \frac{[2(\lambda_i+\gamma), \theta+\zeta+\lambda_i]}{[2\lambda_i, \theta+\zeta-\lambda_i-\gamma]}\,\operatorname{Res}_{\lambda_0=-\lambda_i-\gamma} M_i(\lambda_0;\vec{\lambda})\,, \tag{3.13}$$

where we used (1.26). The residue (with only M_i contributing) is given by

$$\operatorname{Res}_{\lambda_0=-\lambda_i-\gamma} M_i(\lambda_0;\vec{\lambda}) = \frac{[\gamma, \theta-(L-1)\gamma]}{f'(0)\,[\theta-L\gamma]}\,\Lambda_{\widetilde{\mathcal{D}}}(\lambda_i)\prod_{\substack{j=1\\ j\neq i}}^{L}\frac{[\lambda_i-\lambda_j+\gamma, \lambda_i+\lambda_j+2\gamma]}{[\lambda_i-\lambda_j, \lambda_i+\lambda_j+\gamma]}\,. \tag{3.14}$$

Using the symmetry of F the residue of (3.6) as $\lambda_0 \to -\lambda_i - \gamma$ becomes

$$\Big(\frac{[2(\lambda_i+\gamma),\theta+\zeta+\lambda_i]}{[2\lambda_i,\theta+\zeta-\lambda_i-\gamma]}\,F(\vec{\lambda})+F(\vec{\lambda})|_{\lambda_i\longmapsto-\lambda_i-\gamma}\Big)\,\mathrm{Res}_{\lambda_0=\lambda_i}M_i(\lambda_0;\vec{\lambda})=0\,. \tag{3.15}$$

As (3.14) is generically nonzero and F is analytic, (3.15) implies that F is invariant under crossing $\lambda_i \longmapsto -\lambda_i - \gamma$, which is what we wanted to demonstrate. □

Special zeroes. Suppose that $L \geq 2$ and fix $1 \leq k \leq L$. Any solution of (3.6) vanishes when two of its variables are set to λ_+ and λ_-, where the pair (λ_+, λ_-) is one of

$$\begin{array}{ccc}(\mu_k-\gamma,\mu_k) & \longleftrightarrow & (\mu_k-\gamma,-\mu_k-\gamma)\\ \updownarrow & & \updownarrow\\ (-\mu_k,\mu_k) & \longleftrightarrow & (-\mu_k,-\mu_k-\gamma)\end{array} \tag{3.16}$$

[When $\lambda_+ = -\mu_k$ or $\lambda_- = \mu_k$ this vanishing is evident for the partition function (1.27) by Tsuchiya–Filali–Kitanine (2.1).] The grey arrows in (3.16) indicate how the four different 'special zeroes' for given k are related by crossing one or both entries.

Proof. The idea of the proof is again as in Section II.3.2. Fix any $k \in \{1,\cdots,L\}$; by symmetry in the spectral parameters we may take specialize the last two variables. It is easy to see that M_{L-1} and M_L disappear when $\lambda_{L-1} = \lambda_+$ and $\lambda_L = \lambda_-$ for $\lambda_\pm$ as above. Under this specialization (3.6) thus reduces to an equation analogous to (II.3.19). By swapping $\lambda_0 \leftrightarrow \lambda_j$ we obtain $L-1$ further functional equations of a similar form. Recasting this system of linear functional equations in matrix form our task is to show that the determinant of the matrix is nonzero.

As a result of the reflecting end the coefficients are more involved than in Section II.3.2, and we have not yet found suitable specializations of the parameters to prove that the matrix is indeed nonsingular. Nevertheless we have little doubt that this is possible. Analytic and numerical inspection confirm that the determinant is nonzero for $L \leq 15$. There does not seem to be any reason to disbelieve that this is the case for larger L as well. □

3.3 Reduction, recursion and solution

The upshot of the preceding discussion is that it is reasonable to look for solutions of (3.6) within the space of analytic functions on $\mathbb{C}^L$. To solve the equation, which involves one more spectral parameter than F depends on, we may specialize any single spectral parameter to any value we like. Together, (1.25) and (3.2) show that the equation simplifies most when for some $k \in \{1,\cdots,L\}$ we set

- $\lambda_0 = \pm\mu_k - \gamma$, whence $M_0(\pm\mu_k-\gamma;\vec{\lambda}) = \bar{\Lambda}_{\mathcal{A}}(\pm\mu_k-\gamma)$ consists of a single $\vec{\lambda}$-independent product that is nonzero for generic values of the parameters.

Notice the difference with the situation in Section II.3.3. On the one hand, in the presence of a reflecting end, there is no obvious value of λ_i that makes M_i vanish (or even constant): the latter consists of two terms, involving either $\Lambda_{\mathcal{A}}$ or $\Lambda_{\widetilde{\mathcal{D}}}$, which do not have simultaneous zeroes. On the other hand, and more importantly, reflection does allow for a counterpart of the interesting option from Section II.3.3; because of the vertical staggering this now comes in twice as many versions as we may choose a sign [cf. the special zeroes above].

The specialization $\lambda_0 = \pm\mu_k - \gamma$ allows us to express $F(\vec{\lambda})$ as a linear combination of F's that each depend on only $L-1$ free spectral parameters. In particular, when $L = 1$ this procedure completely determines the solution up to an overall factor:

Case $L = 1$. Set $\lambda_0 = \pm\mu_1 - \gamma$ in (3.6) to see that $F(\lambda) \propto [2\lambda]/[\theta + \zeta + \lambda]$ for some proportionality constant not involving λ. Normalizing this solution to match (1.34) or (1.35) we reproduce the partition function (1.28).

This is another instance where the elliptic case forces one to think a bit further. In the trigonometric case the functional equation for $L = 1$ can easily be solved by separation of variables e^{λ_v}, which of course is fine too, yet the systematic nature of the analysis as L varies is less apparent in that case.

Reduction. For $L \geq 2$ choose any single element of $\{\pm\mu_1 - \gamma, \cdots, \pm\mu_L - \gamma\}$, which we denote by $\lambda_\star := \pm\mu_k - \gamma$. If F is an analytic solution of the functional equation (3.6) for system size L then we can write [cf. (II.3.23)]

$$F(\vec{\lambda}) = \sum_{i=1}^{L} M_i(\lambda_\star; \vec{\lambda})\, \widetilde{F}_\star(\lambda_1, \cdots, \widehat{\lambda_i}, \cdots, \lambda_L) \prod_{\substack{j=1 \\ j\neq i}}^{L} [\lambda_j \mp \mu_k\,, \lambda_j \pm \mu_k + \gamma]\,, \tag{3.17}$$

where $\widetilde{F}_\star$ is a function on $\mathbb{C}^{L-1}$ such that $\widetilde{F}_\star(\lambda_1, \cdots, \lambda_{L-1}) \prod_{j=1}^{L-1} [\theta + \zeta + \lambda_j]$ is a higher-order theta function of order $2L$ and norm $(L-2)\gamma$ in each variable. Furthermore, $\widetilde{F}_\star$ is symmetric in the λ_i, and behaves under crossing like in (3.12).

Proof. The proof is parallel to that in Section II.3.3. Set $\lambda_0 = \lambda_\star$ in (3.6) and solve for $F(\vec{\lambda})$ to get an expression similar to (II.3.24). In view of the special zeroes (3.16) of F let us define [cf. (II.3.25)]

$$\widetilde{F}_\star(\lambda_1, \cdots, \lambda_{L-1}) := -\frac{F(\lambda_1, \cdots, \lambda_{L-1}, \lambda_\star)}{\bar{\Lambda}_{\mathcal{A}}(\lambda_\star) \prod_{j=1}^{L-1} [\lambda_j \mp \mu_k\,, \lambda_j \pm \mu_k + \gamma]}\,, \tag{3.18}$$

where the constant $-\bar{\Lambda}_{\mathcal{A}}(\lambda_\star)$ is included for convenience. Using the analogue of (II.3.26) this yields (3.17). The function $\widetilde{F}_\star = \widetilde{F}_{\pm,k}$ inherits its properties from F since the denominator in (3.18) is a symmetric higher-order theta function of order two and norm $-\gamma$ in

each λ_j ($j \neq i$), has zeroes that match the (special) zeroes of the numerator, and is invariant under crossing $\lambda_j \longmapsto -\lambda_j - \gamma$ [cf. (3.16)]. □

For $\lambda_\star = \pm\mu_L - \gamma$ write $\widetilde{F}_\pm := \widetilde{F}_\star$. Setting $\lambda_L = \pm\mu_L$ in (3.17) yields

$$\begin{aligned} F(\lambda_1,\cdots,\lambda_{L-1},\pm\mu_L) &= M_L(\lambda_\star;\vec{\lambda})|_{\lambda_L=\pm\mu_L}\widetilde{F}_\pm(\lambda_1,\cdots,\lambda_{L-1})\prod_{i=1}^{L-1}[\lambda_i \mp \mu_L\,,\lambda_i \pm \mu_L + \gamma] \\ &= [\gamma\,,\zeta \pm \mu_L\,,\pm 2\mu_L]\frac{[\theta+\zeta\mp\mu_L\,,\theta+L\gamma]}{[\theta+\zeta\pm\mu_L,\theta+(L-1)\gamma]}\,\widetilde{F}_\pm(\lambda_1,\cdots,\lambda_{L-1}) \\ &\quad\times\prod_{i=1}^{L-1}[\lambda_i \pm \mu_L\,,\lambda_i \mp \mu_L + \gamma\,,\pm\mu_L + \mu_i + \gamma\,,\pm\mu_L - \mu_i + \gamma]\,, \end{aligned} \tag{3.19}$$

Up to some constant, i.e. $\vec{\lambda}$-independent, factors we have retrieved the Tsuchiya–Filali–Kitanine recurrence relations (2.1) in the present setting, albeit for two different functions $\widetilde{F}_\pm$. [By symmetry and crossing symmetry of the left-hand side there are again similar relations for any $\lambda_i = \pm\mu_L$ as well as for $\lambda_i = \mp\mu_L - \gamma$. Although one could include constant factors in (3.18) such that (3.19) precisely matches (2.1), this is not necessary since we will fix the normalization to match the partition function later on in any case.] We may hope to be able to show that, up to constant factors, $\widetilde{F}_\pm$ are the same, and obey a functional equation like (3.6) for system size $L-1$.

Recursion. Let us demonstrate that when F is a solution of the functional equation (3.6) then for any choice of $\lambda_\star = \pm\mu_k - \gamma$ the function $\widetilde{F}_\star = \widetilde{F}_{\pm,k}$ defined in (3.18) solves (3.6) for system size $L-1$ but with inhomogeneities shifted as $\mu_j \longmapsto \mu_{j+1}$ whenever $j \in \{k,\cdots,L-1\}$. In particular, $\widetilde{F}_\pm := \widetilde{F}_{\pm,L}$ are both solutions of (3.6) for system size $L-1$.

Proof. Pick a $\lambda_\flat \in \{\pm\mu_k, \mp\mu_k - \gamma\}$, with upper/lower sign and k as in $\lambda_\star$. Carefully using (3.17) to rewrite each F in (3.6) and specializing $\lambda_L = \lambda_\flat$ we find that $\widetilde{F}$ satisfies a reduced functional equation (II.3.28) with coefficients given by [cf. (II.3.29)]

$$\begin{aligned} \widetilde{M}_{\nu,\star}(\lambda_0;\lambda_1,\cdots,\lambda_{L-1}) &= \Big(M_\nu(\lambda_0;\lambda_1,\cdots,\lambda_{L-1},\lambda_\flat)\,M_L(\lambda_\star;\lambda_0,\cdots,\widehat{\lambda_\nu},\cdots,\lambda_{L-1},\lambda_\flat) \\ &\quad + M_L(\lambda_0;\lambda_1,\cdots,\lambda_{L-1},\lambda_\flat)\,M_{\nu+1}(\lambda_\star;\lambda_0,\cdots,\lambda_{L-1})\Big) \\ &\quad\times\frac{1}{[2\lambda_\flat\,,\theta+\zeta-\lambda_\flat-\gamma]}\prod_{\substack{\rho=0\\ \rho\neq\nu}}^{L-1}[\lambda_\rho \mp \mu_k\,,\lambda_\rho \pm \mu_k + \gamma]\,. \end{aligned} \tag{3.20}$$

The factor $1/[2\lambda_\flat\,,\theta+\zeta-\lambda_\flat-\gamma]$ ensures that the right-hand side does not depend on the choice of $\lambda_\flat$ for a given $\lambda_\star$, which is why we did not indicate $\lambda_\flat$ in our notation for the

reduced coefficients. Moreover one can verify that the sign in $\lambda_\star$ only results in an overall (ν-independent) factor for the reduced coefficients. Indeed, the choice of this sign only appears in the following overall factor for the (3.20) [cf. (3.19)]:

$$\begin{aligned}&[\zeta \pm \mu_k\,, \theta + \zeta \pm \mu_k - \gamma]\frac{[\theta + \zeta \mp \mu_k]}{[\theta + \zeta \pm \mu_k]}\\ &\times \prod_{\substack{j=1\\ j\neq k}}^{L}[\lambda_j \pm \mu_k\,, \lambda_j \mp \mu_k + \gamma\,, \pm\mu_k - \mu_j + \gamma\,, \pm\mu_k + \mu_j + \gamma]\,.\end{aligned} \tag{3.21}$$

At the same time, unlike in Section II.3.3, when $L \geq 3$ there does not seem to be a simple relation between the reduced coefficients for different choices of k for $\lambda_\star$.

The reduced functional equation (II.3.28) has the same structure as our original functional equation when we take $L-1$ instead of L in (3.6); the coefficients (3.20) also exhibit the symmetries from (3.7). Moreover, when $L = 2$ the left-hand side of (II.3.28) is proportional to that of (3.6) with $L = 1$ for any choice of $\lambda_\star$. Unlike in Section II.3.3, however, this simple relation does unfortunately not persist to $L \geq 3$.

At the end of Section 3.1 we noticed that interchanging $\lambda_0 \leftrightarrow \lambda_i$ in (3.6) for any $i \in \{1, \cdots, L\}$ yields another functional equation that is also solved by F. Thus, for system size $L-1$, in fact we have L different functional equations: (3.6) together with the $L-1$ equations having coefficients (II.3.13) with $L-1$ rather than L. (Recall that not all of these equations are linearly independent.) We are done if we can establish the following

> *Claim.* For any system size L the left-hand side of the reduced functional equation (II.3.28) with $\lambda_\star = \pm\mu_k - \gamma$ can be written as some linear combination of the left-hand sides of these L functional equations corresponding to system size $L-1$, provided we shift the inhomogeneities in the (II.3.13) as $\mu_j \longmapsto \mu_{j+1}$ whenever $j \in \{k, \cdots, L-1\}$.

To see that this is indeed the case we form the $L \times L$ matrix with entries given by (II.3.13) for system size $L-1$, except that the last row is replaced by the coefficients (3.20) of the reduced equation. Our claim is true if this matrix has zero determinant. Whilst we have not managed to prove this rigorously, analytic and numerical investigations for $L \leq 10$ confirm that this is indeed the case for these system sizes, and we see no obstruction for this pattern to continue to larger L too. □

Uniqueness. A consequence of the above discussion is that the functional equation (3.6) has, up to normalization, a *unique* solution within the class of analytic functions on $\mathbb{C}^L$.

Proof. The proof is as in Section II.3.3. The key observation is that none of the preceding proofs involves an algebraic choices, unlike e.g. when solving the equation $\lambda^2 = 1$. Since for $L = 1$ the solution is unique, up to a constant normalization factor, it follows

that the procedure only has one possible result up to normalization: through (II.3.23) any solution for system size L is expressed in terms of one for system size $L-1$. □

Solution. Iterating (3.17) we can find a closed expression for the solution to (3.6).

Symmetrized sum. Any solution to the functional equation (3.6) for $L \geq 2$ can be written as [cf. (II.3.31)]

$$F(\lambda_1,\cdots,\lambda_L) = \Omega_L \sum_{\sigma\in S_L} \prod_{l=1}^{L} M_l(\mu_l-\gamma;\lambda_{\sigma(1)},\lambda_{\sigma(2)},\cdots,\lambda_{\sigma(l)}) \times \prod_{1\leq i<j\leq L} [\lambda_{\sigma(i)}-\mu_j,\lambda_{\sigma(i)}+\mu_j+\gamma] \tag{3.22}$$

for some normalization constant Ω_L. Here S_L the symmetric group in L symbols, and the factor M_l is to be understood as given by (3.2) for system size l. Fixing Ω_L by (1.34) or (1.35) we obtain a closed formula for the reflecting-end partition function [cf. (II.3.32)]:

$$\begin{aligned} Z(\vec{\lambda}) = [\gamma]^L \Big(\prod_{i=1}^{L} \frac{[\zeta-\mu_i,2\lambda_j,\theta+\zeta+\mu_i,\theta+(2i-L-2)\gamma]}{[\zeta+\mu_i,2\lambda_j+\gamma,\theta+\zeta-\mu_i,\theta+(i-2)\gamma]}\Big) \frac{[\theta,\theta-\gamma]}{[\theta+L\gamma,\theta+(L-1)\gamma]} \\ \times \sum_{\sigma\in S_L} \prod_{l=1}^{L} m_l(\lambda_{\sigma(1)},\lambda_{\sigma(2)},\cdots,\lambda_{\sigma(l)}) \prod_{1\leq i<j\leq L} \frac{[\lambda_{\sigma(i)}-\mu_j,\lambda_{\sigma(i)}+\mu_j+\gamma]}{[\lambda_{\sigma(i)}-\lambda_{\sigma(j)},\lambda_{\sigma(i)}+\lambda_{\sigma(j)}+\gamma]}, \end{aligned} \tag{3.23}$$

where

$$\begin{aligned} m_l(\lambda_1,\cdots,\lambda_l) &:= \Big([\gamma]\frac{[2\lambda_l]}{[2\lambda_l+\gamma]}\Big)^{-1} M_l(\mu_l-\gamma;\lambda_1,\cdots,\lambda_l) \\ &= [\zeta+\lambda_l,\lambda_l+\mu_l+\gamma]\frac{[\theta+\zeta-\lambda_l,\theta+l\gamma+\lambda_l-\mu_l]}{[\theta+\zeta+\lambda_l,\theta+(l-1)\gamma]} \\ &\quad\times \prod_{j=1}^{l-1}[\lambda_l-\mu_j+\gamma,\lambda_l+\mu_j+\gamma,\lambda_j-\lambda_l+\gamma,\lambda_j+\lambda_l] \\ &\quad + (-1)^{l-1}[\zeta-\lambda_l-\gamma,\lambda_l-\mu_l]\frac{[\theta+\zeta+\lambda_l+\gamma,\theta+(l-1)\gamma-\lambda_l-\mu_l]}{[\theta+\zeta+\lambda_l,\theta+(l-1)\gamma]} \\ &\quad\times \prod_{j=1}^{l-1}[\lambda_l-\mu_j,\lambda_l+\mu_j,\lambda_l-\lambda_j+\gamma,\lambda_l+\lambda_j+2\gamma]. \end{aligned} \tag{3.24}$$

Proof. The corresponding proof from Section II.3.3 applies verbatim. □

Multiple-integral formula. Finally one may recast (3.22)–(3.23) in the form of a repeated contour integral using (II.3.34).

Proof. The function $f(\lambda) \propto \vartheta_1(\mathrm{i}\lambda|\tau)$ and the function $g(\vec{\lambda})$ determined by the second line in (3.22) satisfy the conditions for the use of (II.3.34) stated in Section II.3.3. □

To conclude this section let us look at the analytic structure of (3.23)–(3.24). Although (3.23) has apparent poles at $\lambda_l = -\gamma/2$, the fixed point under crossing symmetry, these simple poles are removable: the residues at these points vanish. The simple pole of (3.24) at $\lambda_l = -\theta - \zeta$ was already anticipated in (1.29).

As far as the simple poles in (3.24) at $\lambda_l = \lambda_j$ are concerned we first note that these are precisely cancelled by the zeroes in the numerator in (II.3.34). To see that their residues must vanish from the point of view of the symmetrized sum we observe that the second line in (3.23) can be rewritten as

$$\frac{\sum_{\sigma\in S_L} \operatorname{sgn}\sigma \prod_l m_l(\lambda_{\sigma(1)},\cdots,\lambda_{\sigma(l)}) \prod_{i<j}[\lambda_{\sigma(i)} - \mu_j\,, \lambda_{\sigma(i)} + \mu_j + \gamma]}{\prod_{i<j}[\lambda_i - \lambda_j\,, \lambda_i + \lambda_j + \gamma]}\,. \tag{3.25}$$

The numerator is explicitly antisymmetrized in all spectral parameters, which means that the denominator actually divides it: the residues do indeed vanish [cf. the proofs of (II.2.3) and (2.3)]. Finally, the poles at $\lambda_l = -\lambda_j - \gamma$ are related to those at $\lambda_l = \lambda_j$ by crossing symmetry.

One can verify that both terms in (3.24) have precisely the same dependence on all parameters and variables, as indicated in Table 1. Thus it should be possible to recast (3.24) as single product using some relation for the odd Jacobi theta function. When $l = 1$ the addition rule for f guarantees such factorization, but unfortunately we have not been able to see it explicitly for general l. Nevertheless we expect that our result can be rewritten as Tsuchiya–Filali–Kitanine's determinant in a way similar to the procedure in Appendix II.A. In particular, factorizing m_l should lead to several simplifications in (3.23), especially regarding the factors containing θ.

4 Summary, discussion and outlook

Summary. In this chapter we considered the elliptic SOS model with one reflecting end and domain walls on the three other boundaries. The main object was the model's partition function, which we call the reflecting-end partition function. The discussion was parallel to that in Chapter II, with some additional levels of complexity due to reflection, the dynamical nature, and the presence of elliptic functions (but see below).

The characterization of the reflecting-end partition function in the context of the dynamical reflection algebra was described in Section 1, where we also studied several general properties of that partition function.

	order	norm
ζ	2	θ
θ	2	$\zeta + l\gamma - \mu_l$
γ	$l^2 + 3l - 2$	$l\theta + 2l\lambda_l + \sum_j \lambda_j - (l-1)\mu_l$
λ_l	$4l$	$2l\gamma$
$\lambda_1, \cdots, \lambda_{l-1}$	2	γ
μ_l	2	$-\theta - (l-1)\gamma$
$\mu_1, \cdots, \mu_{l-1}$	2	0

Table 1. Up to a factor of $[\theta + \zeta + \lambda_l\,, \theta + (l-1)\gamma]$ the function m_l defined in (3.24) is a higher-order theta function in all variables and parameters, with orders and norms as indicated.

The work of Tsuchiya, Filali and Kitanine, applying the Korepin–Izergin method to find an expression for the partition function in terms of a single determinant, was surveyed in Section 2.

Our work on the reflecting-end partition function was the topic of Section 3. Using the dynamical reflection algebra we derived a cyclic linear functional equation for the partition function in Section 3.1. By construction this functional equation has a solution. In Section 3.2 we showed that any analytic solution necessarily shares several properties with the partition function. In Section 3.3 we further provided quite compelling evidence for the uniqueness, up to normalization, within the class of analytic functions on $\mathbb{C}^L$. This allowed us to obtain a new expression for the partition function as a symmetrized sum (3.23), which may also be rewritten as a multiple contour integral. We saw that the analytic and algebraic properties of the Jacobi theta functions in fact allow for a deeper insight into the analytic and functional properties of the functional equation. Unlike in Chapter II there are a few points where we do not have a complete proof yet, notably for the special zeroes and the reduction step. In those cases, however, numerical checks provide evidence confirming the validity of these steps beyond a physicist's doubt.

Discussion. There are several things to notice when comparing the analysis and results from Section 3 with those in Section 2 or with the domain-wall case from Section II.3.

Comparison with Tsuchiya–Filali–Kitanine. Concerning the similarities and differences between the approaches of Sections II.2 and II.3 the general discussion in Section II.4 carries over to the present case. As we discussed at the end of Section 3.3 we have unfortunately not yet succeeded in explicitly matching our solution with the determinant of Tsuchiya, Filali and Kitanine.

Trigonometric and non-dynamical limits. By taking the trigonometric limit $e^{i\pi\tau} \to 0$ of vanishing elliptic nome the function $f(\lambda) \propto \vartheta_1(i\lambda|\tau)$ degenerates into the

hyperbolic sine. By reinterpreting $[\lambda]$ as $\sinh(\lambda)$ like in Chapter II one thus immediately obtains the analogous results for the trigonometric SOS model on the same lattice. Note that the degree of the limiting trigonometric polynomials may turn out to be lower than the order of the original higher-order theta function due to cancellations, as happens in $[2\lambda]$ or in (II.3.16). In the trigonometric case one may again derive PDEs in the manner described in Section II.4; for the non-dynamical case this was done in [1].

The non-dynamical limit is formally taken by letting $\theta \to \infty$. This yields some additional exponential factors with respect to the conventions from Section II.1.1; in particular one obtains the $U_q(\widehat{\mathfrak{sl}_2})$-invariant form of the six-vertex R-matrix. However, we have chosen our conventions such that factors involving θ always come in ratios, so that one precisely recovers all formulas from [1] by simply dropping all such ratios.

Comparison with domain-wall case. Although we started from the (dynamical) reflection algebra, the functional equation (3.1) has the same form as (II.3.1). The reflection-algebra structure [compare (3.5) with (II.3.6)] reveals itself in the fact that the eigenvalue $\bar{\Lambda}_{\mathcal{A}}$, featuring in M_0, now consist of two terms; the same is true for all coefficients M_i [compare (3.2) with (II.3.2)]. Another notable difference with the functional equation from [58] is that, due to the reflecting boundary, our equation does not determine the behaviour of the partition function with respect to the dynamical parameter θ. This can already be anticipated at the algebraic level by comparing the θ-dependence of the monodromy matrices in the defining relations (1.10) of the dynamical Yang-Baxter algebra $\mathfrak{A} = A_{\tau,\gamma}(\mathfrak{sl}_2)$ with that in (1.18) for the dynamical reflection algebra $\mathfrak{B} \subseteq \mathfrak{A}$. This results in the presence of shifts in (I.3.42), while these are absent in (1.27).

Outlook. There are various problems left that we do not address in this thesis, such as

- completing the proofs in Sections 3.2–3.3;
- the homogeneous limit, in which our expressions for the partition function might be easier to handle than (2);
- the relation to combinatorial problems for the homogeneous model at the ice-like point $\gamma = \mathrm{i}\pi/3$;
- the thermodynamic limit, which has been studied for the ordinary six-vertex model with the same boundary conditions in [38];
- investigating whether this method can also be applied to models associated with Lie algebras $\mathfrak{sl}_N$ of higher rank, or even Lie superalgebras.

For the trigonometric SOS model it should also be quite straightforward to convert our functional equation into a family of partial differential equations as in [1], which might offer new insights into the symmetries of the partition function.

A Jacobi theta functions

The odd Jacobi theta function is rather economic: we only need a few of its properties to be able to work with it, and these properties characterize it.

A.1 The odd Jacobi theta function

The elliptic solution of the dynamical Yang-Baxter equation, see (1.1), features the function

$$f(\lambda) := -\frac{\mathrm{i}}{2}\,\mathrm{e}^{-\mathrm{i}\pi\tau/4}\,\vartheta_1(\mathrm{i}\lambda|\tau) = \frac{1}{2}\sum_{n\in\mathbb{Z}}(-1)^n\,\mathrm{e}^{\mathrm{i}n(n+1)\pi\tau}\,\mathrm{e}^{-(2n+1)\lambda} = \sum_{n\in\mathbb{N}_0}(-1)^n\,\mathrm{e}^{\mathrm{i}n(n+1)\pi\tau}\sinh((2n+1)\lambda)\,. \tag{A.1}$$

Here ϑ_1 is a Jacobi theta function and $\mathbb{N}_0 := \mathbb{N}\cup\{0\}$. The series in (A.1) converge absolutely when the elliptic nome $\mathrm{e}^{\mathrm{i}\pi\tau}$ satisfies $|\,\mathrm{e}^{\mathrm{i}\pi\tau}\,| < 1$. When $\mathrm{e}^{\mathrm{i}\pi\tau}$ tends to zero the theta function degenerates into a trigonometric function, and the prefactor in (A.1) is chosen such that $\lim_{\tau\to\mathrm{i}\infty} f(\lambda) = \sinh(\lambda)$.

In Section 3 we often use the short-hand $[\lambda] := f(\lambda)$ and $[\lambda_1,\lambda_2,\cdots] := [\lambda_1]\,[\lambda_2]\cdots$. The properties that we need to work with the special function f are directly inherited from the odd Jacobi theta function:

- *Analytic structure:* f is entire (holomorphic on all of $\mathbb{C}$) and only has simple zeroes;
- *Double quasiperiodicity:* $[\lambda+\mathrm{i}\pi] = -[\lambda]$ and $[\lambda+\mathrm{i}\pi\tau] = -\,\mathrm{e}^{-\mathrm{i}\pi\tau}\,\mathrm{e}^{-2\lambda}\,[\lambda]$;
- *Parity:* f is odd, $[-\lambda] = -[\lambda]$.

These properties readily follow from the series (A.1). The zeroes of f form a lattice, $\mathrm{i}\pi\,\mathbb{Z}+\mathrm{i}\pi\tau\,\mathbb{Z}\subseteq\mathbb{C}$. Using Liouville's theorem it is not hard to see that the above properties imply that f obeys the *addition rule*

$$[\lambda_1+\lambda_3,\lambda_1-\lambda_3,\lambda_2+\lambda_4,\lambda_2-\lambda_4] - [\lambda_1+\lambda_4,\lambda_1-\lambda_4,\lambda_2+\lambda_3,\lambda_2-\lambda_3] = [\lambda_1+\lambda_2,\lambda_1-\lambda_2,\lambda_3+\lambda_4,\lambda_3-\lambda_4]\,. \tag{A.2}$$

Reversely, the addition rule implies that f is odd. Moreover, up to a constant factor, (A.2) uniquely characterizes f along with its trigonometric and rational limits amongst all entire functions with only simple zeroes.

Since we occasionally encounter $f'(0)$ in Chapter III let us also mention the identities $\vartheta_1'(0|\tau) = \vartheta_2(0|\tau)\,\vartheta_3(0|\tau)\,\vartheta_4(0|\tau) = 2\,\mathrm{e}^{\mathrm{i}\pi\tau/4}\,(\mathrm{e}^{2\mathrm{i}\pi\tau};\mathrm{e}^{2\mathrm{i}\pi\tau})_\infty^3$, where ϑ_2, ϑ_3 and ϑ_4 are the other Jacobi theta functions, and $(p;q)_\infty := \prod_{n\in\mathbb{N}_0}(1-p\,q^n)$ is the q-Pochhammer symbol (q-shifted factorial). More about Jacobi theta functions can be found in [11, §15], [77] or [78, §21]. A useful quick reference is [79, §20].

A.2 Higher-order theta functions

Fix $\tau \in \mathbb{C}$ with $\mathrm{Im}(\tau) > 0$ and consider the function f from (A.1). For $N \in \mathbb{N}_0$ and $t \in \mathbb{C}$ one defines a *theta function of order N and norm t* to be a complex function $F(\lambda)$ for which there exist numbers $\Omega, t_1, \cdots, t_N \in \mathbb{C}$ with $\sum_{n=1}^{N} t_n = t$ such that F can be written in the factorized form

$$F(\lambda) = \Omega \prod_{n=1}^{N} [\lambda + t_n] = \Omega\, [\lambda + t_1, \cdots, \lambda + t_N]\,. \tag{A.3}$$

Let $\Theta_{N,t}$ be the set of theta functions of order N and norm t with respect to the variable λ. A classic result [80, §15] is that $F(\lambda) \in \Theta_{N,t}$ if and only if $F(\lambda)$ is entire and doubly quasiperiodic with quasiperiods $\mathrm{i}\pi$ and $\mathrm{i}\pi\tau$ such that

$$F(\lambda + \mathrm{i}\pi) = (-1)^N F(\lambda)\,, \qquad F(\lambda + \mathrm{i}\pi\tau) = \mathrm{e}^{-2t}\, (-\mathrm{e}^{-2\lambda}\, \mathrm{e}^{-\mathrm{i}\pi\tau})^N F(\lambda)\,. \tag{A.4}$$

For example, $F(\lambda) \coloneqq [n\lambda + \gamma]$ lies in $\Theta_{n^2,n\gamma}$ with respect to λ. As a corollary of (A.4) we see that $\Theta_{N,t}$ is a vector space: any linear combination of functions in $\Theta_{N,t}$ also satisfies (A.4). This factorization property for higher-order theta functions is very useful.

For completeness we also mention that when $N \geq 2$ the dimension of $\Theta_{N,t}$ is equal to N, and that there is an interpolation formula expressing $F(\lambda) \in \Theta_{N,t}$ in terms of its values at N generic points $\lambda_n \in \mathbb{C}$:

$$F(\lambda) = \sum_{n=1}^{N} F(\lambda_n) \frac{[\lambda - \lambda_n + t + \sum_{m=1}^{N} \lambda_m]}{[t + \sum_{m=1}^{N} \lambda_m]} \prod_{\substack{m=1 \\ m \neq n}}^{N} \frac{[\lambda - \lambda_m]}{[\lambda_n - \lambda_m]}\,. \tag{A.5}$$

Further details can be found in [81, 82].

In addition, by Liouville's theorem any elliptic function can be written as a ratio of two higher-order theta functions. Since an elliptic function is doubly periodic these two higher-order theta functions must have the same order and norm. From this we can deduce that an elliptic function, unless constant, has the same number of poles and zeroes in any parallelogram between points in its period lattice Λ.

B Computing the vacuum eigenvalues

In this appendix we ascertain that the eigenvalues (1.24) of the pseudovacua (1.23) for the double-row quantum operators $\mathcal{A}$ and $\widetilde{\mathcal{D}}$ are given by (1.25).

In terms of the ordinary monodromy matrices (1.9) and the reflection matrix (1.15) the

entries (1.19) of the double-row monodromy matrix (1.17) read [cf. (I.3.34)]

$$\begin{aligned}
\mathcal{A}(\lambda) &= k_+(\lambda,\theta)\,A(\lambda,\theta)\,\bar{A}(\lambda,\theta) + k_-(\lambda,\theta)\,B(\lambda,\theta)\,\bar{C}(\lambda,\theta)\,,\\
\mathcal{B}(\lambda) &= k_+(\lambda,\theta)\,A(\lambda,\theta)\,\bar{B}(\lambda,\theta) + k_-(\lambda,\theta)\,B(\lambda,\theta)\,\bar{D}(\lambda,\theta)\,,\\
\mathcal{C}(\lambda) &= k_+(\lambda,\theta)\,C(\lambda,\theta)\,\bar{A}(\lambda,\theta) + k_-(\lambda,\theta)\,D(\lambda,\theta)\,\bar{C}(\lambda,\theta)\,,\\
\mathcal{D}(\lambda) &= k_+(\lambda,\theta)\,C(\lambda,\theta)\,\bar{B}(\lambda,\theta) + k_-(\lambda,\theta)\,D(\lambda,\theta)\,\bar{D}(\lambda,\theta)\,.
\end{aligned} \tag{B.1}$$

Thus we first compute the action of the generators of the dynamical Yang-Baxter algebra $\mathfrak{A}$ on the vectors (1.23). Due to (1.2) and (1.3), $|\Omega\rangle$ is a simultaneous eigenvector of A, C, D and $\bar{A}, \bar{C}, \bar{D}$, with corresponding eigenvalues [cf. (II.1.11)]

$$\begin{aligned}
&\Lambda_A(\lambda,\theta) = \prod_{j=1}^{L}[\lambda-\mu_j+\gamma]\,, && \Lambda_{\bar{A}}(\lambda,\theta) = \prod_{j=1}^{L}[\lambda+\mu_j+\gamma]\,,\\
&\Lambda_C(\lambda,\theta) = 0\,, && \Lambda_{\bar{C}}(\lambda,\theta) = 0\,,\\
&\Lambda_D(\lambda,\theta) = \frac{[\theta+\gamma]}{[\theta-(L-1)\gamma]}\prod_{j=1}^{L}[\lambda-\mu_j]\,, && \Lambda_{\bar{D}}(\lambda,\theta) = \frac{[\theta-L\gamma]}{[\theta]}\prod_{j=1}^{L}[\lambda+\mu_j]\,.
\end{aligned} \tag{B.2}$$

Likewise $\langle\bar{\Omega}|$ is an eigenvector of these operators, with eigenvalues

$$\begin{aligned}
&\bar{\Lambda}_A(\lambda,\theta) = \frac{[\theta-\gamma]}{[\theta+(L-1)\gamma]}\prod_{j=1}^{L}[\lambda-\mu_j]\,, && \bar{\Lambda}_{\bar{A}}(\lambda,\theta) = \frac{[\theta+L\gamma]}{[\theta]}\prod_{j=1}^{L}[\lambda+\mu_j]\,,\\
&\bar{\Lambda}_C(\lambda,\theta) = 0\,, && \bar{\Lambda}_{\bar{C}}(\lambda,\theta) = 0\,,\\
&\bar{\Lambda}_D(\lambda,\theta) = \prod_{j=1}^{L}[\lambda-\mu_j+\gamma]\,, && \bar{\Lambda}_{\bar{D}}(\lambda,\theta) = \prod_{j=1}^{L}[\lambda+\mu_j+\gamma]\,.
\end{aligned} \tag{B.3}$$

Combining these with (B.1) we find that $\Lambda_{\mathcal{A}}$ is given by the expression in (1.25). In contrast, neither pseudovacua is an eigenvector of B or $\bar{B}$. This prevents a simple evaluation of $C\,\bar{B}|\Omega\rangle$ needed for $\Lambda_{\mathcal{D}}$ in view of (B.1). This issue can be circumvented using the (3,2)-component of the relation (1.13), together with (1.21), to rewrite the problematic term as

$$\begin{aligned}
C(\lambda,\theta)\,\bar{B}(\lambda,\theta) &= \bar{B}(\lambda,\theta+\gamma)\,C(\lambda,\theta+\gamma)\\
&\quad+\frac{[\gamma]}{[2\lambda+\gamma]}\Big(\frac{[\theta-\gamma(H-1)+2\lambda]}{[\theta-\gamma(H-1)]}\,\bar{A}(\lambda,\theta+\gamma)\,A(\lambda,\theta+\gamma)\\
&\qquad-\frac{[\theta+\gamma+2\lambda]}{[\theta+\gamma]}\,D(\lambda,\theta)\,\bar{D}(\lambda,\theta)\Big)\,.
\end{aligned} \tag{B.4}$$

Together with (B.1) and (B.2) this yields the result for $\Lambda_{\widetilde{\mathcal{D}}}$ from (1.25), where $\widetilde{\mathcal{D}}$ was defined in (1.20) and we also used the addition rule for f to rewrite the prefactor.

For $\bar{\Lambda}_{\mathcal{A}}$ we proceed analogously. The evaluation of $\langle\bar{\Omega}|B\,\bar{C}$ is avoided by exploiting the (2,3)-component of following relation contained in (1.13):

$$\begin{aligned} B(\lambda,\theta)\,\bar{C}(\lambda,\theta) &= \bar{C}(\lambda,\theta-\gamma)\,B(\lambda,\theta-\gamma) \\ &\quad + \frac{[\gamma]}{[2\lambda+\gamma]}\Big(\frac{[\theta-\gamma(H+1)-2\lambda]}{[\theta-\gamma(H+1)]}\,\bar{D}(\lambda,\theta-\gamma)\,D(\lambda,\theta-\gamma) \\ &\qquad - \frac{[\theta-\gamma-2\lambda]}{[\theta-\gamma]}\,A(\lambda,\theta)\,\bar{A}(\lambda,\theta)\Big)\,. \end{aligned} \tag{B.5}$$

In combination with (B.1) and (B.3) this establishes the last expression in (1.25), again invoking the addition rule for the prefactor.

Part Two

Exact solvability in long-range spin chains

Chapter IV

The partially isotropic generalization of Inozemtsev's spin chain

In this chapter we delve into the realm of *quantum* mechanics. The main character is Inozemtsev's spin chain, which involves long-range interactions governed by an elliptic potential. Inozemtsev introduced this model in 1990 [83] and studied it in detail in the following decade, see the review [84]. In 2004 the model also made an appearance in the context of the gauge-gravity duality, when Serban and Staudacher [85] realized that it fairly accurately (viz. perturbatively up to three loops) describes the dilatation operator in planar $\mathcal{N} = 4$ super-Yang–Mills theory.

Spin chains are quantum-mechanical models with only spin degrees of freedom, yet they exhibit rich physics. Taking into account time we are once more in two dimensions, and quantum integrability also has a role to play for certain special spin chains. Inozemtsev's spin chain interpolates between the celebrated Heisenberg XXX spin chain on the one hand, which only has nearest-neighbour interactions and can be solved via the Bethe ansatz, and the Haldane–Shastry model on the other, featuring long-range interactions and whose solvability relies on quantum-group symmetry present for any finite L. Many features that one tends to take for granted for those limiting cases turn out to be much more delicate for this more general spin chain. Inozemtsev found the exact solution, taking the form of a generalized Bethe ansatz, and proposed a set of conserved charges (symmetries) which are believed to commute with each other. On the other hand, the model does not have a known description via the quantum inverse-scattering method from Section I.4.2.

Challenging the precise meaning of notions such as quantum integrability and exact solvability, Inozemtsev's spin chain is of great theoretical interest. Its integrability was recently examined through the statistical properties of its spectrum by Finkel and González-López [86]. Another way of trying to get a deeper understanding of the model is to see whether it is possible to modify it in a way that preserves some of the salient features, in particular some sort of solvability. Studying such generalizations allows one to investigate whether Inozemtsev's model is an isolated model, for which any change destroys its analytical tractability, or whether it is more robust. In fact, some other spin chains that are related to Inozemtsev's model have already been studied.

- The (hyperbolic) Frahm–Inozemtsev spin chain of finite length has sites that, rather than being uniformly spaced, are located at the zeroes of a Laguerre poly-

nomial [87]. It has an effective Ising-model description that enables one to evaluate the free energy in the thermodynamic limit.

- Finkel and González-López [88] found that Inozemtsev's spin chain also has an $\mathfrak{su}_{1|1}$ counterpart, which can be mapped to a system of free spinless fermions allowing one to solve the model and to study the thermodynamics exactly.

We will be interested in another, more conservative, way to alter the model: deforming it to break a part of the rotational symmetry, just as the XXZ spin chain is a one-parameter extension of the XXX model with deformation parameter Δ.

Outline. This chapter is set up as follows. We start by reviewing the background that we will need to follow Inozemtsev's work. The relevant spin chains are introduced in Section 1.1. To understand Inozemtsev's solution we further need to know some things about yet another, but closely related, class of exactly solvable models: quantum many-body systems with particles moving in one dimension. The relevant parts of this topic are summarized in Section 1.2. Inozemtsev's solution for the isotropic case is recalled in Section 1.3, at least in the easier case of infinite length.

With all these preliminaries in place we are ready for the main part, Section 2. After introducing the partially isotropic version of Inozemtsev's model and collecting some basic facts we describe our efforts to solve this model. The reader should be warned that this is work in progress, and—spoiler!—we have not yet been able to find evidence that this model might be solvable too. Preliminary conclusions and an outlook are given in Section 3.

Notation. In Part One of this thesis we used H to denote (twice) the spin-z operator. In the present chapter we switch to the usual quantum-mechanical notation S^z for the spin-z operator, as we prefer to reserve 'H' for the various Hamiltonians that we will encounter. The parametrization of Δ via the crossing parameter differs by a factor of i from that in Part One: in this chapter we use $\Delta = \cos(\gamma)$ instead of $\cosh(\gamma)$.

1 Exactly solvable spin chains

In this section we cover the background that will be needed in Section 2.

1.1 Spin chains

We begin with a brief review of spin chains, focussing on the nearest-neighbour Heisenberg–Ising model, the long-range Haldane–Shastry spin chain, and of course Inozemtsev's spin chain. We start with the case of finite system size.

Finite spin chains. A *spin chain* of length L is a quantum-mechanical model whose Hilbert space W of states is a tensor product [cf. Section I.3.2]

$$W = \bigotimes_{l \in \mathbb{Z}_L} V_l \tag{1.1}$$

of finite-dimensional irreducible $\mathfrak{su}_2$-representations V_l associated to the sites of a one-dimensional lattice. In (1.1) we have chosen periodic boundary conditions, so the lattice $\mathbb{Z}_L := \mathbb{Z}/L\mathbb{Z}$ forms a circular chain; this choice is convenient for computations and compatible with translational symmetry. The microscopic degrees of freedom are quantum-mechanical spins that live in a 'local quantum space' V_l. The spin Lie algebra $\mathfrak{su}_2$ acts on these V_l by local spin operators (S_l^x, S_l^y, S_l^z), where we employ the tensor-leg notation introduced in Section I.3.2 [cf. (I.3.10)] so that

$$[S_k^\alpha, S_l^\beta] = \mathrm{i}\hbar\,\delta_{kl} \sum_{\gamma=x,y,z} \varepsilon^{\alpha\beta\gamma}\, S_l^\gamma\,, \tag{1.2}$$

with the totally antisymmetric $\mathfrak{su}_2$-structure constant fixed by $\varepsilon^{xyz} = 1$. For computations it is convenient to pass to the $[\mathfrak{sl}_2(\mathbb{C}) \cong (\mathfrak{su}_2)_{\mathbb{C}}]$ ladder operators $S_l^\pm := S_l^x \pm \mathrm{i}\, S_l^y$ which, together with S_l^z, satisfy

$$[S_k^z, S_l^\pm] = \pm\hbar\,\delta_{kl}\, S_l^\pm\,, \qquad [S_k^+, S_l^-] = 2\hbar\,\delta_{kl}\, S_l^z\,, \qquad [S_k^\pm, S_l^\pm] = 0\,. \tag{1.3}$$

The Hilbert space W also carries a 'global' $\mathfrak{su}_2$-representation, given by the total spin operator (S^z, S^y, S^z) defined as

$$S^\alpha := \sum_{l \in \mathbb{Z}_L} S_l^\alpha \in \mathrm{End}(W)\,, \qquad \alpha = x, y, z\,. \tag{1.4}$$

We are interested in the case of spin 1/2, where $V_l = \mathbb{C}|{\uparrow}\rangle_l \oplus \mathbb{C}|{\downarrow}\rangle_l$ is a copy of the defining (fundamental) representation of $\mathfrak{su}_2$, and the S_l^α are represented by the Pauli spin matrices as $S_l^\alpha = \hbar\,\sigma^\alpha/2$ as usual. Such a spin chain is illustrated in Figure 1. The Hilbert space (1.1) comes with an (orthonormal) basis constructed by taking tensor products of the local spin (standard-basis) vectors $|{\uparrow}\rangle_l$ and $|{\downarrow}\rangle_l$. Let us rescale the energy to set $\hbar = 1$ from now on.

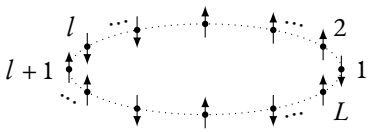

Figure 1. A spin chain of length L with spin 1/2 and periodic boundary conditions.

In this set-up it remains to specify a (hermitean) Hamiltonian $H \in \mathrm{End}(W)$ describing the interactions between the spins. We will consider spin chains that

- are *homogeneous*, i.e. translationally invariant;
- are at least *partially isotropic*, i.e. $[S^z, H] = 0$; and
- involve only *pairwise* interactions.

The goal is to understand the spectrum of the Hamiltonian. First we review the general consequences of these properties.

Partial isotropy. Note that the partial isotropy is an incarnation of the ice rule from Part One. As in Section I.4.2 it implies that W decomposes into sectors of fixed total spin-z [cf. (I.4.24)]:

$$W = \bigoplus_{M=0}^{L} W_M \,, \qquad\qquad S^z|_{W_M} = (\tfrac{1}{2}L - M)\,\mathbb{1} \,. \tag{1.5}$$

The M-particle sector W_M comes with an orthonormal *coordinate* (Wannier) basis

$$|\vec{l}\rangle = |l_1, \cdots, l_M\rangle := S^-_{l_1} \cdots S^-_{l_M} |\Omega\rangle \in W_M \,, \qquad\qquad l_1 < \cdots < l_M \,, \tag{1.6}$$

constructed from the (highest-weight) pseudovacuum (I.3.21) by flipping M spins. To avoid overcounting the components of $\vec{l}$ in (1.6) are required to lie in the 'standard domain' $\{1, \cdots, L\}$—at the expense of manifest periodicity—and to be strictly increasing. Thus $\dim(W_M) = \binom{L}{M}$ and any vector in the M-particle sector can be written as

$$|\Psi_M\rangle = \sum_{l_1<\cdots<l_M} \Psi(\vec{l})\, |\vec{l}\rangle \in W_M \,. \tag{1.7}$$

The partial isotropy allows us to focus on diagonalizing the Hamiltonian in the M-particle sector: we want to solve the eigenvalue problem

$$H\,|\Psi_M\rangle = E_M\,|\Psi_M\rangle, \qquad |\Psi_M\rangle \in W_M \tag{1.8}$$

for every $M \in \mathbb{N}_0$.

Translational invariance. The one-particle sector is completely determined by homogeneity. Translational invariance fixes the one-particle wave function to a plane wave, $\Psi(l) \propto \mathrm{e}^{\mathrm{i}p\,l}$. Here $p \in \mathbb{R}/2\pi\mathbb{Z}$ is the *(total) momentum*, which in general is determined by the eigenvalue $\mathrm{e}^{\mathrm{i}p}$ of the (unitary) shift operator U acting by translations by one site. Periodic boundary conditions imply that $U^L = \mathbb{1}$ is the identity operator on W, leading to momentum quantization $p \in (2\pi/L)\,\mathbb{Z}_L$ as expected for quantum particles on a circle. In this way we obtain another orthonormal basis for W_1, describing *magnons*,

$$|\Psi_1; p\rangle = \frac{1}{\sqrt{L}} \sum_{l\in\mathbb{Z}_L} \mathrm{e}^{\mathrm{i}p\,l}\,|l\rangle \in W_1 \,. \tag{1.9}$$

With respect to this (Bloch) basis any translationally invariant Hamiltonian is diagonal in the one-particle sector. Of course the corresponding energy eigenvalues depend on the Hamiltonian and determine whether or not magnons are 'quasiparticles' describing low-lying excitations in the physical spectrum.

For $M \geq 2$ the situation is more interesting. Homogeneity does no longer suffice for determining the wave functions $\Psi_p(\vec{l}) = \langle \vec{l} | \Psi_M; p \rangle$, see e.g. [5, §2.1]. For the special spin chains for which it is known how to diagonalize the Hamiltonian by analytic methods the strategy for doing so differs from case to case, as we will see in Section 1.3.

Pairwise interactions. The most general spin chain that is homogeneous, partially isotropic and involves pairwise interactions has a Hamiltonian of the form

$$H = -\frac{J}{2} \sum_{k,l \in \mathbb{Z}_L}^{\star} V(k-l) \left(S_k \cdot_\Delta S_l - \frac{\Delta}{4} \right), \tag{1.10}$$

where we use a star to indicate that equal values of k and l are to be excluded from the sum. For brevity we have introduced the 'Δ-deformed scalar product'

$$S_k \cdot_\Delta S_l := S_k^x S_l^x + S_k^y S_l^y + \Delta S_k^z S_l^z = \frac{1}{4} \left(2 \left(\sigma_k^+ \sigma_l^- + \sigma_k^- \sigma_l^+ \right) + \Delta \sigma_k^z \sigma_l^z \right) \tag{1.11}$$

describing hopping and interactions between sites k and l. The interactions depend on the anisotropy parameter Δ; at $\Delta = 1$ full rotational invariance is restored. Since (1.11) is symmetric in k and l we may take the pair potential V to be an even function, $V(-l) = V(l)$, on $\mathbb{Z}_L \setminus \{0\}$. We have divided the coupling constant J by two to compensate for the fact that each summand appears twice. Finally, the shift in (1.10) ensures that the pseudovacuum $|\Omega\rangle \in W_0$ has zero energy. This pseudovacuum is a ground state when $J\Delta > 0$ and $|\Delta| \geq 1$ if we assume V to be nonnegative.

Regarding the one-particle sector we have for $j \neq k$

$$\left(S_j \cdot_\Delta S_k - \frac{\Delta}{4} \right) |l\rangle = \frac{1}{2} \delta_{k,l} \left(|j\rangle - \Delta |l\rangle \right) + (j \leftrightarrow k), \tag{1.12}$$

so it follows that the energy of the magnon (1.9) is given by

$$\varepsilon(p) := E_1(p) = \frac{J}{2} \sum_{l \in \mathbb{Z}_L \setminus \{0\}} (\Delta - \mathrm{e}^{\mathrm{i}pl}) V(l) = \frac{J}{2} \sum_{l \in \mathbb{Z}_L \setminus \{0\}} (\Delta - \cos pl) V(l). \tag{1.13}$$

If we would set $V(0) := 0$ the Δ-independent part is the discrete Fourier transform of V up to a factor. Note that (1.13) is an 'off-shell' quantity: 'on shell' the momenta are restricted to $p \in (2\pi/L)\mathbb{Z}_L$. Also observe that for $M = 1$ the shift by $\mathbb{1}$ in (1.10) ensures that $\varepsilon(0)$ vanishes when $\Delta = 1$. The resulting degeneracy in the energy spectrum is a direct consequence of the isotropy in that case: the zero-momentum magnon is nothing but the properly normalized first $\mathfrak{sl}_2(\mathbb{C})$-descendant of the pseudovacuum, $|\Psi_1; 0\rangle \propto S^- |\Omega\rangle$.

Let us turn to some examples.

Heisenberg–Ising spin chain. In Section I.4.1 we already encountered the *Heisenberg–Ising* or *xxz* model (I.4.8). It involves nearest-neighbour (contact) interactions only:

$$\begin{aligned} V_{\mathrm{xxz}}(l) &= \delta_{|l \bmod L|,1}\,, \\ \varepsilon_{\mathrm{xxz}}(p) &= J\,(\Delta - \cos p)\,. \end{aligned} \tag{1.14}$$

The completely isotropic case $\Delta = 1$ is the *Heisenberg* or *xxx* spin chain, introduced by Heisenberg in 1928 [89]. Three years later Bethe presented the solution of this model in his seminal work [90], using an ansatz written down by Bloch one year prior [91]. The partially isotropic version (1.14) was put forward by Kasteleijn in 1952 [92] and solved by Orbach six years later [93] following Bethe's analysis.

Haldane–Shastry spin chain. In 1988 Haldane and Shastry [94, 95] independently proposed and (partially) diagonalized a spin chain with long-range interactions, obtained (for $\Delta = 1$) from the Hubbard model at half filling when the on-site repulsion grows to infinity. The Hamiltonian is given by

$$\begin{aligned} V_{\mathrm{HS}}(l) &= \frac{\pi^2}{L^2 \sin^2(\pi l/L)}\,, \\ \varepsilon_{\mathrm{HS}}(p) &= \frac{\pi^2 J}{2L^2}\Big[\frac{1}{3}(L^2-1)\,\Delta - \sum_{l=1}^{L-1} \frac{\cos p\, l}{\sin^2(\pi l/L)}\Big]\,. \end{aligned} \tag{1.15}$$

This pair potential has a nice geometric interpretation: thinking of the spin chain as embedded in the circle of circumference L centered at the origin, with site l sitting at $x_l = (L/2\pi)\,\mathrm{e}^{2\pi \mathrm{i}\, l/L}$, the potential is of $1/r^2$ form with $r = d(x_k, x_l) = (L/\pi)\,|\sin(\pi(k-l)/L)|$ the chord distance between the positions of the interacting spins. On shell the one-particle energy in (1.15) simplifies to a quadratic function:

$$\varepsilon_{\mathrm{HS}}(p)\big|_{p \in \frac{2\pi}{L}\mathbb{Z}_L} = \frac{\pi^2 J}{6L^2}(L^2-1)\,(\Delta - 1) - \frac{J}{4} p\,(p - 2\pi)\,. \tag{1.16}$$

As we will see this model is also exactly solvable, yet in a completely different way than the xxz spin chain.

Inozemtsev spin chain. Two years after the papers of Haldane and Shastry another long-range spin chain, this time completely isotropic and with *elliptic* interactions, was put forward by Inozemtsev [83]:

$$\Delta = 1\,; \qquad V_\kappa(l) = \frac{\sinh^2\kappa}{\kappa^2}\Big[\wp_L(l) + \frac{2\kappa}{\mathrm{i}\pi}\zeta_L\Big(\frac{\mathrm{i}\pi}{2\kappa}\Big)\Big]\,. \tag{1.17}$$

Here $\wp_L$ and ζ_L denote the Weierstraß elliptic functions with (quasi)periods $(L, \mathrm{i}\pi/\kappa)$ for $\kappa \in \mathbb{R}_{>0}$, so that (1.17) is real for $l \in \mathbb{Z} \subseteq \mathbb{R}$. What we need to know about these functions is collected in Appendix A.

The remarkable feature of Inozemtsev's spin chain is that it interpolates between the xxx and isotropic Haldane–Shastry spin chains. As κ tends to infinity the nearest-neighbour interactions start to dominate while for vanishing κ the elliptic functions degenerate into trigonometric ones. The constant prefactor and shift in (1.17) are included to get a precise match in both limits.

On shell the one-particle energy [83, §4] can be written as

$$\varepsilon_\kappa(p)\big|_{p\in\frac{2\pi}{L}\mathbb{Z}_L} = \frac{J\,\sinh^2\kappa}{2\,\kappa^2}\Big[\frac{2\kappa}{\mathrm{i}\pi}\,\zeta_1\Big(\frac{\mathrm{i}\pi}{2\kappa}\Big) - \frac{1}{2}\,\wp_1\Big(\frac{\mathrm{i}p}{2\kappa}\Big) - 2\kappa^2\lambda_\kappa(p)^2\Big]\,, \tag{1.18}$$

where for later convenience we have defined the (complex) function

$$\lambda_\kappa(z) \coloneqq \frac{1}{\pi}\Big[\frac{\mathrm{i}\pi}{2\kappa}\zeta_1\Big(\frac{\mathrm{i}z}{2\kappa}\Big) - \frac{\mathrm{i}z}{2\kappa}\zeta_1\Big(\frac{\mathrm{i}\pi}{2\kappa}\Big)\Big] \tag{1.19}$$

with quasiperiods $(1, \mathrm{i}\pi/\kappa)$. Useful properties of λ_κ are collected in Appendix B.

Infinite spin chains. Let us now describe the spin chains that are (morally) obtained from the above setting in the infinite-length limit in which L tends to infinity. To avoid a proliferation of sub- or superscripts we abuse notation and use the same symbols for the infinite-length counterparts of the spaces and operators encountered before. For a *much* more rigorous description we refer to [96, §6.2].

To each site $l \in \mathbb{Z}$ of the lattice we once more associate a copy $V_l \cong \mathbb{C}^2$ of the spin-1/2 $\mathfrak{su}_2$-irrep. The *global* quantum space W is the infinite-dimensional (separable) Hilbert space obtained as a completion of the linear span of all vectors differing from a fixed reference vector, which we again denote by $|\Omega\rangle \in W$, at only finitely many sites: the coordinate vectors (1.6) form a basis that is declared to be orthonormal, and the completion is with respect to that norm. By construction this Hilbert space comes with a decomposition into M-particle sectors

$$W = \bigoplus_{M\in\mathbb{N}_0} W_M\,, \qquad\qquad W_M \cong \ell^2(\{\vec{l} \in \mathbb{Z}^M \mid l_1 < \cdots < l_M\})\,. \tag{1.20}$$

Here $\mathbb{N}_0 \coloneqq \mathbb{N}\cup\{0\}$. The zero-particle sector is once again spanned by the pseudovacuum, $W_0 = \mathbb{C}\,|\Omega\rangle$. All other W_M are infinite-dimensional.

Although each local quantum space V_l carries an $\mathfrak{su}_2$-representation, let us show that this structure breaks down at the global level. The number operator $S^z \in \mathrm{End}(W)$, which is (densely) defined by

$$S^z|_{W_M} \coloneqq M\,\mathbb{1}\,, \tag{1.21}$$

keeps track of the number flipped spins with respect to $|\Omega\rangle$. As the notation indicates (1.21) plays the role of the total spin-z operator: one can think of it as $-\sum_l(S^z_l - 1/2)$,

where the shifts are a renormalization and we included an overall sign to get a positive operator. Although S^z is an unbounded operator on W—for each $M \geq 1$ pick a normalized $|\psi_M\rangle \in W_M$ and consider $\sum_M M^{-1}|\psi_M\rangle \in W$—the restrictions (1.21) are clearly bounded. The global spin raising- and lowering-operators are formally defined on W as $S^\pm = \sum_l S^\pm_l$ but, unlike (1.21), S^- cannot be rescued by any sort of (translationally invariant) renormalization: even $S^-|\Omega\rangle$ has infinite norm. Globally we can really only make sense of the total spin-z operator, and any spin chain on the infinite line is at most partially isotropic. As before we consider a spin chain whose Hamiltonian enjoys partial isotropy and homogeneity.

Partial isotropy. When $[H, S^z] = 0$ the Hamiltonian preserves the decomposition (1.20). As before we focus on solving the eigenvalue problem (1.8) for given M.

Translational invariance. Homogeneity again determines the one-particle sector, although the present case is a bit more subtle; the situation is rather like that for the free quantum-mechanical particle. Magnons with momentum p, i.e. translationally invariant one-particle vectors, are formally defined as [cf. (1.9)]

$$|\Psi_1; p\rangle := \frac{1}{\sqrt{2\pi}} \sum_{l\in\mathbb{Z}} \mathrm{e}^{\mathrm{i}p\,l}\,|l\rangle\,, \qquad\qquad p \in \mathbb{R}/2\pi\mathbb{Z}\,. \tag{1.22}$$

However, one can check that $\langle\Psi_1; p|\Psi_1; p'\rangle = \delta(p - p')$ whence these vectors are orthogonal but not normalizable, and therefore do not lie in W_1. Physical one-particle states are wave (magnon) packets of the form $\int_0^{2\pi} \mathrm{d}p\, A(p)\,|\Psi_1; p\rangle \in W_1$ with a square-integrable momentum profile $A \in L^2(\mathbb{R}/2\pi\mathbb{Z})$.

Pairwise interactions. The infinite-length versions of (1.10) and (1.13) are straightforward generalizations:

$$H = -\frac{J}{2} \sum_{k,l\in\mathbb{Z}}^{\star} V(k-l)\left(S_k \cdot_\Delta S_l - \frac{\Delta}{4}\right), \tag{1.23}$$

the pseudovacuum still has zero energy, and the magnon-dispersion relation reads

$$\varepsilon(p) := E_1(p) = \frac{J}{2} \sum_{l\in\mathbb{Z}_{[0]}} (\Delta - \mathrm{e}^{\mathrm{i}p\,l})\, V(l) = J \sum_{l\in\mathbb{N}} (\Delta - \cos p\,l)\, V(l)\,, \tag{1.24}$$

where we abbreviate $\mathbb{Z}_{[0]} := \mathbb{Z} \setminus \{0\}$. Set $V(0) := 0$. In this case the Δ-independent part is just the Fourier transform of V up to a factor.

Let us show that if V, viewed as a sequence, has absolutely convergent series, i.e. $V \in \ell^1(\mathbb{Z})$, then the restriction of (1.23) to any M-particle sector is bounded.

Proof. The action on the coordinate basis is determined by [cf. (1.12)]

$$\Big(S_j \cdot_\Delta S_k - \frac{\Delta}{4}\Big)\,|\vec{l}\rangle = \frac{1}{2}\,(1-\delta_{j,\vec{l}})\Big[\Big(\sum_{m=1}^{M}\delta_{k,l_m}\,|l_1,\cdots,j,\cdots,\widehat{l_m},\cdots,l_M\rangle\Big) - \Delta\,\delta_{k,\vec{l}}\,|\vec{l}\rangle\Big] + (j\leftrightarrow k)\,, \tag{1.25}$$

which assumes $j \neq k$. Here we employ the short-hand $\delta_{k,\vec{l}} \coloneqq \sum_{m=1}^{M}\delta_{kl_m}$ and the caret indicates that l_m is to be omitted. Using this we obtain

$$H\,|\vec{l}\rangle = \frac{J}{2}\sum_{m=1}^{M}\sum_{k\in\mathbb{Z}_{[\vec{l}]}} V(k-l_m)\,(\Delta\,|\vec{l}\rangle - |l_1,\cdots,k,\cdots,\widehat{l_m},\cdots,l_M\rangle)\,, \tag{1.26}$$

where we abbreviate $\mathbb{Z}_{[\vec{l}]} \coloneqq \mathbb{Z}\setminus\{l_1,\cdots,l_M\}$. Since the coordinate basis vectors are orthonormal and $V(l)\geq 0$ we arrive at the following bound for the (operator) norm of the restriction of the Hamiltonian:

$$\|H|_{W_M}\| \leq \frac{J}{2}\sqrt{M\,(M\,\Delta^2+1)}\,\|V\|_1\,, \qquad \|V\|_1 = \sum_{l\in\mathbb{Z}}|V(l)|\,. \tag{1.27}$$

□

In our examples $V(l)\geq 0$, so the absolute value in the last expression may be dropped.

Heisenberg–Ising spin chain. The infinite xxz spin chain has

$$V_{\mathrm{xxz}}(l) = \delta_{|l|,1}\,, \qquad \varepsilon_{\mathrm{xxz}}(p) = J\,(\Delta-\cos p)\,. \tag{1.28}$$

The spectrum of this model was analysed by Yang and Yang in 1966 [97].

Haldane–Shastry spin chain. Taking the limit $L\to\infty$ of (1.15) we arrive at the infinite Haldane–Shastry spin chain, with inverse-square potential

$$V_{\mathrm{HS}}(l) = \frac{1}{l^2}\,, \qquad \varepsilon_{\mathrm{HS}}(p) = \frac{\pi^2 J}{6}(\Delta-1) - \frac{J}{4}p\,(p-2\pi)\,. \tag{1.29}$$

Note that the one-particle energy is most easily obtained from (1.16).

Inozemtsev spin chain. When L tends to infinity the Weierstraß functions in (1.17) degenerate to hyperbolic functions, and the interactions are short ranged, decaying exponentially with increasing distance between the excited spins. The infinite Inozemtsev spin chain is given by

$$\begin{aligned} &\Delta = 1; \qquad V_\kappa(l) = \frac{\sinh^2\kappa}{\sinh^2\kappa\,l}\,,\\ &\varepsilon_\kappa(p) = \frac{J\,\sinh^2\kappa}{2\,\kappa^2}\Big[\frac{2\kappa}{\mathrm{i}\pi}\,\zeta_1\Big(\frac{\mathrm{i}\pi}{2\kappa}\Big) - \frac{1}{2}\,\wp_1\Big(\frac{\mathrm{i}p}{2\kappa}\Big) - 2\kappa^2\lambda_\kappa(p)^2\Big]\,. \end{aligned} \tag{1.30}$$

Note that the dispersion relation has precisely the same form as the on-shell result (1.18) for finite L. Although this might be surprising it is easy to understand: the right-hand side of (1.18) is independent of L while that relation holds for all L. A direct computation of ε_κ by evaluating the series in (1.24) can be found in Appendix C. When $\kappa \to \infty$ or $\kappa \to 0$ the magnon dispersion relation reproduces the isotropic limits $\Delta \to 1$ of (1.28)–(1.29), see also Figure 2.

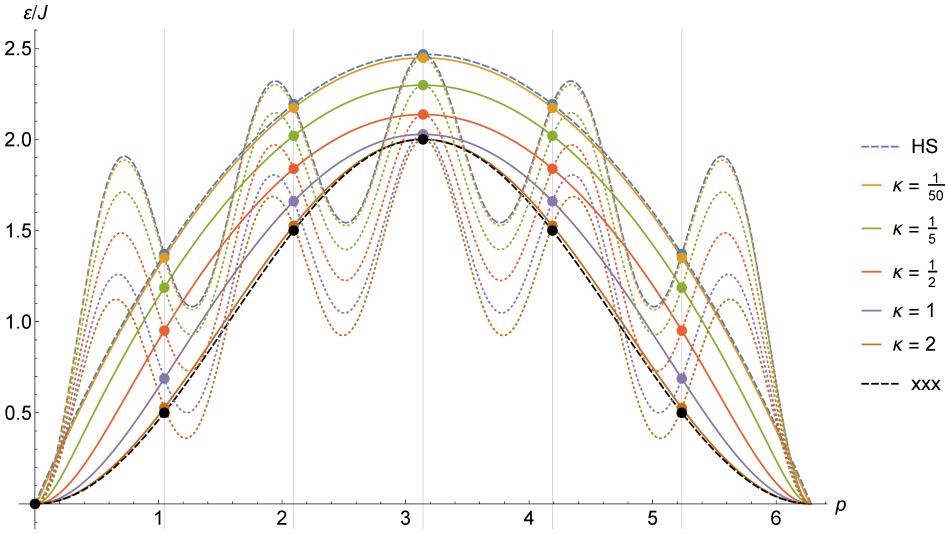

Figure 2. [Colour online] The one-particle energies for various spin chains. The asymptotic dispersion relations are indicated by solid curves for Inozemtsev's spin chain (1.30) at different κ, and by dashed curves for the Haldane–Shastry (1.29) and Heisenberg (1.28) spin chains. The dotted curves show the off-shell result for $L = 6$ obtained by computing (1.13) for Inozemtsev's spin chain (1.17), and are bounded from above by the wavy dashed curve (1.15). At the values $p \in (2\pi/6)\,\mathbb{Z}_6$ we see that the on- and off-shell curves intersect. Note that the curves for $\kappa = 1/50$ and $\kappa = 2$ already lie very close to the limiting cases.

Unification. The examples discussed in this section are related by the following limits of the pair potential of Inozemtsev's finite spin chain (1.17):

Heisenberg Inozemtsev Haldane–Shastry

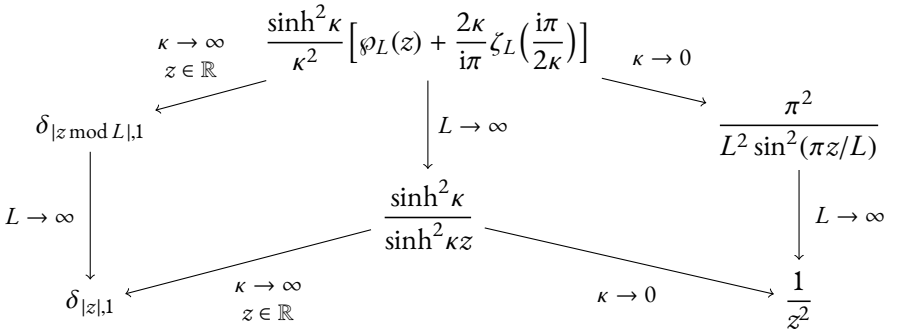

(1.31)

valid for $z\in\mathbb{C}$ when κ is finite, and for $z\in\mathbb{R}$ in the limit $\kappa\to\infty$ as indicated. For the spin chains of infinite length the estimate (1.27) implies that the corresponding limits of the Hamiltonians entail convergence with respect to the operator norm. Note that the infinite-length limit simplifies matters: the pair potential for Inozemtsev goes from elliptic to hyperbolic, and for Haldane–Shastry from trigonometric to rational.

1.2 Intermezzo: quantum many-body systems

To understand the solution of Inozemtsev's spin chain we need to know some things about another topic related to quantum integrability: that of integrable quantum-mechanical models with several interacting identical particles possessing dynamical degrees of freedom. These systems form exceptions to the rule in mechanics, where usually even three-body motion is not analytically tractable. This is a beautiful topic in mathematical physics, related to other topics such as representation theory and special functions. We will not be able to do it justice, only scratching the surface to highlight the parts that we will need. For more we refer to e.g. [98, 99].

Calogero–Sutherland–Moser models. Consider a quantum-mechanical system with M identical particles moving in one dimension. As in Section 1.1 we focus on translationally invariant models in which the particles interact pairwise. In units where $\hbar^2/m=1$ the Schrödinger equation thus acquires the form

$$-\frac{1}{2}\nabla^2\psi(\vec{x})+\frac{1}{2}\beta(\beta-1)\sum_{m,n=1}^{M}{}^{\star}V(x_m-x_n)\,\psi(\vec{x})=E\,\psi(\vec{x})\,, \tag{1.32}$$

where $\beta \in \mathbb{R}_{>0}$ is a coupling constant setting the interaction strength. (As in (1.10) the star indicates that equal values are to be omitted from the sum.) For $M = 1$ we get the Laplace equation, and the solutions are plane waves. Let us briefly review some different choices of the potential V yielding quantum-integrable systems known as Calogero–Sutherland–Moser (CSM) models. The classical-mechanical limit of the rational and trigonometric versions, see below, were studied by Moser in 1975 [100], who proved that they are integrable in the sense of Liouville.

Prequel: Lieb–Liniger. We start with a model that is usually not considered to be of CSM type, although it is of the form (1.32) with contact interactions governed by a repulsive delta-function potential,

$$V_{\mathrm{LL}}(x) = \delta(x)\,. \tag{1.33}$$

This model for a one-dimensional gas of bosons was introduced and solved by Lieb and Liniger in 1963 [101]. Their solution uses Bethe's method, see Section 1.3. In some sense this is not too surprising as the Heisenberg spin chain can be seen as a lattice version of the Lieb–Liniger model. Indeed, $\sum_l (S_l \cdot S_{l+1} - 1/4)$ is essentially the discrete Laplace operator, cf. (1.12), and $\Delta < -1$ yields nearest-neighbour repulsion.

Rational case. The prototype for CSM models is Calogero's model for particles on an infinite line interacting through an inverse-square potential, possibly together with a harmonic potential,

$$V_{\mathrm{rat}}(x) = \frac{1}{x^2} + \frac{\omega}{2}\,x^2\,. \tag{1.34}$$

This model was proposed and solved for the three-body case in 1969 [102], followed by the general M-particle case after two years [103].

Trigonometric case. Only months after Calogero's general solution Sutherland [104] came with a version of the CSM model for particles on a circle of circumference L. The potential is obtained by making (1.34), without the harmonic potential, periodic:

$$V_{\mathrm{tri}}(x) = \sum_{k\in\mathbb{Z}} V_{\mathrm{rat}}(x + k\,L)\big|_{\omega=0} = \frac{\pi^2}{L^2 \sin^2(\pi x/L)}\,. \tag{1.35}$$

The result should be familiar: it is the continuous version of the pair potential of the Haldane–Shastry spin chain (1.15). Sutherland found that the (unnormalized) symmetric ground-state M-particle wave function has a simple factorized (Jastrow) form

$$\psi_{\mathrm{tri}}(\vec{x}) = \prod_{1\le m<m'\le M} \left|\sin(\pi(x_m - x_{m'})/L)\right|^{\beta}, \tag{1.36}$$

with eigenvalue $\pi^2\beta^2 M(M^2-1)/(6L^2)$. Upon conjugation of the Hamiltonian by this ground state the other wave functions are given by Jack polynomials.

Hyperbolic case. By replacing π/L in (1.35) by $\mathrm{i}\kappa$ one arrives at another model for particles on an infinite line, governed by the short-range potential

$$V_{\mathrm{hyp}}(x) = \frac{\kappa^2}{\sinh^2 \kappa\, x}\,, \tag{1.37}$$

where κ sets the interaction range. This result is rather similar to the potential of Inozemtsev's infinite spin chain (1.30), and this many-body model will be most relevant for us. Before discussing its solution we finish our list of examples.

Elliptic case. If we put the previous system on a circle of circumference L we obtain, with the help of (A.4), an elliptic pair potential that closely resembles (1.17):

$$V_{\mathrm{ell}}(x) = \sum_{k\in\mathbb{Z}} V_{\mathrm{hyp}}(x + k\,L) = \wp_L(x) + \frac{2\kappa}{\mathrm{i}\pi}\zeta_L\Big(\frac{\mathrm{i}\pi}{2\kappa}\Big)\,. \tag{1.38}$$

This is the most general integrable system of the form (1.32). The explicit form of the eigenfunctions for arbitrary M was found by Felder and Varchenko while solving the elliptic Knizhnik–Zamolodchikov–Bernard equations [105].

Solution of hyperbolic case. To understand Inozemtsev's solution of the infinite spin chain we need the solution of the hyperbolic CSM model at coupling $\beta = 2$, which is already fairly involved. The starting point is the observation of Chalykh and Veselov [106] that when $\beta = 2$ the M-particle solution for the rational model (with $\omega = 0$) can be written in the form $D_M\, \mathrm{e}^{\mathrm{i}\vec{p}\cdot\vec{x}}$, having total momentum $\sum_m p_m$ and energy $\sum_m p_m^2/2$. Here D_M is a recursively defined differential operator, with $D_2 = \partial_1 - \partial_2 - 2/(x_1 - x_2)$ found by explicitly solving the two-particle problem. In the hyperbolic case one may proceed likewise to obtain a similar analytic expression, with the same energy but now with e.g. $D_2 = \partial_1 - \partial_2 - 2\kappa \coth \kappa(x_1 - x_2)$. Inozemtsev [107] turned this into an explicit formula featuring coefficients that are determined by a set of linear equations. The derivation can be found in [84, 107] and [108, §3.9]. In order to have the correct singularities, asymptotics and periodicity (with period $\mathrm{i}\pi/\kappa$) one shows that the M-particle wave function is necessarily of the form

$$\psi_{\vec{p}}(\vec{x}) = \frac{\mathrm{e}^{-\kappa(M-1)\,\vec{1}\cdot\vec{x}}}{\prod_{1\le m<m'\le M}\sinh\kappa(x_m - x_{m'})}\;\mathrm{e}^{\mathrm{i}\vec{p}\cdot\vec{x}} \sum_{\vec{n}\in\{0,\cdots,M-1\}^M} c_{\vec{n}}(\vec{p})\;\mathrm{e}^{2\kappa\,\vec{n}\cdot\vec{x}}\,, \tag{1.39}$$

where we write $\vec{1} := (1, \cdots, 1)$. The Schrödinger equation (1.32) then reduces to the following system of linear equations for the coefficients $c_{\vec{n}}$:

$$\sum_{m,m'=1}^{M\star} \Big[\Big(\frac{n_m - n_{m'}}{M} \Big(n_m - n_{m'} + \frac{\mathrm{i}p_m - \mathrm{i}p_{m'}}{\kappa} \Big) + \frac{M+1}{6} \Big) c_{\vec{n}}(\vec{p}\,) - \sum_{\text{allowed } k} \operatorname{sgn} k \, \Big(n_m - n_{m'} + 2k + \frac{\mathrm{i}p_m - \mathrm{i}p_{m'}}{2\kappa} \Big) c_{\vec{n}+k\,\vec{e}_m - k\,\vec{e}_{m'}}(\vec{p}\,) \Big] = 0 \tag{1.40}$$

under the convention $\operatorname{sgn} 0 = 1$, and

$$\sum_{\text{allowed } k} \Big(n_m - n_{m'} + 2k + \frac{\mathrm{i}p_m - \mathrm{i}p_{m'}}{2\kappa} \Big) c_{\vec{n}+k\,\vec{e}_m - k\,\vec{e}_{m'}}(\vec{p}\,) = 0\,, \tag{1.41}$$

where we define $\vec{e}_m \in \{0, \cdots, M-1\}^M$ by $(\vec{e}_m)_{m'} = \delta_{m,m'}$, and for given $\vec{n}$, m and m' the allowed $k \in \mathbb{Z}$ satisfy both $0 \le n_m + k \le M-1$ and $0 \le n_{m'} - k \le M-1$, so that $\vec{n} + k\,\vec{e}_m - k\,\vec{e}_{m'} \in \{0, \cdots, M\}^M$ and the resulting coefficient appears in (1.39). The conditions (1.40)–(1.41) should hold for all $\vec{n} \in \{0, \cdots, M-1\}^M$.

The simpler relations (1.41) are consistency conditions for (1.40) related to polynomiality. It appears to be the case that solutions to (1.41) automatically obey (1.40), although there is no general proof of this. Let us take a closer look at the system (1.41) of equations. When $M = 1$ the prefactor vanishes, allowing for a nonzero solution $c_0(p)$. For $M \ge 2$ it can be shown that most of the M^M coefficients $c_{\vec{n}}$ in (1.39) vanish:

- the prefactor in (1.41), being nonzero for generic p_m, is not relevant here and may be absorbed by a redefinition of the coefficients;
- it is easy to see that (1.41) implies that $\vec{n}$ can have at most one 0 and at most one $M-1$;
- one can now prove that we must have $\sum_m n_m = M(M-1)/2$.

When $M = 2$, for example, only c_{01} and c_{10} are nonzero, while for $M = 3$ the nonvanishing coefficients are those obtained from c_{012} by permuting the subscripts, together with c_{111}. In fact, for any M the system (1.41) admits a unique solution $\{c_{\vec{n}}(\vec{p}\,)\}_{\vec{n}}$ up to an overall normalization constant. Indeed, when $\vec{n}$ is a permutation of $(0, \cdots, M-1)$ there is a simple general formula,

$$c_{\sigma(0), \cdots, \sigma(M-1)}(\vec{p}\,) = C \prod_{1 \le m < m' \le M} \Big(1 + \frac{\mathrm{i}p_{\sigma^{-1}(m)} - \mathrm{i}p_{\sigma^{-1}(m')}}{2\kappa} \Big)\,, \tag{1.42}$$

which further determines all coefficients with coinciding subscripts n_m through (1.41).

1.3 Exact solvability in spin chains

We have seen that for any partially isotropic homogeneous spin chain the zero- and one-particle sectors are fixed by symmetries. In general there is no reason to expect there to be exact analytic expressions for any M-particle sector with $M \geq 2$. Special cases such as the models introduced in Section 1.1 form exceptions: they are exactly solvable for all M. To be fair this may, as for the xxz spin chain, amount to solvability 'in principle', where one is able turn the problem of finding the spectrum to that of solving a set of coupled equations, but the latter cannot be done analytically. Nevertheless, in such cases it can still be a very fruitful approach for studying the thermodynamic limit where L and M tend to infinity in such a way that the filling fraction M/L remains fixed. In addition, such exactly solvable models tend to exhibit properties like additive energies and factorization (two-particle reducibility) of general scattering processes. In this section we recall the basics of the exact solutions of the spin chains from Section 1.1.

Coordinate Bethe ansatz. In Section I.4.2 we discussed a very powerful algebraic approach to analysing the Heisenberg–Ising model by exploiting the (quantum-)algebraic structure underlying the spin chain (see Appendix I.A), which in fact explains its exact solvability. Nevertheless it will be useful to recapitulate the salient features of Bethe's original approach, the coordinate Bethe ansatz, which does not rely on the presence of such an algebraic structure.

Finite L. We start with the finite xxz model given by (1.10) and (1.14). In the two-particle sector the ansatz

$$\Psi_{p_1,p_2}(l_1,l_2) = A(p_1,p_2)\ \mathrm{e}^{\mathrm{i}(p_1 l_1 + p_2 l_2)} + A'(p_1,p_2)\ \mathrm{e}^{\mathrm{i}(p_2 l_1 + p_1 l_2)} \tag{1.43}$$

produces eigenvectors of H_{xxz} parametrized by p_1, p_2 such that $p = p_1 + p_2 \bmod 2\pi$ is the momentum. The corresponding energy is *additive*, i.e. $E_2(p_1,p_2) = \varepsilon_{\mathrm{xxz}}(p_1) + \varepsilon_{\mathrm{xxz}}(p_2)$, provided the two-particle scattering matrix depends on the parameters p_m as

$$S_{\mathrm{xxz}}(p_1,p_2) := \frac{A'(p_1,p_2)}{A(p_1,p_2)} = -\frac{1 - 2\,\Delta\,\mathrm{e}^{\mathrm{i}p_2} + \mathrm{e}^{\mathrm{i}(p_1+p_2)}}{1 - 2\,\Delta\,\mathrm{e}^{\mathrm{i}p_1} + \mathrm{e}^{\mathrm{i}(p_1+p_2)}}\,. \tag{1.44}$$

The additive behaviour of the energy justifies a quasiparticle interpretation, where we can think of (1.43)–(1.44) as describing a superposition of two magnons with quasimomentum p_m, each contributing p_m to the momentum and $\varepsilon_{\mathrm{xxz}}(p_m)$ to the energy. Since we work in the coordinate basis (1.6) the periodicity $\Psi_{p_1,p_2}(l_2, l_1 + L) = \Psi_{p_1,p_2}(l_1,l_2)$ has to be imposed by hand. This yields the *Bethe-ansatz equations*

$$\mathrm{e}^{\mathrm{i}p_1 L} = S_{\mathrm{xxz}}(p_1,p_2)\,, \qquad \mathrm{e}^{\mathrm{i}p_2 L} = S_{\mathrm{xxz}}(p_2,p_1)\ [= S_{\mathrm{xxz}}(p_1,p_2)^{-1}] \tag{1.45}$$

that determine the allowed values of the quasimomenta. It turns out that these equations do not have the desired $L = \dim(W_1)$ solutions in $\mathbb{R}$, which can be remedied by allowing

for $p_m \in \mathbb{C}$ such that p and $E_2(p_1, p_2)$ are real, requiring $p_1 = p_2^*$ to be complex conjugate. (Note that additive energy is an off-shell property, and does not directly translate into obvious patterns in the spectrum: the allowed values of the p_m depend on M.)

It is often convenient to pass to *rapidities* λ_m related to the quasimomenta via

$$e^{ip_m} = \frac{\sinh\gamma\,(\lambda_m + i/2)}{\sinh\gamma\,(\lambda_m - i/2)}, \tag{1.46}$$

where we parametrize $\Delta = \cos(\gamma)$. (These coincide with the spectral parameters from Part One up to some constants.) Solving (1.46) for λ_m as a function of p_m one obtains

$$\begin{aligned} \lambda_{xxz}(p_m) &= \frac{1}{\gamma}\operatorname{arctanh}\Big(\tan\frac{\gamma}{2}\,\cot\frac{p_m}{2}\Big) \\ &\to \frac{1}{2}\cot\frac{p_m}{2} = \lambda_{xxx}(p_m) \qquad \text{as } \gamma \to 0\,, \end{aligned} \tag{1.47}$$

where we have also indicated the isotropic (rational) limit. One of the convenient features of the formulation in terms of rapidities resides in the fact that the two-particle S-matrix (1.44) only depends on the difference of these variables:

$$\begin{aligned} S_{xxz}(\lambda_1, \lambda_2) &= \frac{\sinh\gamma\,(\lambda_1 - \lambda_2 - i)}{\sinh\gamma\,(\lambda_1 - \lambda_2 + i)} \\ &\to \frac{\lambda_1 - \lambda_2 - i}{\lambda_1 - \lambda_2 + i} = S_{xxx}(\lambda_1, \lambda_2) \qquad \text{as } \gamma \to 0\,. \end{aligned} \tag{1.48}$$

For general M the coordinate Bethe ansatz can be written as

$$\Psi_{\vec{p}}(\vec{l}) = \sum_{\sigma \in S_M} A_\sigma(\vec{p})\, e^{i\vec{p}_\sigma \cdot \vec{l}}, \tag{1.49}$$

where $\vec{p}_\sigma$ is the image of the (right) action of the permutation group S_M by switching components: $(\vec{p}_\sigma)_m = p_{\sigma(m)}$. The results for the two-particle sector extend to general M: the corresponding energy is additive, $E_M(\vec{p}) = \sum_m \varepsilon_{xxz}(p_m)$, so (1.49) may be interpreted as a superposition of magnons with total momentum $p = \sum_m p_m \bmod 2\pi$. Due to periodicity the quasimomenta p_m must obey the Bethe-ansatz equations [cf. (I.A.10) via rapidities]

$$e^{ip_m L} = \prod_{\substack{m'=1 \\ m' \neq m}}^{M} S_{xxz}(p_m, p_{m'})\,, \qquad 1 \le m \le M \tag{1.50}$$

and reality of p and $E_M(\vec{p})$ requires complex $p_m \in \mathbb{C}$ to come in conjugate pairs. Moreover, one finds that, up to an overall normalization factor, the coefficients A_σ are products of two-particle S-matrices: magnon scattering *factorizes* into two-body processes.

The derivation of (1.50) exploits the fact that the right-hand side of (1.49) is symmetric in the l_m, as in the right-hand side of the expression (1.6) for the coordinate basis vectors. This allows one to extend the Bethe wave function (1.49) to symmetric functions on all of $\mathbb{Z}^M$, which is convenient for computations. Note that this extension does not affect the physical components, featuring in (1.7), for which $l_1 < \cdots < l_M$. The computations are worked out in full detail in [5, §B].

Thermodynamic limit. Remarkably the preceding analysis, relying on periodicity to obtain Bethe-ansatz equations (1.50), turns out to offer insight into the *infinite* XXZ spin chain as well. Since the XXZ pair potential is the same for all $L \in \mathbb{N} \cup \{\infty\}$ the coordinate Bethe ansatz (1.49) also yields M-particle eigenvectors of the infinite spin chain, again exhibiting factorized scattering. In general these formal eigenvectors asymptotically behave as plain waves and are not normalizable; they can be used to build normalizable wave packets representing scattering states. A special class of eigenvectors is formed by *bound states*, given by (1.49) with allowed (necessarily complex) values of the quasimomenta determined through (bound-state) equations obtained by demanding that $|\Psi_M; \vec{p}\rangle \in W_M$ *is* normalizable. This requires certain terms in (1.49) to vanish for asymptotic positions. But the A_σ are given in terms of the two-particle S-matrix, and it turns out that the bound-state equation for given M can also be found by matching the poles and zeroes of the two sides of (1.50) as $L \to \infty$. In terms of rapidities the solutions $\vec{\lambda}$ take the form of vertical strings in $\mathbb{C}$, each centred around the real axis and with $\lambda_{m+1} = \lambda_m + \mathrm{i}$ [cf. (1.48)]. Invoking the 'string hypothesis', the (unproven) conjecture that the thermodynamic behaviour is completely determined by these bound states, one can proceed to compute quantities like the free energy per site [109].

Let us finally mention that as $L \to \infty$ an algebra of (quantum-group) symmetries emerges: for general $\Delta = (q + q^{-1})/2$ it is quantum-affine $\mathfrak{sl}_2$, $U_q(\widehat{\mathfrak{sl}_2})$, reducing to the Yangian $Y_\hbar(\mathfrak{sl}_2)$ at $\Delta = 1$ [110].

Haldane–Shastry spin chain. The solution of the Haldane–Shastry model takes an entirely different form. The case $\Delta = 1$ has received by far the most attention; other values of Δ seem be discussed in only a handful of papers [94, 111, 112].

For finite L the Sutherland ground states (1.36) yield wave functions $\mathrm{e}^{\mathrm{i}p\vec{1}\cdot\vec{l}}\psi_{\mathrm{s}}(\vec{l})$, of (total) momentum $p \in (2\pi/L)\,\mathbb{Z}_L$ provided the anisotropy parameter is of the form $\Delta = \beta\,(\beta - 1)/2$ with $\beta \in 2\mathbb{N}$ including $\Delta = 1$. For $M = 1$ this reproduces (1.9), while in general the entire wave function is factorized as a product of two-particle contributions. Although the energy is not quite additive it exhibits a very regular pattern, especially at $\Delta = 1$ where it comes in multiples of $J\pi^2/L^2$. [In fact, additivity is restored for the general $\mathfrak{su}_{m|n}$-version of the HS spin chain, see [112, §3] and references therein.]

Now the preceding does not yield enough eigenfunctions to span the M-particle sector, but Haldane numerically found that all remaining states have the same eigenvalues as the simple polynomial ones, cf. Figure 3 below. This highly degenerate spectrum is a con-

sequence of an underlying [$U_q(\widehat{\mathfrak{sl}_2})$ or $Y_\hbar(\mathfrak{sl}_2)$] symmetry present at *finite* L [111, 113]. The above wave functions correspond to highest-weight vectors of these symmetry algebras, enabling one to construct the full spectrum. Thus the quantum-group symmetries allow for a much more detailed solution at finite L than a Bethe-ansatz analysis does for the Heisenberg-type spin chains. The thermodynamics of the Haldane–Shastry spin chain can be obtained using the asymptotic Bethe ansatz, which amounts to imposing periodicity on the (simpler) asymptotic form of the wave function [114].

Inozemtsev spin chain. Inozemtsev managed to find exact solutions for his spin chain for all M and L. The result is some sort of hybrid of the coordinate Bethe ansatz and the polynomial solutions of the Haldane–Shastry model.

Finite case. Due to the elliptic pair potential the case of finite L is rather complicated, and Inozemtsev solved it in the period 1995–2000 [115], only *after* he tackled the infinite spin chain. The solution is based on that of the elliptic CSM model on a circle, exploiting the resemblance between the two models. The system of Bethe-ansatz-type equations for the parameters p_m is rather complicated. It turns out that the M-particle energy is nearly, but not quite, additive. Nevertheless, Inozemtsev recursively defined a set of L operators that commute with the spin-chain Hamiltonian [116], cf. [83, §3]. At least two of these symmetries commute with each other [117], and it is expected that this extends to form an involutive family of operators, which would essentially demonstrate that the model is integrable.

Infinite case. The solution for the infinite-length spin chain was obtained by Inozemtsev in 1992 [107] based on the similarity of his two-particle solution [83] with that of the hyperbolic CSM model with potential (1.37). Suppose that a set of coefficients $\{c_{\vec{n}}(\vec{p})\}_{\vec{n}}$ from (1.39) satisfies (1.40)–(1.41), hence yielding a wave function for the hyperbolic CSM model. Then Inozemtsev showed that if we define

$$a_{\vec{n}}(\vec{p}) := c_{\vec{n}}(2\kappa\,\lambda_\kappa(p_1),\cdots,2\kappa\,\lambda_\kappa(p_M))\,,\qquad \vec{n}\in\{0,\cdots,M-1\}^M \tag{1.51}$$

then the symmetrization of (1.39) in the positions, restricted to $x_m = l_m \in \mathbb{Z}$,

$$\begin{aligned}\Psi_{\vec{p}}(\vec{l}) &:= \sum_{\sigma\in S_M}\psi_{\vec{p}}(\vec{l}_\sigma)|_{c_{\vec{n}}\mapsto a_{\vec{n}}} = \sum_{\sigma\in S_M}\psi_{\vec{p}}(\vec{l}_{\sigma^{-1}})|_{c_{\vec{n}}\mapsto a_{\vec{n}}} \\ &= \frac{\mathrm{e}^{-\kappa(M-1)\,\vec{1}\cdot\vec{l}}}{\prod_{1\le m<m'\le M}\sinh\kappa(l_m-l_{m'})}\sum_{\sigma\in S_M}\operatorname{sgn}(\sigma)\;\mathrm{e}^{\mathrm{i}\vec{p}_\sigma\cdot\vec{l}}\sum_{\vec{n}\in\{0,\cdots,M-1\}^M} a_{\vec{n}}(\vec{p})\,\mathrm{e}^{2\kappa\,\vec{n}_\sigma\cdot\vec{l}}\,,\end{aligned} \tag{1.52}$$

are wave functions for the spin chain given by (1.23) and (1.30). Note that this is a generalization of the coordinate Bethe ansatz (1.49) with coefficients A_σ that depend on the positions l_m as well as the parameters p_m. When $M = 1$ we reproduce the single-magnon wave function, with overall factor $a_0(p)$ independent of p. As $\kappa\to\infty$ (1.51)–(1.52) reduces to the coordinate Bethe ansatz.

A very nontrivial result is that for all M the corresponding energies are additive. Moreover, when the difference between all positions becomes asymptotically large the solution factorizes, acquiring the form (1.49) with A_σ consisting of products of two-particle S-matrices [obtained from (1.55) below as $\bar{l} \to \infty$]. This simplification enables one to use the asymptotic Bethe ansatz to study the thermodynamic properties under the assumption of the string hypothesis [118]. Interestingly, unlike for the xxz spin chain in this case one cannot work with only rapidities (see below) instead of quasimomenta.

Example: $M = 2$. Let us examine (1.52) for the two-particle sector. In this case (1.41) implies that $a_{00} = a_{11} = 0$ while $a_{01}(p_1, p_2) \propto 1 - \coth \varphi_\kappa(p_1, p_2)$ and $a_{10}(p_1, p_2) \propto 1 + \coth \varphi_\kappa(p_1, p_2)$. Here the function φ_κ is determined by the relation

$$\coth \varphi_\kappa(p_1, p_2) = \mathrm{i}\, \lambda_\kappa(p_1) - \mathrm{i}\, \lambda_\kappa(p_2)\,. \tag{1.53}$$

It follows that (1.52) can be written in the form first used by Inozemtsev to tackle the two-particle sector [83, §4],

$$\begin{aligned} \Psi_{p_1,p_2}(l_1, l_2) &= \frac{\sinh(\kappa\, \bar{l} - \varphi_\kappa(p_1, p_2))}{\sinh \kappa\, \bar{l}}\, \mathrm{e}^{\mathrm{i}(p_1 l_1 + p_2 l_2)} + \frac{\sinh(\kappa\, \bar{l} + \varphi_\kappa(p_1, p_2))}{\sinh \kappa\, \bar{l}}\, \mathrm{e}^{\mathrm{i}(p_2 l_1 + p_1 l_2)} \\ &= \sinh \varphi_\kappa(p_1, p_2) \Big[(\coth \varphi_\kappa(p_1, p_2) - \coth \kappa \bar{l}\,)\, \mathrm{e}^{\mathrm{i}(p_1 l_1 + p_2 l_2)} \\ &\qquad + (\coth \varphi_\kappa(p_1, p_2) + \coth \kappa \bar{l}\,)\, \mathrm{e}^{\mathrm{i}(p_2 l_1 + p_1 l_2)} \Big]\,, \end{aligned} \tag{1.54}$$

with $\bar{l} := l_2 - l_1$ the distance between the magnons. The 'two-particle interaction matrix'

$$\begin{aligned} S_\kappa(\bar{l}; p_1, p_2) &= \frac{\sinh(\kappa\, \bar{l} + \varphi_\kappa(p_1, p_2))}{\sinh(\kappa\, \bar{l} - \varphi_\kappa(p_1, p_2))} = \frac{\coth \varphi_\kappa(p_1, p_2) + \coth \kappa\, \bar{l}}{\coth \varphi_\kappa(p_1, p_2) - \coth \kappa\, \bar{l}} \\ &= \frac{\lambda_\kappa(p_1) - \lambda_\kappa(p_2) - \mathrm{i} \coth \kappa\, \bar{l}}{\lambda_\kappa(p_1) - \lambda_\kappa(p_2) + \mathrm{i} \coth \kappa\, \bar{l}}\,, \end{aligned} \tag{1.55}$$

now depends on (the distance between) the positions of the magnons to account for the long-range interactions. As κ tends to infinity this dependence disappears: $\coth \kappa\, \bar{l} \to \operatorname{sgn} \bar{l} \in \{\pm 1\}$ ($\bar{l} \neq 0$) while $\lambda_\kappa(p_m) \to \lambda_{\mathrm{xxx}}(p_m)$ by (B.3). In particular, we may think of $\lambda_\kappa(p_m)$ as being the rapidities for the Inozemtsev spin chain [cf. (1.47)–(1.48)].

2 Partially isotropic version of Inozemtsev's spin chain

In the discussion of Section 1.1 one model was conspicuous by its absence: the partially isotropic version of Inozemtsev's spin chain. In this section we collect the basic facts of this model and initiate the investigation into the question whether the model might be exactly solvable.

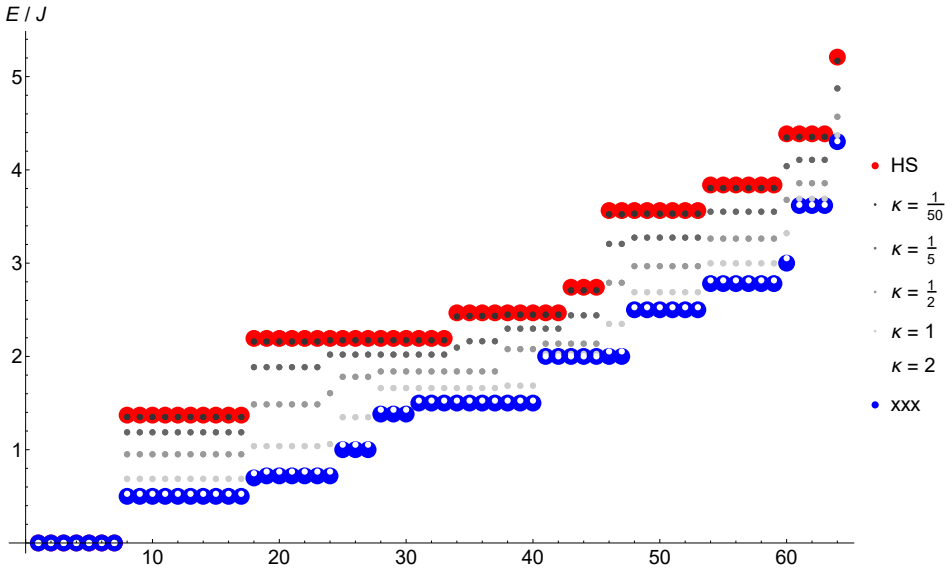

Figure 3. [Colour online] The complete spectrum for $L = 6$ in the isotropic case ($\Delta = 1$) of the spin chains whose one-particle energies are shown in Figure 2 . The horizontal axis simply enumerates the $2^L = 64$ eigenvalues, sorted by their magnitude. The high degeneracy in the spectrum of the Haldane–Shastry spin chain is clearly visible, with energies equal to $0, 5, 8, 9, 10, 13, 14, 16, 19$ times $\pi^2/6^2 \approx 0.27$. For the Heisenberg spin chain the pseudovacua and one-particle states, together with their $\mathfrak{sl}_2(\mathbb{C})$-descendants, are found at $E/J = 0, 1/2, 3/2, 2$. Inozemtsev's spin chain nicely interpolates between these limiting cases, already being very close to them for $\kappa = 1/50$ and $\kappa = 2$, respectively.

2.1 The spin chain

It is natural to consider the partially isotropic (xxz-like) extensions of Inozemtsev's spin chain with pair potential (1.17) or (1.30) by including an anisotropy parameter $\Delta = \cos\gamma$ in the usual way. This model interpolates between the xxz and partially isotropic Haldane–Shastry spin chains, and contains Inozemtsev's isotropic spin chain as a special case. Inozemtsev mentioned this extension in [83, §5], and briefly commented on some technical issues that might have to be dealt with in order to solve the model.

Finite case. When L is finite the partially anisotropic version of Inozemtsev's spin chain (1.17) is governed by the Hamiltonian [cf. (1.10)]

$$H_{\gamma,\kappa} = -\frac{J}{2} \sum_{k,l \in \mathbb{Z}_L}^{\star} \frac{\sinh^2\kappa}{\kappa^2} \Big[\wp_L(k-l) + \frac{2\kappa}{\mathrm{i}\pi}\zeta_L\Big(\frac{\mathrm{i}\pi}{2\kappa}\Big)\Big] \Big(S_k \cdot_\Delta S_l - \frac{\Delta}{4}\Big) . \tag{2.1}$$

As special cases it includes the Heisenberg–Ising and partially isotropic Haldane–Shastry spin chains, cf. (1.31). An example of the spectrum of this model and its limits is given in Figure 4.

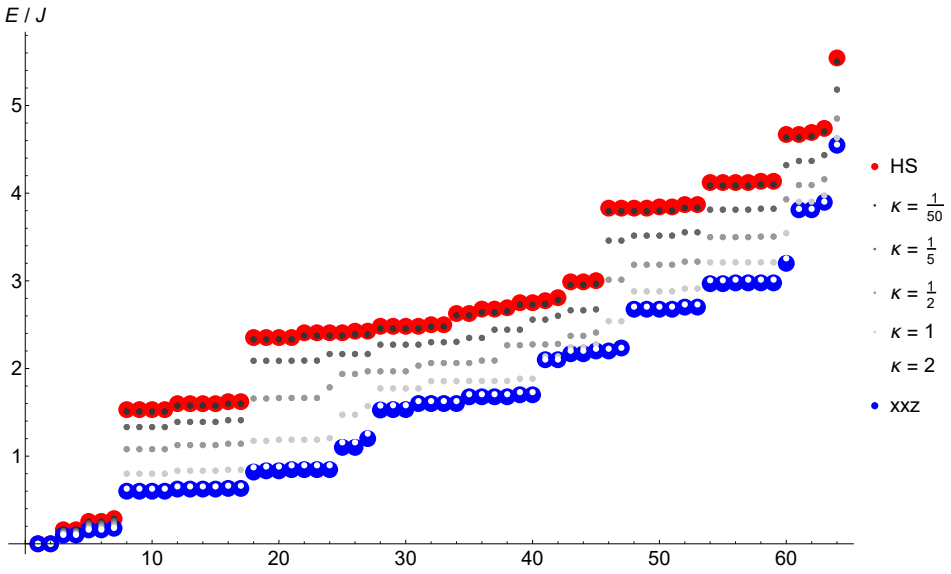

Figure 4. The complete spectrum for the spin chains from Figure 3, with $L = 6$, now in a mildly anisotropic case $\Delta = 1.1$. The original multiplets can still be recognized, but most degeneracies are lifted by the anisotropy.

Infinite case. The infinite-length spin chain has Hamiltonian

$$H_{\gamma,\kappa} := -\frac{J}{2} \sum_{k,l\in\mathbb{Z}}^{\star} V_\kappa(k-l)\big(S_k \cdot_\Delta S_l - \frac{\Delta}{4}\big), \qquad V_\kappa(l) := \frac{\sinh^2\kappa}{\sinh^2\kappa\, l}. \tag{2.2}$$

Its restriction to the M-particle sector is a bounded operator by (1.27), with

$$\tau_\kappa := \|V_\kappa\|_1 = \sum_{l\in\mathbb{Z}_{[0]}} V_\kappa(l) = \frac{\sinh^2\kappa}{\kappa^2}\Big[\frac{\kappa^2}{3} + \frac{2\kappa}{\mathrm{i}\pi}\,\zeta_1\Big(\frac{\mathrm{i}\pi}{2\kappa}\Big)\Big] \tag{2.3}$$

involving a series computed in Appendix C. (As before the second equality holds when we set $V_\kappa(0) := 0$.)

Magnons. As always the pseudo-vacuum has zero energy for any L. By translational invariance the one-particle sector still has eigenvectors (1.22), formal for infinite L, with energy eigenvalues (1.24) determined by

$$\begin{aligned}\frac{2}{J}\,\varepsilon_{\gamma,\kappa}(p) &= \Delta\,\tau_\kappa + \frac{\sinh^2\kappa}{\kappa^2}\Big[-\frac{\kappa^2}{3} + \frac{1}{2}\,\wp_1\Big(\frac{\mathrm{i}p}{2\kappa}\Big) - 2\kappa^2\lambda_\kappa(p)^2\Big] \\ &= \frac{\sinh^2\kappa}{\kappa^2}\Big[(\Delta-1)\frac{\kappa^2}{3} + \Delta\,\frac{2\kappa}{\mathrm{i}\pi}\,\zeta_1\Big(\frac{\mathrm{i}\pi}{2\kappa}\Big) - \frac{1}{2}\,\wp_1\Big(\frac{\mathrm{i}p}{2\kappa}\Big) - 2\kappa^2\lambda_\kappa(p)^2\Big]\,. \qquad (2.4)\end{aligned}$$

This expression generalizes all of those in (1.28)–(1.30). For finite length (2.4) has to be restricted to on-shell $p \in (2\pi/L)\,\mathbb{Z}_L$. Plotting this one-particle energy yields something very similar to Figure 2, where the curves are now shifted in the horizontal direction due to the constant (p-independent) term proportional to $\Delta - 1$ in (2.4): the curves no longer pass through the origin.

The properties of the Weierstraß functions (Appendix A) imply that the analytic function defined by (2.4) is even, $\varepsilon_{\gamma,\kappa}(-z) = \varepsilon_{\gamma,\kappa}(z)$, and doubly quasiperiodic with quasiperiods $(2\pi, 2\mathrm{i}\kappa)$:

$$\varepsilon_{\gamma,\kappa}(z+2\pi) = \varepsilon_{\gamma,\kappa}(z)\,, \qquad \varepsilon_{\gamma,\kappa}(z+2\mathrm{i}\kappa) = \varepsilon_{\gamma,\kappa}(z) + J\sinh^2\kappa\,(2\mathrm{i}\lambda_\kappa(z)+1)\,. \qquad (2.5)$$

In particular we also have $\varepsilon_{\gamma,\kappa}(2\pi - z) = \varepsilon_{\gamma,\kappa}(z)$, cf. Figure 2.

2.2 Towards an exact solution for the two-particle sector?

As we have seen in Section 1.3 each of the limiting cases of our spin chain is exactly solvable, albeit in a different way for each case. This naturally leads one to wonder whether the partially isotropic version of Inozemtsev's spin chain could be exactly solvable as well. In fact, for the XXZ and Haldane–Shastry spin chain the solution method is not too sensitive to the value of Δ: for the former the coordinate Bethe ansatz has precisely the same form, and only the two-particle S-matrix takes a slightly different form (1.44), while according to Haldane the solution of the latter also generalizes in a fairly straightforward manner, at least for discrete values $\Delta = \beta\,(\beta-1)/2$ with $2\beta \in \mathbb{N}$. One could hope that, at least for some values of $\Delta \neq 1$, it is also possible to use Inozemtsev's solution as a starting point for obtaining the spectrum of the deformed Inozemtsev spin chain presented above.

In this section we describe our efforts in this direction so far. We focus on the infinite spin chain, which, as for $\Delta = 1$, is less involved than its elliptic finite-size counterpart. Unfortunately we will not be able to provide a positive answer. Nevertheless we think the problem is intriguing, and the following might still be of interest to other researchers too.

***M*-particle difference equation.** Consider the M-particle sector. The sum over k in (1.26) can be evaluated for the Δ-dependent term to find [cf. (2.3)]

$$\begin{aligned}\frac{2}{J}\,H_{\gamma,\kappa}\,|\vec{l}\rangle = \Delta\left(M\,\tau_\kappa - \sum_{m,m'=1}^{M\,\star} V_\kappa(l_m - l_{m'})\right)|\vec{l}\rangle \\ - \sum_{m=1}^{M}\sum_{k\in\mathbb{Z}_{[\vec{l}]}} V_\kappa(k-l_m)\,|l_1,\cdots,k,\cdots,\widehat{l_m},\cdots,l_M\rangle\,.\end{aligned} \tag{2.6}$$

A wave function must therefore satisfy the lattice version of the Schrödinger equation, the *M-particle difference equation*

$$\begin{aligned}\sum_{k\in\mathbb{Z}_{[\vec{l}]}}\sum_{m=1}^{M} V_\kappa(k-l_m)\,\Psi(l_1,\cdots,k,\cdots,\widehat{l_m},\cdots,l_M) \\ = \left(M\,\Delta\,\tau_\kappa - \frac{2}{J}\,E_M - \Delta\sum_{m,m'=1}^{M\,\star} V_\kappa(l_m-l_{m'})\right)\Psi(\vec{l})\,.\end{aligned} \tag{2.7}$$

Strictly speaking, in writing k on the left of l_m for all k and m we assume that the wave function is symmetric in the positions l_m. It seems very reasonable to expect this to be true since it holds for all known limiting cases, and is in accordance with the symmetry of the formula for the coordinate-basis vectors (1.6).

In the one-particle sector the wave function is obtained from (1.22) so (2.7) boils down to (2.4). Our ultimate goal is to solve (2.7) for $M \geq 2$. In the remainder of this section we describe the current status of our attempts for doing so for the two-particle sector. In this case (2.7) reads

$$\begin{aligned}\sum_{k\in\mathbb{Z}_{[l_1,l_2]}} \left(V_\kappa(k-l_1)\,\Psi(k,l_2) + V_\kappa(k-l_2)\,\Psi(l_1,k)\right) \\ = \left(2\,\Delta\,(\tau_\kappa - V_\kappa(l_2-l_1)) - \frac{2}{J}\,E_2\right)\Psi(l_1,l_2)\,.\end{aligned} \tag{2.8}$$

Therefore the two-particle energy can be expressed in terms of the coefficients as

$$E_2 = \frac{J}{2}\sum_{k\in\mathbb{Z}_{[0,l_2-l_1]}} V_\kappa(j)\left(2\,\Delta - \frac{\Psi(l_1+k,l_2)+\Psi(l_1,l_2-k)}{\Psi(l_1,l_2)}\right). \tag{2.9}$$

Since this energy cannot depend on the positions we have to find wave functions such that the right-hand side of this equation becomes independent of the l_m.

First attempt. Recall that the ansatz used by Bethe to solve the xxx model can also be used to tackle the xxz spin chain, just resulting in the modified two-particle scattering matrix (1.48) and correspondingly altered conditions (bound-state equations) for the allowed values of the parameters p_m. This motivates simply trying Inozemtsev's ansatz (1.54) where we hope to determine the phase $\varphi_{\gamma,\kappa}(p_1,p_2)$, which we now expect to depend on $\Delta = \cos\gamma$ as well as κ, and the allowed values of the parameters p_m by demanding (1.54) to yield actual eigenvectors.

Assuming $\varphi_{\gamma,\kappa}(p_1,p_2)$ to be *independent* of the l_m, the right-hand side of (2.9) equals

$$\begin{aligned}
&\Delta\,[(\mathrm{e}^{\mathrm{i}p_1\bar{l}}+\mathrm{e}^{\mathrm{i}p_2\bar{l}})\coth\varphi_{\gamma,\kappa}(p_1,p_2)+(\mathrm{e}^{\mathrm{i}p_1\bar{l}}-\mathrm{e}^{\mathrm{i}p_2\bar{l}})\coth\kappa\,\bar{l}\,]\sum_{k\in\mathbb{Z}_{[0,\bar{l}]}}V_\kappa(k)\\
&-\frac{1}{2}\coth\varphi_{\gamma,\kappa}(p_1,p_2)\sum_{k\in\mathbb{Z}_{[0,\bar{l}]}}[(\mathrm{e}^{\mathrm{i}p_1k}+\mathrm{e}^{-\mathrm{i}p_2k})\,\mathrm{e}^{\mathrm{i}p_2\bar{l}}+(\mathrm{e}^{-\mathrm{i}p_1k}+\mathrm{e}^{\mathrm{i}p_2k})\,\mathrm{e}^{\mathrm{i}p_1\bar{l}}\,]V_\kappa(k)\\
&+\frac{1}{2}\sum_{k\in\mathbb{Z}_{[0,\bar{l}]}}\coth\kappa(\bar{l}-k)\,[(\mathrm{e}^{\mathrm{i}p_1k}+\mathrm{e}^{-\mathrm{i}p_2k})\,\mathrm{e}^{\mathrm{i}p_2\bar{l}}-(\mathrm{e}^{-\mathrm{i}p_1k}+\mathrm{e}^{\mathrm{i}p_2k})\,\mathrm{e}^{\mathrm{i}p_1\bar{l}}\,]V_\kappa(k)
\end{aligned}\tag{2.10}$$

up to an overall factor of $J/[(\mathrm{e}^{\mathrm{i}p_1\bar{l}}+\mathrm{e}^{\mathrm{i}p_2\bar{l}})\coth\varphi_{\gamma,\kappa}(p_1,p_2)+(\mathrm{e}^{\mathrm{i}p_1\bar{l}}-\mathrm{e}^{\mathrm{i}p_2\bar{l}})\coth\kappa\,\bar{l}\,]$. Using (C.1)–(C.2) from Appendix C one finds that (2.10) equals

$$\begin{aligned}
&\frac{1}{J}\,(\varepsilon_{\gamma,\kappa}(p_1)+\varepsilon_{\gamma,\kappa}(p_2))\,[(\mathrm{e}^{\mathrm{i}p_1\bar{l}}+\mathrm{e}^{\mathrm{i}p_2\bar{l}})\coth\varphi_{\gamma,\kappa}(p_1,p_2)+(\mathrm{e}^{\mathrm{i}p_1\bar{l}}-\mathrm{e}^{\mathrm{i}p_2\bar{l}})\coth\kappa\,\bar{l}\,]\\
&+[(1-\mathrm{e}^{\mathrm{i}p_1\bar{l}})\,(1-\mathrm{e}^{\mathrm{i}p_2\bar{l}})-(\Delta-1)\,(\mathrm{e}^{\mathrm{i}p_1\bar{l}}+\mathrm{e}^{\mathrm{i}p_2\bar{l}})]\,V_\kappa(\bar{l}\,)\,\coth\varphi_{\gamma,\kappa}(p_1,p_2)\\
&-(1-\mathrm{e}^{\mathrm{i}p_1\bar{l}})\,(1-\mathrm{e}^{\mathrm{i}p_2\bar{l}})\,V_\kappa(\bar{l})\,(\mathrm{i}\,\lambda_\kappa(p_1)-\mathrm{i}\,\lambda_\kappa(p_2))-(\Delta-1)\,(\mathrm{e}^{\mathrm{i}p_1\bar{l}}-\mathrm{e}^{\mathrm{i}p_2\bar{l}})\,V_\kappa(\bar{l}\,)\,\coth\kappa\,\bar{l}\,.
\end{aligned}\tag{2.11}$$

At the isotropic point $\Delta = 1$ the last two lines in (2.11) simplify and we recover (1.55): for $\coth\varphi_{0,\kappa} = \coth\varphi_\kappa$ given by (1.53) these last two lines cancel and one obtains an additive two-particle dispersion relation. When $\Delta \neq 1$, however, such an additive spectrum requires $\coth\varphi_{\gamma,\kappa}(p_1,p_2) = \coth\varphi_\kappa + O(\Delta-1)$ to depend on (the difference of) positions—the $a_{\vec{n}}$ in (1.52) become position-dependent—which contradicts the assumption that we used in the preceding computation. One can check that the resulting two-particle S-matrix does not reduce to (1.44) in the xxz limit $\kappa\to\infty$. Moreover, direct numerical checks confirm that the resulting wave function does not solve (2.8); the right-hand side of (2.9) even depends on the l_m. We must conclude that, unfortunately, Inozemtsev's ansatz (1.54) does not straightforwardly extend to the partially isotropic case.

Second attempt. We can try to cook up another ansatz for the two-particle wave function, hoping to be able to stick to a generalized coordinate Bethe ansatz of the form

$$\Psi_{p_1,p_2}(l_1,l_2) = A(l_1,l_2;p_1,p_2)\;\mathrm{e}^{\mathrm{i}(p_1l_1+p_2l_2)}+A'(l_1,l_2;p_1,p_2)\;\mathrm{e}^{\mathrm{i}(p_2l_1+p_1l_2)}\,,\tag{2.12}$$

where the dependence of the coefficients on l_m and p_m, together with the allowed values of the parameters p_m, are to be determined. Then the two-particle interaction matrix is

$$S_{\gamma,\kappa}(l_1, l_2; p_1, p_2) := \frac{A'(l_1, l_2; p_1, p_2)}{A(l_1, l_2; p_1, p_2)} \,. \tag{2.13}$$

Our ansatz must satisfy the following properties.

i) *Limiting behaviour.* In the isotropic limit $\gamma \to 0$ (2.12) must become proportional to (1.54); in particular (2.13) has to reduce to (1.55). Similarly, when κ tends to infinity (2.12) has to become proportional to (1.43), and (2.13) should boil down to (1.48). Of course the limit of vanishing κ should also be compatible with the solution of Haldane–Shastry, but that limit is a bit more subtle, and we will leave it for now.

ii) *Homogeneity.* Translational invariance requires that $\Psi_{p_1,p_2}(l_1 + 1, l_2 + 1) = \mathrm{e}^{\mathrm{i}p}\, \Psi_{p_1,p_2}(l_1, l_2)$ for some total momentum $p \in \mathbb{R}/2\pi\mathbb{Z}$. The latter equals $p_1 + p_2$ if and only if the coefficients in (2.12), and thus the S-matrix (2.13), depend on the positions through the difference $\bar{l} = l_2 - l_1$.

iii) *Feasibility.* For our approach to work, we should be able to actually compute the series in (2.9), and the result must be independent of the positions to make sense. (It would of course be extremely nice if we would find additive energies.)

By (i) we seek an S-matrix that fits in the commutative diagram

$$\begin{array}{ccc} S_{\gamma,\kappa}(l_1, l_2; p_1, p_2) & \xrightarrow{\gamma \to 0} & \dfrac{\lambda_\kappa(p_1) - \lambda_\kappa(p_2) - \mathrm{i}\,\coth \kappa\, \bar{l}}{\lambda_\kappa(p_1) - \lambda_\kappa(p_2) + \mathrm{i}\,\coth \kappa\, \bar{l}} \\ \Big\downarrow{\scriptstyle \kappa \to \infty} & & \Big\downarrow{\scriptstyle \kappa \to \infty \atop (\bar{l} > 0)} \\ \dfrac{\sinh \gamma\, (\lambda_{\mathrm{xxz}}(p_1) - \lambda_{\mathrm{xxz}}(p_2) - \mathrm{i})}{\sinh \gamma\, (\lambda_{\mathrm{xxz}}(p_1) - \lambda_{\mathrm{xxz}}(p_2) + \mathrm{i})} & \xrightarrow{\gamma \to 0} & \dfrac{\lambda_{\mathrm{xxx}}(p_1) - \lambda_{\mathrm{xxx}}(p_2) - \mathrm{i}}{\lambda_{\mathrm{xxx}}(p_1) - \lambda_{\mathrm{xxx}}(p_2) + \mathrm{i}} \end{array} \tag{2.14}$$

Besides the above requirements one might expect on physical grounds that this S-matrix shares the following features with its limiting cases.

iv) *Symmetry.* We presume that the wave function (2.12) is symmetric in the positions.

v) *Pauli exclusion principle.* For all γ and κ we anticipate $S_{\gamma,\kappa}(l_1, l_2; p_1, p_1) = -1$, so that the wave function obeys a Pauli exclusion principle $\Psi_{p_1,p_1} = 0$ for the p_m.

vi) *Bose–Einstein statistics.* At the same time it is quite likely that $\Psi_{p_2,p_1} = \Psi_{p_1,p_2}$, whence $S_{\gamma,\kappa}(l_1, l_2; p_2, p_1) = S_{\gamma,\kappa}(l_1, l_2; p_1, p_2)^{-1}$. (Recall that in 1 + 1 dimensions this is compatible with the previous property.)

vii) *Physical unitarity*. Finally, when $p_m \in \mathbb{R}$ we expect that $|S_{\gamma,\kappa}(l_1,l_2;p_1,p_2)|^2 = 1$.

Inspired by (1.48) and (1.55) a possible guess for the S-matrix is of the form

$$\frac{\sinh\!\big(\gamma\,(\coth\varphi_{\gamma,\kappa}(p_1,p_2) + \coth\kappa\,\bar{l}\,)\big)}{\sinh\!\big(\gamma\,(\coth\varphi_{\gamma,\kappa}(p_1,p_2) - \coth\kappa\,\bar{l}\,)\big)}\,. \tag{2.15}$$

This function satisfies (i) provided $\coth\varphi_{\gamma,\kappa}(p_1,p_2)$ fits in the commutative diagram

$$\begin{array}{ccc} \coth\varphi_{\gamma,\kappa}(p_1,p_2) & \xrightarrow{\ \gamma\to 0\ } & \coth\varphi_{\kappa}(p_1,p_2) = \mathrm{i}\,\lambda_\kappa(p_1) - \mathrm{i}\,\lambda_\kappa(p_2) \\ \Big\downarrow{\scriptstyle \kappa\to\infty} & & \Big\downarrow{\scriptstyle \kappa\to\infty} \\ \mathrm{i}\,\lambda_{\mathrm{xxz}}(p_1) - \mathrm{i}\,\lambda_{\mathrm{xxz}}(p_2) & \xrightarrow[\ \gamma\to 0\ ]{} & \mathrm{i}\,\lambda_{\mathrm{xxx}}(p_1) - \mathrm{i}\,\lambda_{\mathrm{xxx}}(p_2) \end{array} \tag{2.16}$$

featuring the rapidities from (1.47). Observe that (2.15) fulfils (ii). Moreover, (v) and (vi) are satisfied when $\coth\varphi_{\gamma,\kappa}(p_2,p_1) = -\coth\varphi_{\gamma,\kappa}(p_1,p_2)$, whereas (vii) is true if $\coth\varphi_{\gamma,\kappa}(p_1,p_2)^* = -\coth\varphi_{\gamma,\kappa}(p_1^*,p_2^*)$. Of course (2.15) is not the only possibility; for example, further common factors could be included after the γ in (2.15) without affecting (i).

The idea, then, is to proceed like in our first attempt and try to determine $\coth\varphi_{\gamma,\kappa}(p_1,p_2)$ by imposing (2.12) with an S-matrix of the form (2.15) to solve (2.9), hopefully for additive energies. Before doing so, however, let us spend some more time to examine if our new ansatz has any chance of meeting our requirements and wishes. In view of (2.16) it seems natural to guess that $\coth\varphi_{\gamma,\kappa}(p_1,p_2)$ is of the form

$$\mathrm{i}\,\lambda_{\gamma,\kappa}(p_1) - \mathrm{i}\,\lambda_{\gamma,\kappa}(p_2) \tag{2.17}$$

with new rapidities fitting in the commutative diagram

$$\begin{array}{ccc} \lambda_{\gamma,\kappa}(p) & \xrightarrow{\ \gamma\to 0\ } & \lambda_\kappa(p) \\ \Big\downarrow{\scriptstyle \kappa\to\infty} & & \Big\downarrow{\scriptstyle \kappa\to\infty} \\ \lambda_{\mathrm{xxz}}(p) = \dfrac{1}{\gamma}\,\mathrm{arctanh}\Big(\tan\dfrac{\gamma}{2}\,\cot\dfrac{p_m}{2}\Big) & \xrightarrow[\ \gamma\to 0\ ]{} & \lambda_{\mathrm{xxx}}(p) = \dfrac{1}{2}\cot\dfrac{p}{2} \end{array} \tag{2.18}$$

In that case (v)–(vi) are automatic, and (vii) requires $\lambda_{\gamma,\kappa}$ to be real analytic, $\lambda_{\gamma,\kappa}(p_m)^* = \lambda_{\gamma,\kappa}(p_m^*)$. A candidate is the function

$$\frac{1}{\gamma}\,\mathrm{arctanh}\Big(\tan\frac{\gamma}{2}\;\lambda_\kappa(p_m)\Big)\,. \tag{2.19}$$

Together with (2.15) and (2.17) this meets most of our demands and wishes. It remains to inspect the feasibility requirement (iii).

Let us go back to the more general (2.12) with S-matrix of the form (2.15), for some $\coth \varphi_{\gamma,\kappa}(p_1, p_2)$ that is to be determined like in our first attempt. Our new ansatz is feasible if we can compute the series

$$\sum_{k \in \mathbb{Z}_{[0,\bar{l}]}} \mathrm{e}^{\mathrm{i}p\,k}\, V_\kappa(k)\, \sinh[\gamma\,(\coth \varphi_{\gamma,\kappa}(p_1, p_2) \pm \coth \kappa(\bar{l} - k))]\,. \tag{2.20}$$

However, we run into a problem as a result of the nested trigonometric functions in the summand: Inozemtsev's trick for computing such series, explained in Appendix C, breaks down. Indeed, we would hope to find (2.20) in the expansion of the complex functions

$$F_\pm(z) := \sum_{k \in \mathbb{Z}} \mathrm{e}^{\mathrm{i}p\,k}\, V_\kappa(k + z)\, \sinh[\gamma\,(\coth \varphi_{\gamma,\kappa}(p_1, p_2) \pm \coth \kappa(\bar{l} - k - z))]\,. \tag{2.21}$$

By construction these functions are doubly quasi-periodic, $F_\pm(z+1) = \mathrm{e}^{-\mathrm{i}p}\, F_\pm(z+1)$ and $F_\pm(z + 2\mathrm{i}\pi/\kappa) = F_\pm(z)$. However, they have an *essential* singularity at $k = \bar{l}$ so there does not seem to be any hope to express them via a finite number of $\wp$'s to find a closed formula for the series (2.20).

A third option. Rather than directly using or trying to adapt the formulae of Inozemtsev's solution we could go back to its origin. The partially isotropic Haldane–Shastry model suggests considering the eigenfunctions of the hyperbolic CSM model at arbitrary value of the coupling β. For $M = 2$ it is a combination of hypergeometric functions, cf. [98, §A] and [79, §15]. The symmetrization of this eigenfunction in the positions, with an appropriate replacement of quasimomenta by rapidities as in (1.51), might yield wave functions for the deformed Inozemtsev model for appropriate values of the parameters. We have not yet had an opportunity to execute this plan due to time constraints, but will certainly do so in the near future.

3 Summary and discussion

Summary. In this chapter we reported on the current status of our research regarding the question whether the partially isotropic version of Inozemtsev's elliptic spin chain might be exactly solvable. We have focussed on the spin chain of infinite length since that case is easier, with the elliptic functions degenerating into hyperbolic ones. The first nontrivial case is the two-particle sector, consisting of vectors with two overturned spins with respect to the ferromagnetic reference state. Inozemtsev's solution of the isotropic case exploits a relation with quantum many-body systems. To understand all of this we reviewed

Inozemtsev's spin chain and its limits in Section 1.1, the relevant quantum many-body systems in Section 1.2, and Inozemtsev's solution in Section 1.3.

Our work on the partially isotropic Inozemtsev model is described in Section 2. Unlike for the XXZ spin chain, naively trying Inozemtsev's two-particle ansatz does not work: the resulting 'solution' violates a crucial assumption made along the way. Secondly we attempted writing down a more general ansatz and trying to guess the form of the two-particle S-matrix from its limits and other properties it should obey. We wrote down a guess that appears to satisfy most wishes, but it involves nested trigonometric functions, which obstructs the computation of the action of the Hamiltonian with Inozemtsev's trick for evaluating certain infinite series. Finally we came with another option, by going back to the relevant quantum many-body system, but have not yet had time to work it out.

Discussion. Of course the obvious next step is to try our third option to see if we can find exact solutions for $M = 2$. In case the corresponding energies behave additively and allow for bound states, we would take this as an indication that it might be possible to find exact solutions for higher M as well.

Related open problems. Besides the question that we have looked at there are several other unresolved issues pertaining to Inozemtsev's model. The most interesting one seems to be whether it is possible to solve the model via some Yang–Baxter equation; in particular one may expect quantum-group symmetry to appear for the infinite lattice. Another intriguing question concerns the relation to quantum many-body systems. There exists relativistic, or more precisely one-parameter [119], integrable generalizations of CSM models due to Ruijsenaars and Schneider [120]. These again come in the four flavours rational, trigonometric, hyperbolic and elliptic. The rational case turns out to be dual to the hyperbolic CSM model. It would be interesting to investigate whether it is possible to find a direct relation between the rational Ruijsenaars–Schneider (RS) model and Inozemtsev's spin chain, and if so, whether this can be pushed to find novel, possibly even exactly solvable, spin chains related to the other RS models.

A Weierstraß elliptic functions

In this appendix we collect the properties of three functions that are collectively known as the Weierstraß elliptic functions, even though only one of them is actually elliptic. The symbol $\wp$ is known as the 'Weierstraß P'. A useful quick reference is [79, §23]; see also [78, §20].

A.1 Weierstraß $\vec{\wp}$, $\vec{\zeta}$ and $\vec{\sigma}$

Let $L \in \mathbb{N} := \mathbb{Z}_{>0}$ and $\kappa \in \mathbb{R}_{>0}$. The complex numbers $\omega_1 = L$ and $\omega_2 = \mathrm{i}\pi/\kappa$ generate the lattice $\Lambda := L\,\mathbb{Z} \oplus \mathrm{i}\pi\,\mathbb{Z}/\kappa$ in $\mathbb{C}$. Write $\Lambda^\times := \Lambda \setminus \{0\}$. The Weierstraß functions with

(quasi)periods $(L, \mathrm{i}\pi/\kappa)$ are defined as

$$\begin{aligned}
\wp_L(z) &\coloneqq \wp(z|\Lambda) \coloneqq \frac{1}{z^2} + \sum_{\omega\in\Lambda^\times}\left(\frac{1}{(z-\omega)^2} - \frac{1}{\omega^2}\right),\\
\zeta_L(z) &\coloneqq \zeta(z|\Lambda) \coloneqq \frac{1}{z} + \sum_{\omega\in\Lambda^\times}\left(\frac{1}{(z-\omega)\,\omega} + \frac{z}{\omega^2}\right),\\
\sigma_L(z) &\coloneqq \sigma(z|\Lambda) \coloneqq z\prod_{\omega\in\Lambda^\times}\left(1-\frac{z}{\omega}\right)\exp\left(\frac{z}{\omega}+\frac{z^2}{2\,\omega^2}\right).
\end{aligned} \tag{A.1}$$

The series for $\wp_L$ and σ_L converge absolutely and uniformly on compact subsets of $\mathbb{C}\setminus\Lambda$. For $z\notin\Lambda$ the three functions are related by

$$\wp_L(z) = -\zeta_L'(z)\,, \qquad\qquad \zeta_L(z) = \sigma_L'(z)/\sigma_L(z)\,. \tag{A.2}$$

Each of these functions is real valued on $\mathbb{R}$.

The basic properties of the elliptic function $\wp_L$ are

- *Analytic structure:* meromorphic, with second-order poles at Λ with zero residue;
- *Double periodicity:* $\wp_L(z+\omega_i) = \wp_L(z)$;
- *Parity:* $\wp_L$ is even.

If we define $\eta_i \coloneqq \zeta(\omega_i/2)$, which obey the Legendre relation $\eta_1\,\omega_2 - \eta_2\,\omega_1 = \mathrm{i}\pi$, the function ζ_L satisfies

- *Analytic structure:* ζ_L is meromorphic, with simple poles at Λ;
- *Double (arithmetic) quasiperiodicity:* $\zeta_L(z+\omega_i) = \zeta_L(z) + 2\,\eta_i$;
- *Parity:* ζ_L is odd.

Finally, σ_L has properties that are very similar to those of the odd Jacobi theta function:

- *Analytic structure:* σ_L is entire with simple zeroes at Λ;
- *Double (geometric) quasiperiodicity:* $\sigma_L(z+\omega_i) = -\,\mathrm{e}^{\omega_i\eta_i}\,\mathrm{e}^{2\eta_i\,z}\,\sigma(z)$;
- *Parity:* σ_L is odd.

By Section III.A.1 it follows that σ_L is proportional to the odd Jacobi theta function. The explicit relation between the two is

$$\sigma_L(z) = \frac{\omega_1}{\pi}\,\mathrm{e}^{\eta_1 z^2/\omega_1}\,\frac{\vartheta_1(\pi z/\omega_1|\tau)}{\vartheta_1'(0|\tau)} \tag{A.3}$$

A.2 Trigonometric series

We have the following trigonometric series: $\wp_L$ is given by

$$\begin{aligned}\wp_L(z) &= -\frac{2}{\omega_2}\,\eta_2 + \frac{\pi^2}{\omega_2^2}\sum_{l\in\mathbb{Z}}\frac{1}{\sin^2(\pi\,(z+l\,\omega_1)/\omega_2)}\\ &= -\frac{2\kappa}{\mathrm{i}\pi}\,\zeta_L\Big(\frac{\mathrm{i}\pi}{2\kappa}\Big) + \kappa^2\sum_{l\in\mathbb{Z}}\frac{1}{\sinh^2(\kappa\,(z+l\,L))}\,,\end{aligned} \tag{A.4}$$

while ζ_L is given by

$$\begin{aligned}\zeta_L(z) &= \frac{2}{\omega_2}\,\eta_2\,z + \frac{\pi}{\omega_2}\sum_{l\in\mathbb{Z}}\cot\frac{\pi\,(z+l\,\omega_1)}{\omega_2}\\ &= \frac{2}{\omega_2}\,\eta_2\,z + \frac{\pi}{\omega_2}\cot\frac{\pi\,z}{\omega_2} + \frac{\pi}{\omega_2}\sum_{l\in\mathbb{N}}\frac{\sin(2\pi z/\omega_2)}{\sin(\pi(z+l\,\omega_1)/\omega_2)\,\sin(\pi(z-l\,\omega_1)/\omega_2)}\\ &= \frac{2\kappa}{\mathrm{i}\pi}\,\zeta_L\Big(\frac{\mathrm{i}\pi}{2\kappa}\Big)\,z - \kappa\coth(\kappa\,z) + \kappa\sum_{l\in\mathbb{N}}\frac{\sinh(2\kappa z)}{\sinh(\kappa\,(z+l\,L))\,\sinh(\kappa\,(z-l\,L))}\,.\end{aligned} \tag{A.5}$$

In the first line of (A.5) the summands for $\pm l$ should be taken together to ensure that the series converge. This yields the expression in the second line.

B The function $\vec{\lambda}_\kappa$

The properties of the Weierstraß ζ-function collected above imply the following for

$$\lambda_\kappa(z) := \frac{1}{\pi}\Big[\frac{\mathrm{i}\pi}{2\kappa}\zeta_1\Big(\frac{\mathrm{i}z}{2\kappa}\Big) - \frac{\mathrm{i}z}{2\kappa}\zeta_1\Big(\frac{\mathrm{i}\pi}{2\kappa}\Big)\Big]\,. \tag{B.1}$$

This function is odd and doubly quasiperiodic with quasiperiods $(\omega_1,\omega_2) = (2\pi, 2\mathrm{i}\kappa)$,

$$\lambda_\kappa(-z) = -\lambda_\kappa(z)\,, \qquad \lambda_\kappa(z+2\pi) = \lambda_\kappa(z)\,, \qquad \lambda_\kappa(z+2\mathrm{i}\kappa) = \lambda_\kappa(z) - \mathrm{i}\,, \tag{B.2}$$

where the last equality also uses the Legendre relation $\omega_2\,\zeta(\omega_1/2) + \omega_1\,\zeta(\omega_2/2) = \mathrm{i}\pi$. Also, λ_κ has zeroes at $z = 0$ and $z = \pi$, whence at $\pi\mathbb{Z} \subseteq \mathbb{R}$. In addition we have the following trigonometric series for λ_κ:

$$\lambda_\kappa(z) = \frac{1}{2}\cot\frac{z}{2} + \frac{1}{2}\sum_{n\in\mathbb{N}}\frac{\sin z}{\sin(\frac{z}{2}+\mathrm{i}\kappa n)\,\sin(\frac{z}{2}-\mathrm{i}\kappa n)} = \frac{1}{2}\cot\frac{z}{2} + \sum_{n\in\mathbb{N}}\frac{\sin z}{\cosh 2\,\kappa\,n - \cos z}\,. \tag{B.3}$$

Under complex conjugation λ_κ obeys $\lambda_\kappa(z)^* = \lambda_\kappa(z^*)$, i.e. $\lambda_\kappa(z)$ is real analytic (and $\lambda_\kappa(\mathbb{R}) \subseteq \mathbb{R}$).

C Inozemtsev's trick for computing certain series

In this appendix we compute the series that we encounter in this chapter. Recall the notation $V_\kappa(l) := \sinh^2\kappa/\sinh^2\kappa\, l$ and $\mathbb{Z}_{[\vec{l}]} := \mathbb{Z} \setminus \{l_1, \cdots, l_M\}$.

One-particle sector. To compute the one-particle dispersion relation one needs the following series

$$\sum_{l\in\mathbb{Z}_{[0]}} V_\kappa(l) = \frac{\sinh^2\kappa}{\kappa^2}\Big[\frac{\kappa^2}{3} - \frac{2\mathrm{i}\kappa}{\pi}\,\zeta_1\Big(\frac{\mathrm{i}\pi}{2\kappa}\Big)\Big]\,, \tag{C.1}$$

$$\sum_{l\in\mathbb{Z}_{[0]}} \mathrm{e}^{\mathrm{i}p\,k}\, V_\kappa(l) = \frac{\sinh^2\kappa}{\kappa^2}\Big[\frac{\kappa^2}{3} + \frac{1}{2}\,\wp_1\Big(\frac{\mathrm{i}p}{2\kappa}\Big) - 2\kappa^2\lambda_\kappa(p)^2\Big]\,. \tag{C.2}$$

Let us outline how these series can be evaluated using a trick that appears to be due to Inozemtsev. We follow the nice explanation in [88, §B] and refer to [108, §3.4] for detailed calculations.

Proof. Notice that (C.1) is a special case of (C.2). In fact, it is the exponential that will allow us to compute the latter. The reason is that by Liouville's theorem in complex analysis any function F that is doubly (geometrically) quasiperiodic,

$$F(z+1) = \mathrm{e}^{-\mathrm{i}p}\,F(z)\,, \qquad\qquad F(z+\mathrm{i}\pi/\kappa) = F(z)\,, \tag{C.3}$$

and analytic on the closed period parallelogram necessarily vanishes. It follows that quasiperiodic meromorphic functions are determined by their singularities.

Consider the complex function

$$F(z) := \sum_{l\in\mathbb{Z}} \mathrm{e}^{\mathrm{i}pl}\, V_\kappa(z+l) = \sinh^2\kappa \sum_{l\in\mathbb{Z}} \frac{\mathrm{e}^{\mathrm{i}pl}}{\sinh^2(\kappa(z+l))}\,. \tag{C.4}$$

One checks that it is meromorphic, obeys (C.3), and has a double pole at the origin:

$$F(z) = \frac{\sinh^2\kappa}{\kappa^2\,z^2} + 2\pi\mathrm{i}\Big(-\frac{\sinh^2\kappa}{3} + \sum_{l\in\mathbb{Z}_{[0]}} \mathrm{e}^{\mathrm{i}p\,l}\, V_\kappa(l)\Big) + O(z)\,. \tag{C.5}$$

At zeroth order we recognize the series that we want to compute, which can now be done by cooking up another function with the same quasiperiodicity and singularities, so that the series in (C.5) are given by the zeroth order of the Laurent series of this new function. Let us show that such a new function can be constructed as a product $G(z)\,H(z)$, where G accounts for the quasiperiodicity and H is doubly periodic and accommodates the singularities.

Take $G(z) := \sigma_1(z + r\,p)\exp(s\,p)/\sigma_1(z - r\,p)$, where σ_1 is the Weierstraß elliptic function with quasiperiods $(1, \mathrm{i}\pi/\kappa)$. G satisfies (C.3) when we take $r = -\mathrm{i}/4\kappa$ and $s = \zeta_1(\mathrm{i}\pi/2\kappa)/\pi$; the price that we pay is an unwanted simple pole at $z = r\,p$ and a simple zero at $z = -r\,p$. Thus H should have a double pole at the origin to match (C.5), and a simple zero at $z = r\,p$ and a simple pole at $z = -r\,p$ to counter those of G. Any doubly periodic function with these properties can be written as a linear combination of $\wp_1(z) - \wp_1(r\,p)$, $\zeta_1(z) - \zeta_1(r\,p)$ and $\zeta_1(z + r\,p) - \zeta_1(2r\,p)$, where the coefficients are fixed to ensure the correct residues and double periodicity. □

Two-particle sector. For the two-particle sector (alas, with $\Delta = 1$) one can use the series

$$\sum_{k\in\mathbb{Z}_{[0,-\bar{l}]}} \mathrm{e}^{\mathrm{i}p\,k}\, V_\kappa(k)\, \coth\kappa(\bar{l}+k) = \Big(-\frac{2}{J}\,\varepsilon_\kappa(p) + \Delta\,\tau_\kappa - (1 + 2\,\mathrm{e}^{\mathrm{i}p\bar{l}})\, V_\kappa(\bar{l})\Big)\coth\kappa\,\bar{l} + 2\,(1 - \mathrm{e}^{\mathrm{i}p\,\bar{l}})\, V_\kappa(\bar{l})\,\mathrm{i}\,\lambda_\kappa(p)\,, \tag{C.6}$$

where ε_κ is the one-particle energy (1.30) for the infinite spin chain. The proof is as before: the series $\sum_{k\in\mathbb{Z}} \mathrm{e}^{\mathrm{i}p\,k}\, V_\kappa(k + z)\, \coth\kappa(\bar{l} + k + z)$ defines a quasiperiodic function with a double pole at the origin, and contains (C.6) at the zeroth order of its Laurent expansion. The details may be found in [108, §3.7].

References

[1] W. Galleas and J. Lamers, *Reflection algebra and functional equations*, Nucl. Phys. B 886, 1003 (2014), arxiv:1405.4281.

[2] W. Galleas and J. Lamers, *Differential approach to on-shell scalar products in six-vertex models*, arxiv:1505.06870.

[3] J. Lamers, *Integral formula for elliptic SOS models with domain walls and a reflecting end*, Nucl. Phys. B 901, 556 (2014), arxiv:1510.00342.

[4] R. Klabbers and J. Lamers, *A partially isotropic extension of Inozemtsev's elliptic spin chain*, in preparation.

[5] J. Lamers, *A pedagogical introduction to quantum integrability, with a view towards theoretical high-energy physics*, PoS Modave2014, 001 (2014), arxiv:1501.06805.

[6] R. Keesman, J. Lamers, R. A. Duine and G. T. Barkema, *Finite-size scaling at infinite-order phase transitions*, in preparation.

[7] Y. Shibukawa, *Dynamical braided monoids and dynamical Yang–Baxter maps*, J. Gen. Lie Theory Appl. 5, 1 (2011), http://ci.nii.ac.jp/naid/110007699245/en/.

[8] T. Kinoshita, T. Wenger and D. S. Weiss, *A quantum Newton's cradle*, Nature 440, 900 (2006).
M. Mourigal, M. Enderle, A. Klöpperpieper, J.-S. Caux, A. Stunault and H. M. Rønnow, *Fractional spinon excitations in the quantum Heisenberg antiferromagnetic chain*, Nat. Phys. 9, 435 (2013), arxiv:1306.4678.

[9] E. P. Wigner, *The unreasonable effectiveness of mathematics in the natural sciences*, Commun. Pure Appl. Math. 13, 1 (1960), Richard courant lecture in mathematical sciences delivered at New York University, May 11, 1959.

[10] S. Weigert, *The problem of quantum integrability*, Physica D56, 107 (1992).
J.-S. Caux and J. Mossel, *Remarks on the notion of quantum integrability*, J. Stat. Mech. 2011, 02023 (2011), arxiv:1012.3587.

[11] R. J. Baxter, *Exactly solved models in statistical mechanics*, Dover Publications (2007).

[12] H. A. Kramers and G. H. Wannier, *Statistics of the two-dimensional ferromagnet. Part I*, Phys. Rev. 60, 252 (1941).
H. A. Kramers and G. H. Wannier, *Statistics of the two-dimensional ferromagnet. Part II*, Phys. Rev. 60, 263 (1941).

[13] L. Onsager, *Crystal statistics. I. A two-dimensional model with an order-disorder transition*, Phys. Rev. 65, 117 (1944).

[14] J. D. Bernal and R. H. Fowler, *A theory of water and ionic solution, with particular reference to hydrogen and hydroxyl ions*, J. Chem. Phys. 1, 515 (1933).

[15] L. Pauling, *The structure and entropy of ice and of other crystals with some randomness of atomic arrangement*, J. Am. Chem. Soc. 12, 2680 (1935).

[16] G. Algara-Siller, O. Lehtinen, F. C. Wang, R. R. Nair, U. Kaiser, H. A. Wu, A. K. Geim and I. V. Grigorieva, *Square ice in graphene nanocapillaries*, Nature 519, 443 (2015), [but see also Zhou, W. et al, *The observation of square ice in graphene questioned*, Nature 528, E1-E2 (2015)].

[17] E. H. Lieb, *Residual entropy of square ice*, Phys. Rev. 162, 162 (1967).

[18] E. H. Lieb, *Exact solution of the F model of an antiferroelectric*, Phys. Rev. Lett. 18, 1046 (1967).
E. H. Lieb, *Exact solution of the two-dimensional Slater KDP model of a ferroelectric*, Phys. Rev. Lett. 19, 108 (1967).

[19] B. Sutherland, *Exact solution of a two-dimensional model for hydrogen-bonded crystals*, Phys. Rev. Lett. 19, 103 (1967).

[20] P. Bennema, *Spiral growth and surface roughening: developments since Burton, Cabrera and Frank*, J. Cryst. Growth 69, 182 (1984).

[21] W. Kossel, *Zur Theorie des Kristallwachstums*, Nachr. Ges. Wiss. Göttingen 1927, 135 (1927), http://eudml.org/doc/59220.

[22] H. v. Beijeren and I. Nolden, *The roughening transition*, in: *Structure and dynamics of surfaces II: Phenomena, models, and methods*, ed.: W. Schommers and P. Blanckenhagen, Springer (1987).

[23] W. K. Burton, N. Cabrera and F. C. Frank, *The growth of crystals and the equilibrium structure of their surfaces*, Phil. Trans. R. Soc. A 243, 299 (1951).

[24] H. v. Beijeren, *Exactly solvable model for the roughening transition of a crystal surface*, Phys. Rev. Lett. 38, 993 (1977).

[25] R. J. Baxter, *Perimeter Bethe ansatz*, J. Phys. A: Math. Gen. 20, 2557 (1987).

[26] H. J. Brascamp, H. Kunz and F. Y. Wu, *Some rigorous results for the vertex model in statistical mechanics*, J. Math. Phys. 14, 1927 (1973).

[27] V. E. Korepin, *Calculation of norms of Bethe wave functions*, Commun. Math. Phys. 86, 391 (1982).

[28] A. G. Izergin, *Partition function of the six-vertex model in finite volume*, Sov. Phys. Dokl. 32, 878 (1987).

[29] V. Korepin and P. Zinn-Justin, *Thermodynamic limit of the six-vertex model with domain wall boundary conditions*, J. Phys. A: Math. Gen. 33, 7053 (2000), cond-mat/0004250.

[30] P. Zinn-Justin, *Six-vertex model with domain wall boundary conditions and one-matrix model*, Phys. Rev. E 62, 3411 (2000), math-ph/0005008.

[31] T. S. Tavares, G. A. P. Ribeiro and V. E. Korepin, *The entropy of the six-vertex model with variety of different boundary conditions*, J. Stat. Mech. 2015, P06016 (2015), arxiv:1501.02818.

[32] I. V. Cherednik, *Factorizing particles on a half-line and root systems*, Theor. Math. Phys. 61, 977 (1984).

[33] E. K. Sklyanin, *Boundary conditions for integrable quantum systems*, J. Phys. A: Math. Gen. 21, 2375 (1988).

[34] R. E. Behrend, P. A. Pearce and D. O'Brien, *Interaction-round-a-face models with fixed boundary conditions: the ABF fusion hierarchy*, J. Stat. Phys. 84, 1 (1996), hep-th/9507118.

[35] O. Tsuchiya, *Determinant formula for the six-vertex model with reflecting end*, J. Math. Phys. 39, 5946 (1998), solv-int/9804010.

[36] G. Filali and N. Kitanine, *The partition function of the trigonometric SOS model with a reflecting end*, J. Stat. Mech. 06, L06001 (2010), arxiv:1004.1015.

[37] G. Filali, *Elliptic dynamical reflection algebra and partition function of SOS model with reflecting end*, J. Geom. Phys. 61, 1789 (2011), arxiv:1012.0516.
G. Filali, *Dynamical reflection algebra and associated boundary integrable models*, PhD thesis, https://tel.archives-ouvertes.fr/tel-00664076.

[38] G. A. P. Ribeiro and V. Korepin, *Thermodynamic limit of the six-vertex model with reflecting end*, J. Phys. A: Math. Theor. 48, 045205 (2015), arxiv:1409.1212.

[39] G. Kuperberg, *Another proof of the alternating sign matrix conjecture*, Inter. Math. Res. Notes 1996, 139 (1996), math/9712207.

[40] H. Rosengren, *An Izergin–Korepin type identity for the 8VSOS model with applications to alternating sign matrices-*, Adv. Appl. Math. 43, 137 (2009), arxiv:0801.1229.

[41] H. Rosengren, *The three-colour model with domain wall boundary conditions*, Adv. Appl. Math. 46, 481 (2011), arxiv:0911.0561.

[42] G. Kuperberg, *Symmetry classes of alternating-sign matrices under one roof*, Ann. of Math. 156, 835 (2002), math/0008184.

[43] J. Propp, *The many faces of alternating-sign matrices*, math/0208125, in: *Discrete models: combinatorics, computation, and geometry (DM-CCG 2001)*, ed.: R. Cori, J. Mazoyer, M. Morvan and R. Mosseri.
D. Bressoud, *Proofs and confirmations: the story of the alternating sign matrix conjecture*, Cambridge University Press (1999).

[44] E. N. Lassettre and J. P. Howe, *Thermodynamic properties of binary solid solutions on the basis of the nearest neighbor approximation*, J. Chem. Phys. 9, 747 (1941).

[45] L. A. Takhtadzhan and L. D. Faddeev, *The quantum method of the inverse problem and the Heisenberg XYZ model*, Russ. Math. Surv. 34, 11 (1979).

[46] N. Kitanine, J. M. Maillet and V. Terras, *Correlation functions of the XXZ Heisenberg spin-1/2 chain in a magnetic field*, Nucl. Phys. B 567, 554 (2000), math-ph/9907019.
J. M. Maillet and V. Terras, *On the quantum inverse scattering problem*, Nucl. Phys. B 575, 627 (2000), hep-th/9911030.
F. Göhmann and V. E. Korepin, *Solution of the quantum inverse problem*, J. Phys. A: Math. Gen. 33, 1199 (2000), hep-th/9910253.

[47] R. J. Baxter, *Partition function of eight-vertex lattice model*, Ann. Phys. 70, 193 (1972).

[48] G. Felder and A. Varchenko, *Algebraic Bethe ansatz for the elliptic quantum group* $E_{\tau,\eta}(sl_2)$, Nucl. Phys. B 480, 485 (1996), q-alg/9605024.

[49] J.-L. Gervais and A. Neveu, *Novel triangle relation and abscense of tachyons in Liouville string field theory*, Nucl. Phys. B B238, 125 (1984).

[50] G. Felder, *Conformal field theory and integrable systems associated to elliptic curves*, hep-th/9407154, in: *Proc. ICM, Zürich 1994*, ed.: S. D. Chatterji, Birkhäuser (1995), 1247-1255p.

[51] G. E. Arutyunov, L. O. Chekhov and S. A. Frolov, *R-Matrix quantization of the elliptic Ruijsenaars–Schneider model*, Theor. Math. Phys. 111, Issue 2, 536 (1997), q-alg/9612032.
G. E. Arutyunov and S. A. Frolov, *Quantum dynamical R-matrices and quantum Frobenius group*, Comm. Math.Phys. 191, 15 (1998), q-alg/9610009.

[52] G. Felder, *Elliptic quantum groups*, hep-th/9412207, in: *Proc. ICMP, Paris 1994*, ed.: D. Iagolnitzer, Intern. Press Boston (1995).

[53] B. Enriquez and G. Felder, *Elliptic quantum groups* $E_{\tau,\eta}(\mathfrak{sl}_2)$ *and quasi-Hopf algebras*, Commun. Math. Phys. 195, 651 (1998), q-alg/9703018.

[54] P. Bleher and V. Fokin, *Exact solution of the six-vertex model with domain wall boundary conditions. Disordered phase*, Commun. Math. Phys. 268, 223 (2006), math-ph/0510033.
P. Bleher and K. Liechty, *Exact solution of the six-vertex model with domain wall boundary conditions. Ferroelectric phase*, Commun. Math. Phys. 286, 777 (2009), arxiv:0712.4091.
P. Bleher and K. Liechty, *Exact solution of the six-vertex model with domain wall*

boundary conditions. Critical line between ferroelectric and disordered phases, J. Stat. Phys. 134, 463 (2009), arxiv:0802.0690.
P. Bleher and K. Liechty, *Exact solution of the six-vertex model with domain wall boundary conditions. Antiferroelectric phase*, Commun. Math. Phys. 286, 777 (2009), arxiv:0904.3088.
P. Bleher and T. Bothner, *Exact solution of the six-vertex model with domain wall boundary conditions. Critical line between disordered and antiferroelectric phases*, Random Matrices: Theory Appl. 01, 1250012 (2012), arxiv:1208.6276.

[55] W. Galleas, *Functional relations for the six-vertex model with domain wall boundary conditions*, J. Stat. Mech. 06, P06008 (2010), arxiv:1002.1623.

[56] W. Galleas, *A new representation for the partition function of the six-vertex model with domain wall boundaries*, J. Stat. Mech. 01, P01013 (2011), arxiv:1010.5059.

[57] W. Galleas, *Multiple integral representation for the trigonometric SOS model with domain wall boundaries*, Nucl. Phys. B 858, 117 (2012), arxiv:1111.6683.

[58] W. Galleas, *Refined functional relations for the elliptic SOS model*, Nucl. Phys. B 867, 855 (2013), arxiv:1207.5283.

[59] W. Galleas, *Functional relations and the Yang–Baxter algebra*, J. Phys.: Conf. Ser. 474, 012020 (2013), arxiv:1312.6816.

[60] J. Aczél, *On history, applications and theory of functional equations*, in: *Functional equations: history, applications and theory*, D. Reidel Publishing Company (1984).

[61] M. Kuczma, *A survey of the theory of functional equations*, Univ. Beograd. Publ. Elektrotehn. Fak., Ser. Mat. Fiz. 130, 1 (1964).

[62] P. Zinn-Justin, *Six-vertex, loop and tiling models: integrability and combinatorics*, arxiv:0901.0665, habilitation thesis.

[63] M. Zuparic, *Studies in Integrable Quantum Lattice Models and Classical Hierarchies*, arxiv:0908.3936, PhD thesis.

[64] W. Galleas, *Scalar product of Bethe vectors from functional equations*, Commun. Math. Phys. 329, 141 (2014), arxiv:1211.7342.

[65] A. G. Izergin, D. A. Coker and V. E. Korepin, *Determinant formula for the six-vertex model*, J. Phys. A: Math. Gen. 25, 4315 (1992).

[66] N. A. Slavnov, *Calculation of scalar products of wave functions and form factors in the framework of the algebraic Bethe ansatz*, Theor. Math. Phys. 79, 502 (1989).

[67] Y.-S. Wang, *The scalar products and the norm of Bethe eigenstates for the boundary XXX spin-1/2 finite chain*, Nucl. Phys. B 622, 633 (2002).

[68] N. Kitanine, K. K. Kozlowski, J. M. Maillet, G. Niccoli, N. A. Slavnov and V. Terras, *Correlation functions of the open XXZ chain: I*, J. Stat. Mech. 10, P10009 (2007), arxiv:0707.1995.

[69] W. Galleas, *Off-shell scalar products for the XXZ spin chain with open boundaries*, Nucl. Phys. B 893, 346 (2015), arxiv:1412.5389.

[70] W. Galleas, *Elliptic solid-on-solid model's partition function as a single determinant*, arxiv:1604.01223.

[71] H. Rosengren, private correspondence (2016).

[72] F. Göhmann, M. Bortz and H. Frahm, *Surface free energy for systems with integrable boundary conditions*, J. Phys. A: Math. Gen. 38, 10879 (2005), cond-mat/0508377.
K. K. Kozlowski and B. Pozsgay, *Surface free energy of the open XXZ spin-1/2 chain*, J. Stat. Mech. 05, P05021 (2012), arxiv:1201.5884.

[73] J. Cao, H.-Q. Lin, K.-J. Shi and Y. Wang, *Exact solution of XXZ spin chain with unparallel boundary fields*, Nucl. Phys. B 663, 487 (2003), cond-mat/0212163.

[74] W.-L. Yang and Y.-Z. Zhang, *On the second reference state and complete eigenstates of the open XXZ chain*, JHEP 2007, 044 (2007), hep-th/0703222.

[75] H. Fan, B.-Y. Hou and K.-H. Shi, *Representation of the boundary elliptic quantum group $\mathcal{B}E_{\tau,\eta}(sl_2)$ and the Bethe ansatz*, Nucl. Phys. B 496, 551 (1997).

[76] J. M. Maillet and J. Sanchez de Santos, *Drinfel'd twists and algebraic Bethe ansatz*, q-alg/9612012, in: *L. D. Faddeev's Seminar on Mathematical Physics*, ed.: M. Semenov-Tian-Shansky, AMS (2000).
T.-D. Albert, H. Boos, R. Flume, R. H. Poghossian and K. Ruhlig, *An F-twisted XYZ model*, Lett. Math. Phys. 53, 201 (2000), nlin/0005023.

[77] H. MacKean and V. Moll, *Elliptic curves: function theory, geometry, arithmetic*, Cambridge University Press (1999).

[78] E. T. Whittaker and G. N. Watson, *A course of modern analysis*, fourth edition, Cambridge University Press (1927).

[79] W. Reinhardt and P. Walker, *Digital library of mathemaical functions*, Accessed during 2015–2016, http://dlmf.nist.gov.

[80] H. Weber, *Elliptische Functionen und algebraische Zahlen*, fourth edition, Friedrich Vieweg und Sohn (1891).

[81] G. Felder and A. Schorr, *Separation of variables for quantum integrable systems on elliptic curves*, J. Phys. A: Math. Gen. 32, 8001 (1999), math/9905072.

[82] S. Pakuliak, V. Rubtsov and A. Silantyev, *SOS model partition function and the elliptic weight function*, J. Phys. A: Math. Gen. 41, 295204 (2008), arxiv:0802.0195.

[83] V. I. Inozemtsev, *On the connection between the one-dimensional $s = 1/2$ Heisenberg chain and Haldane–Shastry model*, J. Stat. Phys. 59, 1143 (1990).

[84] V. I. Inozemtsev, *Integrable Heisenberg–Van Vleck chains with variable range exchange*, Phys. Part. Nucl. 34, 166 (2003), hep-th/0201001, [Fiz. Elem. Chast. Atom. Yadra 34 (2003) 332-387].

[85] D. Serban and M. Staudacher, *Planar $\mathcal{N} = 4$ gauge theory and the Inozemtsev long range spin chain*, JHEP 0406, 001 (2004), hep-th/0401057.
A. Rej, *Review of AdS/CFT Integrability, Chapter I.3: Long-range spin chains*, Lett. Math. Phys. 99, 85 (2012), arxiv:1012.3985.

[86] F. Finkel and A. González-López, *A new perspective on the integrability of Inozemtsev's elliptic spin chain*, Annals Phys. 351, 797 (2014), arxiv:1405.7855.

[87] H. Frahm and V. I. Inozemtsev, *New family of solvable 1D Heisenberg models*, J. Phys. A: Math. Gen. 27, L801 (1994), cond-mat/9405038.

[88] F. Finkel and A. González-López, *Exact solution and thermodynamics of a spin chain with long-range elliptic interactions*, J. Stat. Mech. 1412, P12014 (2014), arxiv:1407.6922.

[89] W. Heisenberg, *Zur Theorie der Ferromagnetismus*, Z. Phys. 49, 619 (1928).

[90] H. Bethe, *Zur Theorie der Metalle*, Z. Phys. 71, 205 (1931), see also the English translation by T.C. Dorlas (2009).

[91] F. Bloch, *Zur Theorie des Ferromagnetismus*, Z. Phys. 61, 206 (1930).

[92] P. W. Kasteleijn, *The lowest energy state of a linear antiferromagnetic chain*, Physica 18, 104 (1952).

[93] R. Orbach, *Linear antiferromagnetic chain with anisotropic coupling*, Phys. Rev. 112, 309 (1958).

[94] F. D. M. Haldane, *Exact Jastrow–Gutzwiller resonating-valence-bond ground state of the spin-1/2 antiferromagnetic Heisenberg chain with $1/r^2$ exchange*, Phys. Rev. Lett. 60, 635 (1988).

[95] B. Shastry, *Exact solution of an $s = 1/2$ Heisenberg antiferromagnetic chain with long-ranged interactions*, Phys. Rev. Lett. 60, 639 (1988).

[96] O. Bratelli and D. W. Robinson, *Operator algebras and quantum statistical mechanics II: equilibrium states, models in quantum statistical mechanics*, Springer-Verlag (2003).

[97] C. N. Yang and C. P. Yang, *One-dimensional chain of anisotropic spin-spin interactions. I. Proof of Bethe's hypothesis for ground state in a finite system*, Phys. Rev. 150, 321 (1966).

[98] B. Sutherland, *Beautiful models: 70 years of exactly solved quantum many-body problems*, World Scientific (2004).

[99] A. P. Polychronakos, *Generalized statistics in one dimension*, hep-th/9902157, in: *Topological aspects of low-dimensional systems: Proceedings, Les Houches summer school of theoretical physics, Session LXIX*.

[100] J. Moser, *Three integrable Hamiltonian systems connected with isospectral deformations*, Adv. Math. 16, 197 (1975).

[101] E. H. Lieb and W. Liniger, *Exact analysis of an interacting Bose gas. I. The general solution and the ground state*, Phys. Rev. 130, 1605 (1963).
E. H. Lieb, *Exact analysis of an interacting Bose gas. II. The excitation spectrum*, Phys. Rev. 130, 1616 (1963).

[102] F. Calogero, *Solution of a three-body problem in one dimension*, J. Math. Phys. 10, 2191 (1969).

[103] F. Calogero, *Solution of the one-dimensional N body problems with quadratic and/or inversely quadratic pair potentials*, J. Math. Phys. 12, 419 (1971), [see also *"Erratum"*, J. Math. Phys. 37, 3646 (1996)].

[104] B. Sutherland, *Exact results for a quantum many-body problem in one dimension*, Phys. Rev. A 4, 2019 (1971).

[105] G. Felder and A. Varchenko, *Integral representation of solutions of the elliptic Knizhnik–Zamolodchikov–Bernard equations*, Inter. Math. Res. Not. 1995, 221 (1995), hep-th/9502165.

[106] O. Chalykh and A. Veselov, *Commutative rings of partial differential operators and Lie algebras*, Commun. Math. Phys. 126, 597 (1990).

[107] V. I. Inozemtsev, *The extended Bethe ansatz for infinite $s = 1/2$ quantum spin chains with non-nearest-neighbour interaction*, Commun. Math. Phys. 148, 359 (1992).

[108] R. Klabbers, *Inozemtsev's elliptic spin chains*, MSc thesis, http://dspace.library.uu.nl/handle/1874/306868.

[109] M. Takahashi, *Thermodynamics of one-dimensional solvable models*, Cambridge University Press (1999).

[110] D. Bernard, *An Introduction to Yangian symmetries*, Int. J. Mod. Phys. B7, 3517 (1993), hep-th/9211133, in: *Advanced research workshop on integrable quantum field theories, Como, Italy, September 14–19, 1992*, 3517p.
B. Davies, O. Foda, M. Jimbo, T. Miwa and A. Nakayashiki, *Diagonalization of the XXZ Hamiltonian by vertex operators*, Commun. Math. Phys. 151, 89 (1993), hep-th/9204064.

[111] D. Bernard, M. Gaudin, F. Haldane and V. Pasquier, *Yang–Baxter equation in long-range interacting systems*, J. Phys. A: Math. Gen. 26, 5219 (1993).

[112] F. D. M. Haldane, *Physics of the ideal semion gas: spinons and quantum symmetries of the integrable Haldane–Shastry spin chain*, cond-mat/9401001, in: *Correlation effects in low-dimensional electron systems*, ed.: A. Okiji and N. Kawakami, Springer (1994).

[113] F. D. M. Haldane, Z. D. M. Ha, J. C. Talstra, D. Bernard and V. Pasquier, *Yangian symmetry of integrable quantum chains with long-range interactions and a new description of states in conformal field theory*, Phys. Rev. Lett. 69, 2021 (1992).

[114] N. Kawakami, *Asymptotic Bethe-ansatz solution of multicomponent quantum systems with* $1/r^2$ *long-range interaction*, Phys. Rev. B 46, 1005 (1992).
Z. N. C. Ha and F. D. M. Haldane, *Squeezed strings and Yangian symmetry of the Heisenberg chain with long-range interaction*, Phys. Rev. B 47, 12459 (1993).

[115] V. I. Inozemtsev, *On the spectrum of* $s = 1/2$ xxx *Heisenberg chain with elliptic exchange*, J. Phys. A: Math. Gen. 28, L439 (1995).
V. I. Inozemtsev, *Solution to three-magnon problem for* $s = 1/2$ *periodic quantum spin chains with elliptic exchange*, J. Math. Phys. 37, 147 (1996).
V. I. Inozemtsev, *Bethe-ansatz equations for quantum Heisenberg chains with elliptic exchange*, Regul. Chaot. Dyn. 5, 243 (2000), math-ph/9911022.

[116] V. I. Inozemtsev, *Invariants of linear combinations of transpositions*, Lett Math. Phys. 36, 55 (1996).

[117] J. Dittrich and V. I. Inozemtsev, *The commutativity of integrals of motion for quantum spin chains and elliptic functions identities*, Regul. Chaot. Dyn. 13, 19 (2008), arxiv:0711.1973.

[118] R. Klabbers, *Thermodynamics of Inozemtsev's elliptic spin chain*, Nucl. Phys. B 907, 77 (2016), arxiv:1602.05133.
J. Dittrich and V. I. Inozemtsev, *On the second-neighbour correlator in 1D* xxx *quantum antiferromagnetic spin chain*, J. Phys. A: Math. Gen. 30, L623 (1997), cond-mat/9706263.

[119] H. W. Braden and R. Sasaki, *The Ruijsenaars–Schneider model*, Prog. Theor. Phys. 97, 1003 (1997), hep-th/9702182.

[120] S. N. M. Ruijsenaars and H. Schneider, *A new class of integrable systems and its relation to solitons*, Ann. Phys. 170, 370 (1986).

Samenvatting

Dit hoofdstuk geeft een samenvatting in het Nederlands van de inhoud van dit proefschrift. Omdat de meeste lezers ervan geen experts zijn in het vakgebied begin ik met een schets van de wetenschappelijke context: de theoretische natuurkunde, en elliptische kwantumintegreerbaarheid in het bijzonder. Ik hoop met dit hoofdstuk vrienden en familie een indruk te geven van het onderzoek waar ik mij de afgelopen jaren mee bezig heb gehouden.

Wetenschappelijke context

Theorieën en modellen. Het doel van de natuurwetenschappen is de wereld en het heelal om ons heen te begrijpen. Beginnend met de waarneming van verschijnselen probeert men een *theorie* te formuleren die de waarneming omvat en waarvan verdere voorspellingen kunnen worden getest. Door een combinatie van experimenteren en abstraheren kan dit proces leiden tot een algemene theorie die naast nieuwe voorspellingen ook meer inzicht geeft in de onderliggende mechanismen. Dit wordt geïllustreerd door een anekdote over Newton: een appel die van een boom viel—een voorbeeld van zwaartekracht op aarde ("losgelaten objecten vallen")—zou de aanleiding zijn geweest voor Newton's algemene gravitatietheorie ("massa's trekken elkaar aan").

Alhoewel de werkelijkheid zeer gecompliceerd is, is het vaak mogelijk de situatie enorm te vereenvoudigen. Een *model* is een vereenvoudigde weergave van de werkelijkheid om een verschijnsel te beschrijven. Hoe zo'n model eruitziet verschilt van geval tot geval; voor de vallende appel vergeten we voor het gemak alles behalve de aarde en de appel, terwijl we voor het begrijpen van de baan van de aarde om de zon beiden als puntmassa's beschouwen.

In de theoretische natuurkunde bestuderen we theorieën en modellen die de verschijnselen in de natuur beschrijven. De theorieën en modellen die centraal staan in dit proefschrift komen voort uit twee takken van de theoretische natuurkunde: in Deel Eén is dit de statistische fysica en in Deel Twee de kwantummechanica. Beide onderwerpen hebben te maken met een belangrijke les uit de geschiedenis van de natuurwetenschappen, namelijk dat veel verschijnselen beter kunnen worden begrepen door ze op veel kleinere, 'microscopische' lengteschalen te bestuderen. Bovendien is de natuur in het klein in zekere zin eenvoudiger. De vele materialen die wereld rijk is bestaan uiteindelijk uit slechts een honderdtal verschillende soorten atomen, die op hun beurt allemaal zijn opgebouwd uit elektronen, protonen en neutronen. De *kwantummechanica* is een zeer succesvolle theo-

rie om de wereld van dit soort deeltjes te beschrijven (mits hun snelheden niet al te hoog zijn). De *statistische fysica* beschrijft hoe een microscopisch model met heel veel deeltjes kan worden gebruikt voor het bestuderen van verschijnselen die plaatsvinden op veel grotere, 'macroscopische' lengteschalen. Voor de modellen in dit proefschrift gaat het om uiteenlopende verschijnselen zoals ijs, de groei van kristallen en magnetisme. De hoofdrol in dit proefschrift is echter niet weggelegd voor deze verschijnselen maar voor de wiskundige eigenschappen van de theorie en de modellen: we onderzoeken niet de natuur maar de theorie.

Je zou kunnen zeggen dat ook dit proefschrift gaat over het natuurwetenschappelijke proces waarin men een specifiek verschijnsel herkent als een speciaal geval van iets algemeners, en de zo verkregen theorie vervolgens test met experimenten—maar dan op een abstracter niveau. De plaats van de natuur wordt hier ingenomen door de theorie zelf, in ons geval de theorie van de zogeheten 'kwantumintegreerbaarheid', en experimenten worden vervangen door modellen. We nemen hierbij modellen die zijn ontwikkeld om natuurverschijnselen te begrijpen als uitgangspunt om meer wiskundig gemotiveerde modellen te maken en bestuderen. Het doel is een beter begrip van de theorie, en daarmee uiteindelijk van de modellen die een dieper begrip van de natuur bieden. We zullen een voorbeeld hiervan tegenkomen terwijl we nader ingaan op de twee kernbegrippen in de titel van mijn proefschrift.

Elliptische kwantumintegreerbaarheid. Het wordt wel gezegd dat de wiskunde onredelijk effectief is in de natuurwetenschappen [9]. Voor de 'kwantumintegreerbare' modellen die ik bestudeer is dit al helemaal het geval. In het algemeen is er bij het maken van modellen een spanning tussen de mate waarin het model realistisch is en hoezeer het mogelijk is om dingen uit te rekenen: hoe meer we de situatie 'idealiseren' des te verder we kunnen komen met berekeningen met pen en papier. Kwantumintegreerbare modellen hebben een onderliggende wiskundige structuur die het mogelijk maakt om verscheidene belangrijke natuurkundige grootheden (meetbare eigenschappen) in het model tot in detail uit te rekenen. Met dit laatste bedoel ik dat de resultaten niet alleen heel precies (denk: 3.14159265359) zijn, maar *exact* (denk: π). Een voorbeeld is het ijsmodel voor een platte laag ijs van precies één atoom dik. Dit model speelt een rol in Deel Eén van dit proefschrift. De strikte tweedimensionaliteit maakt het mogelijk om veel grootheden uit te rekenen. Hoewel tweedimensionaal ijs misschien niet realistisch lijkt, is men er in 2015 in geslaagd om het soort ijs waar het hier om gaat te maken in het laboratorium [16]! Het is niet onwaarschijnlijk dat zulk ijs ook écht in de natuur voorkomt, bijvoorbeeld wanneer water in de porieën van materialen doordringt en bevriest.

Het vroegste voorbeeld van een kwantumintegreerbaar model is de spinketen van Heisenberg. Een *spinketen* is een ééndimensionaal kwantummechanisch model voor magnetisme, bestaande uit een rij of ketting van (kwantummechanische) tolletjes—de atomen van het materiaal—die niet verplaatsen maar elkaar wel kunnen 'voelen' (onderling wis-

selwerken). De Heisenberg-spinketen is het prototype voor de modellen uit Deel Twee van dit proefschrift. In een beroemd artikel uit 1931 analyseerde Hans Bethe het energiespectrum van dit model met behulp van een slimme gok ('Ansatz'). Meestal moeten we het doen met allerlei benaderingen als we meer willen weten over grootheden zoals de energie. Het bijzondere van Bethes werk is dat het exacte (!) informatie biedt over het energiespectrum van spinketens die willekéúrig lang zijn, dus zelfs voor macroscopische spinketenlengte. Bovendien blijkt dat de spingolven die door de spinketen reizen en onderweg op elkaar botsen zich veel beschaafder gedragen dan men zou verwachten op basis van de regels die het model definiëren: het lijkt wel alsof de spingolven zich aan extra, verborgen regels houden. Veel modellen in de theoretische natuurkunde hebben een aantal *symmetrieën*: het systeem gedraagt zich dan bijvoorbeeld hetzelfde op ieder ogenblik, of wanneer we het verplaatsen of ronddraaien. Elke symmetrie leidt tot een regel waar de spingolven zich aan moeten houden. De resultaten van Bethe suggereren dus dat de Heisenberg-spinketen nog veel meer symmetriëen zou kunnen hebben. Ruwweg noemen we een model waarvoor dit het geval is *integreerbaar*.

In de decennia na Bethes artikel bleek het mogelijk om diens methode toe te passen op allerlei andere modellen, waaronder ook het ijsmodel en een generalisatie daarvan die bekend staat als het 'zesvertexmodel'. In de jaren zeventig slaagde Rodney Baxter erin, door het zesvertexmodel en het nog algemenere 'achtvertexmodel' te bestuderen, aan te tonen dat het ijsmodel inderdaad een heleboel verborgen symmetrieën heeft. Deze blijken ook verborgen symmetrieën te zijn van de Heisenberg-spinketen met macroscopische spinketenlengte. In de late jaren zeventig werd een zeer krachtig wiskundig formalisme geïntroduceerd waarmee zowel het zesvertexmodel als de Heisenberg-spinketen kan worden bestudeerd met behulp van abstracte algbra. Ook Bethes methode en Baxters resultaten kunnen worden gereproduceerd in dit formalisme. In het kort worden modellen met een dergelijke onderliggende wiskundige structuur *kwantumintegreerbaar* genoemd.

Kwantumintegreerbare modellen worden onderverdeeld in drie klassen. De klasse met 'rationale' modellen bevat onder andere de Heisenberg-spinketen. De klasse met 'goniometrische' modellen omvat bijvoorbeeld het zesvertexmodel. De derde klasse bevat kwantumintegreerbare modellen die *elliptisch* worden genoemd; het achtvertexmodel is hier een voorbeeld van. Aan deze laatste klasse ontleent dit proefschrift zijn titel.

Wat is er zo interessant aan elliptische kwantumintegreerbare modellen? Laten we om dit beter te begrijpen teruggaan naar het zesvertexmodel en zijn vrienden. Nadat Bethe een manier had bedacht om de Heisenberg-spinketen te analyseren bleek deze techniek ook toepasbaar op onder andere het ijsmodel en het algemenere zesvertexmodel. Iedere keer suggereerden de resultaten dat het model een verborgen algebraïsche structuur heeft. Baxter onderzocht het (elliptische) achtvertexmodel, dat in tegenstelling tot het zesvertexmodel geen duidelijke fysische interpretatie heeft—het beschrijft bijvoorbeeld geen ijsachtig materiaal—en waarvoor Bethes methode niet werkt. Dit dwong hem om andere wegen te zoeken om het model op te lossen. Het vinden van verborgen symmetrieën voor meer realistische modellen—zoals het ijsmodel en de Heisenberg-spinketen—was een zeer mooie

bijkomstigheid. Sinds Baxters vondst maken elliptische kwantumintegreerbare modellen het mogelijk om de theorie van de kwantumintegreerbaarheid nauwkeurig te onderzoeken. In dit proefschrift bestudeer ik daarom modellen die ons helpen de theorie beter te begrijpen.

Inhoud van dit proefschrift

Het proefschrift bestaat uit twee delen. Deel Eén speelt zich af in de wereld van vertexmodellen in de statistische fysica terwijl het kortere Deel Twee over kwantummechanische spinketens gaat.

Deel Eén. Dit deel bestaat uit drie hoofdstukken. Inhoudelijk ligt het zwaartepunt bij Hoofdstuk III en zijn de eerste twee hoofdstukken voorbereidend.

Hoofdstuk I. Kwantumintegreerbaarheid is een erg mooi maar technisch onderwerp, en publicaties over dit onderwerp zijn doorgaans lastig voor niet-ingewijden. In de hoop mijn proefschrift toegankelijker te maken begin ik met een introductie tot de relevante kwantumintegreerbare vertexmodellen. Ik denk dat dit eerste hoofdstuk ook los van het proefschrift nuttig kan zijn als een introductie tot het vakgebied.

Naast het zes- en achtvertexmodel bespreek ik in Hoofdstuk I ook het SOS-model (*solid-on-solid*, vaste stof op vaste stof) voor de groei van kristallen. Het SOS-model heeft ook een elliptische variant, die door Baxter werd ontwikkeld in zijn studie van het achtvertexmodel. Op dit elliptische SOS-model kan Bethes methode wél worden toegepast, en de zo verkregen resultaten kunnen worden vertaald naar resultaten voor het achtvertexmodel. Op hun beurt kunnen SOS-modellen ook worden beschouwd als 'gegeneraliseerde' zesvertexmodellen, wat een intuïtieve *diagrammatische notatie* toestaat. Dit is een manier om abstracte algebra te visualiseren die het mogelijk maakt plaatjes te gebruiken in plaats van formules. Een beroemd voorbeeld van zo'n diagrammatische notatie wordt gegeven door Feynmandiagrammen in kwantumveldentheorie. Voor het gewone zesvertexmodel was een diagrammatische notatie ook bekend, maar bij mijn weten is de notatie die ik gebruik voor gegeneraliseerde zesvertexmodellen nieuw [3]. Met behulp van deze notatie behandel ik in Hoofdstuk I de relevante aspecten van de theorie van de kwantumintegreerbaarheid voor elliptische SOS-modellen.

Een andere kwestie die in Hoofdstuk I aan bod komt, en belangrijk is voor de volgende hoofstukken, is het volgende. Bij het berekenen in de statistische fysica van macroscopische natuurkundige grootheden komt een technisch detail kijken: we moeten tussentijds kiezen met welke zogeheten 'randvoorwaarden' we werken. Voor veel modellen is dit een kwestie van slim kiezen en hangt het macroscopische resultaat vervolgens niet meer af van onze keuze. Dit strookt met de intuïtie dat, wanneer we ergens in het midden van een steeds groter wordend systeem metingen doen, de resultaten steeds minder gevoelig zijn voor wat er aan de rand gebeurt. Het zesvertexmodel is hierin een uitzondering: de randvoorwaarden

doen er terdege toe! Periodieke randvoorwaarden worden het meest gebruikt; dit is een handige keuze omdat de resultaten goed aansluiten bij de eigenschappen van ijs. Een andere mogelijkheid is om zogenaamde 'domeinmuren' op de randen te kiezen. Deze keuze blijkt voor het ijsmodel interessante wiskundige toepassingen te hebben in het gebied van de combinatoriek. Het is ook het onderwerp van het volgende hoofdstuk.

Hoofdstuk II. In dit hoofdstuk bestudeer ik het zesvertexmodel met domeinmuren aan de randen. Veel informatie over macroscopische natuurkundige eigenschappen zit verpakt in de zogenaamde *partitiefunctie*. De uitdaging is om de partitiefunctie voor dit model te berekenen voor een willekeurige maar eindige systeemgrootte. Bethes methode kan niet worden gebruikt als we hebben gekozen voor domeinmuren, maar er zijn andere methodes beschikbaar om de 'domeinmuurpartitiefunctie' te bestuderen. Deze functie werd in de jaren tachtig exact berekend door Vladimir Korepin en Anatoly Izergin. Het doel van Hoofdstuk II is het uiteenzetten van een ándere manier om deze partitiefunctie exact te berekenen. Een voordeel is dat onze methode *constructief* is.

Deze alternatieve methode is zes jaar geleden bedacht door Wellington Galleas, en sindsdien verder ontwikkeld door hem en mij. Het idee is de onderliggende algebraïsche structuur te gebruiken om een bepaalde 'functionele' vergelijking af te leiden voor de domeinmuurpartitiefunctie. Deze functionele vergelijking kan worden gebruikt om een expliciet voorschrift te vinden voor de constructie van de partitiefunctie voor willekeurige systeemgrootte. Een dergelijke voorschrift heeft een voordeel ten opzichte van de aanpak van Korepin en Izergin, waarbij men eerst eigenschappen formuleert die de domeinmuurpartitiefunctie vastleggen en vervolgens op een of andere manier een formule moet vinden die aan al die eigenschappen voldoet. Daarnaast illustreert onze methode de kracht van de onderliggende algebraïsche structuur, die terugkomt in de vele mooie eigenschappen van onze functionele vergelijking.

Hoofdstuk III. Hier test ik of onze constructieve methode ook werkt voor een technisch veel ingewikkelder geval: het elliptische SOS-model met domeinmuren en één 'reflecterende' rand. Alhoewel deze randvoorwaarde vanuit natuurkundig oogpunt nog minder realistisch is dan domeinmuren, is het interessant vanuit een algebraïsch oogpunt.

Ook hier was al een formule beschikbaar, wat niet wegneemt dat dit geval een goede toets is om te kijken hoe algemeen onze methode is. Het elliptische karakter van het model dwingt ons om op een abstracter niveau te werken, wat leidt tot een beter begrip van de methode.

Deel Twee. Hierboven is de Heisenberg-spinketen al een aantal keren voorbijgekomen. Spinketens staan in het tweede deel van mijn proefschrift.

Hoofdstuk IV. Dit hoofdstuk beschrijft lopend onderzoek dat ik samen met Rob Klabbers doe naar de vraag of een bepaalde elliptische spinketen exact oplosbaar is.

Er bestaat een zeer interessante elliptische spinketen die in 1990 werd voorgesteld door Vladimir Inozemtsev. Deze spinketen interpoleert tussen de Heisenberg-spinketen en de

zogeheten Haldane–Shastry-spinketen: de Inozemtsev-spinketen is een algemener model dat de andere twee bevat als speciale gevallen. Bovendien is het, net als de andere twee spinketens, exact oplosbaar. Nu hebben de (rationale) Heisenberg- en Haldane–Shastry-spinketens beiden goniometrische varianten die eveneens exact oplosbaar zijn. Het is eenvoudig om een generalisatie te vinden van de Inozemtsev-spinketen die interpoleert tussen deze goniometrische versies van de Heisenberg- en Haldane–Shastry-spinketens. De vraag is of ook deze spinketen exact oplosbaar zou kunnen zijn.

Hiertoe onderzoeken we een aantal methodes die voortkomen uit het werk van Inozemtsev, vooralsnog in de eenvoudigste situatie die interessant is: de tweedeeltjessector van onze spinketen. Helaas leveren onze eerste pogingen niets op. We opperen een derde mogelijkheid, maar zijn nog niet toegekomen aan een verdere uitwerking hiervan. Dit hoofdstuk heeft dus een open eind, en niemand weet nu of het goed of slecht zal aflopen. Als het mogelijk blijkt om de tweedeeltjessector exact te analyseren dan zou dit aanwijzingen kunnen geven of ook de meerdeeltjessectoren exact oplosbaar zijn.

Tot slot. In mijn proefschrift ontwikkel ik voor het elliptische SOS-model een intuïtieve diagrammatische notatie die aansluit bij al bekende notatie voor het zesvertexmodel. Ik geef een gedetailleerde beschrijving van een constructieve methode voor de exacte bepaling van partitiefuncties van dergelijke modellen. Die methode is behoorlijk algemeen: ik laat zien dat zij ook toepasbaar is op het elliptische SOS-model met domeinmuren en een reflecterende rand.

Daarnaast vestig ik de aandacht op een elliptische spinketen die de Inozemtsev-spinketen generaliseert en beschrijf ik lopend onderzoek naar de vraag of deze spinketen exact oplosbaar is.

Hopelijk vormt dit proefschrift een goede introductie tot hedendaags onderzoek naar een prachtig onderwerp: de wondere wereld van kwantumintegreerbaarheid voor vertexmodellen, SOS-modellen en spinketens—en in het bijzonder de elliptische varianten daarvan.

Acknowledgements

Dear Gleb, it is a pleasure to thank you for making this thesis possible, for giving me freedom, and for feedback on my work. I really enjoy our conversations about research, (quantum)physics, and non-scientific subjects.

André, dank je voor de gastvrijheid in Oxford, en voor de nuttige discussies. Je invloed op mijn wiskundige vorming is onmiskenbaar in dit proefschrift, alleen al in het veelvuldige gebruik van grafische notatie. Hjalmar, thank you for the hospitality, *fika*, and for very helpful discussions and feedback.

I learned a lot from my collaborators. Wellington, thank you for many useful discussions, for succeeding to get me into *Mathematica*, and for bringing the problem tackled in Chapter III to my attention. Rob, ik waardeer onze prettige samenwerking zeer; dank je voor de gezelligheid zowel op als buiten het werk in Hamburg, en voor het nauwgezette commentaar op aanzienlijke delen van dit proefschrift. Rick, Rembert en Gerard, ik heb met plezier meegedacht over méétbare eigenschappen van het zesvertexmodel.

Teaching is an important part of academic life. I enjoyed assisting Bernard de Wit and Eric Laenen for a course on advanced quantum field theory, and Mikhail Vasiliev for a course on higher-spin gauge theory. It was also very nice to run a seminar on spin chains with Gleb and André, which culminated in my lecture notes.

Thank you to all my colleagues at the Institute for Theoretical Physics for the pleasant work environment. Special thanks to my office mates Stijn, Riccardo, Panos and Cora; to Nava and to Vivian; and to our supporting staff, Joost, Olga and Wanda. I also thank my colleagues at the Mathematical Institute—in particular Joey and Shan—for their interest in physics; I really enjoyed our seminar on quantum field theory. Thank you to my fellow PhD-representatives at Prout for the nice time and the different perspectives on the position of PhD candidates.

A very attractive aspect of the academic world is its international character. I thank DESY for the kind hospitality during my visits; special thanks to Frau Duarte. Thank you to my peers from DRSTP, GQT, 'Amsterdam–Brussels–Paris', Modave, IGST and the other schools and conferences that I have attended: to fun times!

Lieve familie en vrienden, dank jullie voor alles, in voor- en tegenspoed. Voor de vakanties; voor de concerten en de opera's; voor het tuinieren, het wandelen, fietsen en boulderen; voor de vele gezellige avonden, het samen koken, en het lekkere eten. Lieve Levi, ik ben je voor altijd dankbaar voor al het voorgaande. Lieve ouders, ook bijzonder bedankt voor het meedenken over de vormgeving van dit proefschrift en het uitgebreide commentaar op de Nederlandse samenvatting.

Liefste KaYin, je verdient veel meer dan alleen een eigen bladzijde in mijn dankwoord: dank je voor alles, dank je voor ons, dank je voor dat je jij bent.

Curriculum vitae

I was born in Utrecht on 14 December 1986 and grew up in Hilversum, where I attended the Gemeentelijk Gymnasium from 1999 to 2005. After a year of which I spent half travelling in Southeast Asia I came to Utrecht for my studies at Utrecht University. I obtained a double Bachelor (2006–2009) in the programmes 'Physics & Astronomy' and 'Mathematics', and Master degrees (2009–2012) in 'Theoretical Physics' and 'Mathematical Sciences', graduating *cum laude* in each case. My Master's theses were supervised by Prof. dr. Gleb Arutyunov and by dr. André Henriques.

From September 2012 to 2016 I was a PhD candidate at the Institute for Theoretical Physics at Utrecht University in the group of Prof. dr. Gleb Arutyunov. I have had the opportunity to participate in various schools and conferences during this time, to give lectures about quantum integrability at the Modave Summer School, and to visit DESY (Hamburg, Germany) on several occasions including a five-week period. Besides this I enjoyed acting as a faculty representative for Prout, the PhD network of Utrecht University.

In September 2016 I will start as a postdoc on the mathematics of elliptic integrable systems at Chalmers University of Technology in Gothenburg, Sweden.